NORGES GEOTEKNISKE INSTITUTT

NORWEGIAN GEOTECHNICAL INSTITUTE

PUBLIKASJON NR. 208
PUBLICATION

J.H. Schmertmann
New Concepts for the Mobilization of the Components of Shear Resistance in Clay - a Review of a Large Experimental Study to Determine the Behavior of Mohr-Coulomb Cohesion and Friction in Clay

K.H. Andersen. T. Lunne, T.J. Kvalstad and C.F. Forsberg
Deep Water Geotechnical Engineering

Program for Workshop, 33rd IGC in Lillestrøm Norway
Geohazards - a tribute to Kaare Høeg
A Life in GeoSciences

Program for Workshop, 33rd IGC in Lillestrøm Norway
Theme of the Day
Geohazards: Can society cope?

NGI

OSLO 2012

The NGI Publications is a special and last issue of the series. The NGI Publication Series is published by:

Norwegian Geotechnical Institute
P.O. Box 3930 Ullevaal Stadion
N-0806 Oslo, Norway

Telephone: (+47) 22 02 30 00
Telefax: (+47) 22 23 04 48
E-mail: ngi@ngi.no
*Internet: http://www.ngi.no_*

The first article has not been published before.

The second article is reset and reprinted with permission from the Proceedings of the XXIVth National Conference of the Mexican Society of Soil Mechanics in Aguascalientes, 26-29 Nov. 2008.

Printed and bound by
Interface Media as, Oslo, 2012
400 copies
ISBN-10: 82-546-0195-x
ISBN-13: 978-82-546-0195-2
EAN: 9788254601952
ISSN: 0078-1193

NGI's Publication 208

It is a special pleasure to introduce to our readers the last NGI Publication in printed format. Future publications will be in digital form on the NGI website.

This last publication has special contents. It presents an unpublished paper by Emeritus Professor John H. Schmertmann, an early post-doctoral fellow at NGI: "New Concepts for the Mobilization of the Components of Shear Resistance in Clay - a Review of a Large Experimental Study to Determine the Behavior of Mohr-Coulomb Cohesion and Friction in Clay", where Professor Schmertmann brings together the results of laboratory tests and his experience to explain how soil behaves, which has been one of his areas of expertise all his life. In this context, it is appropriate to quote one paragraph from a letter by Karl Terzaghi to Professor F.E. Richart at University of Florida on the contribution of researchers to soil mechanics. Karl Terzaghi wrote the letter from his home in Winchester, Massachusetts on April 12, 1961:

> "If you have not received a copy of Hvorslev's contribution to the Shear Conference in Boulder, you should get one. Hvorslev did, as usual, a remarkably thorough job. It is a pity that he did not yet know the results of Schmertmann's investigations".

This NGI publication becomes available on the occasion of the official opening of the Schmertmann Research Laboratory at NGI on 15th May 2012, a new laboratory wing dedicated to research, fundamental soil mechanics, geotechnical education and outreach to other researchers.

The second contribution in this publication is the paper "Deep Water Geotechnical Engineering", by Knut. H. Andersen. Tom Lunne, Tore J. Kvalstad and Carl Fredrik Forsberg, all from NGI. The paper brings together excerpts of the wide expertise required for the geotechnical engineering design of offshore installations in deepwater. The paper was first presented by our Technical Director Knut H. Andersen at the 24th National Conference of the Mexican Society of Soil Mechanics in Aguascalientes, Mexico, and is published in the proceedings of the conference.

After the two papers, we present the program for the Kaare Høeg Symposium held in 2008 at the 33rd International Geology Conference in Lillestrøm, Norway, where NGI's earlier Managing Director's life and career were honoured by his mentor Professor Robert V. Whitman, and by students, colleagues and friends. We also present the program for the International Geohazards Day, held at the same 33rd International Geology Conference, where experts in natural hazards from all over the world came to share their experience and case studies. Natural hazards is an area where NGI has worked since 1950, and where the award of Centre of Excellence status with the "International Centre for Geohazards" in 2002 was a recognition of its contributions and potential in this area.

Oslo, 2012-04-20
Lars Andresen
Managing Director, NGI

NEW CONCEPTS FOR THE MOBILIZATION OF THE COMPONENTS OF SHEAR RESISTANCE IN CLAY

Review of a Large Experimental Study to Determine the Behavior of Mohr-Coulomb Cohesion and Friction in Clay

by John H. Schmertmann[1]

Prologue

The Managing Director of the NGI, Dr. Suzanne Lacasse, asked me to write a prologue to the paper to help the reader understand its unusual history. I will briefly review it here. It involves a long association with the NGI.

It all began when I met the first Managing Director of the NGI, Dr. Laurits Bjerrum, in early 1956 after he gave a lecture to graduate students and faculty at Northwestern University. I spoke with him afterwards and he kindly agreed to sell state-of-the-art, Geonor triaxial equipment to the University of Florida, where I started the university teaching and research part of my career later in 1956. By 1958 I had an operating laboratory and started my clay research for a PhD from Northwestern University with Dr. Jorj O. Osterberg as my advisor.

The ASCE's Research Conference on Shear Strength of Cohesive Soils at Boulder, CO in June 1960 gave me the opportunity to publish, together with Dr. Osterberg, the 1st major paper describing the research. By then the lab's Geonor equipment had expanded to that shown in the attached 1960 photo and we had developed and performed our first 100 **IDS**-tests.

Our paper attracted the attention of Dr. Karl Terzaghi, who made favorable comments about it in his taped introductory remarks to the Conference. Dr. Bjerrum, very active at this Conference, asked me to meet with him and Dr. A. Bishop in his hotel suite to discuss my research, at the end of which he invited me to come to the NGI for a year as a visiting post doctoral fellow. After completing my PhD at Northwestern in 1962 I moved my family to Oslo for 15 months, where I interacted with Dr. Bjerrum and the NGI staff and worked on various research projects and this clay research.

The NGI's invitation to participate in honoring Dr. Bjerrum after his sudden death in 1973 led to my 2nd major paper on clay shear in their 1976 Bjerrum Memorial Volume. It provides a summary of the 1958-1971 research and my thoughts about what we had learned. Then a 1978-2005 career change into consulting pre-empted any further major work to interpret the research results.

[1] Professor Emeritus, Dept of Civil and Coastal Engineering, University of Florida, Gainesville, FL 32611, email: schmert@ufl.edu. Please send discussions to the NGI at ngi@ngi.no.

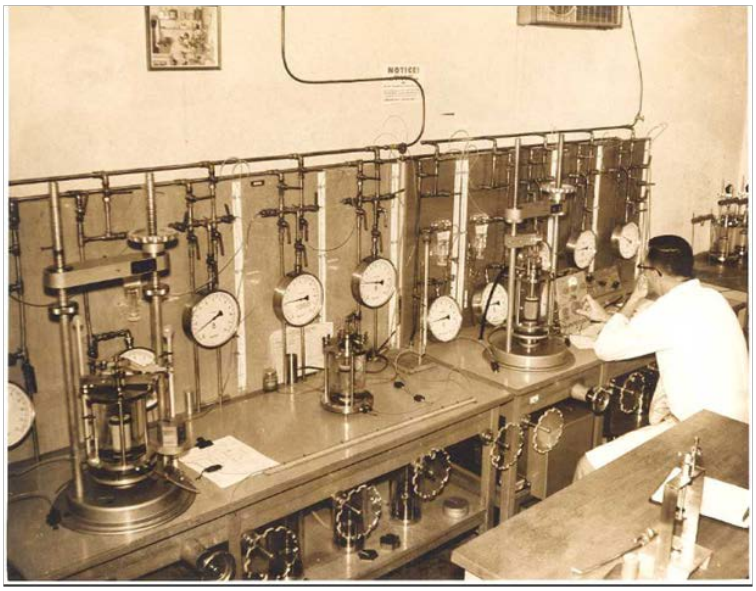

University of Florida Laboratory in 1960

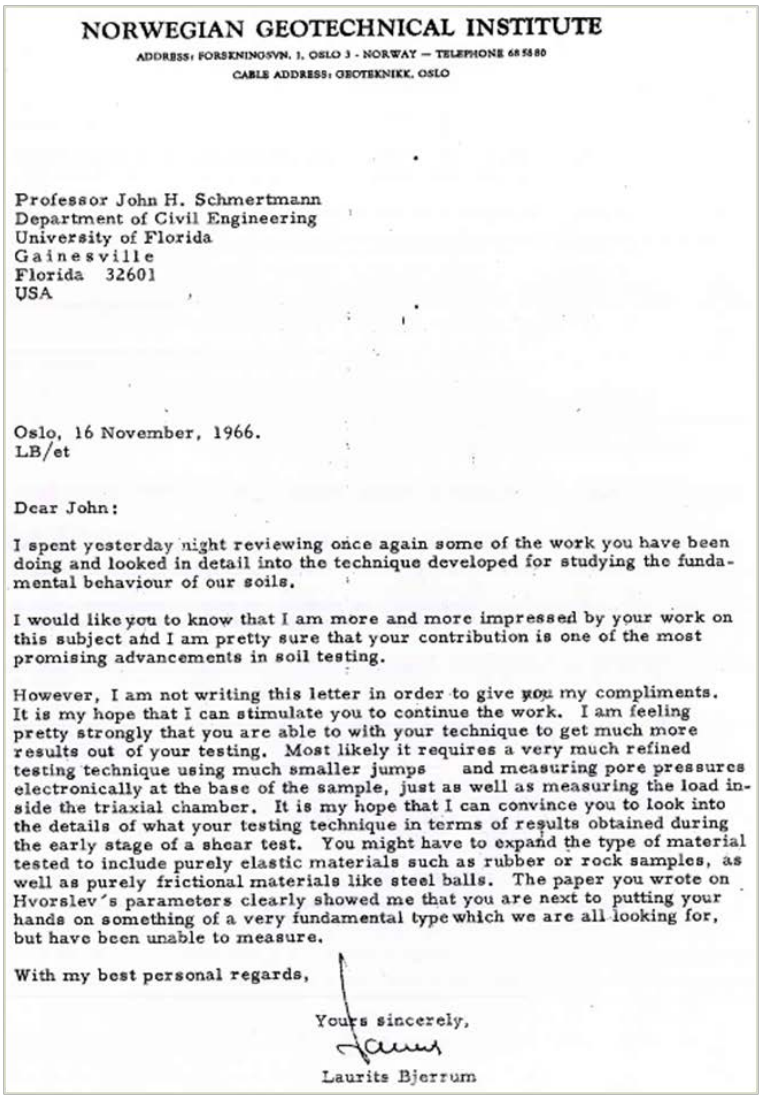

NORWEGIAN GEOTECHNICAL INSTITUTE

ADDRESS: FORSKNINGSVN. 1, OSLO 3 - NORWAY — TELEPHONE 68 58 80

CABLE ADDRESS: GEOTEKNIKK, OSLO

Professor John H. Schmertmann
Department of Civil Engineering
University of Florida
Gainesville
Florida 32601
USA

Oslo, 16 November, 1966.
LB/et

Dear John:

I spent yesterday night reviewing once again some of the work you have been doing and looked in detail into the technique developed for studying the fundamental behaviour of our soils.

I would like you to know that I am more and more impressed by your work on this subject and I am pretty sure that your contribution is one of the most promising advancements in soil testing.

However, I am not writing this letter in order to give you my compliments. It is my hope that I can stimulate you to continue the work. I am feeling pretty strongly that you are able to with your technique to get much more results out of your testing. Most likely it requires a very much refined testing technique using much smaller jumps and measuring pore pressures electronically at the base of the sample, just as well as measuring the load inside the triaxial chamber. It is my hope that I can convince you to look into the details of what your testing technique in terms of results obtained during the early stage of a shear test. You might have to expand the type of material tested to include purely elastic materials such as rubber or rock samples, as well as purely frictional materials like steel balls. The paper you wrote on Hvorslev's parameters clearly showed me that you are next to putting your hands on something of a very fundamental type which we are all looking for, but have been unable to measure.

With my best personal regards,

Yours sincerely,

Laurits Bjerrum

Laurits Bjerrum's letter in 1966

Inspired by rediscovering Bjerrum's 1966 letter in 2005, I decided to make a complete review of my records from the research. This paper, the 3rd major work on the subject and an updated extension of the 2nd in the Memorial Volume, presents a "breakthrough" in my understanding. The reader will see how this evolved from an unsuspected, even paradoxical, special viscous friction behavior of the adsorbed water layer (AWL) on clay particles. This now seems obvious to me, but it did not appear so in the 1970's. Even Bjerrum missed it in his 1973 SOA paper. After making this mental leap all sorts of personal mysteries about clay shear behavior seemed to fall like dominoes and became at least partially resolved in my mind. The paper leads the reader through this personal experience of discovery and resolution.

It took a long time to happen, but this paper has now found a suitable "home" in one of the final printed volumes of a long and distinguished series of NGI publications.

ABSTRACT

This paper reviews a unique "**IDS**" triaxial test designed to separate the Mohr-Coulomb engineering components of shear resistance in soils. Selected results from approximately 500 such tests performed from 1958 to 1971 using saturated cohesive soils, from machine remolded to undisturbed, demonstrate important concepts, some new, about clay shear strength component behavior. These include: (1) The importance of considering strain and its effect on soil structure when measuring the components of shear resistance in clay. (2) A newly recognized "secondary" sliding **friction**, Φ'_{α}, that mobilizes fully at compressive strains of approximately 1% or less and likely results from the shear resistance behavior of an apparent viscous adsorbed water layer (AWL) between particle surfaces. (3) A "primary" friction, Φ'_{β}, measured directly by the **IDS-**test, that results from particle interference effects that mobilize more gradually with strain in laboratory normally consolidated (NC) clays. Overconsolidation (OC) and/or prior creep increase the subsequent strain rate of Φ'_{β} mobilization. (4) A viscous time transfer of AWL Φ'_{α} friction to the more stable Φ'_{β} friction. (5) A plastic cohesion, also likely due to AWL behavior, that provides a tensile strength even in machine remolded clays. (6) The formation of more permanent, but also more brittle, cohesive bonds during OC and/or ageing, and (7) A related practical discussion using the above concepts about the shear components to better understand residual friction, secondary consolidation and "secondary shear", ageing preconsolidation, silts, sands and partial saturation, undrained strength, the low-strain shear modulus, K_o, different types of consolidation, Burland's ICL, the minimum surcharge ratio for effective drainage aids, failure planes and slickensides, the shear components during creep, and similar components when testing drained or undrained.

Key words: adsorbed water layer, ageing, bonds, clay, cohesion, consolidation, creep, drained, drainage aids, double layer, effective stress, failure planes, friction, ICL, IDS-tests, K_o, preconsolidation, primary consolidation, primary shear, remolded, residual strength, saturated, secondary consolidation, secondary shear, shear, shear modulus, slickensides, time effects, tension, triaxial tests, undisturbed, unsaturated, viscosity.

TABLE OF CONTENTS

1. INTRODUCTION

In the early development of soil mechanics, say the 50 years from 1920-1970, many prominent researchers and engineers studied the shear strength of soils, particularly clays. For examples of some references over these 50 years that significantly influenced the research described in this paper see Bjerrum (1967a, 1972), Casagrande (1932), Horn and Deere (1962), Hvorslev (1961), Lambe (1953, 1958, 1960), Rowe and Rowe et. al. (1957, 1962, 1963(a)(b), 1964), Skempton (1953, 1961, 1970), and Terzaghi (1920, 1931, 1941a, 1941b, 1955). However, many questions remain unanswered, such as the nature and importance of the adsorbed water layer (AWL) between clay particle contacts, the existence or non-existence of cohesion in unbonded clays, the reliability of cohesion, the origins of residual shear and secondary consolidation, and the reliability for practice when using ageing-preconsolidation in geologically NC clays. These and other questions still remain for many engineers. This paper provides another perspective and some possible answers.

Herein, as in all the previous reports of his shear resistance research, the writer used the Mohr-Coulomb (M-C) model to express the total shear resistance in cohesion and friction terminology. The following **simple definitions of "cohesion" and "friction"** apply in this paper. The writer assumed that the total mobilized shear resistance of a saturated soil structure subjected to shear loading consists of the sum of two sets of engineering components, as follows: The **cohesion components** that behave approximately independently of the magnitude of compressive effective stress and give a soil its tensile strength, and the **friction components** that depend approximately linearly on the magnitude of compressive effective stress and contribute no tensile strength. He also assumed that all mobilized components = 0 when the shear loading = 0.

The M-C model dominated early research, has the attraction of simplicity, remains in widespread use, and the research results summarized herein seem explainable using this model. But important alternatives exist. Critical State Soil Mechanics (CSSM), using Cam-clay and associated models as described by Schofield and Wroth (1968) and Schofield (1999, 2005), argue for the superiority of these newer models. But, to the writer's knowledge, none of these include a new soil "secondary" friction component with many unusual properties, cohesion in remolded clays, shear component changes with strain, and major time transfer effects between components. The laboratory test results presented herein do not at present fit easily into a mechanistic, continuum mechanics picture of clay shear resistance. But, as interpreted by the writer, they do fit in with the electrochemical, viscous behavior of the adsorbed water layer as described by Terzaghi (1920, 1931, 1941a, 1941b), Lambe (1953, 1958, 1960) and others.

The writer took an original approach to the experimental study of the shear strength of clays at the University of Florida from 1958 to 1971. During this time he and his students (the "we" herein) developed and performed approximately 500 axisymmetric triaxial tests of a then new type, referred to herein as **IDS**-tests and described subsequently, in a then state-of-the-art laboratory (See **14. ACKNOWLEDGEMENTS** and photo in the **PROLOGUE**). Publications authored or co-authored by the writer in 1960, 1962, 1963(a)(b), 1964, 1976, 1981, 1991 and 1993, all referenced herein, document and summarize many of the previous findings from this research. Ho (1971 pp. 3-26) reviewed much of the M-C cohesion and friction component research and resulting theories over the years 1932-1971. This includes the **IDS-**test research, to which he added. This paper provides a fresh review of this research.

The catch-all word "structure" as used herein refers to a particular state of the extremely complex 'fabric' of the 3-dimensional packing and arrangement of particles and aggregates, its specific volume or void ratio, the attractive and repulsive forces and the resultant adsorbed water layer (AWL) on and between particles, and the cementation and other bonds that may form between particles or aggregates of particles. All soils have "structure". **Strain** distorts and changes structure. Schmertmann (1964) describes in some detail the need to consider strain and its effect on structure when measuring the components of shear resistance in clay.

The reader should treat all stresses as effective and, unless noted otherwise, all strains refer to axial compressive strains denoted by "Є" with the time-rate of strain denoted by "Ė". Some of the data and concepts presented herein may require more explanation than allowed by the length of this paper. The reader can supplement this paper by referring to the references cited and will find copies of many of these references in a website by using the following link: http://geotechnical.schmertmann.info/.

2. SUMMARY OF THE IDS-TEST

2.1 Preview of Shear Components

The writer's interpretation of the results from this large laboratory research program using the **IDS**-test led to the concepts developed herein. As a guide to this development, it might help the reader to see some of this interpretation in advance in the form of the summary Equation (5). Unfortunately, important strain and time effects such as strain rate and creep complicate any attempt to present a realistic yet simple equation to express the Mohr-Coulomb envelope shear behavior of clays. The writer offers the following equation (5) as a still simplified, but hopefully informative, summary of the components developed herein.

$$\{\tau = \mathbf{I}_c + \mathbf{I}_b + \sigma' \tan [\Phi'_\alpha + (\Phi'_\beta \approx \Phi'')]\}_{\epsilon,t} \quad \text{.....(5)}$$

Wherein:

- τ = Mobilized **shear resistance**.
- $\mathbf{I}_c$ = Plastic **cohesion**, probably slowly decreasing with reducing strain rate.
- $\mathbf{I}_b$ = Bond **cohesion**, generally relatively brittle and increasing with rest time at constant load.
- Φ'_α = Sliding **friction** through adsorbed water layer lubricant, viscous, decreasing with rest time, and also referred to subsequently as "secondary friction".
- Φ'_β = **Friction** due to particle/particle geometrical interference effects, increasing with OC, dry density, anisotropic consolidation, creep, secondary compression, and rest time, and clearly more stable than Φ'_α. Also referred to subsequently as "primary friction".
- ϵ,t = Subscripts denote that the mobilized shear and its components refer to the same axial strain at a particular time, and emphasizes they can vary with strain and time.

2.2 Explanation of the IDS-test

The writer developed the **IDS**-test as a **strain rate controlled**, **drained** triaxial test procedure for separating the apparent effective stress independent (**I**) and dependent (**D**) Mohr envelope components, 'nominal cohesion' and 'friction', respectively, as functions of initial structure and subsequent strain (**S**) – hence "**IDS**". Figure 1 shows the progress of an **IDS**-test in 4 steps, the first two experimental and the final two analytical.

Referring to Figure 1a, points A and B, unloaded from σ'_c, show the best locations in a consolidation load-unload cycle to have approximately (meaning 'close enough for the purposes of this research') the same after-consolidation structure, including void ratio, but with a measurable difference in effective stress. The researcher then subjects these two isotropically (in this research) consolidated specimens to triaxial compression, as in Figure 1b, and keeps each at a constant effective stress of σ'_{1A} and σ'_{1B}, respectively, by continually **controlling pore pressures** to match deviator stress while continuing the same axial strain rate. This produces a constant σ'_1, decreasing σ'_3 stress path.

Figure 1b* also shows schematically the stress-strain path of the test performed with a single specimen using the method described subsequently under **3.2 Curve Hopping**. At any strain, such as ϵ_X, specimen A will mobilize shear τ_{AX} and specimen B will mobilize a lower τ_{BX}, depending on the soil structure's reaction at ϵ_X to a change from σ'_{1A} to a lower σ'_{1B}. The researcher will then have measured directly a value of friction using two (or one) specimens with approximately the same initial structure along very similar stress and time paths to the

* In Figure 1b and generally herein, the writer refers to the **IDS**-tests as strain (Є) controlled with a constant rate of strain (Ė). But, more accurately, we performed them with a constant rate of downward movement of the top of a strain-gage load cell. We corrected for load cell and triaxial cell load column compressions. These compressions reduced Ė, especially during the low Є, high-modulus portion of a test. We also corrected approximately for the vertical strains associated with the *c.* ½% volume strains during curve hopping.

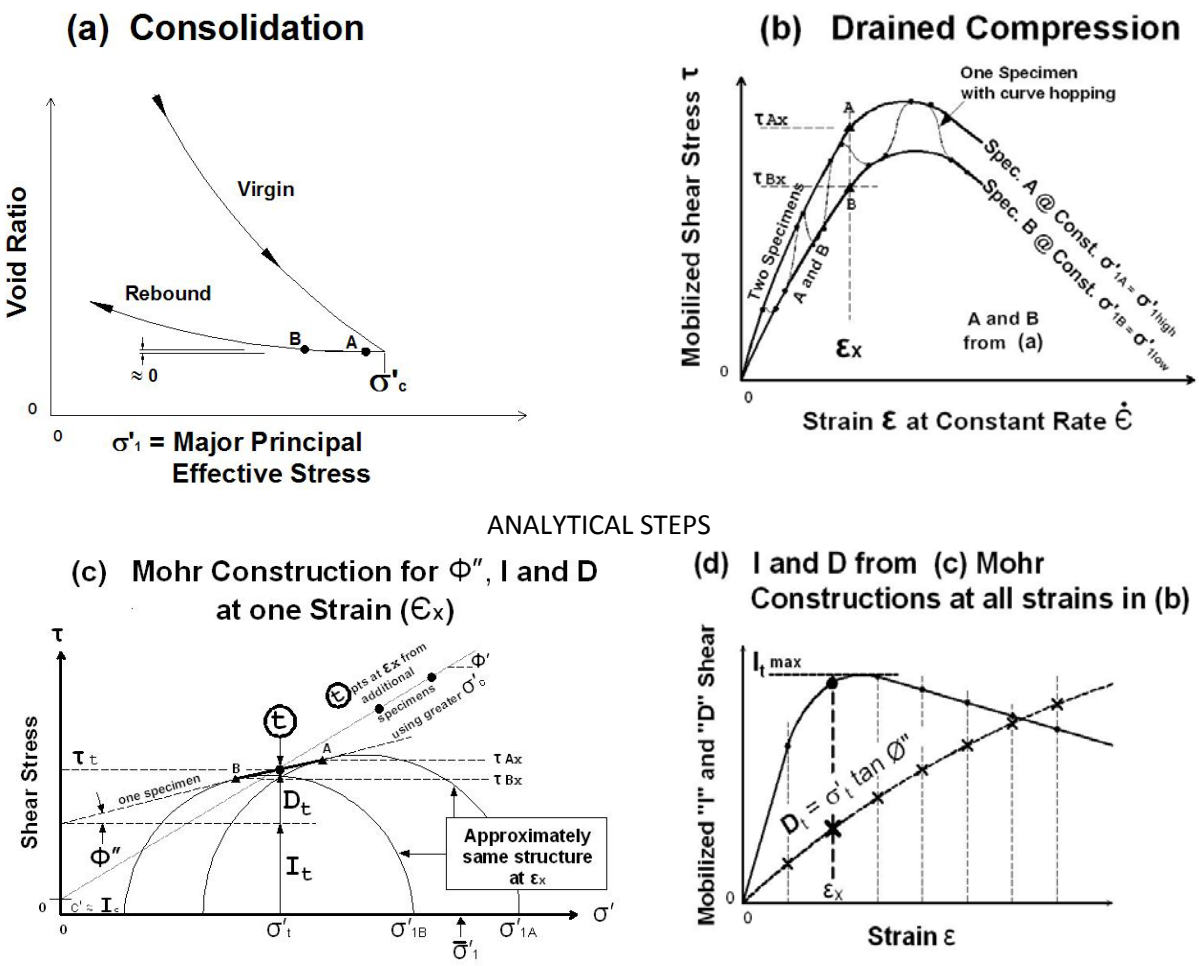

Figure 1: 4 Steps in Constant–σ´₁ IDS-test Using Either One or Two Specimens (Schematic)

same strain, and thus with approximately the same structure.

Figure 1c presents the Mohr circles representing the triaxial stress conditions at τ_{AX} and τ_{BX} as points A and B on the common tangent to the circles. The slope of this tangent gives an experimentally determined friction differential with a slope angle denoted Φ". The writer assumed this tangent slope correct at the midpoint "t" at effective stress σ'_t and shear stress τ_t. This assumption neglects a 1.5% too-low error in the **I** intercept resulting from envelope curvature between points A and B (Schmertmann, 1976 pp. 77, 78). Linearly extrapolating the A-B slope to the σ′ = 0 axis gives an apparent effective stress independent $\mathbf{I}_t$ component, or 'nominal cohesion', which leaves $\mathbf{D}_t$ as the directly measured, effective stress dependent friction component mobilized at σ'_t. The research by Schmertmann and Osterberg (1960, pp. 7-20), and a review by Schmertmann (1976, pp. 76-78), support this use of a linear extrapolation to obtain $\mathbf{I}_t$. Note from Figure 1c that:

$$[\,\tau = \mathbf{I} + \mathbf{D}]_t \quad \text{..... (1a)}$$

$$\mathbf{D}_t = \sigma'_t \tan \Phi'' \quad \text{..... (1b)}$$

and that the writer often uses the angle Φ" or tan Φ" , and later also Φ'_β and tan Φ'_β, to represent the **D** component.

The point "t" comes from one (any) strain in a single **IDS**-test. Finally, as shown in Figure 1d, one plots the $\mathbf{I}_t$ and $\mathbf{D}_t$ values for ϵ_X. Plotting the results from many strains from the same 1- or 2-specimen test in Figure 1b, using the method in Figure 1c, and connecting the points in Figure 1d produces the test objective of determining the mobilization of **I** and **D** with **S**train. **I** typically has a maximum value $\mathbf{I}_m$ at ϵ ≤ 1%, shown schematically in Figure 1d.

3. TEST METHODS

3.1 Extruded Clays, Standard Procedure

Of necessity to have enough comparative test results, we used machine mixed and extruded (severely remolded) specimens. We extruded batches of approximately 40 clay specimens using a "Vac-aire" machine, described in Matlock et. al. (1951), wherein powered augers mixed the clay and forced it, in a vacuum to obtain near-saturation, several times through a 1,000 mm^2 circular die. We then cut the clay into 100 mm length specimen blanks, wrapped them in wax paper coated with a petrowax and stored them in a humid room. Some post-extrusion restructuring occurred. We used the blanks after storage of at least one month and only after determining by miniature vane shear tests that each batch's undrained strength had reached an approximate constant with time. Upon removal for testing, we trimmed each blank to an 80 mm test specimen length in a split miter box for mounting in a triaxial cell. The test specimens had a length/diameter ratio of 2.2, which we assumed high enough to avoid the complication of using frictionless platens. Altogether, we extruded and stored approximately 1,000 specimen blanks from a variety of clays. They had a typical degree of saturation of 99% and a preconsolidation $p_c \approx 50$ kPa from the extrusion and restructuring. Table 1 gives some classification information for these clays, which the writer chose based on availability, variety, availability of undisturbed specimens for comparison testing, and a high enough permeability for convenient **IDS**-test research. Air conditioning kept the temperature of the lab approximately constant within a range of 22° to 26°C.

To simplify comparisons between tests, and recognizing the importance of drainage rate and other time effects (discussed subsequently), we used the following approximate 'standard' procedure for most of the tests: (1) One day, one increment isotropic consolidation to σ'_c; (2) $\dot{\epsilon}$ control $\approx 1.0\ \%/t_{100}$ or less, where t_{100} = isotropic, primary consolidation time for ≈ 100% effective stress increase; (3) Drained test with pore pressure control for $\sigma'_1 \approx$ constant; and (4) Triaxial compression with constant $\sigma'_{1high} \approx 0.95\ \sigma'_c$ and $\sigma'_{1low} \approx 0.75\ \sigma'_c$. The resulting stress path kept σ'_1 below σ'_c to avoid abrupt yielding changes in the structure of the test specimen. Schmertmann (1962) includes an extensive discussion of the method, the accuracy requirements for the successful performance of such an **IDS**-test, and the experimental errors involved.

The volume change occurring during the above 20% σ'_c change in σ'_1 produced a typical 1/2 % volume strain. The writer also investigated a 10% to 60% change in σ'_1 and thus smaller and larger volume strains. As a result he assumed a 20% change produced a change in structure of negligible importance when separating the shear components (see Schmertmann and Osterberg (1960, pp. 649-662) and Schmertmann (1976, pp. 76-78)). The results in these references and herein support this assumption.

Usually only the variable under study would differ from the 'standard procedure'. Using machine extruded clays also had the important advantage of mechanically destroying most or all of any cohesive bonds that had formed in the natural clay due to cementation or other insitu ageing effects. Test results from extruded clays provided a good destructured baseline from which to measure differences

Table 1: Plasticity and Mineralogy of Clays Tested (from Schmertmann 1976)

Extruded Clay	Plasticity Index (PI %)	-0.002 mm. %	Activity PI/-0.002	Clay Minerals
Enid (residual)	9	20	0.45	Kaolinite – 15% Illite – 10%
Jacksonville	14	13	1.08	Montmorillonite – 10%
Boston blue kv ≈ 6 x 10^{-9}cm/s	19	53	0.36	Illite – 45% Chlorite – 25%
Kaolinite kv ≈ 3 x 10^{-8}cm/s	21	60	0.35	Kaolinite – 99%
Lake Wauburg	105	85	1.24	Montmorillonite – 85% Illite – 5%

when comparing with the same clay when testing a restructured or an undisturbed specimen.

3.2 Curve Hopping

Schmertmann and Osterberg (1960, Figs. 1-13) describe the learning transition from performing **IDS** (then called "CFS")–tests using up to five duplicate specimens versus the two shown in Figure 1, and eventually to only a single specimen using a "curve hopping" technique (Figure 1b). This technique involves imposing controlled and continuous pore pressure changes on the specimen during its continuing drained compression and hopping back and forth between the two levels of σ'_1 and determining successive points along each σ'_1 hop. Connecting final "●" points before the next hop forms 'dash' increments along each σ'_1 curve. Then one connects the 'dashes' to estimate the two complete curves as if the hopping had not occurred. Schmertmann (1962) showed 15 comparisons between 1 and 2 specimen **IDS**-tests from a variety of extruded and undisturbed soils. They confirm the practical validity of the use of a single specimen with the curve hopping, **even with 'undisturbed' specimens**.

3.3 Uniform Pore Pressure

An accurate drained, strain-controlled **IDS-**test requires that the controlled pore pressures applied at the specimen base distribute practically uniformly throughout. The writer believes we attained this goal by using a combination of drainage and monitoring techniques, including: 1) External filter strips and caps, 2) One or more needle-punched 1.8 mm diameter longitudinal **internal** drains filled with saturated, twisted wool yarn, 3) Occasional check tests using slower rates of strain to allow more time for pore pressure uniformity, and/or using back pressure to force 100% saturation, and/or checking uniformity with pore pressure needles, 4) Using strain rates based on the prior measured time for isotropic consolidation and thus link rate to the actual specimen drainage, permeability and stiffness conditions, and 5) Monitoring the progress of the above described curve hopping and using only the final two data points when they both appeared to have reached the next σ'_1 level curve, as in Figure 1b. See Schmertmann and Osterberg (1960, pp. 648-668) for a description of the development of test procedures designed, in part, to assure uniform pore pressure.

4. MOHR ENVELOPE RESULTS FROM EXTRUDED CLAYS

The conventional c′-Φ′ Mohr envelope usually presents the results of strength tests as the linear or curved tangent to a sequence of Mohr circles at different stresses and void ratios, each at some given shear strength condition such as maximum shear. The condition could occur at different strains. Thus, the circles and envelope could apply to different structures with a different mobilization of the components of shear resistance. Again, see Schmertmann (1964, 1976 pp. 65-66).

Herein the writer uses a more constant structure variation–with the envelope defined by the locus of tangent points ("t" in Figure 1c) from a sequence (see below) of **IDS**-tests at the **same strain**. This permits introducing test strains, and their effects on clay structure and shear mobilization, into the study of the components of clay shear. The reader will soon see that such Mohr envelopes using a constant strain have little or no curvature when testing 99% saturated, nominally normally consolidated (OCR = 1.05 and 1.33 during the **IDS-**test for σ'_1 = 0.95 σ'_c and 0.75 σ'_c, respectively) extruded clays within the 50 to 700 kPa range of σ'_c investigated. The OCRs given subsequently refer to values before the **IDS-**test.

The following envelopes in Figures 2, 3 and 5 come from comparing **IDS**-test results from many nearly duplicate extruded specimens, each test providing a point "t" as shown in Figure 1c, with each envelope for a different constant axial strain Є. Most of the data points in the subsequent figures result from tests that substantially followed the 'standard procedure' but had different magnitudes of isotropic consolidation σ'_c, and therefore of void ratio, σ'_{1h}, σ'_{1l}, and σ'_t.

4.1 Normally Consolidated (NC) Clays

Note that Figures 2a and 3a show data and shear component envelopes for the total ($\mathbf{I}_t + \mathbf{D}_t$) components, = τ_t, versus σ'_t, and Figures 2b, 3b and 5 only show data and envelopes for the $\mathbf{I}_t$ component versus σ'_t.

Figure 2a shows comparative τ_t versus σ'_t results from extruded Boston blue clay (BBC) at representative compressive strains of ϵ = 0.5, 4.0, and 10.0%. A computer has fit a least-squares straight line through the individual test data points with each point weighted equally. The numbers next to each line indicate the slope angle (Φ'), the extrapolated zero intercept (c') and the R^2 value of the linear fit, which in this figure varies from 0.949 to 0.999. All the subsequent R^2 values also fall within this range and support the validity of the linearity of the Mohr envelopes over the stresses, strains and strain rates investigated.

Figure 2b shows the results from the same tests but with only the $\mathbf{I}_t$ component instead of the total $\tau_t = \mathbf{I}_t + \mathbf{D}_t$ mobilized shear in Figure 2a. The numbers denote the slope angle (Φ'_α), the extrapolated zero intercept ($\mathbf{I}_c$), and R^2. Note the dramatic difference versus Figure 2a – all three strains plot almost identically. $\mathbf{I}_c$ and Φ'_α do not vary much with strain and in this respect appear to behave plastically over the axial strain range of 0.5-10%.

Figures 3a and 3b show the similar results obtained from a commercial kaolinite powder mixed with distilled water (reconstituted). Comparing the extruded kaolinite with the Boston blue clay provides one example of how reconstituted kaolinite matches test results in natural clays. Kaolinite, used extensively in this research, has many desirable properties for laboratory research. See Schmertmann (1963) for more information about the kaolinite used and the usefulness of kaolinite.

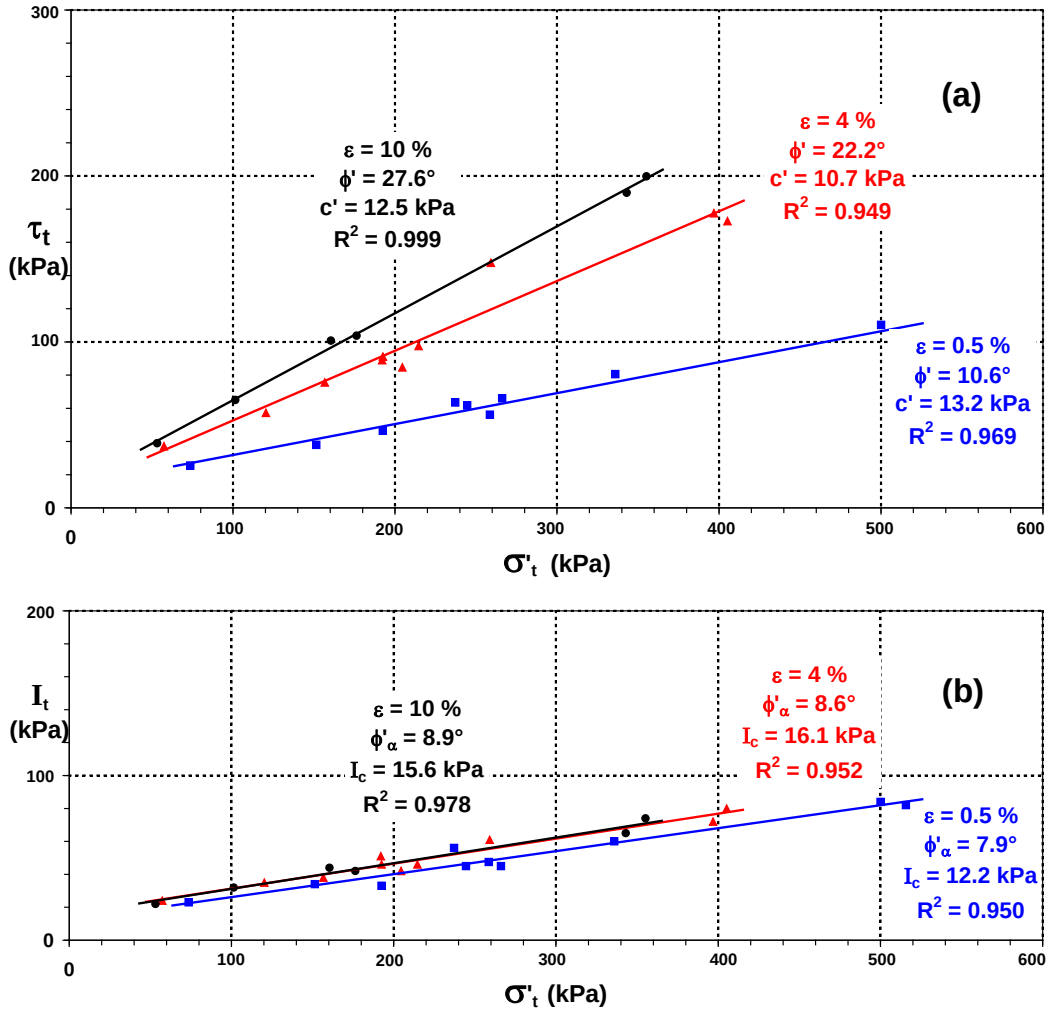

Figure 2: IDS-test Mohr Envelopes, Extruded NC Boston Blue Clay

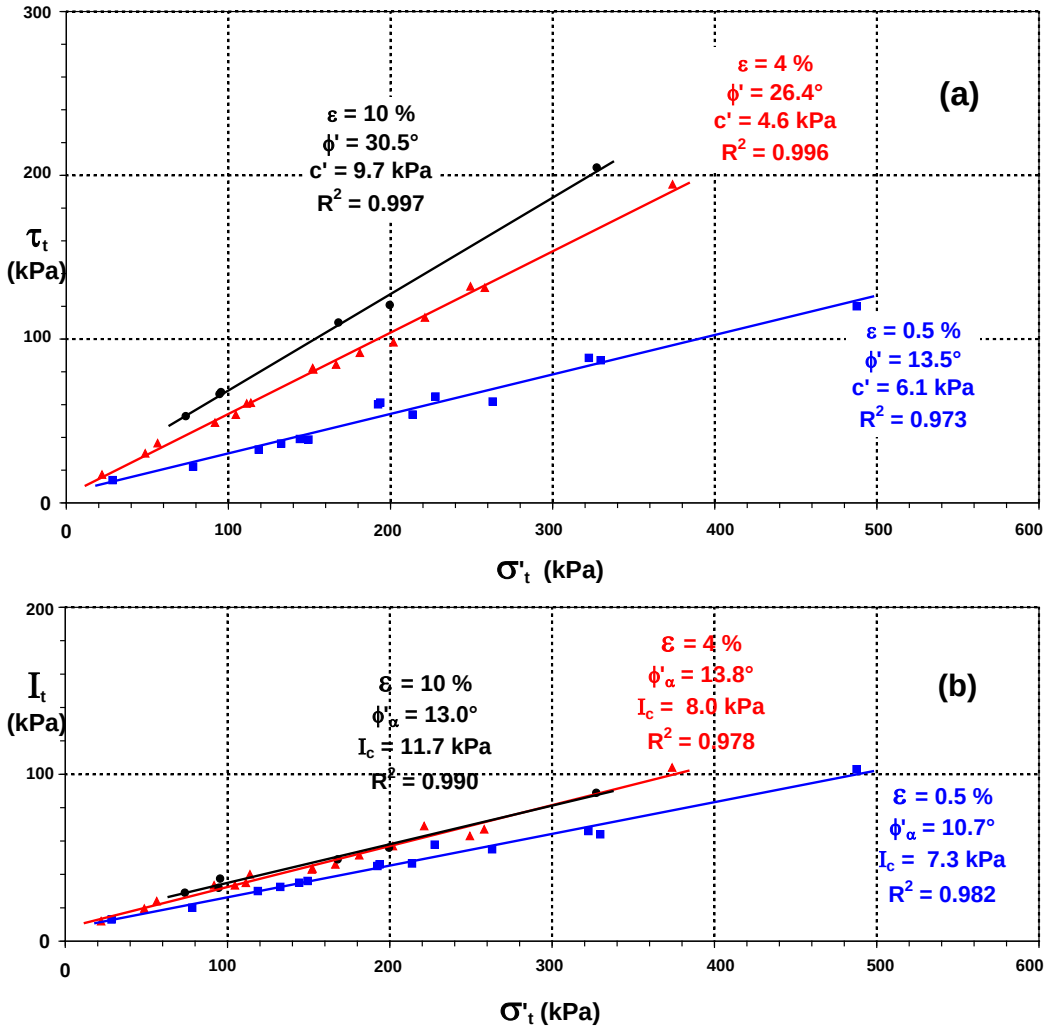

Figure 3: IDS-test Mohr Envelopes, NC Kaolinite

4.2 Normally Consolidated (NC) versus Overconsolidated (OC) Clays

4.2.1 Kaolinite Clay

Figure 4, based on Schmertmann (1976, Figure 6), presents results from a sequence of isotropic NC and OC consolidation tests followed by **IDS**-tests. As discussed below, they demonstrate further the remarkable insensitivity of the **I** component to clay structure, for example its void ratio, dilatancy and OCR, and also its linear dependence on effective stress over the stress range investigated. Figures 2b and 3b have already shown this linearity.

Figure 4a shows an arithmetic void ratio versus major principal effective stress σ'_1 graph of the results from four normally consolidated specimens (test Nos. 111, 112, 106, 105) and five overconsolidated specimens (test Nos. 107, 109, 110, 108, 113). All the test specimens came from the same batch of extruded clay with the narrow range of computed initial void ratios shown. The figure shows the position on the graph of each specimen after NC or OC and the variation of σ'_1 and void ratio during the **IDS**-test curve hopping at the axial strain of the maximum value of **I** = $\mathbf{I}_m$, which typically occurred at $\epsilon \approx 1\%$. Figure 4c shows the key to reading the void ratio and σ'_1 changes associated with consolidation, rebound, and the **IDS**-test curve hopping at the strain of $\mathbf{I}_m$.

Figure 4b shows the values of $\mathbf{I}_m$ (see Figure 1d) from each test using the same effective stress scale as in Figure 4a, with each point located at the average $\overline{\sigma}'_1$ of the test σ'_{1h} and σ'_{1l} values. Clearly, void ratio does not significantly affect $\mathbf{I}_m$ – compare the three test groups 111-113, 112-108, and 106-107-109-110, each group with decreasing void ratios but at approximately the same effective stress.

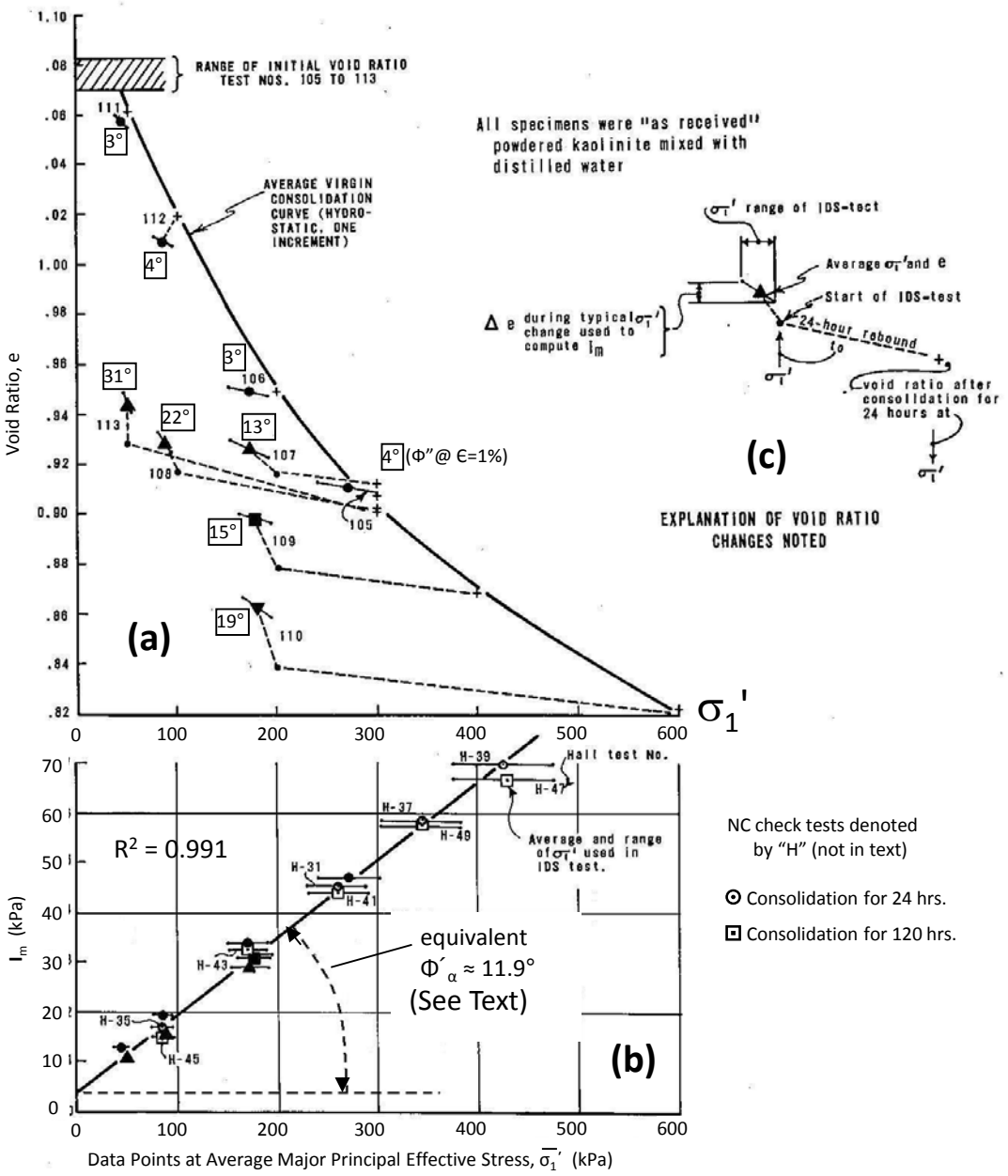

Figure 4: Demonstration of I_m independence from void ratio, dilatancy, secondary consolidation time and OCR in extruded kaolinite (annotated from Schmertmann 1976)

Unlike the approximately constant $\mathbf{I}_m$, Φ″ increases with the progressive reduction in void ratio due to the increase in the OCR within each of these three groups – with Φ″ increasing from 3° to 31°, 4° to 22°, and 3° to 19°, respectively.

However, $\mathbf{I}_m$ does vary with effective stress – consider test group (105-107-108-113) at roughly the same void ratio but with an approximate five-fold reduction in effective stress and $\mathbf{I}_m$. Figure 4b shows convincingly that $\mathbf{I}_m$ in kaolinite depends linearly on $\overline{\sigma}_1'$ and not on void ratio.

The **IDS**-test results in Figure 4 also show something important concerning $\mathbf{I}_m$ and dilatancy, interlocking and friction. The NC-OC test pairs 111-113 and 112-108 had contractant and dilatant structures (- and + dilatancy), respectively, yet each pair had ≈ $\mathbf{I}_m$. The sequence of tests at the same effective stress but with progressively increasing +dilatancy, test Nos. 106, 107, 109, and 110, also have ≈ $\mathbf{I}_m$ despite the OCR increasing from 1 to 3.

The writer converted $\overline{\sigma}_1'$ to the equivalent σ'_t to get the equivalent Φ'_α angle in Figure 4b. This $\Phi'_\alpha \approx 11.9°$ at the $\mathbf{I}_m$ strain ≈ 1% and fits

nicely within the Figure 3b values of Φ'_α = 8.0°, 13.8° and 13.0° at strains of 0.5, 4 and 10%, respectively. If dilatancy results primarily from particle interlocking effects, the above data show that dilatancy and interlocking have only a minor, if any, effect on $\mathbf{I}_m$ and Φ'_α in extruded kaolinite over the strain interval of at least 0.5-10%.

The writer will show subsequently that Φ'_α represents an unexpected component of clay friction. If true, we have the unusual situation of a friction not sensitive to OC and interlocking. This requires an unusual explanation, also given subsequently.

4.2.2 Enid Clay

Note that the writer also performed an unpublished series of tests similar to those in Figure 4 using the extruded natural residual Enid clay, with similar results, and obtained $\Phi'_\alpha \approx 13.2°$ from this series at $\epsilon \approx 1\%$.

Figure 5 shows an $\mathbf{I}_t$ versus σ'_t graph from **IDS**-tests using Enid clay, similar to those shown in Figures 2b and 3b except it shows only the data points and linear fit for a representative $\epsilon = 4\%$. In addition it shows results from three **IDS**-tests on specimens with overconsolidation ratios of OCR = 2, 4 and 7. They fit almost exactly on the best fit line for the NC tests. This provides another example, in addition to that shown for the kaolinite in Figure 4, that the **I**-component depends on effective stress but not on the OCR.

As expected, these OCR tests in Figure 5 produced a clearly stronger OC versus NC Mohr envelope (not shown). Figure 4 just showed that $\mathbf{I}_m$ at a given $\overline{\sigma}'_1$ remains approximately constant at all OCRs investigated. Any increase in mobilized shear in Figure 5 at $\epsilon = 4\%$ must result from an increase in $\mathbf{D}_t$, or Φ''. Figure 5 shows the measured increases in Φ'' = 6.1°, 11.9°, and 18.7° for OCR = 2, 4 and 7, respectively, when compared to Φ'' at $\epsilon = 4\%$ when only NC to the reduced σ'_{cu} that produced the OC. These increases in Φ'' explain the stronger OC versus NC envelope.

5. APPARENT PARADOX

Figures 2b, 3b, 4b and 5, from tests on extruded NC and OC clays, all show the **I** component linearly dependent on effective stress with an extrapolated $\sigma'_t = 0$ intercept. Schmertmann (1976, Figure 11) provides further evidence of this linearity from other clays, a silt and two sands. This reference provides still further evidence from **undrained IDS**-tests on three **undisturbed**, soft clays in Figures 17, 18, and 19 as explained therein. Ho (1971 p. 79) also confirmed this linearity in great detail using specimens of extruded kaolinite and glass spheres. The writer therefore considers it well established that this linear relationship exists, to the maximum σ'_c = 700 kPa investigated, in some, and probably many, remolded and undisturbed clays, silts and sands.

The above leads to an apparent paradox, expressed as follows:

> *The ($\mathbf{I}_t$ - $\mathbf{I}_c$) component obtained from the Figure 1c linear extrapolation to the effective stress origin as part of a nominal cohesion intercept presumed independent of effective stress, instead increases linearly with applied effective stress.*

Therefore, whatever the detailed reasons for such linear behavior, ($\mathbf{I}_t$-$\mathbf{I}_c$) **behaves as an engi-**

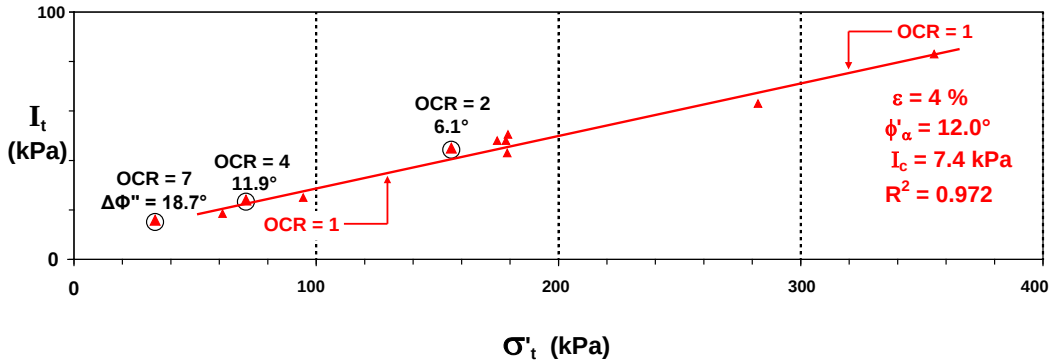

Figure 5: IDS-test Mohr It Envelope, Extruded NC and OC ENID Clay at $\epsilon = 4\%$

neering friction with an angle here denoted Φ'_α and a value denoted $\mathbf{I}_\alpha$. Equation (2) expresses this friction:

$$\mathbf{I}_\alpha = (\mathbf{I}_t - \mathbf{I}_c) = \sigma'_t (\tan \Phi'_\alpha) \quad \text{.....(2)}$$

The writer's subsequent explanation of this apparent paradox involves the viscous friction behavior of the adsorbed water layers (AWLs) on clay particles and seems consistent with other data about Φ'_α behavior and with Terzaghi's (1941a and 1941b) concepts. He called it "liquid friction" in 1941b. **The demonstration herein of a viscous Φ'_α friction, whatever the detailed reasons for the apparent viscous and friction behavior, should and does help explain the unique engineering behavior of clay.**

6. COHESION IN EXTRUDED KAOLINITE

The kaolinite's $\sigma'_t = 0$ intercepts of c′ and $\mathbf{I}_c$ at $\epsilon = 0.5$, 4 and 10% in Figure 3 suggest that a real cohesion may exist at the 'standard' $\dot{\epsilon} \approx 0.007$%/min. The c′ intercepts in Figure 3a = 6.1, 4.6, and 9.7, and average 6.8 kPa. In Figure 3b the $\mathbf{I}_c$ intercepts = 7.3, 8.0, and 11.7, with an average of 9.0 kPa. As part of our comprehensive effort to prove or disprove that the extruded kaolinite had a real cohesion, one of the writer's students, Topshøj (1970), also performed 8 NC and 6 OC, constant σ'_1, kaolinite **IDS extension** tests. They produced a similar $\mathbf{I}_c$ = 8.4 kPa using $\mathbf{I}_m$ at an average ϵ = -2.5%. Now consider the results from two **non-IDS** test methods.

Topshøj (1970) also checked directly the mobilized shear with zero effective stress on the plane of shear by performing a series of 11 Bishop and Garga (1969) type effective stress triaxial tension tests on hourglass-shaped duplicate specimens of the same kaolinite used for Figures 3 and 4. Figure 6 shows the maximum-shear Mohr's circle from each test. The then difficult-to-measure-accurately tensile strains for each point varied from -0.4 to -2.4%, with an average of -1.14%. Topshøj used an axial strain rate that she deliberately varied between $\dot{\epsilon}$ = 0.0015 to 0.015%/min, and concluded that this rate variation had no significant effect on the $\mathbf{I}_o$ result in Figure 6. Note the greatly expanded scale to show the detail at low stresses, and that 8 of the 11 circles extend into effective tension at maximum shear. All tests had an imposed zero pore pressure at specimen mid height via a base drain connection to an external tank with a free water surface.

All the specimens apparently failed in shear, some with a visible network of parallel shear planes. The writer measured an approximate failure plane angle of 29° from horizontal from her tests. The points on the Mohr circles in Figure 6 show the mobilized shear on that average plane. A least squares linear fit through the points gives a $\sigma' = 0$ shear mobilization intercept of $\mathbf{I}_o$ = 7.7 kPa. The scatter in the data points results from the experimental difficulties with accurately measuring small effective stresses, and initial differences between the extruded duplicate specimens, all emphasized by the expanded scale. Considering Topshøj had 11 tests, the writer believes she had sufficient data to support the $\mathbf{I}_o$ = 7.7 kPa

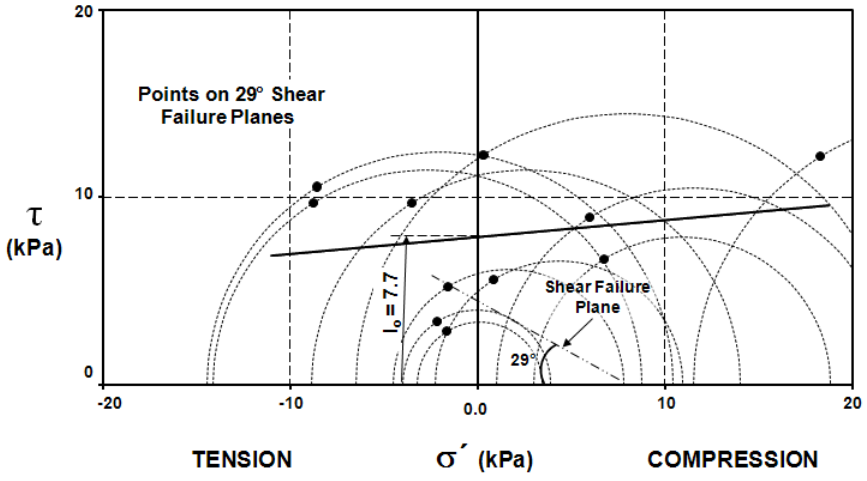

Figure 6: I_o from Tension Tests on Extruded Kaolinite

cohesion intercept in this kaolinite when testing at $\dot{\epsilon}$ = 0.0015 to 0.015%/min.

The tension tests in Figure 6 all increased void ratio, or dilated, during the test. The work to dilate against cell pressure might account for some or all of the cohesion intercept. Topshøj (1970, pp. 65-68) corrected for the work involved using the method in Rowe (1962), which reduced $\mathbf{I}_o$ approximately 30% to 7.7 kPa. The writer believes that capillarity (computed avg. 99.9% saturation), negative pore pressures (slow strain rate), dilatancy (corrected), and experimental error (all known significant errors corrected) did not produce this 7.7 kPa cohesion from these tension tests. Topshøj (1970) also performed four NC, back-pressured, compression stress-dilatancy tests using the Rowe et.al. (1963) method and obtained an average 8.3 kPa for the cohesion intercept, with ϵ from 0.3 to 1.9%. These 7.7 and 8.3 kPa results from non-**IDS** tests also fit within the aforementioned c´ and $\mathbf{I}_c$ of 6.8 and 9.0 kPa from the two **IDS-**test methods. The writer therefore believes that all these results from a comprehensive investigation prove that a real cohesion existed in this kaolinite clay. If it can exist in a reconstituted-from-powder, low activity, machine mixed and extruded saturated clay, it seems likely it can and does exist in most or all natural clays at the strain rates investigated. However, its magnitude may depend on strain rate. See **11.2 $\mathbf{I}_c$ Reliability** for further discussion of rate effects.

7. LINKING IDS AND CONVENTIONAL TESTS ($\Phi'' \approx \Phi'_\beta$)

Figure 7 shows the graphical link between Φ'' from an **IDS-**test and a new, subsequently explained, Φ'_β as determined from Φ' in Figures 2a and 3a minus Φ'_α from Figures 2b and 3b. $\Phi'_\beta = (\Phi' - \Phi'_\alpha)$ at the same strain as Φ''. Equation (3) expresses the link mathematically.

$$\tan \Phi'' = \sin \Phi'_\beta / [\cos \Phi'_\alpha \cos (\Phi'_\alpha + \Phi'_\beta)] \quad \ldots\ldots\ldots\ldots (3)$$

Using typical values of Φ'_β and Φ'_α in equation (3) shows Φ'' exceeds Φ'_β, usually by less than 2° in clays. For the purposes of this paper the writer considers this difference minor and assumes $(\Phi' - \Phi'_\alpha) = \Phi'_\beta \approx \Phi''$ and will use Φ'' and Φ'_β interchangeably.

8. THE MOHR ENVELOPE COMPONENTS OF EXTRUDED SHEAR RESISTANCE AND THEIR TIME DEPENDENCIES

Figure 8 shows a schematic diagram of the Mohr envelope components of mobilized shear resistance as demonstrated in this paper from the results of many **IDS** triaxial compression and some extension and tension tests (Topshøj, 1970), on extruded, isotropically consolidated, near-saturated, duplicate specimens. The data herein comes from only three extruded clays but the previously cited references refer to similar data from other clays,

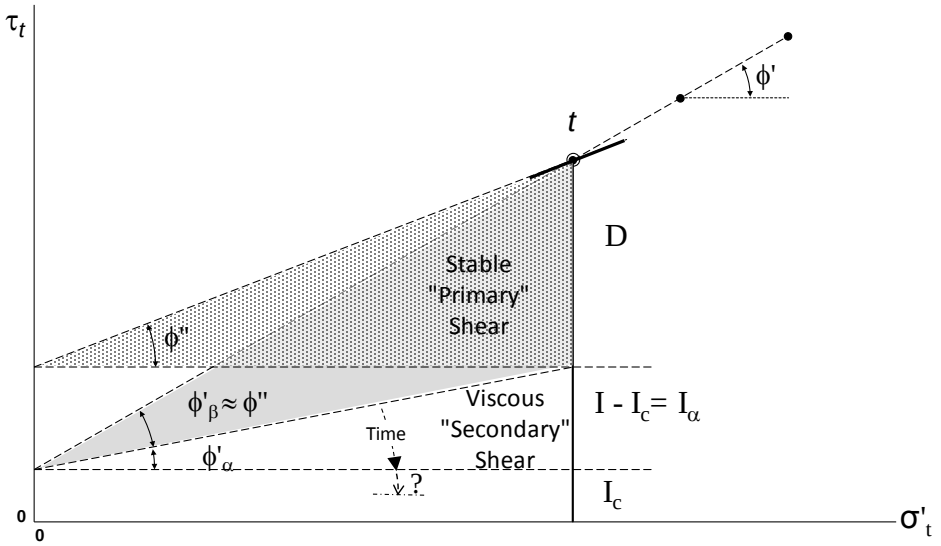

Figure 7: Test Ø˝ ≈Ø´-Ø´$_\alpha$ = Ø´$_\beta$ "Primary" Shear
(Also see Figures 1c and 8, Equation 2)

including 'undisturbed', and also from silt, sands, and glass spheres.

Working from zero to increasing shear in Figure 8, we first have the cohesion component $\mathbf{I}_c \approx c'$, approximately constant with strain, which this paper demonstrates behaves as a real cohesion by showing a comparable tensile shear strength in one example clay. Section **10** discusses a possible additional, more brittle bond cohesion, $\mathbf{I}_b$. The next component, the $\sigma'_t \tan \Phi'_\alpha$ part of **I**, or $\mathbf{I}_\alpha$, has a range of approximately 8-14° in the extruded and 'undisturbed' clays investigated, and in compression usually has only a minor dependence on axial strain after **I** develops fully at $\epsilon \approx 1\%$.

The third and last component, herein denoted Φ'_β, which, as discussed in the previous section, approximately equals the Φ'' soil friction component demonstrated directly by the **IDS**-test. In NC clay it increases slowly and roughly linearly with strain, at least to strains of approximately 5%. Figure 8 illustrates a typical value of Φ'_β for a strain of 10%. Note that at ϵ=10% the clays tested had nearly reached their maximum **IDS**-test drained shear mobilization. Thus the 10% envelope in Figure 8 would also approximately match the c'-Φ' conventional maximum drained shear envelope. Figure 8 also shows schematically how the additional mobilized shear in overconsolidated clays at the same 10% strain produces a stronger envelope that results entirely from additional Φ'_β ($\approx \Phi''$). It appears, from previous and with subsequent further discussion under **9.3 Explanation of Φ'_β**, that Φ'_β results from particle geometrical interference effects.

Early in the **IDS**-test research, which began in 1958, it became obvious that the shear components of the clays tested exhibited significant time effects, especially during time with constant shear, including zero shear. The **D-**component increased with time, usually accompanied by a measurable decrease in the **I**-component. The following Sections **8.1** to **8.5** present some examples from a variety of test conditions to illustrate the generality of this time-transfer behavior and its importance. For additional details and related testing see the references cited.

8.1 Undrained Creep with Shear

Bea (1960, 1963) performed and discussed **undrained** compression creep tests and results from specimens of machine extruded kaolinite and extruded and undisturbed Boston Blue Clay (BBC). After 2½ to 19 days of undrained creep using stress control, he performed an **IDS**-test on each specimen to determine the change in shear components, at the same strain, after creep versus results from an **IDS-**test after undrained compression with strain control and no creep. For all three clays he found that creep produced an increase in the **D** (or Φ'' or Φ'_β) component and a decrease in the **I** component. A short extrapolation back to the strain at the end of creep showed that the **IDS-**tests mobilized a shear resistance at the same axial strain that increased from 10-13% due to the prior creep. The soil structures had stiffened and particle geometrical interference effects had increased during the time of creep. For example, the extruded kaolinite's Φ'_β after

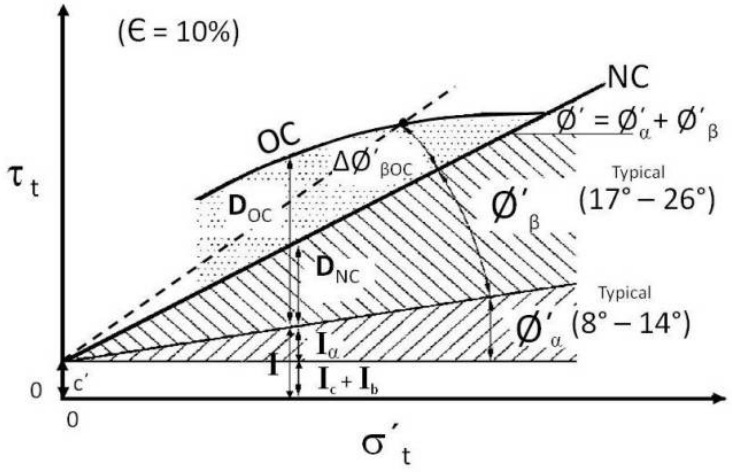

Figure 8: Schematic Summary of Components (NC, OC Extruded Clays)

19% strain had increased from 24° to 33° while **I** dropped from 27 kPa to near 0. The reader will also find details from Bea's tests in Schmertmann (1976, p. 87 and 1981, p. 472).

8.2 Drained Stress Control with Rest Time versus Strain Control

Strain control testing imposes a forced, continuing axial strain on a test specimen and allows little or no time for the structure to rest at constant shear load and develop any rest-related ageing effects. In contrast, stress control with increments of loading spaced after periods of constant-load rest does permit the soil structure time to adjust and develop rest-related ageing effects. Now consider the example in Figure 9a.

The strain-controlled test (solid lines) used the previously described curve hopping technique and used only a single specimen tested to a strain of 2.3% in 29 days with $\dot{\epsilon}$= 0.079%/d. The stress control test, tested over 37 days to a strain of 3.6%, used two duplicate specimens with 12 increments of loading and approximate three day rest periods between increments, for an average $\dot{\epsilon}$= 0.097%/d. We used one specimen for the same constant high σ'_{1h} used in the strain control test, and a duplicate specimen for the same constant low σ'_{1l}. Both stress control curves show the strain after each increment's 3 days of drained creep. They clearly show greater response to the same σ'_{1h} to σ'_{1l} change in effective stress, or in other words a greater Φ'' or Φ'_β versus the strain control test. We then followed each with an **IDS-**test component analysis (see Figure 1c,d).

Figure 9b shows the comparative **IDS**-test component results from stress versus strain control. The 1-specimen strain control test produced the usual rapid increase in **I** followed by constant or slowly decreasing **I** with additional strain (see Figure 1d). In contrast, the 2-specimen stress control test reaches the same initial maximum **I** but then **I** drops abruptly with further strain to 45% of its initial value at a strain of 2.3%. Over the same strains the Φ'_β (**D**) component increased substantially from approximately 11° to 18° at 2.3% strain. This figure provides an example of the time transfer of **I** to **D** when allowing versus not allowing periods of rest under constant load with similar average axial strain rates.

8.3 Rate of Strain ($\dot{\epsilon}$)

Although the rate of strain in a strain-control test does not have a major effect on the mobilization of the **I** and **D** components at a given strain and on the time transfer from **I** to **D**, it does have a measurable effect when considering orders-of-magnitude changes in strain rate. Part (a) of Figure 10 provides an example from extruded specimens of kaolinite at ϵ=1%. **I** decreased from approximately 60 to 50 kPa while Φ'_β increased from approximately 3 to 6°

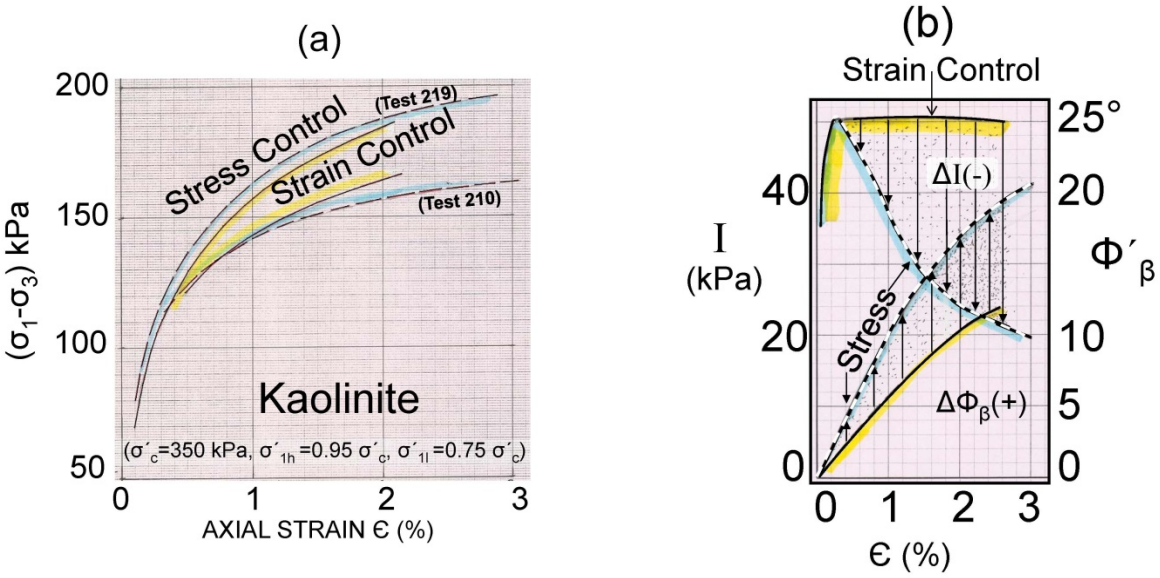

Figure 9: 29 Day Strain versus 37 Day Stress Control IDS-tests
(Also see Schmertmann (1963(b), Figs 27-28))

over a strain rate reduction factor of approximately 300. It appears that a sufficiently small strain rate and the increased time involved will permit some **I** to **D** transfer even with a continuously forced strain increase. A subsequent discussion in **10.1** under **BOND COHESION** will consider part (b) of Figure 10.

8.4 Secondary Consolidation (Drained Creep without Applied Shear)

We also learned early in this research that longer times for isotropic secondary consolidation increased the mobilization of **D** in a subsequent **IDS**-test while leaving the **I** component somewhat reduced. For example, in one series of kaolinite tests increasing the isotropic secondary time from 100 to 52,000 minutes increased Φ'_β at Є = ½% from 1° to 6° with **I** decreasing from 52 to 45 kPa. In another series of four undrained tests the compression modulus over the $(\sigma'_1-\sigma'_3)$ interval of 10 to 50 kPa increased from 900 to 8,800 kPa when the secondary time increased from 115 to 35,600 minutes. These and other comparisons provided clear evidence of significant soil structural changes resulting from secondary consolidation. The changes produce an increase in Φ'_β. The reader can find other and more detailed information about secondary

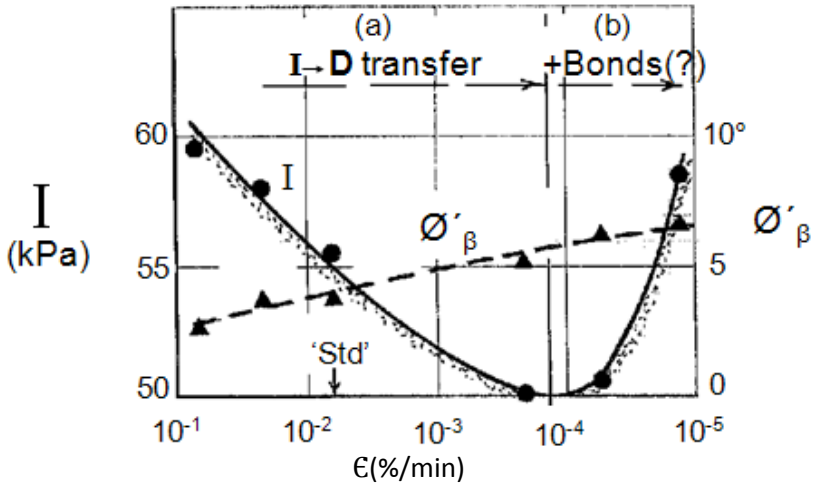

Figure 10: Effect of IDS-test Strain Rate on Kaolinite Shear Components @ ε = 1%

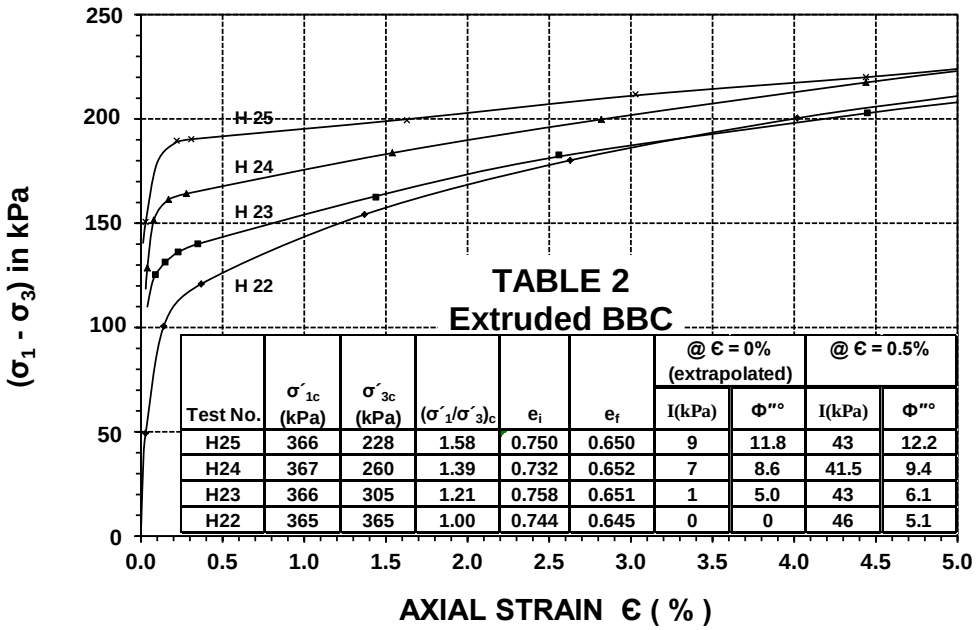

TABLE 2
Extruded BBC

Test No.	σ'_{1c} (kPa)	σ'_{3c} (kPa)	$(\sigma'_1/\sigma'_3)_c$	e_i	e_f	@ Є = 0% (extrapolated) I(kPa)	@ Є = 0% (extrapolated) Φ"°	@ Є = 0.5% I(kPa)	@ Є = 0.5% Φ"°
H25	366	228	1.58	0.750	0.650	9	11.8	43	12.2
H24	367	260	1.39	0.732	0.652	7	8.6	41.5	9.4
H23	366	305	1.21	0.758	0.651	1	5.0	43	6.1
H22	365	365	1.00	0.744	0.645	0	0	46	5.1

Figure 11: Superposed IDS-test axial stress curves at constant σ'_{1h} = 343 kPa versus Strain, after Anisotropic, Normal Consolidation, with related details in Table 2.

consolidation and **IDS** component effects in Schmertmann (1976, p. 87; 1981 p. 474; and 1991, Figs. 27-30).

8.5 Anisotropic Consolidation (Drained Creep with Shear)

Schmertmann and Hall (1961) devoted an entire paper to showing the **IDS**-test shear component results after the 24h and 120h anisotropic, normal consolidation of extruded kaolinite and Boston blue clay over the $(\sigma'_1/\sigma'_3)_c$ range of 1 to 1.6. In all cases the **D**-component increased to carry the additional shear as this ratio increased. At the same time the **I**-component decreased. We thus found an **I** to **D** (or Φ'_α to Φ'_β) transfer during drained creep with shear. Also see Schmertmann (1976, Figure 23).

To illustrate the above consider the data in Figure 11. The figure shows comparative **IDS**-test σ'_{1h} curves from one series of extruded, duplicate BBC specimens after various levels of 24h anisotropic NC. As with the aforementioned secondary consolidation, the increase in the **D**-component (or Φ'_β) produces stiffening and strengthening of the clay's structure over a limited additional strain of about 4% in this case. Table 2 in Figure 11 gives the components and other comparative information when this additional (to consolidation) strain = 0 (using a short back-extrapolation) and at 0.5%. The reader can see how **D** (or Φ''_β) increased gradually and **I** dropped to near-zero at $\epsilon = 0$ and then increased abruptly, to typical isotropic consolidation values, at $\epsilon = 0.5\%$ as the anisotropic consolidation ratio increased from 1 to 1.6. At a ratio of 1.6, which $\approx 1/K_o$, the mobilized compressive strength increased 50 percent at 0.5% additional axial strain due to the **I** to **D** time transfer induced by the anisotropic consolidation. This occurred despite the NC octahedral $(\sigma'_1 + 2\sigma'_3)/3$ effective stress at $\epsilon = 0.5\%$ decreasing from 259 kPa in H22 to 214 kPa in H25 and their almost identical void ratios.

9. ADSORBED WATER LAYER (AWL)

The possible importance of the adsorbed water layer (AWL) on the surface of all wet soil particles, but especially clays, has provided a subject of interest and controversy since the early years of soil mechanics. As shown below, this paper now continues by presenting more examples supporting its importance in the shear and consolidation behavior of clays.

Bjerrum (1973 p. 126) showed that undrained shear strength data requires a correction for rate of shear effects. Leroueil (1996), showed that viscous shear effects in clays produced a 27% increase in the preconsolidation stress p_c in the more rapid CRS versus CLI oedometer tests. He also showed a 40% increase in p_c when strain rate increased by a factor of over 1000 and how decreasing temperature also increased p_c due to its effect of increasing shear viscosity. Perkins and Sjursen (2009) showed that a *c.* 20°C decrease from lab room to N. Sea seabed temperatures increased Troll clay s_u and p_c by *c.* 20%, using "very good" to "excellent" quality undisturbed samples. Similarly, the profession has known for a long time that increasing temperature in the laboratory versus insitu also increases the rate of secondary consolidation. Anderson and Richart (1974) provide an example, also discussed in Section **12.6**. What might cause these significant effects in the shear resistance of clays? The writer believes that the special and viscous behavior of the adsorbed water layer surrounding the typical layer-lattice clay mineral particles provides the most likely answer.

Horn and Deere (1962, Table 1) showed a dramatic difference between the saturated and dry sliding friction (each denoted tan Φ'_μ in the subsequent Table 3a) shear behavior of "massive-structured soil minerals" such as quartz, feldspar and calcite, versus the "layer-lattice minerals" (now called phyllosilicates) common in clays. The massive minerals **increase** their sliding friction coefficient with saturation and the layer-lattice minerals **decrease** theirs. The decrease factor for the clay minerals in Table 3a averages 2.2. The authors referred to water as an "antilubricant" for the massive minerals, and as a "lubricant" in the layer-lattice minerals. Many lubricants behave as thin low-friction layers, which leads to the writer's explanation of the Section **5** paradoxical Φ'_α.

Table 3: Comparing Clay Mineral Φ'_μ with Saturated Clay Φ'_α

(a) Minerals

Clay Minerals[1]	tan Φ'_μ	
	dry	saturated
Biotite	0.310	0.130
Chlorite	.529	.220
Muscovite	.431	.231
Phlogopite	.310	.149
	Avg = 0.395	**Avg = 0.183**

[1] From Horn and Deere (1962), Mitchell (1993)

(b) Clays

Extruded Clays (in this paper)	tan Φ'_α	
	dry	saturated
Kaolinite (avg. of 3), Fig. 3	0.543[1]	0.222
BBC (avg. of 3), Fig. 2		.148
Enid, Fig. 5		.212
		Avg = 0.194

[1] From one not-extruded test (Schmertmann, 1976, Fig. 10)

9.1 Explanation of Φ'_α

The left side of Figure 12 shows Terzaghi's (1941a, 1941b) concept of the interaction of the adsorbed water layers in contact around two solid soil particles. The relative thickness of the layer to the particle size, the shear and normal forces acting across the contacts, and time, determine the closeness of the particles to each other. Time implies a viscosity that increases with closeness due to colloidal effects. This, in turn, determines the hydraulic properties of the water between the particles, including its ability to transmit pore pressures. Particles with the AWL effectively squeezed out have an effective solid particle-particle contact with associated more rigid bonding, a very high AWL viscosity, and little or no pore pressure transmission over the contact area. That part of the water between particles relatively far apart has little viscosity and can transmit full pore pressures. In-between distances have 'contacts' with in-between viscosities and pore pressure transmission capabilities.

On the right side of Figure 12 the writer has greatly simplified the contact between two particles and their AWLs as transmitting full pore pressure over the area (A – a) and no pore pressure over the area "a" of a contact, with "A" representing the total shear section area per contact. Recognizing that the ratio (a/A) probably has a very small value, the math suggests that the sliding shear resistance through the contacts represents the tan Φ'_α frictional part of the **I**-component. This assumes a negligible contribution from Φ'' in the extruded clays, because at low strain Φ'' mobilizes much slower with strain than Φ'_α (compare **D** or Φ'' with **I** versus ϵ in the schematic Figure 1d and in Table 2). The subsequent Figures 17 and 18 suggest that Φ'', or Φ'_β, will mobilize even slower in natural clays because any bonding therein will inhibit the early strain development of Φ'_β.

Now consider in Table 3 how the extruded clay (tan Φ'_α) values developed herein compare with the sliding friction (tan Φ'_μ)

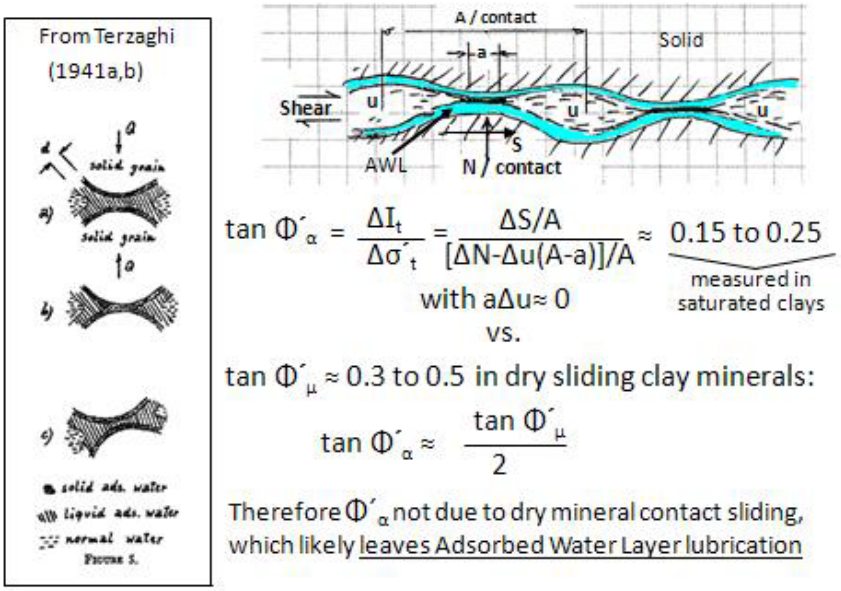

Figure 12: Paradox likely due to lubrication by adsorbed water layer

values along cleavage planes in some layer-lattice (phyllosilicate) minerals typical in clays. In such minerals water reduces Φ'_μ as detailed in Horn and Deere (1962) and summarized by Mitchell (1993) and in Table 3a. The writer added the previously documented saturated clay (tan Φ'_α) values into Table 3b. The (tan Φ'_μ) values range from 0.130 to 0.231, with an average of 0.183. The (tan Φ'_α) values range from 0.148 to 0.222, with an average of 0.194. A coincidence? Possibly, but the writer does not think so. These and subsequent data show that the paradoxical AWL Φ'_α from **IDS**-tests ≈ the sliding Φ'_μ in saturated clay minerals.

9.2 Φ'_α varies with d_{10}

If the shear behavior of the adsorbed water layer determines Φ'_α, and colloidal theory indicates the relative importance of this layer increases with a reduction in particle size, then it seems reasonable to expect a relationship between Φ'_α and particle size. Figure 13 shows a graph of Φ'_α versus d_{10} (log scale) from ten 'soils', including the three extruded BBC, kaolinite and Enid clays. The other seven soils include three clays—one from **undrained IDS**-tests using undisturbed specimens of a Norwegian, soft, Manglerud quick clay from Schmertmann (1976, Fig. 17) and identified by "U", a finely ground quartz silt, two sands, and glass spheres. The writer then added a $\Phi'_{residual}$ point from a mixed sandy, clayey silt from under the Pisa tower (see **12.1**).

Figure 13 suggests a roughly linear, semi-log relationship between Φ'_α and d_{10}. This provides further evidence, in the form of Φ'_α, for the existence and importance of the adsorbed water layer in clays, with reducing importance in silts, but still measurable in sands (see Schmertmann 1976, Figs. 11 and 28), and with the importance generally increasing with the log of a decreasing d_{10}. A related discussion in Section **12.2** shows that the time needed for secondary consolidation increases with Φ'_α.

9.3 Explanation of Φ'_β

Terzaghi et. al. (1996, p. 147) describe, as have others, a soil's frictional shear resistance Φ' as the sum of a particle/particle sliding component Φ'_μ, and a geometrical interference component Φ'_g, or $\Phi' = \Phi'_\mu + \Phi'_g$. According to the above discussion of Figure 12, the (σ' tan Φ'_α) part of the **I**-component from **IDS**-tests on clays results from AWL particle/particle sliding. Therefore the saturated $\Phi'_\mu = \Phi'_\alpha$. Having previously established under **7. LINKING...** that $\Phi' \approx \Phi'_\alpha + \Phi'_\beta$, **then the geometrical interference component $\Phi'_g \approx \Phi'_\beta$**. As in Figure 7, the writer also describes these Φ'_α and Φ'_β frictional components as "secondary" and "primary", and "unstable" and "stable", respectively.

10. BOND COHESION I_b

In the writer's opinion this paper demonstrates in Section **6**, and in Figures 3, 4 and 6 the existence of a real cohesion in extruded kaolinite clay. It seemed roughly constant with strain between ϵ = 1/2 to 10%. Figure 2 shows the same for extruded BBC. Based on the available

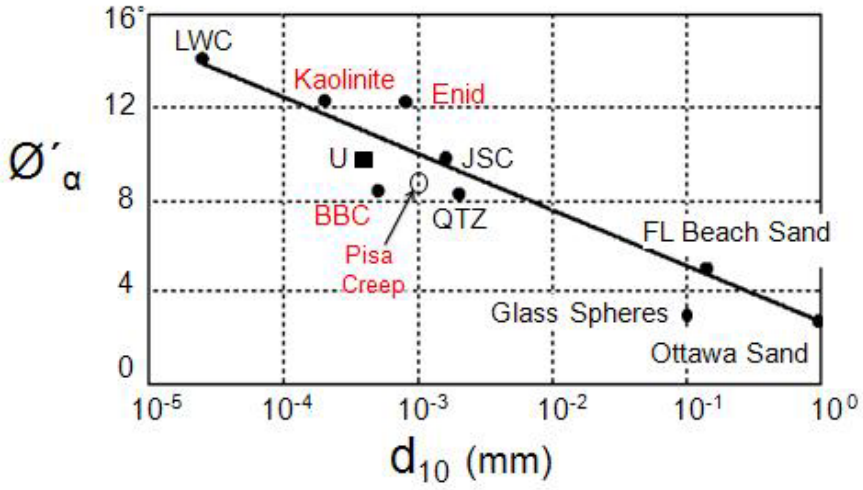

Figure 13: Dependence of Ø´α on d_{10}

IDS-test data, the strains of extrusion and **IDS**-testing do not destroy the $\mathbf{I}_c$ cohesion. This type of cohesion most likely results from the electrochemical forces of attraction between the clay particles and their AWLs and has a magnitude approximately independent of strain. In this sense it behaves plastically after Є>1/2%.

However, Lambe (1960, Figure 9) and Mitchell (1993, p. 373) detailed at least five different types of cohesion, including the above, with some more easily destroyed by strain. The writer will now present examples of more brittle cohesion than the plastic $\mathbf{I}_c$, resulting from bonding that appears to have developed during testing in the laboratory or from ageing in the field. Denoting such bond cohesion as the "$\mathbf{I}_b$" part of **I**, Equation (4) expresses the total **I**. But, keep in mind that the $\mathbf{I}_\alpha$ part denotes the paradoxical AWL friction and not a cohesion.

$$\mathbf{I} = \mathbf{I}_\alpha + \mathbf{I}_b + \mathbf{I}_c \quad \text{.....(4)}$$

10.1 During Very Low Rates of Shear

A previous discussion of Figure 10(a) in **8.3** noted a measurable decrease in **I** at Є = 1% with a large decrease in $\dot{Є}$. However, at $\dot{Є} \approx 10^{-4}$ %/min a decreasing **I** somewhat abruptly (on a log rate scale) turned to an increase in the next log cycle of strain rate while Φ'_β continued to increase. The writer speculates that in Figure 10(b) the strain rate became so low that the considerable ageing time involved (10^5 min or 70d) allowed measurable $\mathbf{I}_b$ bonds to form, which caused **I** at Є = 1% to increase in this extruded kaolinite. Subsequent Figure 17 also showed the $\mathbf{I}_b$ increase.

10.2 From Overconsolidation

Simple, one day isotropic overconsolidation to an OCR = 4 appears sufficient to start the formation of brittle bonds. Figure 14 shows data from **IDS**-tests on extruded specimens of kaolinite and Enid clays. The writer used $\dot{Є} \approx 8.5 \times 10^{-4}$ %/min to permit the curve hopping procedure at very low strains, which in turn permitted separating the components at these strains. For both OC clays we measured a distinct peak in the otherwise expected smooth trend for the increase of the **I** component with strain. The stippled shading in Figure 14 shows the peaks. It looks like brittle $\mathbf{I}_b$ bonding, that developed during only one day of OC, increased the **I** component over the first approximately 0.1 to 0.2% of **IDS**-test strain.

Note the connection between the postulated development of bonding in kaolinite due to ageing in the **10.1** discussion with the demonstrated bond development in **10.2** due to OC. This evidence supports the possibility of accelerating some ageing effects by OC – and implies the reverse, that ageing could produce OC (subsequently demonstrated in **12.3 AGE-**

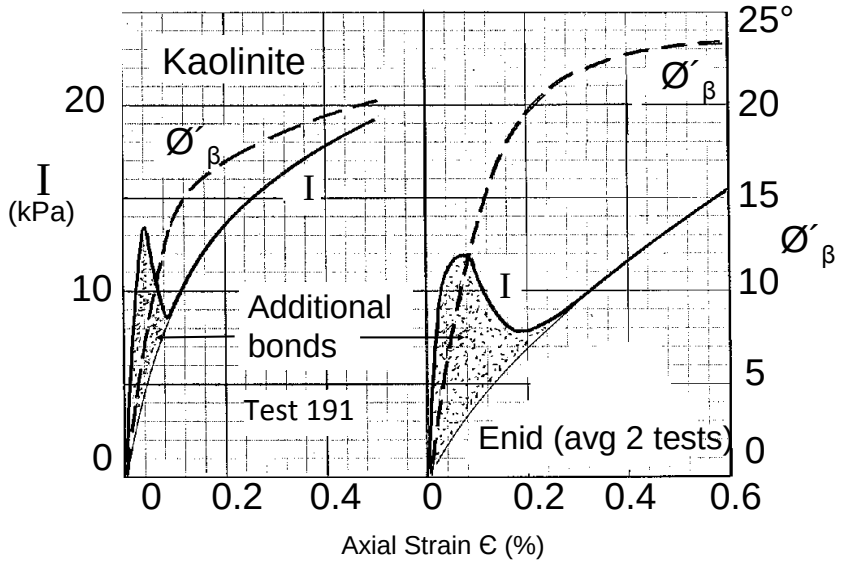

Figure 14: Evidence of Rigid Bonds after 1 day, Isotropic OCR = 4 (σ'_c = 700, σ'_{cu} = 175, σ'_{1h} = 170, σ'_{1l} = 135 kPa)

ING PRECONSOLIDATION). Mitchell (2008) supports the latter possibility for sands, as did Terzaghi (1941b, pp 3,4).

10.3 In Undisturbed Clays

Those $\mathbf{I}_b$ bonds that remain after undisturbed sampling, trimming and handling in a laboratory should show up as additional **I**-component compared to the same clays after severe remolding by machine mixing and extrusion. Comparative **IDS**-tests using specimens from the same undisturbed block of BBC provide an example. The undisturbed e = 0.82 and the machine extruded e = 0.65, both after isotropic NC to $\sigma_c' = 400$ kPa. **I** values at $\epsilon = 1\% \approx 70$ and 50 kPa, respectively, indicating an $\mathbf{I}_b \approx 20$ kPa destroyed by the extrusion. That allowed the additional $\Delta e = 0.17$ consolidation. For this and other **IDS**-test examples of $\mathbf{I}_b$ cohesion using undisturbed clays see Schmertmann and Osterberg (1960, Figures 21-24), and Schmertmann (1962, Figs. 2, 7, and 1976, Figs. 17-19).

10.4 Terzaghi's Bonding

Terzaghi (1941a, 1941b), based on his prior research studying adsorbed water layer behavior and described in Terzaghi (1920, 1931), and illustrated by him on the left side of Figure 12, thought that adjacent clay particles with enough force+time acting between them would eventually come into solid/solid particle contact and form a 'cold-weld' type of rigid bonding. Then it would take a threshold shear force, or a "critical pressure", to break these bonds. This presents another possible type of cohesion, now included in $\mathbf{I}_b$, which also seems consistent with the low-strain, brittle bonds measured by the **IDS**-tests discussed above. See 12.10.3.2 for further discussion of "critical pressure".

11. THE SHEAR COMPONENTS

As developed in this paper, the shear components consist of cohesions that produce a tensile strength plus the Φ'_α and ($\Phi'' \approx \Phi'_\beta$) friction components. The following, starting with cohesion, gives the writer's opinions, based mostly on this research, as to the physical basis for each of the components.

11.1 $\mathbf{I}_c$ Cohesion

In the case of severely remolded clays, such as when machine-extruded, a plastic "$\mathbf{I}_c$" cohesion probably results from the net attractive forces between the surfaces of the particles in near-contact but still separated by adsorbed water layers. It mobilizes rapidly within a compressive strain of 1.0% or less and appears slightly strain rate dependent, as discussed below in **11.2**.

11.2 $\mathbf{I}_c$ Reliability

An issue in geotechnical engineering involves the question of the reliability in practice of $\mathbf{I}_c$ cohesion in natural clays. Critical State Soil Mechanics does not use cohesion in "fully softened" clay because of its supposed unreliability. The research results described herein suggest a complicated but ultimately reliable $\mathbf{I}_c$ in undisturbed clays, partly because of compensating time-transfer effects.

If $\mathbf{I}_c$ cohesion results from the behavior of the AWL, as the writer postulates, then it might exhibit viscous strain rate effects and reduce to zero at very low strain rates. In part to check this, Strømann (1971, pp. 97-103) performed drained, compression, relaxation tests on three extruded, OCR = 2, kaolinite specimens from the same source as the kaolinite used for the **IDS-**tests in Figures 3 and 4. She followed an approximate constant structure Mohr envelope (CSME, see Schmertmann, 1976 pp. 65-66, 78) backwards to a very low effective stress and, by a short extrapolation, obtained an $\mathbf{I}_o$ cohesion (her notation) intercept with the $\sigma' = 0$ axis. The final relaxation drained creep rates of compressive strain that applied to these CSMEs dropped $\dot{\epsilon}$ to less than 1.27×10^{-5} %/min, or more than 55 days/%, by an unknown amount. However, she determined still measurable values of $\mathbf{I}_o$ from 1.0 to 4.8 kPa at $\epsilon \approx 0.9$ to 3.8%.

The above compares with the aforementioned approximate range for $\mathbf{I}_c$ of 7-12 kPa obtained from **IDS-**tests using an average $\dot{\epsilon} \approx 7 \times 10^{-3}$ %/min, or more than 500 times faster. The cohesion reported herein for ex-

truded kaolinite may reduce with reduced strain rate, but, if so, it does so very gradually. We need more experimentation to determine if it can reduce to zero.

It thus appears that $\mathbf{I}_c$ might or might not eventually drop to zero and lose its contribution to the total mobilized shear resistance. But that does not consider the associated time-transfer increase in the **D**-component, σ' tan Φ'_β, which can more than compensate for the loss in $\mathbf{I}_c$ as discussed under **8.1 Undrained Creep** and **8.5 Anisotropic Consolidation**. In addition, any increasing strain and strain rate resulting from an increased loading will rapidly remobilize the AWL-based $\mathbf{I}_\alpha$, and presumably also any lost $\mathbf{I}_c$, producing a stronger clay during this next interval of strain.

Note that if $\mathbf{I}_c$ does reduce with time to zero or near-zero, this change becomes part of the Φ'_α viscous secondary shear behavior shown with a "?" in Figure 7 that transfers to Φ'_β, as discussed in **12.2**.

11.3 $\mathbf{I}_b$ Cohesion

Other types of cohesion behave in a more brittle fashion and with more permanence. For example one can have pressure-induced and/or chemically-induced precipitation and cementation. These effects usually increase with the time allowed for them to develop. This paper has shown in Figures 10 and 14 how they may develop even during laboratory testing times in severely remolded (extruded) clays or, perhaps they develop quickly because of the prior severe remolding. The writer refers to them as "bond cohesion", denotes them by "$\mathbf{I}_b$", and in **10.3** and other references provides examples of $\mathbf{I}_b$ in several undisturbed clays.

11.4 Φ'_α Friction

The writer has shown that this particle/particle sliding friction could, and likely does, result from the particle surface lubrication effects of the viscous adsorbed water layers on the surfaces of all particles, but particularly important on the fine particles of layer-lattice minerals (phyllosilicates) in clays. All of the following findings, from mostly strain-controlled **IDS**-tests using extruded clays, seem consistent with this finding about Φ'_α:

11.4.1 Φ'_α mobilizes rapidly and then decreases gradually with axial strain in extruded clays.

11.4.2 Φ'_α has approximately the same magnitude over ϵ = 0.5 to 10% in extruded clays, and in this sense behaves plastically.

11.4.3 Φ'_α has a magnitude very similar to that reported from research determining the saturated, sliding friction of some phyllosilicates typical in clays.

11.4.4 Φ'_α has a similar magnitude when tested in compression and extension**.**

11.4.5 AWL effects and a viscous Φ'_α friction provide an explanation for the apparent paradox with a σ' = 0 'nominal cohesion' intercept in an **IDS**-test.

11.4.6 Φ'_α appears approximately independent of void ratio, OCR, secondary compression time, dilatancy and interlocking, deflocculation or dispersion, clay mineralogy**,** isotropic or anisotropic consolidation, and the stress-time path for consolidation (see Schmertmann 1976, Tables 1-4a).

11.4.7 A viscous creep behavior of the AWLs would explain the transient and "secondary" behavior of Φ'_α.

11.4.8 Φ'_α behaves as the sliding friction Φ'_μ in Terzaghi et. al. (1996, p. 147).

11.4.9 Φ'_α usually decreases with an increase in particle size.

11.5 Φ'_β Friction

The writer believes (also in Schmertmann, 1976, p. 91), as do Terzaghi et. al. (1996, p. 147) and probably many others, that this component of clay friction, which the 1996 reference denotes as Φ'_g, results from particle, and/or aggregates of particles, geometrical interference effects, including locking and unlocking, rotations, bending and unbending, and breaking or other damage. All of the following findings seem consistent with this description of Φ'_β:

11.5.1 Each **IDS**-test directly measures a primary clay friction Φ'', or approximately Φ'_β, versus axial strain.

11.5.2 Φ'_β increases gradually with compressive strain in NC clays, and more rapidly as the OCR of an extruded clay increases.

11.5.3 At a given strain Φ'_β increases with increases in interlocking and positive dilatancy .

11.5.4 At a given strain Φ'_β increases with the void ratio reduction resulting from overconsolidation.

11.5.5 At a given strain Φ'_β increases due to a time transfer from the transient Φ'_α in stress controlled testing. This demonstrates its stability versus Φ'_α.

11.5.6 At a given compressive strain after anisotropic consolidation, Φ'_β increases with increasing the $(\sigma'_1/\sigma'_3)_c$ ratio.

11.6 Φ'_β versus Φ'_α Reliability

This paper includes some examples of the time transfer of the particle/particle AWL sliding Φ'_α to the more stable particle interference Φ'_β. The cited references have more examples. Testing with strain control continually mobilizes almost all the AWL-controlled Φ'_α. But, this highly viscous Φ'_α may creep to near-zero under constant-load time in the field. This sliding creep will likely produce more geometrical interference between particles and increase Φ'_β. If not, as with residual strain conditions, the clay will become overloaded compared to its strain controlled test strength and respond with continuing creep, some form of structural collapse, or otherwise fail. Note, as shown for example by Figure 9(b), that Φ'_β can increase by suitable cycles of load increase and rest at constant load, but presumably only to some maximum capability, $\Phi'_{\beta max}$, controlled by its current structure. See **12.1** for more discussion of this presumption.

11.7 Summary Equation

The following equation (5) summarizes the Mohr-Coulomb envelope components developed from the writer's interpretation of the research results described herein. The same equation (5) introduced Section **2. SUMMARY OF THE IDS-TEST** with a preview of the interpreted shear components, together with an introductory description of the components.

$$\{\tau = \mathbf{I}_c + \mathbf{I}_b + \sigma' \tan [\Phi'_\alpha + (\Phi'_\beta \approx \Phi'')]\}_{\epsilon,t} \quad (5)$$

12. PRACTICAL CONCEPTS

If the research results and new or refined concepts herein add to the fundamental engineering understanding of soil and clay behavior, then they should find applications in both research and practice, perhaps in the form of adjustments in how engineers assign the causes of and test and model the engineering behavior of clays. The following presents thirteen example concepts and possible adjustments to illustrate the practical potential. They add to the **IDS**-test itself, which makes it practical to identify the M-C shear components in clay.

12.1 Residual $\Phi' \approx \Phi'_\alpha$

At residual strains the particles have, by definition, a minimum of bonding and of interlocking and other particle/particle geometrical interference. That suggests $\mathbf{I}_b$ and Φ'_β might then have only small values. That leads to the possibility that AWL effects might dominate the frictional shear resistance at $\Phi'_{residual}$ and hence Φ'_α might dominate at residual strains in clays. Figure 15 provides data that supports this possibility.

In a discussion Hamel (2004) provided some laboratory test and field back-calculated $\Phi'_{residual}$ versus PI values from colluvial landslides in Pennsylvania. Figure 15 shows his laboratory $\Phi'_{residual}$ test points and the matching range of $\Phi'_{residual}$ from the landslides. The writer has superposed on these data the Φ'_α values available to him from extruded clays within the PI range plotted, including the Φ'_α results from undrained **IDS**-tests using undisturbed specimens from three soft clays—see Schmertmann (1976, Figs. 17-19). The similarity between the two sets of values, $\Phi'_{residual}$ and Φ'_α, shows that the viscous Φ'_α friction shear behavior of the adsorbed water layer may provide a major part of the total residual shear resistance of at least some clays.

Since the initial preparation of Figure 15 the writer has encountered other field and lab residual strength data, now added into Figure 15, that continues to support the possibility that I_c (or c′) and Φ'_α from AWLs provide a major part of residual strength. Tiwari et. al (2005) studied 6 landslides in Japan's Nigata prefecture that failed along slickensides in an OC clay with a PI range of 31 to 68%, averaging 47%. Backfiguring using a Japanese method gave average c'_{res} = 7.7 kPa and Φ'_{res} = 10.4°. Eighteen lab ring shear tests on undisturbed and remolded specimens gave similar results, with an overall average c'_{res} = 4.0 kPa and Φ'_{res} = 12.1°. In addition, Failmetzger and Bullock (2008) reported an insitu Iowa borehole shear test that gave values of c'_{res} = 8.8 kPa and Φ'_{res} = 11.2° in an OC clay with a PI ≈ 24%. Smith et. al. (2006) reported that the OC, slickensided, marine, stiff clays of the Potomac Group Formation underlying parts of Washington D.C. and Baltimore had residual strengths of Φ'_{res} = 10 to 15° (using c'_{res} = 0) and a typical PI ≈ 50%. The above additional data support the initial data in Figure 15.

In further addition, comments and data found in the NGI's 1967 Conference Proceedings seem to reinforce the possibility that $\Phi'_{residual} \approx$ the **IDS**-test-determined Φ'_α. Morgenstern (1967) wrote "It seems possible that the physical basis for the low residual strength exhibited by most clays resides in basal shear plane shear of the platy particles." Hutchinson (1967) noted that field determinations of $\Phi'_{residual}$ in inland slopes of London clay varied from 8°-10° with PIs from 20-28%. Figure 15 includes a box showing these ranges, which fits within the previous data shown. Kenney (1967a) concluded that $\Phi'_{residual}$ does not depend on clay plasticity (as in Figure 15) but does depend on the attractive forces between particles. In Kenney (1967b) he strongly recommended using the **IDS**-test for studying the fundamental strength behavior of clays.

From all the above data it seems possible that the cohesion and friction shear components of the AWL can logically and quantitatively account for much of the residual strength of many clays if bonding and the particle interference friction Φ'_β reduce to small values at residual strains.

However, the above possibility presents the writer with an as yet unresolved mystery. Other Φ'_β component behavior from this research appears to provide counter evidence, namely that time and continuous strain, over the interval of *c.* 1% to the maximum 10% investigated, decreases Φ'_α and increases Φ'_β. One possible resolution involves the progressive destructuring of a clay with Φ'_β reducing to a low $\Phi'_{\beta max}$ capability at higher residual strains, as discussed below.

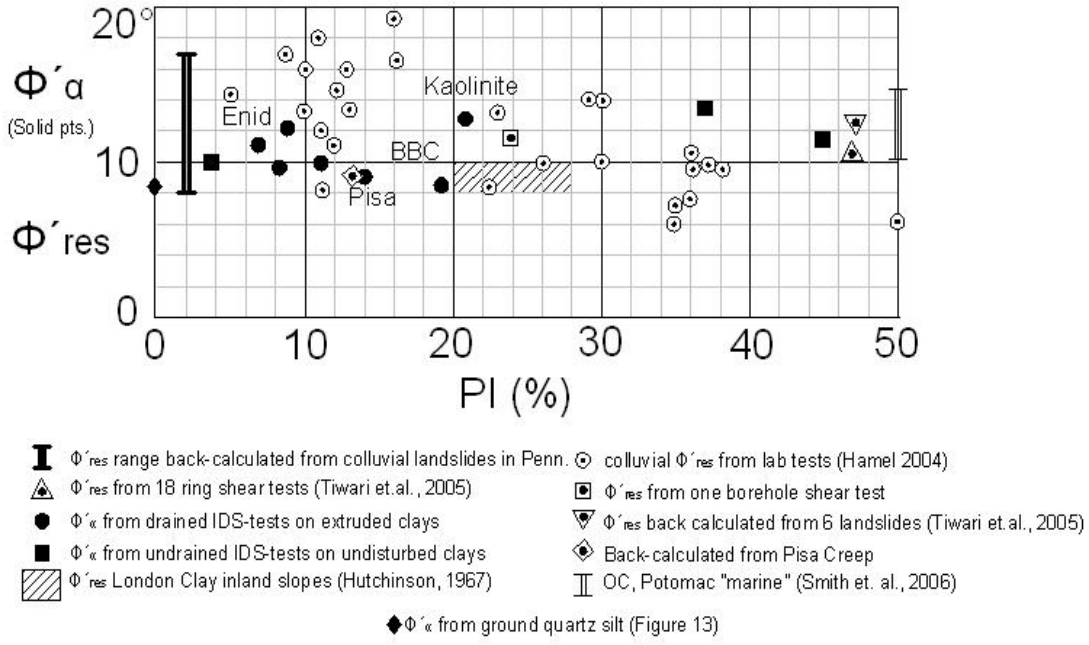

Figure 15: Evidence that Ø´α ≈ Ø´residual

Consider a stable clay slope loaded to a just-beginning creep condition with Φ'_{β} fully mobilized at the clay's current structures' $\Phi'_{\beta max}$ capability. For whatever reason the shear load on the slope increases and it begins to creep with viscous Φ'_{α} partially mobilizing as required. The additional strain causes the clay to destructure a little and $\Phi'_{\beta max}$ reduces. The next cycle of shear load increase and destructuring reduces $\Phi'_{\beta max}$ a little more and mobilizes a little more Φ'_{α}, and the viscous creep rate increases. After more such cycles $\Phi'_{\beta max}$ has reached its destructured minimum of particle geometrical interference and the viscous Φ'_{α} has mobilized almost fully. Thus, the shear resistance to slope movement now becomes primarily due to the unstable, viscous AWL Φ'_{α} and c' with $\Phi'_{\beta max}$ at its current lowest possible value. The next cycle of load increase increases Φ'_{α} to its maximum value with no more Φ'_{β} to transfer to and serious creep begins. Thus, $\Phi'_{residual}$ might $\approx \Phi'_{\alpha}$.

Note that the above scenario resembles the cyclic, progressive destructuring of OC clay slopes described by Bjerrum (1967b) as due to the progressive breaking of bonds. Instead of the breaking of bonds the above scenario has progressive destructuring that reduces $\Phi'_{\beta max}$, and may or may not include breaking bonds.

Discussion of the pro and con evidence of the above scenario falls beyond the scope of this paper. However, one especially interesting piece of pro evidence concerns the reported creep of the upper sandy and clayey silt layer under the Pisa Tower (Burland et. al. (2009)). The writer made a rough calculation of the average operational effective friction angle on the authors-identified, spherical rotational failure surface during the last 50 years of creep and obtained $\Phi'_{creep} \approx \Phi'_{residual} \approx 9°$ (assuming $\mathbf{I}_c$=0). The writer estimated from the data available to him that the silt layer has a PI $\approx$ 13% and a $d_{10} \approx 10^{-3}$mm. These Pisa soil data fit well within Figures 13 and 15 herein and suggest that Φ'_{creep} may also have a major Φ'_{α} component at the estimated (assuming simple shear over a 100mm thick shear zone) equivalent $\dot{\epsilon} \approx 2x10^{-6}$%/min creep rate for this tower's rotation.

12.2 Secondary Consolidation and Secondary Shear

During the effective stress and volume changes that usually define consolidation, the relatively incompressible solid particles, and/or aggregates of particles, must change their positions to accommodate the consolidation. The sum of all the mobilized shear resistance within a clay's structure must resist and eventually match the additional shear applied as the volume change gradually ends. The writer assumes that the internal shear resistance of a clay's structure determines its consolidation behavior, not the reverse. If we have "secondary consolidation" then we must have "secondary shear". This research clearly identifies this secondary shear, as follows:

As illustrated in Figures 1b,c and 7, Φ'' (or Φ'_{β}) results from the rapid shear mobilization response to an effective stress change – much like primary consolidation results from a rapid void ratio reduction response to an effective stress increase. Then, a generally much slower, delayed response occurs as the viscous Φ'_{α} friction reduces, or continues to reduce, as it transfers and adds to the more stable Φ'_{β} friction. It might help understanding to think of the above transfer as a "secondary shear" frictional resistance that adds to the "primary shear" available to resist the next consolidation load increase. Figure 7 illustrates how this transfer develops a larger total $\Phi' = \Phi'_{\beta} \approx (\Phi'_{\alpha}+\Phi'')$ frictional shear resistance at the time when the clay structure has completed this secondary shear transfer process to $\Phi'_{\alpha} = 0$.

According to the above and previous explanations of Φ'_{α} friction resulting from viscous AWL behavior, the time decay of mobilized secondary shear and its slow transfer to primary shear (Φ'_{α} transfers to Φ'_{β}) produces the secondary consolidation during the transfer search for stability. **IDS-**tests after secondary can capture the increase in Φ'_{β}. For example, Schmertmann (1976, Figure 9), (1982, Figure 8) or (1991, Figure 30), showed that progressively increasing the isotropic secondary consolidation time from 85 to 50,000 minutes increased Φ''(or Φ'_{β}) progressively from 1.2° to 6.9° at ϵ = 0.5% in **IDS**-tests on extruded kaolinite.

More evidence comes from the similarity between the $(\Phi'_{\alpha}/\Phi'_{\beta}$ and (C_{α}/C_c) ratios from

clays, silts, and sands. Again according to the above and simplifying for clarity, the primary Φ'_β controls the primary consolidation and C_c and the secondary Φ'_α controls the secondary consolidation and C_α . From many studies, most by G. Mesri and his students, the (C_α/C_c) ratios for inorganic soils typically vary between 0.01 in granular soils to 0.05 in silts and clays (Terzaghi et. al. 1996, p. 110). The (Φ'_α/Φ'_β) ratios typically vary from *c.* (3°/30°) = 0.1 in granular soils to *c.* (10°/20°) = 0.5 in silts and clays (Figs. 7, 8, 13). Thus, each of the ratios vary by a factor of *c.* 5 going from granular to clays. This similarity provides further evidence that the shear components developed herein help explain both primary and secondary normal consolidation behavior.

Terzaghi (1941b) described secondary consolidation as *"…the gradual displacement of the viscous portion of the adsorbed water films…"*, which he then called the *"process of solidification"*. He wrote further that *"…the time required for reaching a given degree of solidification increases with the reciprocal of the square of the grain size."* One can then also say the time increases linearly with the negative value of the log of grain size – as does Φ'_α in Figure 13. We thus have another connection between Φ'_α and secondary consolidation. It suggests that secondary time increases exponentially with Φ'_α, which checks qualitatively with experience.

The present research results also provide evidence related to any remaining controversy about whether or not primary and secondary consolidation occur **(A)** with no secondary during primary or **(B)** secondary also occurs during primary. Many researchers believed **B** correct. For example: Terzaghi (1941b) also wrote that *"Both field and laboratory experience demonstrates that we have to deal almost exclusively with the second case* **(B)***."* Taylor (1942, pp. 65, 136; 1948, p. 243) investigated the **(A)** and **(B)** hypotheses in detail and agreed with **(B)** and the need to include a "plastic structural resistance to compression" throughout the consolidation. Forty-eight years later Leroueil (1996, p. 538) also investigated both and presented data that support his conclusion for **(B)** and also states that *"Hypothesis **(B)** assumes some sort of 'structural viscosity'…"*. Sixteen more years later this paper demonstrates that the AWL's viscous cohesive $\mathbf{I}_c$ and frictional Φ'_α secondary shear components supply this "plastic structural resistance to compression" or 'structural viscosity' and the writer also supports **(B)**.

12.3 Ageing Preconsolidation

12.3.1 Decreasing Rate of Consolidation Loading

As discussed above and shown under the **8.4 Secondary Compression** and **8.5 Anisotropic Consolidation**, time and drained shear+ time can stiffen and strengthen a clay's structure by increasing the **D-**component. It then seemed reasonable to expect that allowing more time for a given effective stress consolidation increase, **when stress controlled with rest times**, could allow time for the **D**-component to increase, the structure to stiffen, and perhaps then the consolidation volume change would reduce versus that with a greater effective stress loading rate. To check this, the writer performed some comparative isotropic consolidation tests with greatly reduced rates of effective stress increase. As shown in Figure 16, decreasing the rate of NC loading in two non-swelling clays did reduce the consolidation volume change due to an isotropic effective stress increase from 100 to 350 kPa. However, it did not happen for the expected reason. The formation of bonds appears to have interfered, as explained below under 12.3.2.

Each of the points in Figure 16 represents a separate test of the isotropic, normal consolidation of a duplicate specimen of extruded, reconstituted kaolinite and the natural Enid residual clay. The writer achieved the greater than 1.0 day times by very small increment (≈ constant rate) or 10-increment loading, both with rest periods. Both methods produced about the same reduced void ratio change.

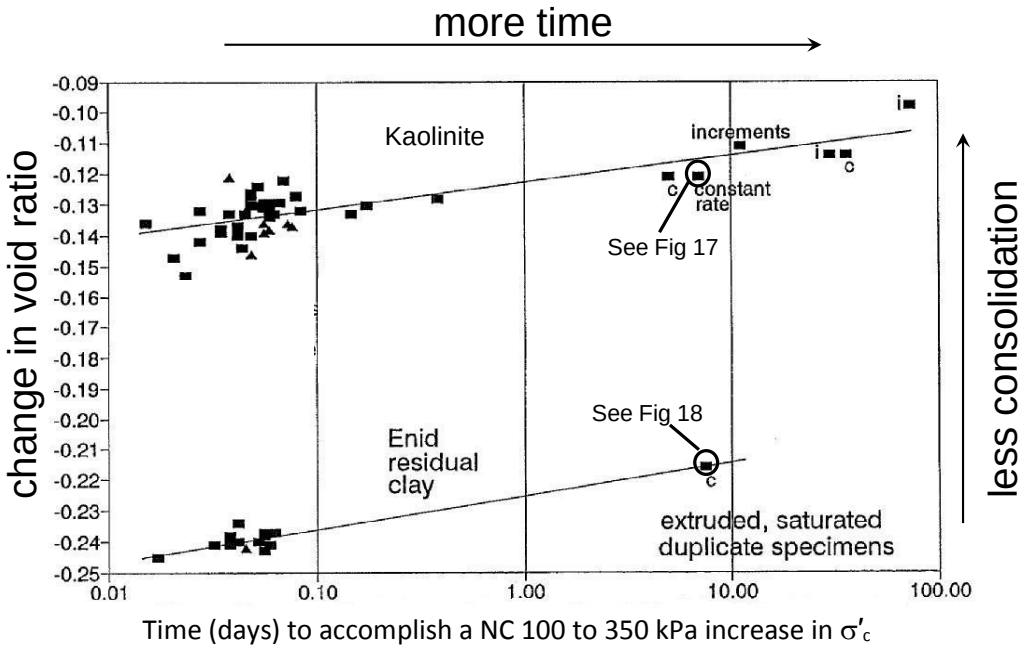

Figure 16: Examples of Decreasing Volume Change by Increasing the NC Time to σ'_c

12.3.2 Components after low rates of consolidation

Consider the two, circled 7-day consolidation time points in Figure 16. For each of these, at the end of the consolidation time, the writer performed an **IDS**-test to separate the components and compare them with duplicate specimens with only approximately one hour of primary consolidation time over the same effective stress interval. Figure 17 shows the results from kaolinite and Figure 18 from the Enid clay, both extruded. Both comparisons produced similar results. The 7-day **I**-component increased and then decreased over a 3% compressive strain interval while the **D**-component (Φ'_β) decreased.

Figures 17 and 18 do not show the aforementioned expected increase in Φ'_β. Instead, Φ'_β decreased. Nevertheless, the consolidation void ratio change did decrease with increasing the time to accomplish the effective stress increase. It appears that each clay's increased resistance to volume change resulted from the addition of cohesive bonding, $\mathbf{I}_b$, as shown by an increase in the **I** component. Then one might also predict that Young's modulus, E, would also increase in the 7-day versus the 1-hr **IDS**-tests because of the rigidity expected from cohesive bonds, as shown in Figure 14.

A check of the $\sigma_1'_{high}$ stress-strain curves showed that E did increase approximately 65% when measured linearly between successive data points over the (σ'_1-σ'_3) stress range of approximately 400 to 800 kPa, all with $\epsilon \leq 0.1\%$. The E for kaolinite increased in drained tests from 900 to 1580 kPa, and for the Enid clay from 1300 to 2060 kPa, despite the low-strain reduction in Φ'_β and the reduced consolidation (greater void ratio) after the 7 day versus 1 hour time to apply the effective stress increase.

The writer now has six measured behaviors which all support that the formation of $\mathbf{I}_b$ cohesive bonds very likely caused the reduced consolidation with increased time, namely:

12.3.2.1 **I** increased
12.3.2.2 Φ'_β decreased
12.3.2.3 E increased
12.3.2.4 $\mathbf{I}_b$ bonds can develop in the lab at $\epsilon = 0.1\%$
12.3.2.5 The bonds inhibited the strain mobilization of the particle interference Φ'_β
12.3.2.6 3% additional axial strain destroyed $\mathbf{I}_b$.

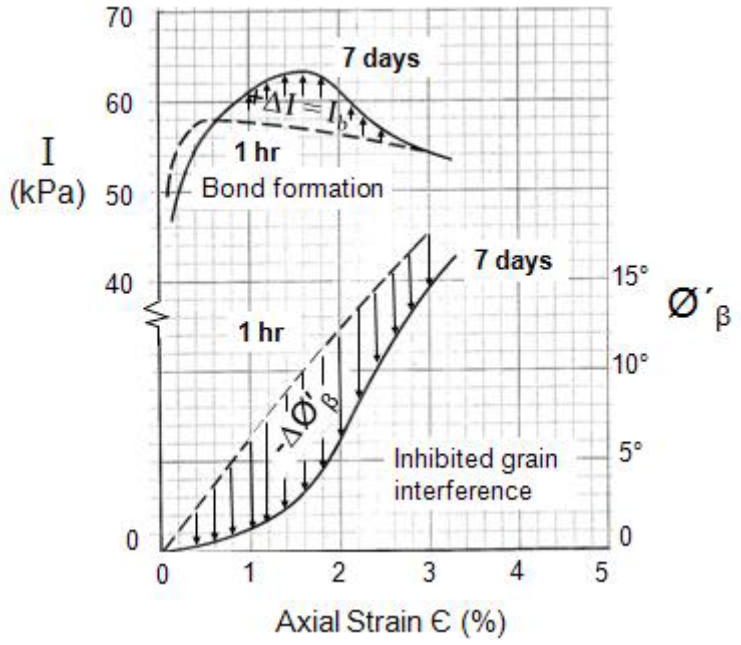

Figure 17 Extruded Kaolinite, 7 days versus 1h for σ'_c Effective Stress Increase from 100-350 kPa

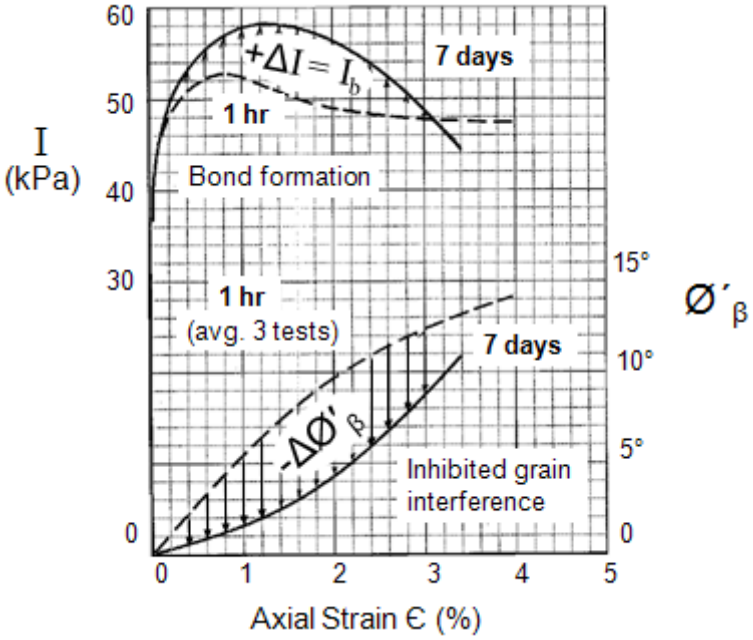

Figure 18: Extruded Enid Clay, 7 days versus 1h for σ'_c Effective Stress Increase from 100-350 kPa

12.3.3 Reliable Ageing Preconsolidation

All the consolidation theories known to the writer, with one important exception, and however they separate and then add primary and secondary consolidation effects, and with whatever load increments used, ***predict more total consolidation with more total time for the effective stress transfer***. Figure 16 shows a counter-intuitive **less** consolidation with **more** time. Terzaghi (1941a) provided the exception. Taylor (1942, pp. 77, 137; 1948 p. 246) supported the exception by also noting that the development of bonds during long sedimentation times would reduce volume change. As described above, bonds did reduce volume change in the lab tests of extruded kaolinite and Enid clay. Terzaghi also provided examples

of the consequences – including almost constant void ratio versus depth profiles in natural, uniform NC clay layers deposited over long periods of time. The writer has found similar profiles in the literature, for example in Landva et. al. (1988) in a clayey silt and in two sensitive Norwegian clays in Lacasse et. al. (1985, Figs. 2, 3) or Burland (1990, Fig. 32), and in Mitchell (1976, Fig. 11.18) (1993, Fig. 11.18).

Terzaghi (1941a) also showed how an ageing preconsolidation or overconsolidation effect would reduce the settlement of real foundations. His Figure 7, partly reproduced as Figure 19, shows **schematically** a sedimentation compression curve "C_s", the real foundation settlement curve without prior excavation, "C", and the consolidation test curve "C_u". The rate of loading increases dramatically from C_s to C to C_u. He showed that he would expect an effective overconsolidation in an otherwise NC deposit, which the writer has labeled the "ageing p_{ca}".

The Bjerrum (1967a, Figures 14-18, 1972, 1973) secondary consolidation creep and quasi-preconsolidation model predicts the ageing preconsolidation, but also that it will eventually disappear with creep. But he also noted (1967a, p. 108), that bonding could slow or stop the secondary creep. Indeed, engineers have successfully used this ageing effect innumerable times in practice to permit the use of shallow foundations with loads below the ageing p_{ca}. Landva et. al. (1988) provided a well documented example for a 9 storey bank building over uniform, sensitive, NC, clayey silt with an average PI ≈ 10%. Schmertmann (1991, pp. 1289-93) also noted the practical use of p_{ca} by engineers in New Orleans, Baton Rouge, Bangkok, and Porto Tolle (also see Schmertmann (2003)). Duncan et. al. (1991) discussed another reliable p_{ca} example with San Francisco Bay clays. Ellstein (1992) noted a reliable p_{ca} in Mexico City clays for 1 and 2 storey construction, but not for 3. Low et. al. (2008) provided a recent example of $(p_{ca} + p_o)/p_o \approx 3$ in a Singapore clay. Clyde Baker (2009, personal communication) reported routinely using p_{ca} in Chicago clays. Typical values of $(p_{ca} + p_o)/p_o$ = 1.25 to 2 in practice. They usually increase in oedometer tests with the quality of the sampling of the clay.

The shear-time Φ'_α to Φ'_β transfer behavior of the AWL and/or the formation of bonds during natural sedimentation rates of loading permit a reliable p_{ca} to develop in many geologically NC clays. Leonards (1972) strongly agreed about reliability. Also see Leroueil (1996, p. 536) and Section **12.10.3** for further agreement.

12.4 Applicability to Silts, Sands, and Partial Saturation

The research and concepts developed herein focused on the engineering shear behavior of saturated clays. But, the writer also found that

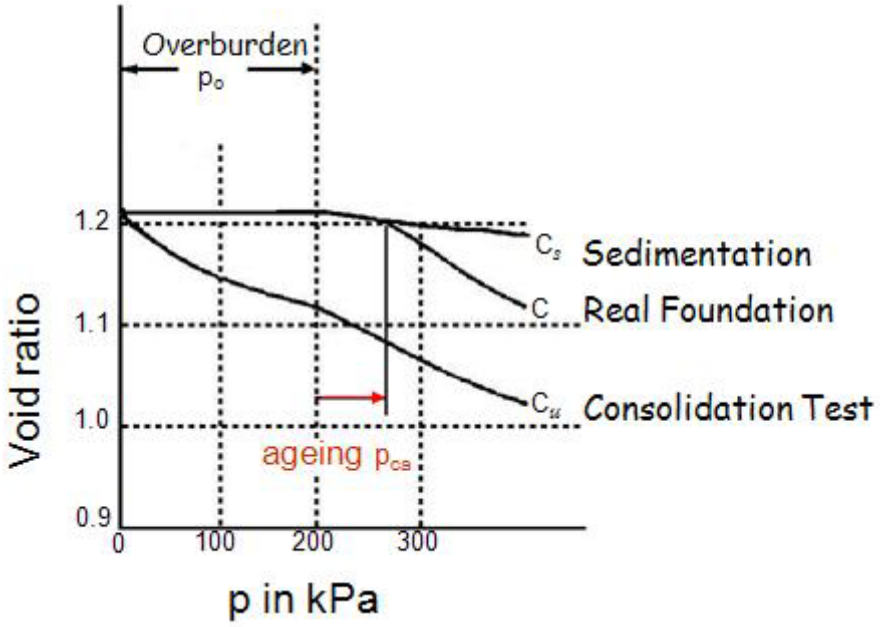

Figure 19: Ageing Preconsolidation p_{ca} from Terzaghi (1941a)

these concepts may apply to many saturated, particulate soils. All such particles have surfaces in contact with a fluid, generally water, with which they interact to form a boundary layer such as the AWL with clays. This layer will have properties different than the truly dry surface of the particle or of pure water and influence any soil's mobilization of its shear resistance components.

Silts, sands and even glass spheres have a measurable Φ'_α-component in **IDS**-tests. Plotting the artificial ground quartz silt with a PI = 0, from Figure 13 into Figure 15 suggests that Φ'_α has a minor dependence on PI that extends to non-plastic silt and sand, and even to glass spheres. Figure 13 shows a natural sand and an artificial Ottawa sand with Φ'_α values of about 5° and 3°, respectively. Schmertmann (1976, Figures 11, 28) provides data from these sand tests.

As noted in **12.2**, granular soils to clays have similar (Φ'_α/Φ'_β) shear and (C_α/C_c) consolidation ratios. This similarity also provides evidence of the importance of the shear components, in particular the viscous Φ'_α, in all mineral soils.

Silt and sand soils also develop ageing effects, including an ageing p_{ca}. As noted in 12.3.3, Landva et.al. (1988) reported an important p_{ca} in the Fredericton N.B. clayey silts. Mitchell (2008) noted the continuing enigma of various ageing effects in sands. Schmertmann (1991, Figure 6) showed a p_{ca} after one day of ageing under a plate load test on 'dry' sand in a humid laboratory. Such ageing effects involve changes in the shear resistance components, as discussed in **12.3**.

All the above suggests to the writer that a better understanding of the strain and time effects associated with AWL behavior has the potential to resolve questions about the mobilized shear components of soils other than clay. Terzaghi (1941b, p. 3) had similar thoughts.

More detailed data from silt and sands in Schmertmann (1976, Fig. 11) comes from a combination of tests on saturated, partially saturated, and lab air dried specimens. All saturation conditions produced approximately the same Φ'_α. This in turn, suggests the possibility that a sufficient AWL exists to develop Φ'_α at all these saturation conditions and that a secondary, viscous, transient shear friction component also forms a part of partially saturated soil mechanics. Various particle/particle attractive forces such as capillary and osmotic pressure provide an additional effective cohesion, as shown in Figure 15 in the reference. The concepts developed herein applied to partially saturated soils seems like a fruitful area for more research.

12.5 Undrained Shear Strength, s_u

A paper by Lunne et. al. (1997) included stress-strain data from 8 CAUC tests (K_o consolidated, undrained triaxial compression with back pressure, and a constant rate of strain) by the NGI on block samples of five low to medium PI Norwegian clays. They produced a common response of a pronounced peak at s_u at compressive strains that ranged from only 0.2 to 1.1%, averaging 0.5%, followed by a steep and then gradually reducing shear resistance with increasing strain. The 6 effective stress paths included in the paper all showed a pseudo-elastic, low dilatancy path to s_u.

The research described herein shows that at ϵ=0.5% the **I**-component has reached, or almost reached, its maximum value while the **D**-component (Φ'_β) remains relatively minor, especially if cohesive bonding inhibits its mobilization as in Figures 17 and 18. The undrained strength at ϵ=0.5% or less when neglecting Φ'_β then consists of plastic $\mathbf{I}_c$ and brittle $\mathbf{I}_b$ cohesions plus a viscous $\mathbf{I}_\alpha$ friction.

The pronounced peak at s_u suggests important $\mathbf{I}_b$ bonding. $\mathbf{I}_c$ and $\mathbf{I}_\alpha$ suggest AWL behavior. The bonding seems consistent with a pseudo-elastic and low dilatancy behavior. As shown herein, the AWL components exhibit little or no dilatancy affects, which also seems consistent. Now consider the implications of this for the possible reduced importance of effective stress in s_u in these Norwegian clays.

For illustration, say we have a clay that when tested undrained has 1/3 of its s_u from each of $\mathbf{I}_b$, $\mathbf{I}_c$ and $\mathbf{I}_\alpha$. By definition, the $\mathbf{I}_b$ and $\mathbf{I}_c$ cohesions do not vary with σ'. In this case a 30% reduction in effective stress due to undrained pore pressure would result in a 10% reduction in s_u. It seems possible, perhaps even likely, that effective stress and any changes in pore pressure may have a significantly reduced role in mobilizing s_u insitu at ϵ=0.5% or less in

similar Norwegian clays. This reasoning may apply to many other clays that have developed significant bonding, as during ageing.

The above may also help explain the observation made during testing and research at the NGI (S. Lacasse, 2010, personal communication) of a mysterious, pronounced increase in s_u at very low strain rates compared to expectations of a continuing log decrease in s_u with decreasing strain rate. Perhaps this represents behavior similar to that shown for the extruded kaolinite in Figure 10. Very slow strain rates may provide the time needed for significant bonds to form or for Φ'_β to increase as in secondary consolidation, or both. The resulting increase in shear strength then exceeds the reduction in viscous AWL shear due to the reducing strain rate, and s_u increases.

12.6 Low Strain Modulus and Secondary Shear (G_o and Φ'_α)

Based on three levels of evidence, the writer proposes a direct connection between G_o, residual strength Φ'_{res}, and the AWL viscous friction Φ'_α, as follows:

The first evidence comes from IDS-tests on isotropically NC clays where the **I**-component typically mobilizes five times more rapidly with strain versus the **D**-component. At the very low shear strains used for the dynamic testing for G_o, typically 10^{-3}% or less, the mobilized shear resistance will come mostly from the **I**-component. Recalling that $\mathbf{I} = \mathbf{I}_c + \mathbf{I}_b + \mathbf{I}_\alpha$, only $\mathbf{I}_\alpha$ depends on the effective stress. Because G_o does increase with effective stress as discussed below, this increase comes from $\mathbf{I}_\alpha$ which, as interpreted herein, depends on the viscous behavior of the adsorbed water layer.

Secondly, G_o increases with approximately $(\bar{\sigma}_o)^{0.5}$ (for example see Anderson and Woods, 1976, Figs. 4, 9). These authors included tests on an extruded, saturated ball kaolinite with a PI = 39% and a d_{50} = 0.00025 mm. Using a reference time of t_{ref} = 1000 min, and assuming their $\bar{\sigma}_o \approx \sigma'_t$, the kaolinite's G_o increased approximately linearly with a $\Phi' \approx 18^o$ over their NC $\bar{\sigma}_o$ range of 69 to 275 kPa. This compares with a Figure 13 $\Phi'_\alpha = 12^o$ for an extruded kaolinite with PI = 21% and a d_{50} of 0.001 mm. A rough correction for PI and d_{50} differences would increase the latter Φ'_α value to *c.* 14-15°. It seems that Φ'_α, and therefore AWL behavior, could account for most of the increasing G_o response to increasing $\bar{\sigma}_o$ in extruded kaolinite and perhaps also in many natural clays.

Thirdly, if G_o in NC clays depends importantly on Φ'_α behavior, then it would have important secondary shear time and temperature effects. The above reference, and many others, document that it does. The N_G term in Eqn. (6) provides a normalized measure of the semi-log increase in G_o (from Schmertmann (1991, p. 1296)) following Δt_{sec} additional time in secondary consolidation after a reference time t_{ref}.

$$\Delta G_o = N_G [\log (t_{ref} + \Delta t_{sec}) - \log t_{ref}] (G_o)_{ref} \quad \text{..... (6)}$$

N_G reduces with the log of grain size from *c.* 0.16 when $d_{50} = 3x10^{-4}$ mm in clay to *c.* 0.02 in sandy gravel with $d_{50} \approx$ 1mm (Anderson and Woods, 1976, Fig. 7; Mesri et. al. 1990, Fig. 1; Schmertmann 1991, Fig. 9). This trend has a striking similarity to Φ'_α versus log d_{10} in Figure 13, and thereby suggests an interdependence between G_o and Φ'_α.

In addition, and as noted in **9. ADSORBED WATER LAYER (AWL)**, temperature changes affect s_u, p_c and C_α. If this results from viscous Φ'_α behavior in the AWL, as postulated, then G_o should also change with temperature. Anderson and Richart (1974) present evidence that it does from test results from 2 artificial and 5 'undisturbed' clays. In one typical example with Detroit clay, G_o increased and decreased 10% when increasing and decreasing the ambient test temperature from 4° to 22°C. The secondary compression drainage also increased and decreased during this temperature increase and decrease. The above further supports the concept that G_o (and secondary compression) depends on a viscous Φ'_α.

From the above attempt to look through the 'fog' of the many variables that can affect G_o to see a bigger picture, it seems the plastic, AWL, $\mathbf{I}_c$ cohesion and $\mathbf{I}_\alpha$ friction provide the "very high viscosity" already used by Terzaghi (1941b, 1955, p. 576) to explain secondary time effects. As described in Section **12.1**, a clay's AWL-controlled behavior also seems to have an important effect on residual strength. It's important effect thus seems to span from the smallest to the largest strains. The writer suggests that the typical semi-log "S" shape of

the entire G versus strain curve obtained from clay, results, at least in part, from the **I**-component behavior of viscous adsorbed water in clays.

12.7 Φ'_β to Understand K_o

12.7.1 K_o Increase During Secondary Consolidation

In Schmertmann (1983) the writer posed the question of what happens to K_o in clay during secondary consolidation. Does it decrease, remain constant, or increase? The experimental data now available shows it slowly increases. Only Soydemir (1984) correctly predicted that K_o would increase during secondary consolidation. He used a mathematical model that included viscosity in the clay's volumetric and deviatoric behavior. The following offers a matching viscous component transfer explanation.

As previously discussed in **12.2**, the secondary part of the consolidation process of a clay's structure adjusting to an increased load involves a time transfer from an unstable Φ'_α to a stable Φ'_β. As developed herein, Φ'_α results from particle/AWL sliding and does not depend on particle interference effects, while Φ'_β does so depend. Despite the one dimensional constraint for the K_o condition, Φ'_α can dissipate with time because of its viscosity. But, a matching increase in Φ'_β cannot fully develop with time because particles, on average, cannot move across, nor can shear strain develop to increase interference along the lateral boundary minor principal plane. This reducing Φ'_α to Φ'_β transfer ability reduces the clay's ability to sustain an increased shear loading and K_o increases with time to maintain equilibrium.

12.7.2 Φ'_β in Jaky's Equation

The writer has some evidence from extruded kaolinite and BBC in Schmertmann and Hall (1961) and Hall (1960) that, when combined with Landva's (2006) work, shows the possible superiority of using $\Phi'' (\approx \Phi'_\beta)$ in Jaky's equation (K_o=1-sin Φ') versus using the current conventional $\Phi' = (\Phi'_\alpha + \Phi'_\beta)$.

Landva reviewed the history and derivation of Jaky's equation, and compared it with Terzaghi's (1943) derivation for K_o when using a friction mobilization factor, and with Mayne and Kulhawy's (1982) empirical correlation data when using Φ'. He concluded that tan Φ' required reduction by a Terzaghi mobilization factor that varied from 0.4 to 1.0, averaging 0.6, to encompass the empirical data. The writer here below suggests the alternative, and gives an example, of using Φ'_β instead of Φ' in Jaky's equation.

From the aforementioned Hall (1961) research the mobilized and maximum values of $\Phi'' \approx \Phi'_\beta$= 12° and 20°, resp., for a mobilization factor = 0.6 at the end of anisotropic K_o consolidation. Using 20° and 0.6 in Figure 4 in Landva's paper gives three correct K_o predictions of 0.63, 0.68 and 0.70. Using a representative Φ'=30° and 0.6 gives a too low K_o=0.50. So does Jaky's equation when using 30°, but it gives a correct 0.66 with 20°. The superior result when using Φ'_β instead of Φ' for estimating insitu K_o seems reasonable because it uses the non-viscous (stable) "primary" Φ'_β friction component for a stable K_o state of stress condition while using Φ' includes the viscous (unstable) "secondary" Φ'_α.

12.8 Normal Consolidation Settlement and the Shear Components

One of the interesting aspects about "consolidation" concerns the various ways it can occur. They do not lend themselves to a simple definition of the word. For example, we can have consolidation settlement with and without pore pressure change, as well as pore pressure change with and without consolidation settlement. We can also have "secondary" before "primary" consolidation, instead of the usual reverse. Including the interaction of the mix of the two cohesion ($\mathbf{I}_c$ and $\mathbf{I}_b$) and two friction (Φ'_α and Φ'_β) shear strength components of clay, as described herein, provides an alternative explanation for these different "normal consolidation" (NC) cases.

12.8.1 Classic Terzaghi Case: Consolidation settlement with excess pore pressure (u_e) dissipation

This case involves consolidation settlement due to a load increase of a magnitude sufficient to generate an excess hydrostatic (u_e) pore pressure in the ordinary water phase, which then drains as it dissipates hydrodynamically to near-zero. The resulting volume change produces the settlement.

Bonds, if any, begin to break and a secondary viscous shear Φ'_α mobilizes fully at very low volume and/or shear strain (see **12.10.3**). Additional Φ'_β tries to mobilize by viscous transfer with low strain to the point that it exceeds the current $\Phi'_{\beta crit}$ mobilized during the prior increment of consolidation volume change. The current stable structure then becomes unstable (yields) and compresses and generates the u_e. This u_e dissipates with a resulting reduction in void ratio, which in turn increases particle interference and allows $\Phi'_{\beta crit}$ and Φ'_β to increase. With the dissipation of u_e the rapid, primary consolidation ends, but the total consolidation continues with the viscous secondary consolidation associated with the time transfer of any remaining Φ'_α, adding to the stable Φ'_β. The consolidation stops when the stable Φ'_β and any remaining and/or developing $\mathbf{I}_b$ can carry the increased loading that initiated the current increment of consolidation.

12.8.2 Consolidation with little or no settlement

For the case of total (σ) and effective (σ') loading increasing very slowly, significant u_e may (or may not) develop and dissipate in very small increments that produce only a small total volume change and settlement. The otherwise normally consolidated clay develops an ageing preconsolidation, p_{ca}, as described in **12.3** and reviewed below.

The slow loading increase permits the time for an almost simultaneous, stable structure stiffening to occur due to the Φ'_α to Φ'_β, unstable to stable transfer and/or the formation of new $\mathbf{I}_b$ bonds, or both. Section **12.3** gives an example from lab testing. Referenced constant void ratio versus depth profiles provide examples from the field.

Schmertmann (1991, Figs. 18, 19) and Schmertmann (1993, Fig. 9) also provide examples of u_e dissipation with settlement followed by more dissipation without settlement. Assuming correct measurements, the clay structure must have stiffened and strengthened during the time of prior u_e dissipation and settlement to the point of greatly reducing the settlement with further dissipation. Again, Φ'_α to Φ'_β transfer and/or an increase in $\mathbf{I}_b$ likely provided the stiffening and strengthening. Section 12.10.3 Lab provides another example from anisotropic consolidation.

12.8.3 Settlement with no σ'_v increase despite u_e dissipation

Crawford and Burn (1976), Larsson (1986), and others have described settlements of test fills while at constant total loading (σ_v) with the resulting u_e remaining approximately constant instead of reducing. However, consolidation settlement did occur. This can only happen if the clay structure collapses when trying to increase σ'_v, but σ'_v cannot increase because the collapse generates u_e at the same rate that it dissipates. We thus have consolidation with a u_e and ($\beta'_{\Phi crit}$ + $\mathbf{I}_b$ + $\mathbf{I}_\alpha$) that continually control each other during the continuing void ratio reduction and settlement so as to maintain a near-constant σ'_v.

If one assumes a negligible or a constant ($\mathbf{I}_c$ + $\mathbf{I}_b$) cohesion, the constant shear loading associated with a constant σ'_v must remain in a creeping equilibrium with the mobilized σ' $\tan(\Phi'_\alpha + \Phi'_\beta)$ frictional resistance. But, Φ'_β should increase with reduced void ratio and the resulting increase in particle interference effects. Because it does not, Φ'_β must be at a $\Phi'_{\beta crit}$ (yield) condition that reduces due to structural yield at the same rate it would otherwise increase. Hence the counter-intuitive consolidation equilibrium between a constant σ'_v and an increasing settlement.

While “temporary”, the above equilibrium will eventually end with σ'_v increasing. But it can take a long time to do so. Crawford and Burn (1976) provide case examples of 15-20 years of equilibrium duration in sensitive clay.

Note that the above presents a variation of the component transfer and residual creep scenario described at the end of **12.1**. Instead

of the residual shear creep in **12.1** we have a consolidation creep. They could also combine.

12.8.4 Settlement with no σ'_v increase and no u_e dissipation

For the near-zero u_e, constant σ' condition after the essentially complete primary u_e dissipation, secondary settlement continues as the viscous Φ'_α continues to transfer to Φ'_β if Φ'_β has not yet reached $\Phi'_{\beta crit}$. If more Φ'_α remains to transfer, but $\Phi'_{\beta crit}$ has reached a maximum, the secondary creep settlement continues as described above, but with u_e a constant value just above zero. Eventually, the decreasing void ratio may let $\Phi'_{\beta crit}$, and therefore Φ'_β increase, and/or $\mathbf{I}_b$ bonds form and the secondary consolidation stops. If not, it continues at a decreasing rate as progressively more viscous AWL water between the particles gets displaced.

12.8.5 Settlement due to fabric collapse

Engineers have identified various other reasons for the weakening and yielding or collapse of soil fabric, such as vibrations and cyclic loading, particle breakage, mechanical remolding, water and other chemical leaching and solution, internal and external erosion, excavations, and high pore pressures leading to unstable low effective stresses. All of these can weaken and overload the shear resistance of a soil and produce settlement. They can also occur in sequence as in leaching prior to undrained loading followed by high pore pressure and collapse. Many combinations have also occurred. They all have in common a weakening resulting in an overloading that exceeds the soil's current stable ($\mathbf{I}_b$ + σ'tan $\Phi'_{\beta crit}$) shear mobilization capability.

12.9 Burland's Clay Intrinsic Consolidation Line (ICL)

According to Burland (1990, pp. 332-334) his ICL results from the normalized, 1D, incremental normal consolidation of a saturated, reconstituted clay started at a void ratio of 1.25 times the void ratio at the Atterberg liquid limit. At this $1.25e_{LL}$ such a clay has a very low and unstable shear resistance and therefore has both the stable $\mathbf{I}_b$ and Φ'_β components near zero. For the reconstituted clays he and others investigated, Burland reported the ICL independent of the starting void ratio in the range of 1.0 to $1.5e_{LL}$ and the time in secondary compression. He also noted that the water used to prepare the reconstituted clay should have the same chemistry as its natural water. All this suggests significant AWL behavior.

That many reconstituted clays closely follow a normalized ICL line may result from the similar plastic $\mathbf{I}_c$ and Φ'_α AWL viscous shear component behaviors in many clays [see Figure 11 in Schmertmann (1976)]. Comparing the consolidation of natural clays to the ICL can then show how the stable Φ'_β and $\mathbf{I}_b$ components change the ICL position of natural clays versus a reconstituted ICL.

12.10 Minimum Surcharge Ratio for Drainage Aids to Reduce Settlement Time

12.10.1 Objective

The writer herein defines a surcharge ratio R_s at any depth z in a NC clay as [(the σ'_{vo} vertical effective stress before the surcharge + the $\Delta\sigma_{vsz}$ added by the surcharge)/(σ'_{vo})]. Then:

$$R_s = (\sigma'_{vo} + \Delta\sigma_{vsz})/\sigma'_{vo} \quad \text{..... (7)}$$

Adding and later removing a surcharge produces overconsolidation in otherwise NC clays. As shown throughout the paper, and illustrated in the schematic Figure 8, overconsolidation increases the subsequent strain rate mobilization of the stable Φ'_β and/or $\mathbf{I}_b$ components. To accomplish this the surcharge must produce enough additional bonds to increase $\mathbf{I}_b$, and/or the strain to increase particle interference to the required increased level of Φ'_β. Using surcharge ratios that cause structural yielding and the generation of u_e also requires the dissipation of that u_e. **However, drainage aids may not help significantly with a too low surcharge ratio because the Φ'_α to Φ'_β transfer occurs because of a highly viscous AWL flow at very low hydraulic gradients instead of a hydrodynamic pore pressure dissipation of low viscosity (ordinary) water at high gradients.** The following attempts to answer the question of

what minimum R_s must one exceed to make drainage aids effective?

12.10.2 A theory for the minimum R_s

12.10.2.1 Normally consolidated (NC) case

In Figure 20 the writer presents a sequence of simplified effective stress paths (ESPs) in (p′-q) Mohr coordinates to explain the derivation of subsequent Equation (8). Point "A" shows the (p′-q) location of a NC clay before surcharging with $\Delta\sigma_v$. Placing the surcharge begins to mobilize the additional q required for eventual stability at point "C" for the illustrated R_s = 2. The dormant **I** component, = σ′ tan Φ'_α, mobilizes first, with a negligible volume change that produces a negligible excess hydrostatic pore pressure u_e (see 12.10.3). Its ESP follows the fully drained AB. The final BC segment produces a new stable, NC state where **I** and u_e have dissipated and mobilized shear comes from only Φ'_β.

The ESP AB develops as $\mathbf{I}_\alpha$ mobilizes fully. The ESP BC develops as $\mathbf{I}_\alpha$ dissipates and one has the volume change associated with NC from σ'_{1A} to 2 $\sigma'_{1A} = \sigma'_{1C}$. But, from σ'_{1A} to σ'_{1B} one has no significant volume change and therefore no u_e to dissipate. Drainage aids would not help until $\sigma'_1 > \sigma'_{1B}$ or, from Equation (7), R_s exceeds the minimum (σ'_{1B} /σ'_{1A}) and the drainage changes from only AWL viscous drainage to include primary hydrodynamic drainage.

A math study of the problem as presented in Figure 20 gives:

$$R_{S\,\min} = \left[\frac{\left(1-\tan\phi'_{\beta NC}\right)+2\tan\left(\phi'_{\beta NC}+\phi'_{\alpha}\right)}{\left(1+\tan\phi'_{\beta NC}\right)}\right] \quad (8)$$

A parametric study using Equation (8) produced R_{smin} in the range of 1.2 to 1.5 when using typical values of the angles involved. However, $\Phi'_{\beta NC}$ has only a minor effect and Equation (9) seems adequate.

$$R_{S\,\min} = 1+2\tan\phi'_{\alpha} \quad \text{..... (9)}$$

For the Figure 20 example, wherein $\Phi'_{\beta NC}$ = 12.8° and Φ'_α = 10°, R_{smin} from equation (8) equals 1.31 and from (9) equals 1.35.

Including $\mathbf{I}_c$: The above NC case neglects any $\mathbf{I}_b$ and $\mathbf{I}_c$ cohesion components. Assume any $\mathbf{I}_b$ mobilizes as part of the OCR determination in the subsequent 12.10.2.2. Further assuming the plastic and viscous $\mathbf{I}_c$ remobilizes fully from zero with the application of a surcharge, then the $\mathbf{I}_c$ cohesion would also increase R_{smin} together with the $\mathbf{I}_\alpha$ friction. The $(\sigma_1-\sigma_3)/2$ in the

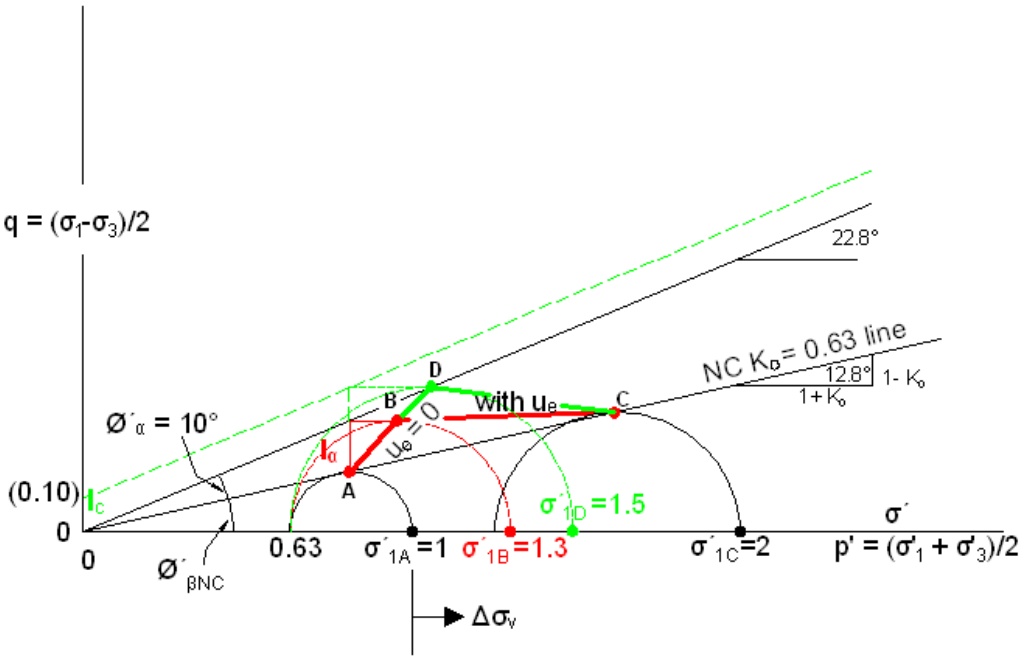

Figure 20: Effective p′-q Stress Paths for Example R_{smin}

envelope in Figure 20 would increase by a constant $\mathbf{I}_c$, as shown by the dashed line. A math study of the above increase shows that R_{smin} would increase by ($2\mathbf{I}_c/\sigma'_1$) in both equations (8) and (9). Reworking the previous example to include an $\mathbf{I}_c = 0.10$, gives R_{smin} =1.51 and 1.55, versus the previous 1.31 and 1.35. Including a range of 5 to 20 kPa for $\mathbf{I}_c$, in an example when σ'_1=100 kPa, would increase the range in R_{smin} from about 1.3 to 1.9 versus the previous 1.2 to 1.5.

12.10.2.2 Overconsolidated (OC) case

Figure 20 can also illustrate the OC case, with NC and OC points "A" and "C" (with OCR = 2). Assume that the AC recompression occurs without significant u_e, and that a new level of **I** can mobilize at "C". The additional **I** then becomes part of the OCR and R_{smin} equals the OCR.

Hansbo and Torstensson (1977, p. 535) describe the results from research on the effectiveness of vertical drains under four test fills over soft clays. On this basis, plus wider practical experience, they emphasize and conclude that the surcharge overpressure in the clay must exceed the preconsolidation pressure. They wrote "*It is amazing how often installation of drains is considered without that those concerned knowing the preconsolidation pressure of the subsoil in question. No doubt, the non-effectiveness of vertical drains sometimes experienced can be explained by the fact that the preconsolidation pressure (p_c) is not exceeded due to loading. In such a case, the rate of consolidation is almost the same, drains or no drains, and …*"

As noted in 12.3.3, many if not most NC clays actually have a reliable p_{ca} due to ageing, with an effective OCR typically between 1.25 and 2. As shown in the previous 12.10.2.1, R_{smin} due to the mobilization of the $\mathbf{I}_\alpha$ component has a predicted range of 1.2 to 1.5, which increases to 1.3 to 1.9 when including ($\mathbf{I}_c/\sigma'_1$) = 0.05 to 0.20. It seems likely that this mobilization and subsequent AWL viscous transfer to Φ'_β could produce a p_{ca} in consolidation tests and become a part of its OCR. This might explain some of the non-effectiveness noted in the above quote when the engineers assumed NC.

12.10.3 Data and Examples

Reviewing the research data from drained NC tests on the extruded BBC, kaolinite, and Enid clays, plus 3 other clays, indicates the volume strain ϵ_v when $\mathbf{I} \approx (\mathbf{I}_c + \mathbf{I}_\alpha)$ occurs with an average $\epsilon_v \approx +0.05\%$. All the checked tests showed a small, positive dilatancy. Mobilizing **I** occurs with very little volume change and with an expanding structure. It would therefore generate negligible positive pore pressure during the mobilization of ($\mathbf{I}_c + \mathbf{I}_\alpha$) when tested undrained**.** After developing the above theory and equations, the writer searched for lab and field examples to check the R_{smin} concept and found the following:

12.10.3.1 Lab

Hall (1960) provides one relevant lab example not found in Schmertmann and Hall (1961). The example shows the isotropic NC of a kaolinite to 228 kPa for 1 day, followed by an 11-step, all in one hour, drained incremental increase in (σ_1-σ_3) to 371 kPa while holding σ_3 constant at 228 kPa.

Hall found that the additional anisotropic consolidation volume change of 1800 mm^3 did not begin until the additional (σ_1-σ_3) reached between 68 and 80 kPa. Hall wrote *"This would fall near the value of twice the peak cohesion (**I**) for the sample."* In this test the measured R_{smin} = [228+(68 to 80)]/228 = 1.30 to 1.35. Both $\Phi'_{\beta NC}$ and Φ'_α equaled approximately 10°, and Equations (8) and (9) would predict 1.32 and 1.35, respectively. Adding an extruded kaolinite $\mathbf{I}_c \approx 8$ kPa would increase the computed R_{smin} to 1.39 and 1.42, respectively, and still near the measured values.

Some experiments and field measurements have shown that clays do not follow Darcy's Law at low gradients. They show a much lower permeability (or hydraulic conductivity) in clay when tested at low versus high gradients – for example, as suggested in Hansbo and Torstensson (1977, p. 534) and as shown in Hansbo [(1973), copied in Mitchell (1993, p. 238)]. Such behavior might occur because the low gradients move mostly the plastic-behaving and very viscous AWL water. When applying Darcy's law one must correct for permeability varying inversely proportional to

viscosity. Perhaps, in a sense, there also exists here an R_{smin} that one must exceed to begin significant "primary" laminar flow movement of low viscosity "ordinary" water. As gradients increase, perhaps one first has mostly a "secondary" slow AWL water flow followed by a mostly faster "primary" water flow, with a consequent increase in the calculated permeability during the transition.

12.10.3.2 Field

Terzaghi (1941b) presented a combination of lab and field experience that relates closely to the R_{smin} concept herein for effective wick drains. He refers to a *"critical (over) pressure, q_c"* required to break the *"solidification"* bonds formed in a layer of (NC) clay. Once broken, the clay enters the *"lubricated state"* and becomes highly compressible and *"undergoes the well known process of consolidation"*. He wrote further *"That this has been repeatedly demonstrated by direct measurement in the field"*. In the present context this means we have an $R_{smin} = (1 + q_c/\sigma'_1)$ to reach before we get the generation of u_e so that drainage aids can increase the rate of u_e dissipation.

In Terzaghi (1941b) he also wrote that *"Construction experience seems to indicate that the critical (over) pressure is of the same order of magnitude as the unconfined compression strength of the clay (q_u)."* Then:

$$R_{smin} \approx (1 + q_c/\sigma'_1) \approx (1 + q_u/\sigma'_1) \approx (1 + 2s_u/\sigma'_1) \quad ..(10)$$

Figure 20 seems to check this indication. From Figure 20, $q_u = (1\text{-}K_o)\sigma'_1 = 0.37$ and $(1+q_u/\sigma'_1) = 1.37$ using only $\mathbf{I}_\alpha$ transfer. The figure shows $R_{smin} = 1.32$. Including a typical $\mathbf{I}_c/\sigma'_1 = 0.05$ transfer increases R_{smin} to = 1.42. Thus, in this case $R_{smin} \approx (1 + q_u/\sigma'_1)$ as indicated by Terzaghi.

The above agreement may have broader implications. Long experience shows that (s_u/σ'_1) in 'NC' clays usually varies from about 0.15 to 0.40. Therefore, because $q_c \approx 2s_u$, $(1 + q_c/\sigma'_1)$ usually varies from about 1.3 to 1.8. Note the similarity to the 1.3 to 1.9 estimated range for R_{smin} developed in 12.10.2.1. Further note the typical range in **12.3** for the ageing $OCR = [(p_{ca} + p_o)/p_o] = 1.25$ to 2, based on experience. We have three similar ranges and that suggests a commonality. For example, perhaps p_{ca} increases with increasing (s_u/σ'_1)?

12.10.3.3 Practice

The writer's ageing OC, his unstable AWL Φ'_α to stable Φ'_β (and $\mathbf{I}_b$) time-transfer to develop R_{smin}, and Terzaghi's AWL solidification and q_c may all describe the same behavior. Practically, determining p_c from high quality clay samples using a CLI oedometer test should provide a good estimate of R_{smin}. Alternatively, one can test for or otherwise estimate the **I**-components, and/or q_u or s_u and use equations (8 and 9 with an $\mathbf{I}_c/\sigma'_1$ addition) and/or (10) to estimate R_{smin}.

12.11 Failure Planes and Slickensides

The one and two specimen **IDS**-test comparisons in Schmertmann (1962), while good enough to show the utility of curve hopping (see **3.2**), do show a general tendency for Φ'_α to decrease and Φ'_β to increase with $\dot{\epsilon}$ in the two specimen versus one specimen tests. This provides still another example of the Φ'_α to Φ'_β time transfer behavior over the approximate 10 hour time of a typical constant $\dot{\epsilon}$ test. The curve hopping in the one specimen test disrupts and slows the transfer compared to the matching two specimen test without the hopping.

Strain disrupts and changes a clay's structure. Strain and time make it progressively easier for the AWL Φ'_α secondary shear reduction to increase the Φ'_β primary shear.

Disrupting structure to the point of developing a visible failure plane concentrates and increases the shear strain on that plane. This tends to deflocculate and disperse the clay's structure into a more parallel arrangement of its platy particles in the direction of the failure plane. This in turn appears to make it easier for the AWL to attract water to the particles. Whatever the reason, the apparent viscosity of the AWL reduces, Φ'_α decreases, and therefore more easily transfers to Φ'_β. Schmertmann and Osterberg (1960, Fig. 13), and Schmertmann (1976, Fig 5 and 1981, Fig 2) show one of many examples of the accelerated Φ'_α to Φ'_β (**I** to **D**) transfer resulting from a failure plane.

The failure plane eventually becomes a slickenside with ageing and insitu movements along that plane. Its parallel fabric minimizes opportunities for stable particle/particle interference and bonding, but maximizes the surfaces for unstable AWL lubrication. We thus have a preferential surface for shear movement and creep. With enough of this minimizing and maximizing the clay approaches the residual state, controlled primarily by the AWL as suggested in **12.1**.

12.12 Creep and the I-component in Drained Compression

As discussed previously, the viscous behavior of the AWL reduces the stability of a clay's structure and causes the time-transfer of mobilized shear to the more stable bond and particle interference components $\mathbf{I}_b$ and Φ'_β, respectively. The transfer also produces creep. The writer will now present experimental evidence to show that the mobilization of the unstable $\mathbf{I}_c$ and $\mathbf{I}_\alpha$ components do not initially produce significant creep until they mobilize fully. The discussion in **12.11** already suggested that **I** must mobilize fully before significant destructuring can occur to generate u_e excess pore pressure. The same appears true for creep in kaolinite clay, as shown below, and perhaps in many other clays. But, as discussed in **12.1** once creep has begun Φ'_α may transfer to Φ'_β and remobilize in cycles that depend on the loading cycles.

12.12.1 Creep Limit

There exists a convenient test and graphical method for obtaining the pressure or stress limit at which significant creep will begin in clay. The test involves incremental load increases and stress control to permit creep at constant stress. As shown in the subsequently discussed Figure 21 example, the writer plotted a creep strain increment ($\Delta\epsilon$) versus the constant $\sigma_a = (\sigma_1 - \sigma_3)$ for that increment. Such plots often produce bi-linear and/or tri-linear slopes. Their intersections define "creep limits" (CL_1 and CL_2 in Figure 21) useful in practice to predict the loading at which significant creep and failure will begin. Housel (1959) showed the use of this method for avoiding creep movement problems in Detroit clays. Stoll (1961) used the method to demonstrate that the creep limit CL_1 applied to piles in both sand and clay. The ASTM Pressuremeter Standard D4719 includes a similar method to determine a creep limit CL_1 from pressuremeter testing. Loadtest Inc. has used the method routinely for pile side shear and end bearing creep limit estimates for over 11 years and most of their pile test reports include an appendix describing it. The method works best with constant increments of loading and a fixed time interval for the determination of creep strains.

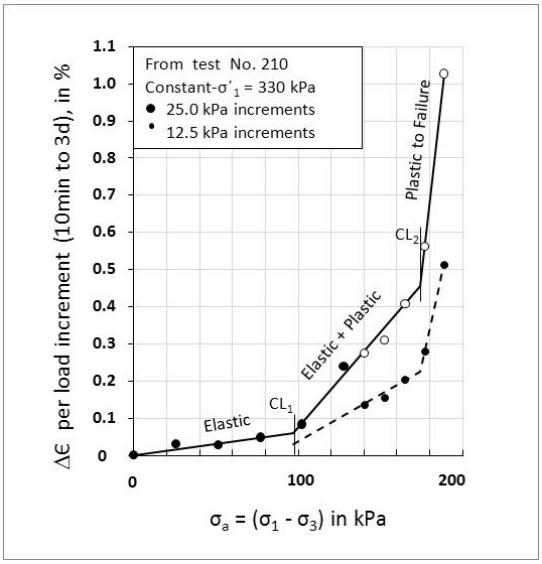

Figure 21: Constant Dead Load, Drained Compression, Creep Limits in Kaolinite

12.12.2 Test Examples

Section **8.1** describes the results from Bea's (1960) undrained creep and **IDS**-testing using extruded kaolinite and extruded and 'undisturbed' BBC. These tests all showed a time transfer from the **I** to the **D** component during creep. They all had a final creep strain that exceeded the strain to reach $\mathbf{I}_{max}$.

Now consider some drained creep data from the stress-controlled, constant–σ'_1, compression tests similar to those in Figure 9(a). First we consolidated isotropically for one day to $\sigma'_c = 350$kPa and rebounded to a reduced σ'_1 of 330 (tests 210, 219) or 260 kPa. We then held each axial load increment constant for approximately three days, and measured the creep strain for each over the 10min to 3day time interval after applying each increment.

Matching increments of σ_a by imposing an equal increment of pore pressure kept σ'_1 constant and reduced σ'_3. Figure 21 shows the creep graph for the constant–σ'_1 = 330kPa test No. 210. For this test we applied 5 initial increments of $\Delta\sigma_a$ = 25.0kPa followed by 5 increments of $\Delta\sigma_a$ = 12.5kPa. The writer then doubled the 12.5kPa increment creep to permit comparing with the prior 25.0kPa increment data. This doubling seemed logical and appeared to produce consistent results. Figure 21 shows both sets of points.

The plotted data from test No.210 show two linear slope intersections, CL_1 at σ_a = 97kPa and CL_2 at σ_a = 174kPa. The matching ϵ values ≈ 0.2% and 1.1%. Similar to the interpretation used for pressuremeter tests, the writer has labeled the resulting 0 to CL_1 slope as "Elastic", CL_1 to CL_2 as "Elastic + Plastic", and greater than CL_2 as "Plastic to Failure". As discussed subsequently, the writer performed 3 more tests similar to No.210 and all produced similar CL_1 and CL_2 results.

Note that only small volume changes occurred during these 4 drained creep tests because of using constant–σ'_1 values below σ'_c. The specimens actually expanded, or swelled slightly because of the progressive reduction of σ'_3 with σ_a. The writer assumed that this swelling had a negligible effect on $\Delta\epsilon$ and the limit interpretations in Figure 21.

12.12.3 $CL_1 \approx 2\ I_{max}$

As developed in this paper, viscous plastic behavior results from the cohesive and frictional shear components that mobilize as particles slide along their AWL contacts. This sliding produces creep. Assuming negligible bonding in the machine extruded specimens used for the Figure 9 tests, the creep should occur in conjunction with the AWL **I** to Φ'_β component transfer behavior. Figure 9(b) shows that it does.

At the CL_1 strain of 0.2% in duplicate test No. 210 in Figure 21, **I** in test 219 in Figure 9(b) has reached an $\mathbf{I}_{max}$ shear of 50 kPa with an approximate compressive strength mobilization of 2 $\mathbf{I}_{max}$ = 100kPa. Thus, the above CL_1 = 97kPa closely matches that expected from only the **I** component. All the stress controlled tests in this 4-test creep study produced similar CL_1 values of 97 to 100kPa.

12.12.4 Elastic I_{max}

Section 12.10.3 has already discussed lab anisotropic consolidation and field surcharge test results as part of the discussion of Figure 20. The results indicate a $u_e \approx 0$, low volume change, pseudo-elastic behavior during the mobilization of the **I** component of shear. The previous 12.12.3 also suggests an elastic mobilization of $\mathbf{I}_{max}$ before starting significant compressive creep.

The destructuring or yielding of a clay during creep occurs in association with the viscous transfer from the unstable AWL components, $\mathbf{I}_c$ and $\mathbf{I}_\alpha$, to the stable $\mathbf{I}_b$ and Φ'_β components. The lack of significant creep from σ_a = 0 to $\mathbf{I}_{max}$ may also indicate the lack of significant transfer until after **I** mobilizes to $\mathbf{I}_{max}$. Many (Figs. 4, 5, 9, 11, 12, 13) of the 2-specimen, strain controlled, **IDS**-tests in Schmertmann (1962) show a very similar **I** and Φ'_β (then called c_ϵ and Φ_ϵ) versus strain behavior when compared to the results presented in Figure 9. After $\mathbf{I}_{max}$, and with continuing strain, one again sees a noticeable transfer from **I** to Φ'_β. In hindsight these 1962 tests already showed that the transfer may occur only after **I** reaches $\mathbf{I}_{max}$ and thus further support the concept of its pseudo-elastic mobilization.

12.12.5 (CL_1/CL_2) Creep Ratio

Prandtl's solution for the plane strain, bearing capacity problem on a weightless, frictionless soil, and which assumes ideal [(elastic + (elastic + plastic)] shear behavior, gives the ratio of [(elastic loading to the beginning of plastic shear along the failure surface)/(failure by plastic shear along the entire surface)] = [$\pi/(\pi+2)$] = 0.61. The same ratio from test No. 210 in Figure 21, (CL_1/CL_2) = (97kPa/174kPa) = 0.56, and (100/156) = 0.64 in a duplicate test No. 219 (not shown). The two tests averaged 0.60 versus the theoretical 0.61.

The above close agreement between elastic-plastic bearing theory and creep behavior supports the concept that CL_1 indicates a transition from elastic deformation to (elastic + plastic)

creep, and that CL_2 indicates the transition to a fully plastic creep failure in kaolinite clay.

Tests 210 and 219 had an isotropic (σ'_C/σ'_1) = OCR = (350kPa/330kPa) = 1.06. Two additional very similar tests, but with constant σ'_1 = 260kPa and an OCR of 1.35, both had $(CL_1/CL_2) \approx 0.73$. The above 0.60 versus 0.73 suggests that (CL_1/CL_2) increases with OCR and therefore this kaolinite clay behaved more elastically with increasing OCR and follows this general experience with almost all clays.

12.13 Drained and Undrained Shear Components

Laboratory research and field design methods for clay often differentiate between two ideal extreme drainage conditions—completely drained or undrained. In saturated soils the former permits volume change but no significant excess pore pressure, u_e, and the latter permits no significant volume change and the development of u_e. One can easily model these extremes in the laboratory by simply turning a drainage valve between open and closed. In the field the drainage always occurs somewhere between the extremes. However, for **IDS**-testing and shear component determinations the presence or absence of u_e does not matter. As shown below, only effective stress matters.

No back Pressure Effect: Numerous **IDS**-tests with and without back pressure of various magnitudes, but with the same effective stresses, showed no difference in the shear components and their mobilization with strain.

Same Drained and Undrained Test Results: The drained tests discussed herein in detail involved controlling pore pressure to match σ_a and thereby keeping σ'_1 constant. They produced the narrow range in Φ'_α and $\mathbf{I}_c$ values shown in Figures 13 and 15 and in Schmertmann (1976, Fig. 12). Undrained tests, as shown in Schmertmann (1976, Figs. 17, 18, 19), produce similar Φ'_α and $\mathbf{I}_c$ values.

With undrained tests one curve hops between two values of constant volume, measures u_e, and analyzes the results in terms of effective stress using the same method as in Figure 1. However, the undrained tests may have less accuracy in the component separations because one can usually measure an independently imposed pore pressure more accurately than the u_e developed in response to stress and strain in an undrained test.

Same Φ'_α to Φ'_β Creep Transfer: Section **8.1** and the associated references described some undrained, stress controlled, creep and **IDS**-test experiments by Bea. They showed a transfer from Φ'_α to Φ'_β during undrained creep. Section **12.12** just demonstrated and discussed the same transfer during drained creep. Qualitatively, both show the same time-transfer in the Φ'_α to Φ'_β friction components. However, the strain rate and magnitude of transfer may, or may not, differ significantly because effective stresses change more rapidly in undrained tests due to the uncontrolled u_e.

13. SUMMARY COMMENTS AND CONCLUSIONS

This research focused on determining the more fundamental engineering components of shear resistance in clays and their relation to strain, structure and time. The writer used the simplest suitable tools and model available at the time, namely the M-C model and the axisymmetric triaxial test. The following results, as developed herein, support this simple approach and should provide a significant step forward in understanding the engineering shear behavior of clay.

13.1 As explained and demonstrated herein, the **IDS**-test provides data for the more fundamental evaluation of the Mohr-Coulomb shear components of soils, including clays. Its use also permits investigating **the important effects of strain, strain-rate and time**.

13.2 A strain-controlled, **IDS**-test on a single specimen of extruded clay mobilizes two distinct groups of components of shear resistance, namely **I** and **D**.

13.3 All test comparisons show that the $\mathbf{I}_\alpha$ part of the **I** 'nominal cohesion' component varies linearly with effective stress. $\mathbf{I}_\alpha$ therefore does not behave as a cohesion but **instead behaves as an engineering friction**, denoted Φ'_α with $\mathbf{I}_\alpha = \sigma' \tan \Phi'_\alpha$. This Φ'_α presents an apparent paradox, compounded by its insensitivity to interlocking, void ratio and OC, plus its transient and plastic behavior, all of which the writer explains by the behavior of

the adsorbed water layer (AWL). Additional data relating Φ'_{α} to grain size, $\Phi'_{residual}$, secondary consolidation, creep, G_o, and p_{ca} provide additional support for this explanation.

13.4 The results from this study support the concept of two dominant clay friction components – a "secondary", viscous Φ'_{α} due to lubricated sliding in the adsorbed water layers, and a "primary" stable Φ'_{β} due to particle geometrical interference effects. The two frictions behave very differently with respect to interlocking and dilatancy, and stress, strain and time paths.

13.5 Linear Mohr envelope extrapolations to the origin determine the intercept $\mathbf{I}_c$ when constructing the envelope at constant strain. $\mathbf{I}_c$ measures a real cohesion in extruded (severely remolded) clays, as confirmed by triaxial effective stress tension and stress-dilatancy tests of the kaolinite. $\mathbf{I} = \mathbf{I}_c + \mathbf{I}_{\alpha}$ and therefore includes both engineering cohesion and friction.

13.6 $\mathbf{I}_c$ behaves plastically when $\epsilon \geq 0.5\%$ and therefore also seems to result from viscous AWL behavior.

13.7 Overconsolidation does not produce a significant change in the **I**-component at a given effective stress and strain. It does increase the **D**-component [σ' tan ($\Phi'' \approx \Phi'_{\beta}$)] and **D** mobilizes earlier with strain as the OCR increases. OC, at a given strain, increases the "primary" Φ'_{β} but not the "secondary" Φ'_{α}.

13.8 The writer found important component time effects in both the shear and the related consolidation behavior of clays. He believes these effects result from the viscous-transient shear behavior of the particle boundary adsorbed water layer and from the more brittle cohesive bonds that can form with time.

13.9 Important differences in the measured values of the components can occur as a result of stress control testing with rest times versus the often more convenient constant strain rate control testing. The component time transfer effects may not occur during strain control or they may occur much more slowly.

13.10 Creep at strains less than residual can produce an important increase in the Φ'_{β} capability of a clay. The soil structure changes that accompany such creep also produce an increase in the shear resistance of a clay mobilized at the same strain after creep versus without the prior creep. This can occur in both drained and undrained creep provided the clay structure and/or time available permits Φ'_{β} to increase.

13.11 If Φ'_{β} can increase, stress-controlled creep with time intervals of rest can provide a reserve strength increase of at least 10% at the same additional strain in the tests described herein. For the creep associated with K_o anisotropic normal consolidation, this increase may = 50% or more.

13.12 The more stable clay friction component that does not appear to have transient decay in this research, Φ'', which $\approx \Phi'_{\beta}$, seems to result from particle geometrical interference effects as shown, at a given **IDS**-test strain, by its increase with reduced void ratio, drained and undrained creep, OC and interlocking, and (from references) a more deflocculated/dispersed structure.

13.13 The formation of bonds can inhibit the low strain mobilization of the particle interference Φ'_{β}.

13.14 The **I**-component appears to mobilize elastically and may require full mobilization before the Φ'_{α} to Φ'_{β} clay structure's stability transfer and plastic creep begin.

13.15 The shear components and their mobilization depend on effective stress and time, and not on whether one tests the specimen drained or undrained.

13.16 The thirteen practical concepts discussed herein show how component behavior can help to explain the causes of residual shear, secondary consolidation, secondary shear, ageing preconsolidation, an applicability to silts, sands, and partially saturated soils, undrained strength insensitive to effective stress, very viscous AWL behavior in the small strain shear modulus, the use of Φ'_{β} when determining K_o, different types of consolidation, Burland's ICL, the minimum surcharge ratio for effective drainage aids, failure planes and slickensides, creep, and the similarity between the drained and undrained shear components.

14. ACKNOWLEDGEMENTS

The writer received important encouragement to pursue his shear strength investigations from Drs.

Jorj Osterberg, Frank Richart Jr. and Karl Terzaghi, but especially from Laurits Bjerrum, the first Director of the Norwegian Geotechnical Institute. Dr. Bjerrum arranged with Arild Andresen of Geonor Inc. for the University of Florida to purchase the high quality triaxial test equipment that made the research possible, provided the opportunity for a 1962-3 postdoctoral fellowship at the NGI, as well as guidance by personal conversations and correspondence. Many students contributed by their research, including Robert Bea, John Hall Jr., KumHung Ho, Helle Strømann and Anne Topshøj. William Whitehead contributed important engineering technician support. Financial support came from three research grants and a post-doctoral fellowship from The National Science Foundation, all supplemented generously by the University of Florida Engineering Experiment Station. Neil Schmertmann helped prepare large spreadsheets of **IDS**-test data and performed the analyses involved to prepare Figures 2, 3 and 5. Michael Ahrens of Loadtest, Inc. also helped with these figures. Suzanne Turner, also from Loadtest, Inc., provided word processing and figure preparation assistance.

15. REFERENCES

Anderson, D. G. and F. E. Richart, Jr. 1974, "Temperature Effect on Shear Wave Velocity in Clays", Technical Note, ASCE Journal of Geotechnical Engineering Division, V100, GT12, pp. 1316-1320. Also in ASCE, GSP 1, p. 16 and GSP 118, p. 1603.

Anderson, D. G. and R. D. Woods 1976, "Time-Dependent Increase in Shear Modulus of Clay", ASCE Journal of the Geotechnical Engineering Division, V102, GT5, May, pp. 525-537.

Bea, R. G. 1960, An experimental study of cohesion and friction during creep in saturated clay. Master's thesis to the University of Florida, 107 pp., published in part by Bea (1963).

Bea, R. G. 1963, Discussion on: Wu, T. H., A. G. Douglas and R. D. Goughmour: Friction and cohesion of saturated clays. A summary of Bea 1960. American Society of Civil Engineers, Journal of the Soil Mechanics and Foundations Division, Vol. 89, No. SM1, pp. 268-277.

Bishop, A. W. and V. K. Garga 1969, "Drained tension tests on London clay", Geotechnique, Vol. XIX, No. 2, pp. 309-313.

Bjerrum, L. 1967a, "Engineering geology of Norwegian normally consolidated clays as related to settlements of buildings", Geotechnique, Vol. 17, pp. 81-118. The 7th Rankine Lecture, reprinted in NGI Publication Nr. 71.

Bjerrum, L. 1967b, "Progressive Failure in Slopes of Overconsolidated Plastic Clay and Clay Shales", The 3rd Terzaghi Lecture, ASCE, JSMFD V93, Part 1, p.16

Bjerrum, L. 1972, "Embankments on Soft Ground", ASCE Proceedings of the Specialty Conference on PERFORMANCE OF EARTH AND EARTH-SUPPORTED STRUCTURES, Vol. II, p. 20.

Bjerrum, L. 1973, "Problems of soil mechanics and construction on soft clays.", State-of-the-art- Paper to Session IV, 8th ICSM & FE, Moscow, Vol. 3, pp. 124, 134.

Burland, J. B., 1990, "On the compressibility and shear strength of natural clays", Geotechnique, V40, 329.

Burland, J.B., Jamiolkowski, M.B., and Viggiani, C. 2009, "Leaning Tower of Pisa: Behavior after Stabilisation Works", Final Draft, to be published in the International Journal of Geoengineering Case Histories.

Casagrande, A. 1932, "The Structure of Clay and its Importance in Foundation Engineering", Journal of the Boston Society of Civil Engineers, April. Reprinted in BSCE Contributions to Soil Mechanics 1925-1940, pp. 72-125.

Casagrande, A. 1950, "Notes on the Design of Earth Dams", Journal of the Boston Society of Civil Engineers, Vol. XXXVII, October. Reprinted in BSCE Contributions to Soil Mechanics 1941-1953, pp. 231-255.

Crawford, C. B. and Burn, K. N. 1976, "Long-term settlements on sensitive clay", Laurits Bjerrum Memorial Volume, NGI, pp. 117-124.

Duncan, J. M. 1991, "The Importance of a Desiccated Crust on Clay Settlements", Soils and Foundations, Vol. 31, No., 3, p. 83.

Ellstein, A. 1992, Discussion of Schmertmann 1991, Journal of Geotechnical Engineering, ASCE, Vol. 118, No. 12, Dec., p. 2012.

Failmezger, R. and Bullock, P. 2008 "Which in-situ test should I use? - A designer's guide", paper submitted for publication by ASCE in Proceedings of Foundations Expo '09, Orlando

Hall, J. Jr. 1960, "An Experimental Study of the Effect of Anisotropical Consolidation on the Cohesion and Friction in Saturated Clay", Master of Science Thesis, University of Florida, p. 29

Hamel 2004, discussion of Mesri et. al., ASCE JGGE, May, p.545

Hansbo, S. 1973, "Influence of mobile particles in soft clay on permeability", Proceedings of the International Symposium of Soil Structure, Gothenburg, Sweden, pp. 132-135.

Hansbo, S. and Torstensson, B. A. 1977, "Geodrain and other Vertical Drain Behavior", Proceedings of the 10th ICSMFE, Tokyo, V.2., p.535.

Ho, K-H 1971, "Theoretical and Experimental Relationships between Stress Dilatancy and IDS Strength Components", University of Florida, Dept. of Civil Engineering, PhD dissertation, 230 pp., unpublished

Horn, H. M., and Deere, D. U. 1962, "Frictional characteristics of minerals", Geotechnique, Vol. 12, No. 4, pp. 319-335.

Horslev, M. J. 1961, "Physical Components of the Shear Strength of Saturated Clays", American Society of Civil Engineers Research Conference on Shear Strength of Cohesive Soils, p. 169.

Housel, W. S. 1959, "Dynamic & Static Resistance of Cohesive Soils", ASTM STP 254, pp. 22-23

Hutchinson, J.N. 1967, "The Free Degradation of London Clay Cliffs", Proceedings of the Geotechnical Conference Oslo 1967 – on Shear Strength Properties

of Natural Soils and Rocks, V.I, p.118

Kenney, T.C. 1967a, "The Influence of Mineral Composition on the Residual Strength of Natural Soils", Proceedings of the Geotechnical Conference Oslo 1967 – on Shear Strength Properties of Natural Soils and Rocks, V.I, p.129

Kenney, T.C. 1967b, "The Influence of Mineral Composition on the Residual Strength of Natural Soils", Proceedings of the Geotechnical Conference Oslo 1967 – on Shear Strength Properties of Natural Soils and Rocks, V.I, p.50

Lacasse, S., Berre, T. and Lefebvre, G. 1985, "Block sampling of sensitive clays", Proc 11th Int. Conf. on Soil Mech., San Francisco, 2, 887-892.

Lambe, T. W. 1953, "The Structure of Inorganic Soil", American Society of Civil Engineers, Proceedings, Vol. 79, Separate No. 315.

Lambe, T. W. 1958, "The Structure of Compacted Clay", ASCE Journal Soil Mechanics and Foundation Division, V. 84, No. SM2, May.

Lambe, T. W. 1960, "A Mechanistic Picture of Shear Strength in Clay", Proceedings Research Conference on Shear Strength of Cohesive Soils, ASCE, Boulder, Colo., pp. 555-580.

Landva, A., Valsangkar, A. J. and Alkins, J. C. 1988, "Performance of a Raft Foundation Supporting a Multistory Structure", Canadian Geotechnical Journal, Feb., see Figure 2, p. 140.

Landva, A. 2006, "A closer look at K_o=sin Φ′ " 59th Canadian Geotechnical Conference, Oct 1-4, Vancouver, BC, pp.291-296.

Larsson, R. 1986, "Consolidation of soft soils", Swedish Geotechnical Institute, Report No. 29, p. 81.

Leonards, G. A. 1972 discussion, ASCE, Performance of Earth and Earth-Supported Structures, Purdue Univ., VIII, p.169.

Leroueil, S. 1996, "Compressibility of Clays: Fundamental and Practical Aspects", ASCE JGE, V122, N7, July, pp. 535, 541. Also in ASCE, GSP No. 40, pp. 63-65.

Low, H-E, Phoon, K-K, Tan, T-S, Leroueil, S 2008, "Effect of soil microstructure on the compressibility of natural Singapore marine clay", Can. Geotech. J. 45, pp. 161-176

Lunne, T., T. Berre and S. Strandvik 1997, "Sample disturbance effects in soft low plastic Norwegian clay", Proceedings of the International Symposium on Recent Developments in Soil and Pavement Mechanics, Rio de Janeiro, Brazil, A. A. Balkema, Rotterdam, pp. 81-102.

Matlock, H., C. W. Fenske and R. F. Dawson 1951: "De-aired, extruded soil specimens for research and for evaluation of test procedures", American Society for Testing and Materials, Bulletin 177, October pp. 51-55.

Mayne, P.W. and Kulhawy, F.H. 1982 "K_o – OCR Relationship in Soil" J. Geotech. Eng. Div., ASCE, 108(6), 851-872.

Mesri, G., Feng, T. W., and J. M. Benak 1990, "Post-densification Penetration Resistance of Clean Sands", ASCE Journal of Geotechnical Engineering, V116, No. 7, pp. 1095-1115.

Mitchell, J. K. 1976, Fundamentals of Soil Behavior, John Wiley & Sons, Inc..

Mitchell, J. K. 1993, Fundamentals of Soil Behavior, 2nd Ed., John Wiley & Sons, Inc., pp. 366, 370.

Mitchell, J. K. 2008, "Aging of Sand – A Continuing Enigma?", 6th Intl. Conference on Case Histories in Geotechnical Engineering, Arlington, VA Aug 11-16, 2008, Paper No.SOAP 11

Morgenstern, N. R. 1967, "Shear Strength of Stiff Clays", Proceedings of the Geotechnical Conference Oslo 1967 – on Shear Strength Properties of Natural Soils and Rocks, V.I, p.67

Perkins, S. W., and M. Sjursen 2009, "Effect of cold temperatures on properties of unfrozen Troll clay", Canadian Geotechnical Journal, NOTE, V46, N12, pp. 1473-1481.

Rowe, P. W. 1957: "c_e = 0 hypothesis for normally loaded clays at equilibrium", 4th I.C.S.M. & F. E., London, Vol. 1, p. 189.

Rowe, P. W. 1962: "The stress-dilatancy relation for static equilibrium of an assembly of particles in contact", Proceedings of the Royal Society, A, Vol. 269, pp. 500-527.

Rowe, P. W., Oates, D. B. and Skermer, N. A. 1963, "The Stress-Dilatancy Performance of Two Clays", ASTM Special Publication No. 361, pp. 134-146.

Rowe, P.W.; Barden, L. and Lee, I. K. 1964 "Energy Component During the Triaxial Cell and Direct Shear Tests", Geotechnique, Vol. 14, pp. 247-261.

Schmertmann, J. H. 1962, "Comparison of one and two-specimen CFS (**IDS**) tests. American Society of Civil Engineers, Journal of the Soil Mechanics and Foundation Division, Vol. 88, No. SM6, pp. 169-205.

Schmertmann, J. H. 1963(a), Discussion on O'Neil, H. M., Direct-shear test for effective strength parameters. American Society of Civil Engineers, Journal of the Soil Mechanics and Foundations Division, Vol. 89, No. SM3, Part 1, pp. 159-161.

Schmertmann, J. H. 1963(b), Discussion of Wu. T .H., A. G. Douglas and R. D. Goughmour: "Friction and Cohesion of Saturated Clays", ASCE, JSMFD, V.89, No.SM1, pp.260-268.

Schmertmann, J. H. 1964 "Generalizing and Measuring the Hvorslev Components of Shear in Clays", ASTM STP 351, pp. 147-162. Reprinted in ASCE GeoInstitute *GSP-180,* FROM RESEARCH TO PRACTICE in GeotechnIcal Engineering honoring J. H. Schmertmann, pp. 34-44.

Schmertmann, J. H. 1976 "The Shear Behavior of Soil with Constant Structure", Laurits Bjerrum Memorial Volume, Norwegian Geotechnical Institute, Oslo, pp. 65-98.

Schmertmann, J. H. 1981, "A General Time-Related Soil Friction Increase Phenomenon", ASTM Special Technical Publication No. 740, pp. 456-484.

Schmertmann, J. H. 1983, "A Simple Question About Consolidation", ASCE Journal of Geotechnical Engineering, Technical Note, Vol. 109, No. 1, pp. 119-122. Discussions and Closure in Vol. 110, No. 5, May 1984, pp. 665-673.

Schmertmann, J. H. 1991, "Mechanical Aging of Soils (25th Terzaghi Lecture)". ASCE Journal of Geotechnical Engineering, Vol. 117, No. 9, see pp. 1308-1325.

Schmertmann, J. H. 1993, "Update on the Mechanical Aging of Soils (25th Terzaghi Lecture)", Symposium,

titled "Sobre Envejecimiento de Suelos", sponsored by The Mexican Society of Soil Mechanics, Mexico City, 26 Aug 93.

Schmertmann, J. H. 2003, Discussion of "Yielding from Field Behavior and its Influence on Oil Tank Settlements" by Riccardo Berardi and Renato Lancellotta, JGGE, Vol. 129, No. 5, p. 481.

Schmertmann, J. H. and Hall, J. R. Jr. 1961: "Cohesion after non-isotropic consolidation", American Society of Civil Engineers, Transactions, Vol. 128, Part I, pp. 949-981. Also publ. in A.S.C.E. as Proceedings Paper 2881, Journal of the Soil Mechanics and Foundation Division, Aug., 1961.

Schmertmann, J. H. and Osterberg, J. O. 1960. "An experimental study of the development of cohesion and friction with axial strain in saturated cohesive soils", Proceedings Research Conference on Shear Strength of Cohesive Soils, ASCE, Boulder, Colo., 643-694

Schofield, A., 1999, "A Note on Taylor's Interlocking and Terzaghi's "True Cohesion" Error", Geotechnical News, V. 17, N4, December

Schofield, A., 2005, "Interlocking, and Peak and Design Strengths", Geotechnique, Letter to the Editor, Vol. 56, No. 5, pp. 357-358.

Schofield, A. and Wroth, P. 1968, Critical state soil mechanics, McGraw-Hill Book Company, 310pp.

Skempton, A.W. 1953, "The colloidal 'activity' of clays", Proc. 3rd Int. Conf. Soil Mechanics, Zurich, V. 1, pp. 57-61. Reprinted in Selected Papers on Soil Mechanics by A. W. Skempton, F.R.S., Tomas Telford Ltd., London, 1984.

Skempton, A.W. 1961, "Effective Stress in soils, Concrete and Rocks", in Pore pressure and suction in soils, Butterworths, London, pp. 4-16. Reprinted in Selected Papers on Soil Mechanics by A.W. Skempton, F.R.S., Thomas Telford Ltd., London, 1984, pp. 106-118.

Skempton, A. W. 1970, "The consolidation of clays by gravitational compaction", Q. J. Geol. Soc. Lond., V 125, pp. 373-412. Reprinted in Selected Papers on Soil Mechanics by A. W.

Smith, R.E., Jahangir, M.E., Rinker, W.C., 2006, "Selection of Design Strengths for Overconsolidated Clays and Clay Shales", 40th Symposium on Engineering Geology and Geotechnica Engineering, Utah State University, Logan, UT, May 24-26.

Soydemir, C. 1984, (Discussion, see Schmertmann, 1983)

Stoll, M.U.W. 1961, Discussion, Proc. 5th ICSMFE, Paris, Vol. III, pp. 279-281

Strømann, H. 1971, "Laboratory Test Techniques for Determining the Constant-Structure Envelopes of Soils", MSCE Thesis, University of Florida, 136 pp., unpublished.

Taylor, D.W. 1942, "Research on consolidation of clays" Serial 82, Massachusetts Inst. of Technol., Cambridge, Mass., 147 pp.

Taylor, D.W. 1948, Fundamentals of Soil Mechanics, John Wiley & Sons, 700 pp.

Terzaghi, K. 1920, "New Facts About Surface Friction", The Physical Review, N.S., Vol. XVI, No. 1, July. Reprinted in From Theory to Practice in Soil Mechanics, Selections of the writing of Karl Terzaghi, 1960, John Wiley & Sons, p. 165.

Terzaghi, K. 1931, "The Static Rigidity of Clays", Journal of Rheology, Vol. 2, No. 3

Terzaghi, K. 1941a. "Undisturbed Clay Samples and Undisturbed Clays". Journal of the Boston Society of Civil Engineers, Vol. xxvii, July. Reprinted in BSCE Contributions to Soil Mechanics 1941-1953, pp. 45-65.

Terzaghi, K. 1941b, "Settlement of Pile Foundations due to Secondary Compression," Proceedings of the Fourth Texas Conference on Soil Mechanics and Foundation Engineering, The University of Texas, Austin, 6pp.

Terzaghi, K. 1943, Theoretical Soil Mechanics, 5th Ed., John Wiley & Sons, p. 181.

Terzaghi, K. 1955, "Influence of Geological Factors on the Engineering Properties of Sediments", Harvard Soil Mechanics Series No. 50, Reprinted from ECONOMIC GEOLOGY 15th Anniversary Volume pp. 557-618

Terzaghi, K., Peck, R.B. and Mesri, G. 1996, Soil Mechanics in Engineering Practice, 3rd Ed., John Wiley & Sons, p. 147.

Tiwari, B., Brandon, T.L., Hideaki, M., and Gyanu R.T. 2005, "Comparison of Residual Shear Strengths from Back Analysis and Ring Shear Tests on Undisturbed and Remolded Specimens", ASCE JGGE, September, p. 1071

Topshøj, A. G. 1970, "Bond strength of extruded Kaolinite by triaxial extension testing", MSCE Thesis, University of Florida, 84 pp., unpublished.

16. NOTATION

The writer usually explains symbols and other notation when they first appear. This paper uses kPa for all stresses, as transferred from original kg/cm^2 units by taking 1 kg/cm^2 = 100 kPa. Thus, this paper has a uniform +2% error in the stresses reported herein, which the writer assumed negligible for the purposes of the paper.

A = total shear plane area per contact a
AWL = adsorbed water layer (also double layer, boundary water layer, etc.)
a = contact area of adsorbed layers between particles wherein the layers do not transmit pore pressures
BBC = Boston blue clay
C = Centigrade
C_c = "primary" consolidation $\Delta e/\Delta \log \sigma'$
C_α = "secondary" consolidation $\Delta e/\Delta \log t$
c′ = cohesion intercept from the τ_t versus σ'_t Mohr envelope
c'_{res} = c′ from non-**IDS** residual shear tests
CLI = Constant Load Increment
CRS = Constant Rate of Strain
CSME = Constant Structure Mohr Envelope developed in Schmertmann (1976, pp.65,76)
CSSM = Critical State Soil Mechanics
D = slope component from an **IDS**-test
d = days
d_{10} = particle size with 10% smaller particles, by weight
E = Young's modulus in axial compression

e = void ratio
e_i = Initial e of specimen
e_f = final e of specimen
e_{LL} = void ratio at liquid limit
G = shear modulus
G_o = dynamic low strain shear modulus
h = hours
IDS-test = triaxial test (in this paper) that determines the **I** and **D** components as functions of **S**tructure and **S**train. Called the CFS-test before 1964.
I = Intercept component from an **IDS**-test when σ′ = 0, extrapolated
$\mathbf{I}_b$ = part of **I** due to relatively brittle, non-viscous bonds
$\mathbf{I}_c$ = part of **I** due to plastic cohesion
$\mathbf{I}_m$ = maximum value of **I** in an **IDS**-test (Fig. 1d)
$\mathbf{I}_o$ = shear at σ′ = 0 from Topshøj's (1970) tension tests, or from Strømann's (1971) relaxation tests
$\mathbf{I}_t$ = **I** on plane of "t"
$\mathbf{I}_\alpha$ = part of **I** due to $\Phi'_\alpha = \sigma' \tan \Phi'_\alpha$
ICL = intrinsic consolidation line
JSC = Jacksonville sandy clay
K = $(\sigma'_{3c}/\sigma'_{1c})$
K_o = K during one dimensional consolidation
kPa = kiloPascals
k_v = coefficient of permeability (hydraulic conductivity) in vertical direction
LWC = Lake Wauburg Clay
M-C = Mohr-Coulomb
min = minutes
N_G = Normalized increase in G_O with time (p.34)
NC = normally consolidated
NGI = Norwegian Geotechnical Institute
OC = overconsolidated
OCR = overconsolidation ratio = σ'_c/σ'_{cu}, not including additional OC due to reduced σ'_1 during an **IDS**-test.
p = normal consolidation pressure
p_0 = p due to overburden
p_c = preconsolidation pressure
p_{ca} = additional p_c due to ageing
PI = plasticity index (%)
q_c = Terzaghi's (1941b) critical pressure
q_u = unconfined compressive strength
R^2 = a statistical measure of the accuracy of a curve fit through data
R_s = surcharge ratio (eqn. 7)
R_{smin} = minimum R_s for effective drains
S = Clay structure, including changes due to strain
S_a = the shear force transmitted per contact area a
s_u = undrained shear strength
t = point of tangency in an **IDS**-test (Fig. 1c), time
t_{100} = isotropic consolidation time for ≈ 100% primary effective stress increase
U = 'undisturbed' specimen
u = pore pressure
u_e = excess hydrostatic pore pressure
w = water content (%)

Δ = change in a value
ϵ = Avg. specimen axial strain (+ compression)
$\dot{\epsilon}$ = time rate of ϵ
Φ = friction angle
Φ' = Φ from the effective stress Mohr envelope used herein and mobilized at constant ϵ with $\dot{\epsilon}$ approximately constant
Φ'_μ = sliding friction
Φ'_{creep} = the back calculated drained friction during creep with c′ = 0
Φ'_g = geometrical interference friction, = Φ'_β and ≈ Φ'' as developed herein
$\Phi''_{residual}$ (or Φ'_{res}) = minimum Φ' at very high shear strain
Φ'' = the part of Φ' from the **D**-component, at a given structure in an **IDS**-test
Φ'_α = the part of Φ' from the **I**-component (Eqn. 2), also referred to as "secondary shear"
Φ'_β = the part of Φ' from the **D**-component ≈ Φ'', (Eqn. 3), also referred to as "primary shear"
$\Phi'_{\beta max}$ = the clay structure's current maximum Φ'_β capability
σ' = normal stress, all stresses effective
σ'_c = isotropic consolidation stress
σ'_{cu} = unloaded σ'_c
$\overline{\sigma}_o$ = octahedral normal effective stress
σ'_1 = major principal stress
σ'_{1h} = high value in **IDS**-test (Fig 1c)
σ'_{1l} = lower value in **IDS**-test (Fig 1c)
σ'_3 = minor principal stress
σ'_t = normal stress on plane of **IDS**-test tangency (Fig. 1c)
$\overline{\sigma'}_1$ = $(\sigma'_{1h} + \sigma'_{1l})/2$
σ'_{vo} = vertical effective stress before a surcharge
$\Delta\sigma'_{vs}$ = vertical stress added by surcharge
τ = mobilized shear stress
τ_t = τ on plane of "t" (Fig. 1c)
τ_{AX}, τ_{BX} = mobilized shear at ϵ_x in specimens A and B (Figs. 1a, 1b, and 1c)

ADDITION to NGI 208 Section 12.2 Secondary Consolidation and Secondary Shear

by John H. Schmertmann[1]

Introduction

A further review of more detailed results from the **IDS** testing described in the writer's paper in NGI Publication 208, and also from some additional testing not reported therein but done during the 1958-60 interval, led to some further insight into the shear component behavior in clays. As discussed in this ADDITION, these involve the effects of low hydraulic gradients, overconsolidation and anisotropic consolidation and their interactions. This leads to an important conclusion, if true, namely that K_o NC consolidation of a clay insitu will produce an inherent ageing preconsolidation p_{ca}. This adds to the evidence for p_{ca} reliability discussed in 12.3.3 and 12.10.2.2.

For convenience, the table and figure numbers continue as if added to the paper, but the section numbers continue as if part of **12.2**, plus an additional comment and conclusion **13.17**.

Consider the test results and analyses prescribed in this ADDITION as potentially important but also incomplete. The writer recommends confirmatory testing.

[1] Professor Emeritus, Dept of Civil and Coastal Engineering, University of Florida, Gainesville, FL 32611, email: schmert@ufl.edu. Please send discussions to the NGI at ngi@ngi.no.

TABLE OF CONTENTS

Page

12.2.1 Additional data indicating lower permeability k_v during secondary consolidation C_α

The writer supervised two laboratory research projects preliminary to the subsequent **IDS**-test research discussed in NGI 208. MacFarlane (1959) performed 12 incremental (CLI) oedometer tests using extruded kaolinite. Marshall (1960) measured permeability k_v in eleven backpressured triaxial specimens of extruded kaolinite and BBC. He used 3 gradients in each, staged. These two studies provide data, that together with data from this paper and Schmertmann (1976), provide further information and support for the concept in **12.2** of high-viscosity AWL flow during secondary compression as measured by $C_\alpha=(\Delta e/\Delta \log t)$.

This support follows the following logic by showing: C_α increases with viscosity η. Knowing that the calculated k_v varies with 1/η, therefore k_v decreases with increasing η which increases C_α. C_α also increases with σ′. Therefore k_v also decreases with increasing σ′ at the low secondary consolidation gradients during C_α. Finally, k_v decreases with decreasing hydraulic gradient i. These combine to show that we likely have a lower, perhaps much lower, k_v during secondary vs. during primary consolidation.

Table 4 – Consolidation and Viscosity using different pore fluids

Fluid	η(cp)	t_{100}(min)	Δt_{sec}(min)	C_α (x10^{-3})
Dry Nitrogen gas	0.02	≈ 0	NA	≈ 0
Methyl Alcohol	0.59	40	900	3.6
Benzene	0.65	7	580	4.8
Distilled Water	1.00	150	1230	6.2
25%/glycerin 75%/water	2.10	230	1080	12.2

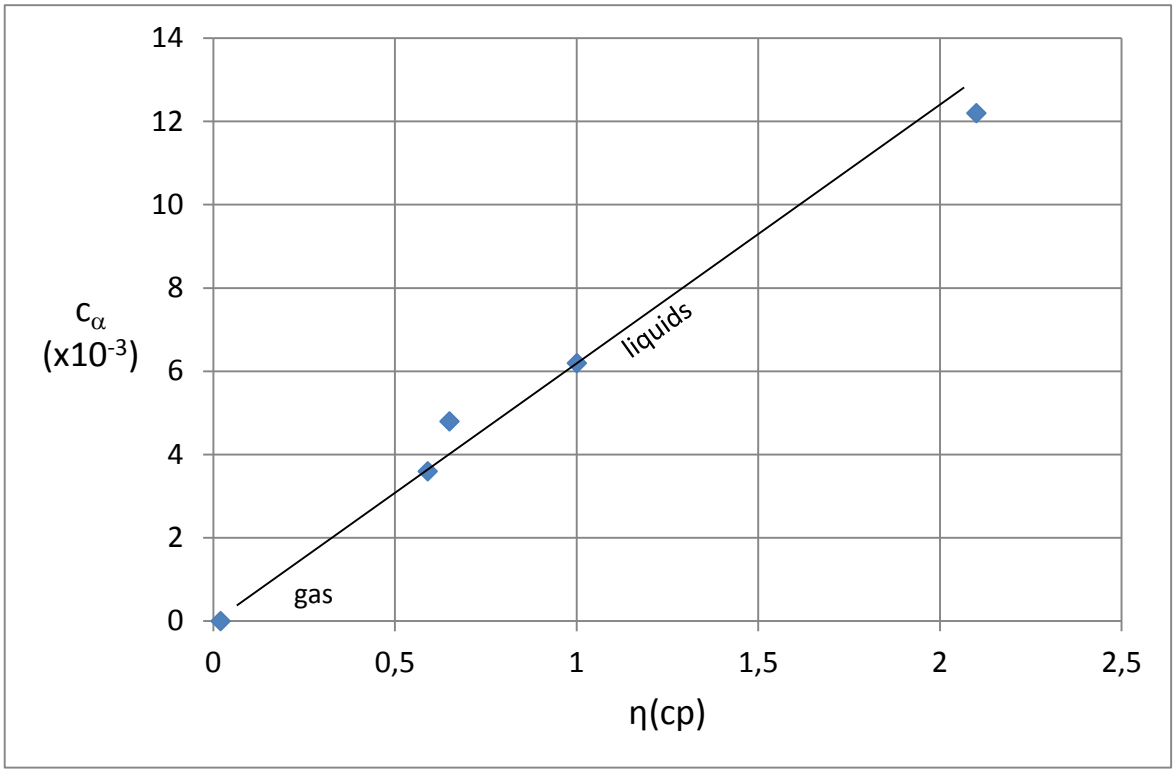

Figure 22: C_α vs. η in powdered, compacted, saturated kaolinite using the pore fluids listed in Table 1.

12.2.1.1 C_α increases with pore fluid viscosity η

Figure 10 and Table 5 in Schmertmann (1976, p.73) provide triaxial test data from an oven dried, compacted kaolinite powder then nearly saturated with five different pore fluids. One-increment isotropic consolidation to 350 kPa using the four liquids produced a primary consolidation behavior followed by secondary compression. The writer determined the transition time graphically using the semilog slope intersection, t_{100}, with the semilog slope C_α measured over a time interval Δt_{sec}. Table 4 lists the η, t_{100} and Δt_{sec} values determined for each fluid. Using dry nitrogen gas as the fluid caused a very rapid consolidation and no discernable secondary C_α. Figure 22 shows a linear fit of the C_α vs. η data passing through the origin. C_α increased approximately linearly with viscosity.

12.2.1.2 C_α increases with effective stress σ'_1 or σ'_c

MacFarlane (1959) found that one series of flocculated kaolinite (PI = 21%) oedometer tests showed C_α increasing from 3.9 to 5.0 x 10^{-3} when σ'_1 increased from 300 to 800 kPa. A similar series using deflocculated kaolinite (PI = 8%) had C_α increasing from 2.7 to 4.0 x 10^{-3} over the same increase in σ'_1.

Most of the comparative C_α vs σ'_c data from Marshall's later, more numerous specimens subjected to triaxial, isotropic consolidation to σ'_c prior to **IDS**-testing, for various reasons seem too scattered to determine trends. Unlike MacFarlane's tests, Marshall's triaxial tests did not usually have the variables controlled adequately nor the secondary volume change measurements made with sufficient precision and/or over sufficient time. However, one set of five triaxial measurements of C_α using deflocculated and then extruded BBC (PI = 11%) did show a definite trend of C_α increasing with NC σ'_c. C_α increased approximately linearly from 5.0 to 7.5 x 10^{-3} when σ'_c increased from 300 to 800 kPa, as shown in Figure 23.

Both the incremental oedometer tests and the one set of isotropic triaxial tests showed an approximate 50% increase in C_α when σ'_1 or σ'_c increased from 300 to 800 kPa.

12.2.1.3 Decreasing vertical gradient i_v decreases permeability k_v

Marshall (1960) made direct, vertical flow with backpressure, measurements of k_v using extruded triaxial specimens of flocculated and deflocculated kaolinite and BBC. He stage-tested each consolidated specimen by successively increasing σ'_c within the 150 to 700 kPa range. At each stage he imposed successive excess pore pressures of 50, 100 and 150 kPa at the top of the specimen to impose the vertical gradient to develop vertical flow and calculate k_v. For the k_v calculation he used the average flow rate into the top and out of the bottom of specimens with a length of *c.* 7.9cm, and after each rate had become constant. The average (flow-in/flow-out) ratio = 1.03. Marshall made his k_v measurements at lab temperatures of *c.* 23°C.

Figure 24 shows the normalized data points from 17 test comparisons of measured k_v at

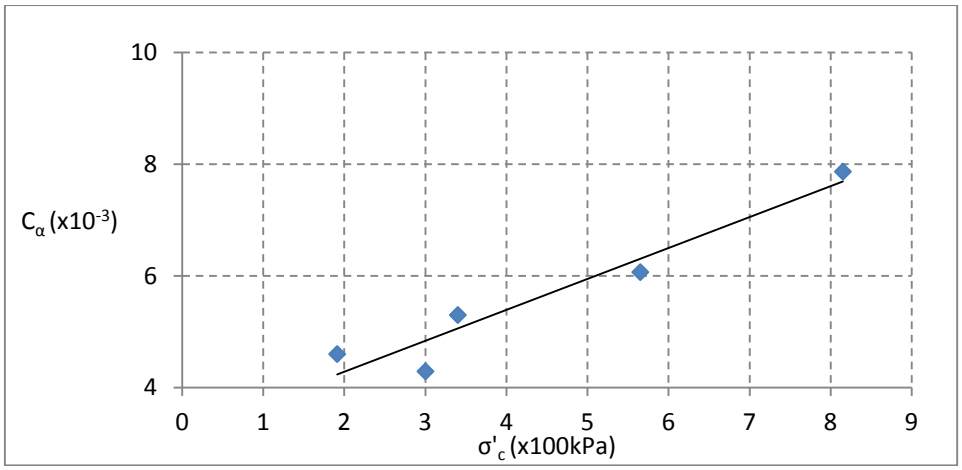

Figure 23: NC C_α vs. isotropic consolidation σ'_c of deflocculated, extruded BBC

higher gradients compared to the lowest gradient = 50x10/7.9 = 63. Marshall had 17 tests with i_v = 63, 11 tests with i_v = 126 and 6 tests with i_v = 189. Each of the two higher gradients showed a definite, but scattered, trend of (k_v/k_{v63}) decreasing with increasing (σ'_c). After gradually applying the pore pressure, and allowing time for gradient equilibrium, the average specimen σ'_1 reduced from σ'_c by 25 kPa when i_v = 63, by 50 kPa when i_v = 126, and by 75 kPa when i_v = 189. Thus the specimens had average OCRs that ranged from 150/(150-75)=2.0 to 700/(700-25)=1.04 in these tests for k_v. These OCRs did not appear important.

It remains possible that the trends shown in Figure 24 result from some unknown effects of stage testing. Marshall did not check this. At the time his results seemed reasonable to the writer and seemed to check with expectations based on unstaged testing.

The writer used the following method to estimate the trend lines in Figure 24: The average σ'_c for the eleven i_v = 126 test points = 450 kPa, and 490 kPa for the six points with i_v = 189. The solid line curve through the 3 average (k_v/k_{v63}) ratio points assumes that a value of σ'_c = 470 kPa applies to this curve. He then interpolated the data scatter to estimate the long-dash curves for σ'_c = 200 and 700 kPa. The extrapolated dotted curves show the trend of (k_v/k_{v63}) ratios for gradients less than 63.

Section 12.10.3.1, in No. 208, presented some evidence of reduced k at reduced i. The writer has seen some new lab testing evidence of reduced permeability at reduced rates of strain $\dot{\varepsilon}$ in soft clay in Santa Monica et.al. (2011, Figs. 6, 8, 11). Reduced rates of strain usually mean reduced seepage gradients (i) and therefore reduced k from this reference.

Figure 22 showed C_α ~ (proportional to) η with η ~ 1/k. Figure 23 and the associated text show that C_α ~ σ'. Therefore, k ~ 1/ σ' and should increase with a decrease in σ'. The high gradient data part of Figure 24 shows such an increase at constant gradient. The extrapolated, low gradient part shows a decrease. We have k both increasing and decreasing with σ' in the same figure. That presents something of a paradox. The writer believes the explanation, as in the No. 208 **5. Apparent Paradox**,

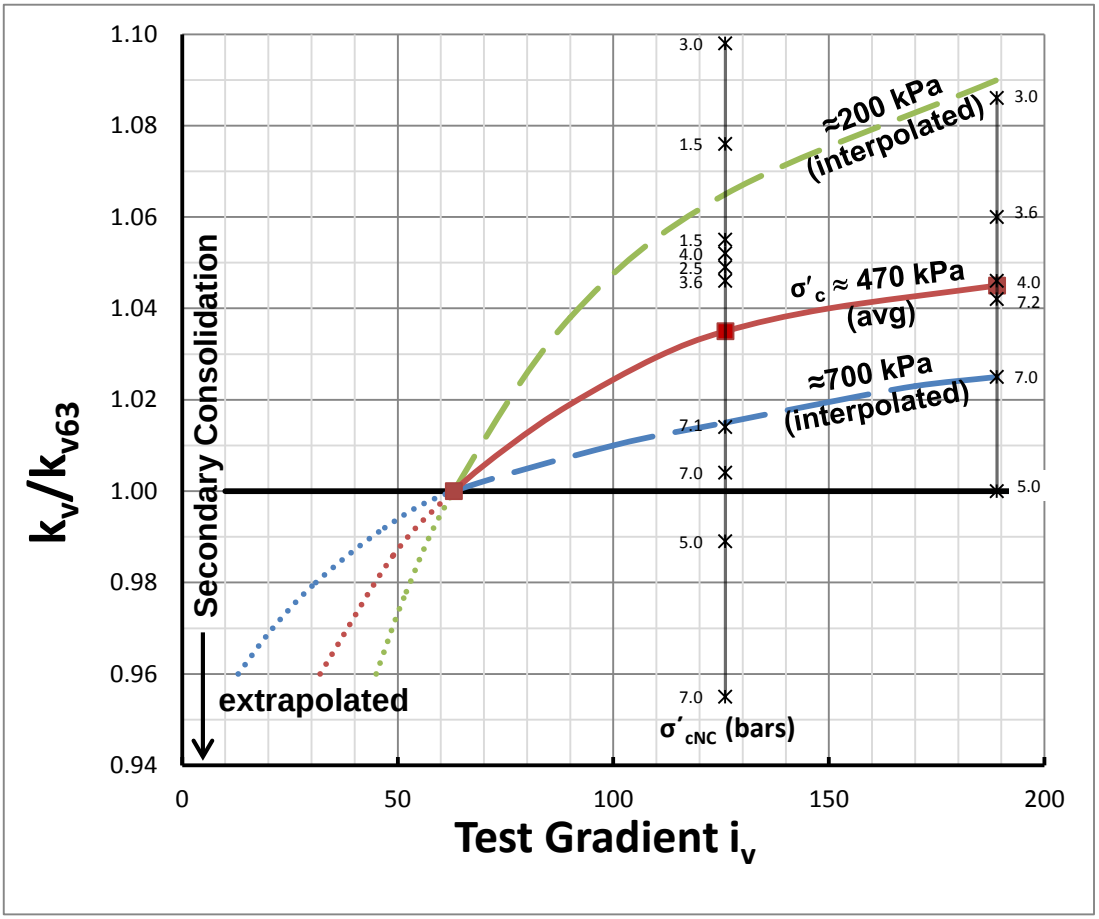

Figure 24: Normalized permeability vs. gradient in extruded kaolinite and BBC

involves the unusual behavior of the viscous, unstable parts of the **I**-component of shear resistance – $\mathbf{I}_c$ and $\mathbf{I}_\alpha$. The following explores some of this behavior and the use of the (**I**/**D**) ratio.

12.2.2 More evidence that C_α due to AWL

The following subsections provide logical steps that further support the **12.2** concept that secondary compression results from AWL behavior – namely from the time dependent transfer from the viscous **I**-component to the stable **D**-component.

12.2.2.1 Secondary consolidation C_α proportional to the I-component

Given that both the **I**-component and C_α involve viscosity, it seems reasonable that a relationship between them could exist. Figure 25 shows the available data relating the **I**-component to C_α from **IDS**-tests on NC extruded clays at an example ϵ_{IDS} = 0.5% immediately after the C_α consolidation. The points come from a mixture of data from *is*NC triaxial and K_o NC oedometer testing as well as a mixture of flocculated and dispersed kaolinite and BBC, plus one 'undisturbed' BBC denoted "U". Figure 25 therefore only gives an overall, rough guide. Assuming $C_\alpha \approx 0$ at $\mathbf{I} \approx 0$, as approximate for sands, the data suggest that C_α may vary approximately linearly with **I** in extruded clays with a constant NC σ'_1.

*12.2.2.2 The ratio of (unstable/stable) components, (**I**/**D**), decreases with Δt_{sec}*

As shown in Schmertmann (1976 Fig. 9, 1991 Fig. 38), the **D**-component increases with an increase in the immediately prior time in isotropic secondary consolidation. Because the **I**-component remains roughly constant at a constant σ'_1, the ratio of (**I**/**D**) decreases. Figure 26 includes data points from eight tests with interpolated curves that show how the (**I**/**D**) ratio decreases in kaolinite **IDS**-tests at ϵ_{IDS}=0.25, 0.50 and 1.0% as a result of increasing isotropic secondary consolidation times from 2 hours to 36 days. Although Figure 26 shows a curve maximum ϵ=1%, the 36-day test's (**I**/**D**) ratio continued to decrease to 0.4 at ϵ_{IDS}=12%, as shown by an additional point "•".

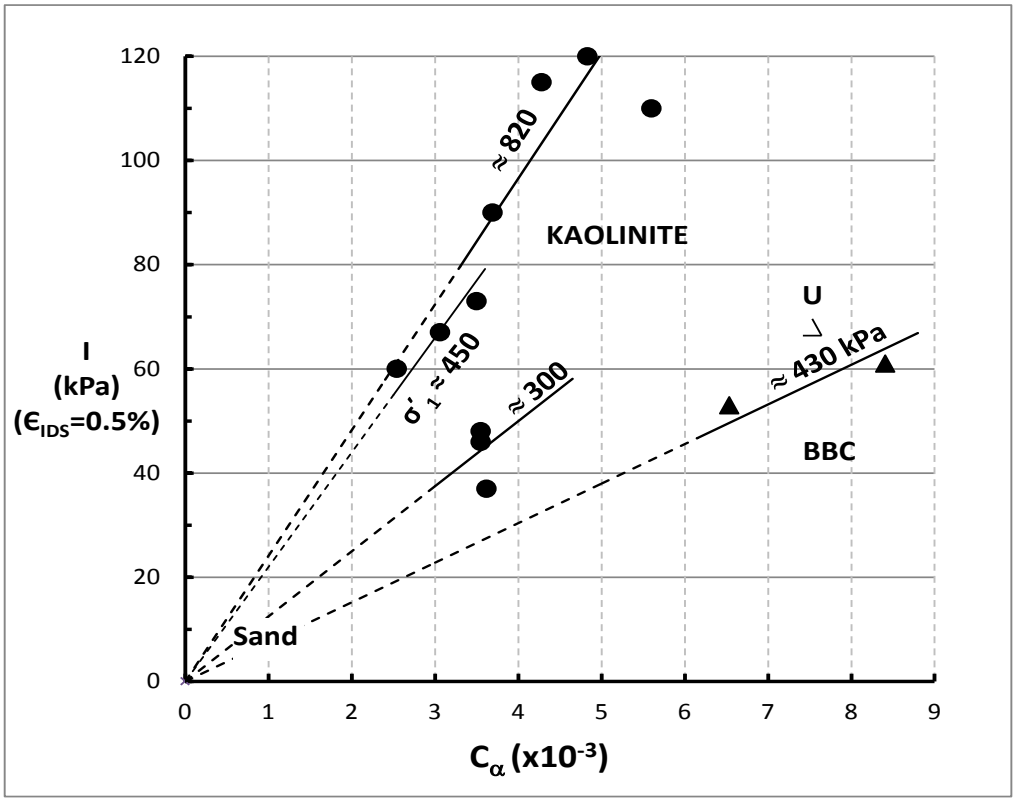

Figure 25: **I** vs. C_α data showing possibility of linear relationship for NC Clays

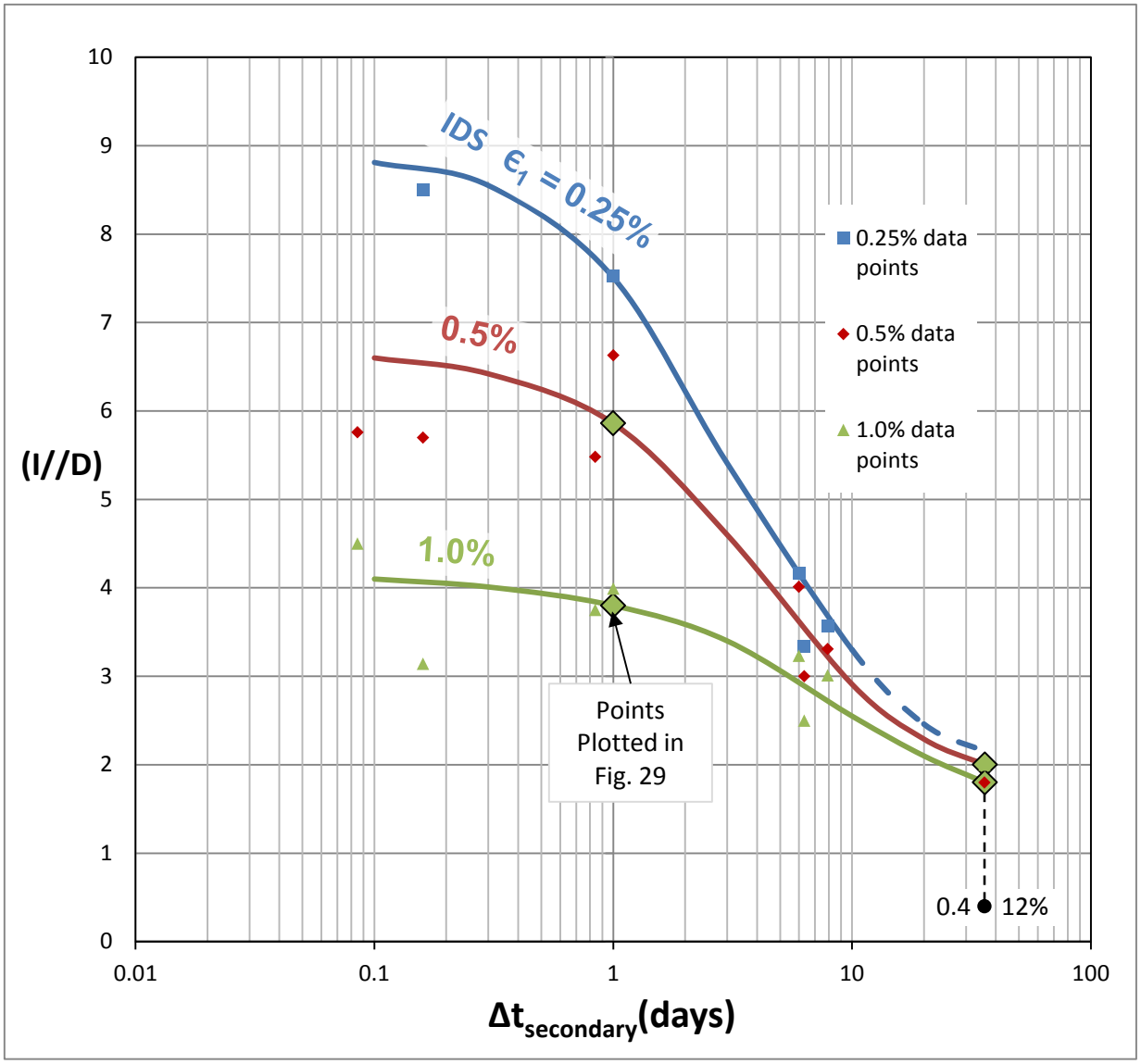

*Figure 26: Illustrating decreasing (**I/D**) during isotropic secondary consolidation in extruded kaolinite All isNC σ´c = 350 kPa*

Also note in Figure 26 that the (**I**/**D**) vs. log Δt_{sec} format shows a semi-log "S" shaped curve similar to the volume strain vs. log time curve during primary consolidation. Perhaps the rate of primary and the rate of secondary component transfers have something more fundamental in common, namely AWL behavior? Clearly the **I**-component dominates at the strains shown in this extruded, *is*NC kaolinite, with the domination reducing with secondary time Δt_{sec}.

*12.2.2.3 (**I/D**) very high at low strain in isNC clay*

Figure 27 shows, again using the (**I**/**D**) ratio, the relative mobilization of the components during **IDS**-testing after isotropic NC secondary consolidation from 50 to 500 kPa. The figure also shows the data points through which the writer estimated the σ´c curves.

The curves in Figure 27 show the (**I**/**D**) ratio rising to very high values at low strain. At a very small strain after the end of a typical lab 1 day time in secondary consolidation the shear mobilization seems overwhelmingly due to the **I**-component and therefore to AWL behavior. Increasing σ´c reduces (**I**/**D**) at all strains shown. All the extruded and assumed bondless (I_b=0) clays tested after *is*NC had (**I**/**D**) vs. strain behavior similar to that in Figures 26 and 27.

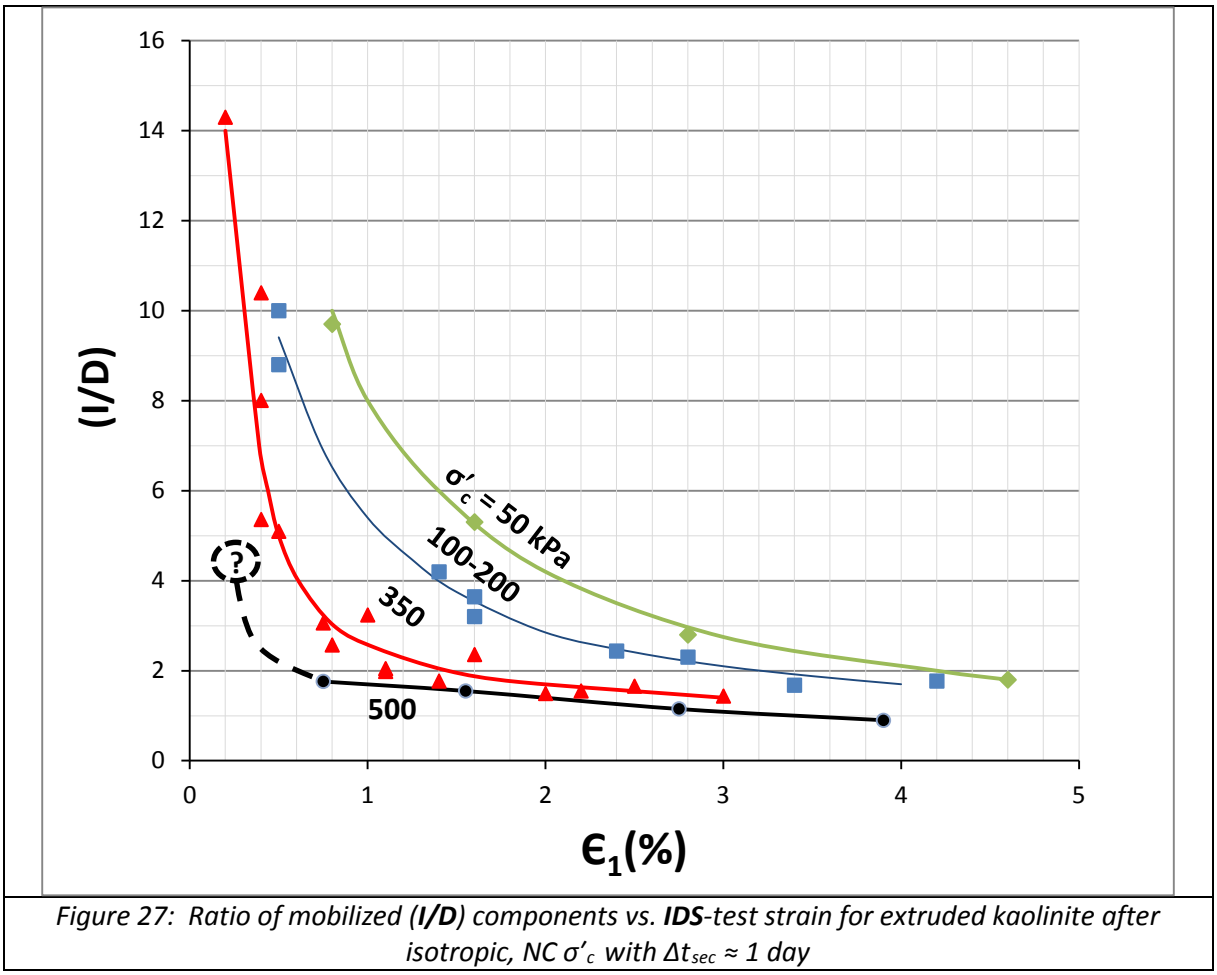

*Figure 27: Ratio of mobilized (**I/D**) components vs. **IDS**-test strain for extruded kaolinite after isotropic, NC σ'_c with $\Delta t_{sec} \approx 1$ day*

12.2.3 Similarities in Component mobilization after isotropic OC (*is*OC) and anisotropic NC (*an*NC)

The previous 12.2.1 and 12.2.2 sections considered only **IDS**-test results using isotropically NC (*is*NC) specimens. The following sections through 12.2.3.3 extend this study to include isotropic OC (*is*OC) and anisotropic NC (*an*NC) specimens.

12.2.3.1 Components and isotropic OCR

Figure 28(a) shows the results from three series of **IDS**-tests using Kaolinite. The red and blue points and lines show data from the 2 series of comparative tests in Figure 4 in #208, involving 7 tests—Series 1: Nos. 105, 107, 108, 113 at roughly constant void ratio but varying σ'_1 in red with "●" points, and Series 2: Nos. 106, 107, 109, 110 at constant σ'_1 but varying void ratio in blue with "♦" points. The black "▲" points show data extracted from an unpublished Series 3 by Hall in 1960 involving 10 *is*NC and 9 *is*OC tests that used both the above methods to obtain the OCR. All three series show approximately the same semilog-linear mobilization of the stable tan ϕ" whether producing the OC at near constant void ratio or at constant σ'_{cu}.

Section **12.7 ϕ'_β to Understand K_O** suggested that ϕ'_β may control K_{ONC} because of its stability. Figure 28(a) shows that tan ϕ", which ≈ tan ϕ'_β, at ϵ_{IDS} = 1% appears to increase linearly vs. log *is*OCR. This suggests that K_O may also increase linearly vs. log *is*OCR, as many others have shown.

Figure 28(b) shows the (**I/D**) mobilization vs. log *is*OCR from the same data as in Figure 28(a). When ϵ_{IDS}=1% this ratio decreases dramatically from roughly 4 to 1 over an OCR increase of only 1 to 1.5 and thereafter remains constant at approximately 1. It appears that even a small OCR has an important effect at ϵ_{IDS}=1%.

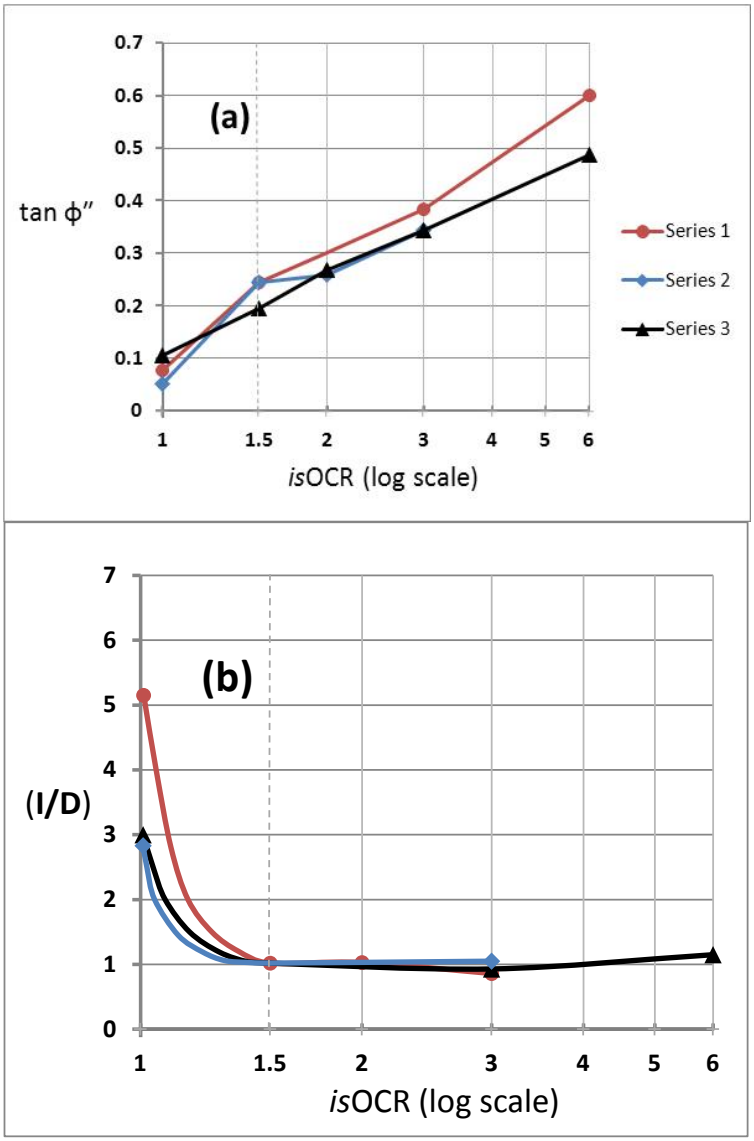

*Figure 28: Mobilized tan(φ″≈φ′$_{\theta}$) and (**I/D**) vs. log OCR in isOC extruded kaolinite at ϵ_{IDS}=1%*

12.2.3.2 Components and anisotropic NC

Figure 29 shows the comparative mobilizations of the **I/D** ratio after *is*NC, *is*OC and *an*NC at $\sigma'_1 \approx$ *350 kPa* and ϵ_{IDS}=1%. Figure 27 already showed the *is*NC mobilization and Figure 29 copies the *is*NC curve when σ'_c = 350kPa. Figure 29 also includes the Figure 28 *is*OC data for ϵ_{IDS}=0.5 to 5% (solid green dots), with interpolation lines for *is*OCR=1.5 to 2, 3 and 6.

Figure 29 also includes something new with the blue K_c data, namely the comparable component **I/D** ratios after various levels of *an*NC at nearly the same σ_1'=366 kPa as the 350 kPa for the isotropic NC and OC data. The new data come from *an*NC $(\sigma_3'/\sigma_1')_c = K_c$ = 0.83, 0.71 and the approximate K_o=0.63. As described in No. 208 Section **8.5**, and in more detail in Schmertmann and Hall (1961), the *an*NC **IDS**-tests permitted determinations of the **I** and **D** components, and hence (**I/D**), at ϵ_{IDS} = 0%.

As K_c and strain increase the extrapolated dotted line shows (**I/D**) vs. strain approaching *is*NC behavior.

12.2.3.3 The OC effect of anisotropic NC

From the comparative data in Figure 29 it appears, in terms of the (**I/D**) ratio of the (unstable/stable) mobilization of components, that decreasing K_c in *an*NC will produce an increasing OC effect. That would mean a greater mobilized shear resistance and modulus at low strain vs. *is*NC specimens despite having a lower octahedral effective stress. Figure 11 in #208 shows exactly that and the associated text notes

a mobilized shear resistance increase of 50% at ϵ_{IDS} = 0.5%. Figure 11 shows that the shear resistance will diminish to approximately the *is*NC value at a strain of 4%. This checks roughly with an imaginary projection in Figure 29 of the *an*NC K_o data to a merger at a strain of c. 3% with the *is*OCR = 1.5 to 2 line.

Figure 26 provides some support for an OC effect from *an*NC. At ϵ=1.0% and Δt_{sec}= 1 and 36 days the corresponding (**I/D**) ratios = 3.8 and 1.8 respectively. At ϵ=0.50% and Δt_{sec}= 1 and 36 days the ratios = 5.8 and 2.0 respectively. Plotting these four secondary points into Figure 29 gives the green diamond points shown. They fit roughly with the previous *is*OCR=1 and *an*NC data. Engineers already know about the OC effect of ageing in secondary consolidation. Thus the Figure 26 and 29 data also reinforce the concept that the OC effect of *an*NC seems inherent because of the similar (**I/D**) ratios developed.

No. 208 Sections **12.3 and 12.10** show that one might expect an ageing OCR = 1.2 to 2 in *an*NC insitu clays. The *anNC* $K_o \approx 0.63$ data in Figure 29 seems to approach the *is*OCR = 1.5 to 2 curve. The writer does not yet have **IDS**-test data after *an*OC but he anticipates it will look similar to the *is*OC behavior in Figure 29. If true, we may then have still another way of explaining the insitu OC of *an*NC clays. Because a decreasing **I/D** means a more stable structure, the above adds to the evidence for p_{ca} reliability given in Section 12.3.3.

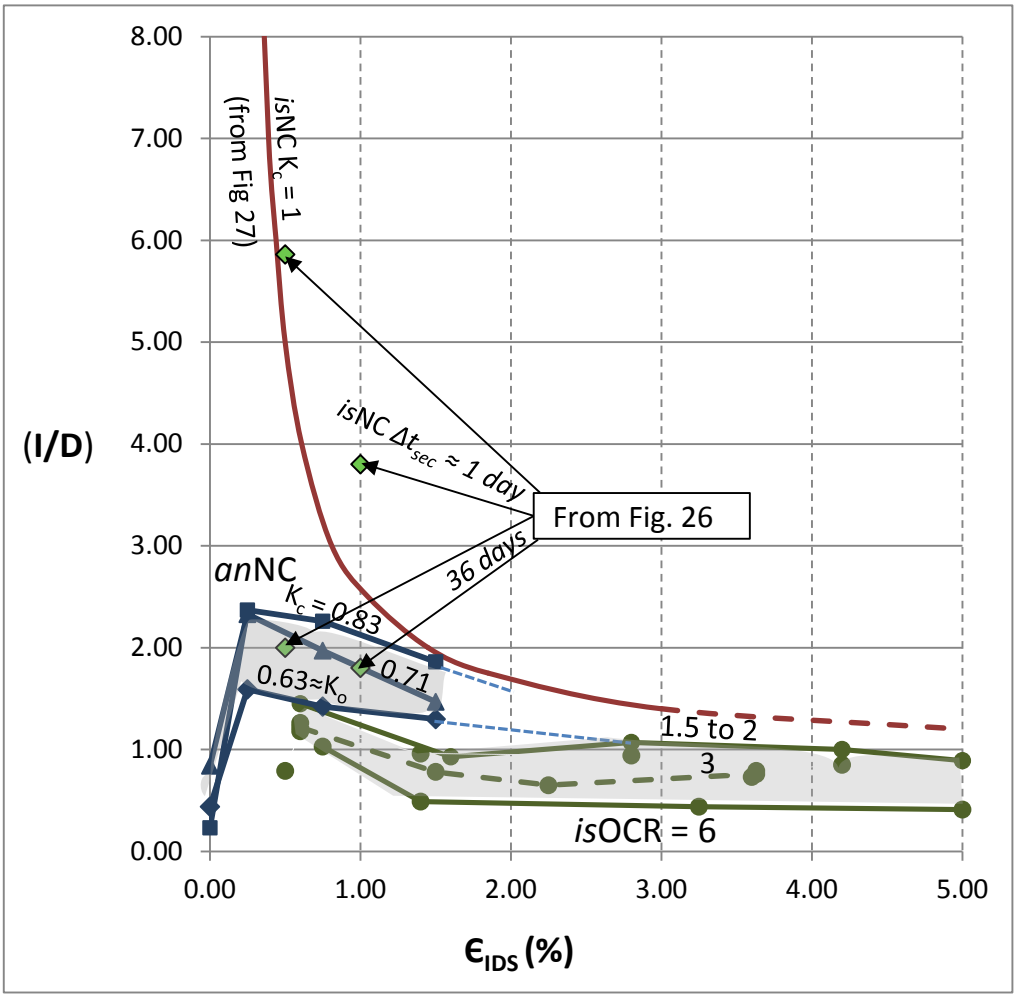

*Figure 29: Comparing component (**I/D**) vs. strain behavior in isNC, isOC and anNC extruded kaolinite*

13.17 Additional comment and conclusion

The work reported in this Addition makes further use of old experiments performed with different objectives. We now need new, more focused research to check the tentative conclusion herein, based on the more fundamental concept of the **I** and **D** components of shear resistance in clay, namely that long-time insitu anisotropic NC produces an inherent and reliable p_{ca} OC effect when increasing σ_v'.

Additional References:

MacFarlane, James W., 1959, "Effect of Structure on Secondary Compression of Kaolinite", An M.S. Thesis Presented to the Graduate Council of The University of Florida, January 1959, 67 pp.

Marshall, Peter W., 1960, "Permeability Studies on Selected Saturated Clays", A High Honors Project under a Fellowship from the National Science Foundation, University of Florida, June 1960, 37 pp.

P.E.L. de Santa Maria, I.S.M. Martins and F.C.M de Santa Maria, "Rheological behavior of soft clays" 2011, Frontiers in Offshore Geotechnics II, Gourvenec & White (eds), Taylor & Francis Group, London, ISBN: 978-0-415-58480-7

Deep Water Geotechnical Engineering

Knut H. Andersen, Tom Lunne, Tore J. Kvalstad, and Carl F. Forsberg
Norwegian Geotechnical Institute, Oslo, Norway

ABSTRACT: This paper describes geology, soil profiles and geohazards for typical deep water areas, identifies design issues, calculation procedures and required soil parameters for geotechnical design of deep water structures and slope stability evaluations, shows how geology and geohazards phenomena can be identified by geophysical and geological methods, and outlines how the required soil parameters can be determined by in situ and laboratory tests. Diagrams that can be used to preliminary estimate the required soil parameters based on simple index properties, without advanced testing on site specific soil, are also presented. The paper concentrates on clay, since clay is the predominant soil type in deep water.

1 INTRODUCTION

The oil and gas exploration and field development continuously move into deeper water. Today a significant part of the offshore field development worldwide takes place in water depths of more than 500m, like in the Gulf of Mexico, Gulf of Guinea, offshore Brazil, the North Sea, offshore Australia, the Adriatic Sea, offshore China, and the Bay of Bengal.

New production concepts are required when moving into deeper water. Fixed platforms are no longer feasible, and floating production and storage facilities and fixed subsea systems have been developed. If the distance to shore is not prohibitive, the oil and gas can be brought on land through pipelines, and all the necessary structures can be kept on the seafloor (e.g. Figure 1.1). Alternatively, a combination of subsea structures and floating structures can be used. The oil and gas are then loaded into and transported by large tankers (e.g. Figure 1.2). Floating systems require anchoring, such as suction anchors, plate anchors, drag anchors, piles, or torpedo anchors. Subsea systems require seabed support, such as plate bearing, skirted systems or piles. Flowlines are used to transport the oil and gas within the field components, and risers are needed if the oil and gas are brought from the sea floor to tankers.

In deep water areas there is also an increasing need to identify and evaluate the consequence of various geohazards, like excess pore water pressure due to rapid sedimentation, gas hydrates, shallow gas, shallow water flow, pockmarks, mud volcanoes, and salt domes. Some areas also have seismic activity and active faulting. Slope instability is an essential part of the geohazards evaluation and involves determination of the possible triggering and failure mechanism of a potential slide, slide dynamics and run out distance, forces against down slope structures, and tsunami generation.

The sediments in the deep water areas are generally soft clay that can be underconsolidated. However, over-consolidated clay can exist in areas where overburden has been removed by previous slides. Active sedimentation and erosion can also occur.

The new field development concepts require new geotechnical solutions and additional soil parameters. For instance, suction anchors involve calculation of skirt penetration resistance and capacity of skirted structures under tension, and pipelines and risers need soil parameters from the soil very close to the seabed.

The larger water depths require improved geotechnical and geophysical investigation techniques and procedures. In particular, soil sample quality may be reduced due to large stress relief when the samples are brought up to the sea surface, especially if there is dissolved gas in the pore water.

This paper (1) describes geology, soil profiles and geohazards for typical deep water areas, (2) identifies design issues, calculation procedures and required soil parameters for geotechnical design of deep water structures and slope stability evaluations, (3) shows how geology and geohazards phenomena can be identified by geophysical and geological methods, and (4) outlines how the required soil parameters can be determined by *in situ* and laboratory tests. Diagrams that can be used for preliminary estimate of the required soil parameters based on simple index properties, without advanced testing on site specific soil, are also presented. The paper concentrates on clay, since clay is the predominant soil type in deep water.

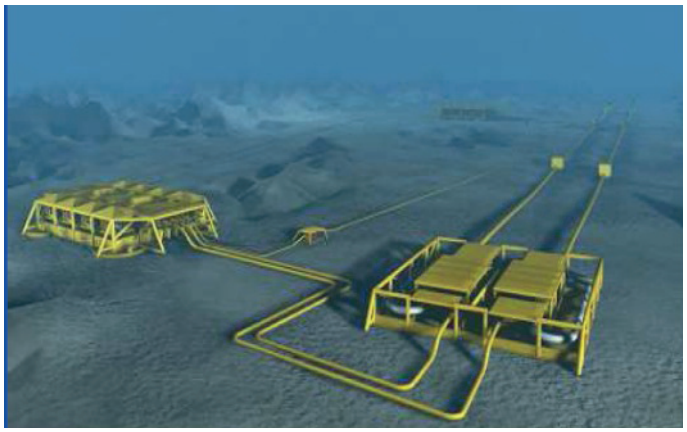

Figure 1.1 Subsea to shore layout for the Ormen Lange Field (Fausa, 2006).

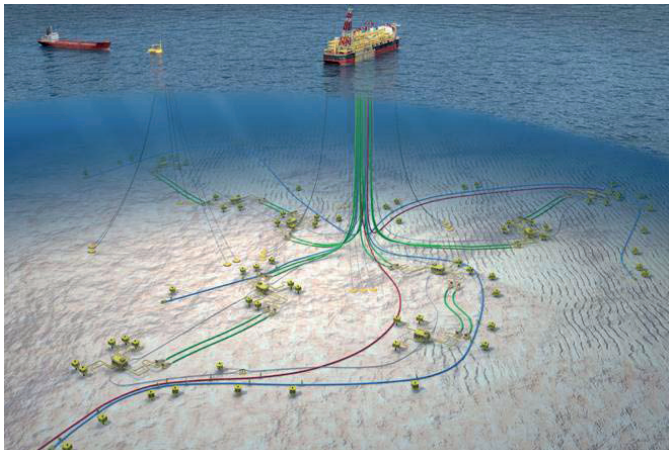

Figure 1.2 Field offshore Nigeria with floating system (Picard et al., 2007).

2 TYPICAL GEOLOGY AND SOIL PROFILES

2.1 *Geological setting*

In order to determine whether or not a soil profile is characteristic for an area, an evaluation of the geological setting can be useful. While soil profiles for specific soil types do not exhibit differences between deep and shallow water settings, there are nonetheless some considerations that mark differences between shallow and deep water. In general, there is a less energetic environment in deep water, and therefore a greater dominance of fine grained sediments as well as a greater distance to sediment sources on land, and thus a lower sedimentation rate. However, there are important exceptions to this, because many deep water areas are on the continental slope where there is extensive evidence for mass movements. Mass transport deposits (MTD) are therefore found both on the slope and on the basin floor (Posamentier and Kolla, 2003). Canyons are another characteristic of slope morphology that form the conduits for both mass transport and density currents that in turn can bring sand and gravel out to the ocean basin.

Some important aspects to consider when evaluating the geological setting are:

– Sediment supply from the hinterland, and the location of major rivers draining onto the continental margin. In areas where the distance to a sediment source is large, sedimentation can be dominated by biogenic debris from for example coral reefs or silica or calcareous plankton. The first forms calcareous deposits that may have special properties whereas the latter two form diatomaceous and calcareous oozes respectively.
– The slope configuration. How steep, are there canyons present? Is there any evidence of previous sliding?
– The presence of ocean currents, both on the shelf and especially along the slope (contour currents).
– In what way has the setting been influenced by lower sea levels (approx. -120m when glacial ice accumulated on the northern hemisphere), and how has this influenced the present morphology, e.g. inactive canyons, shelf edge deltas etc.
– Are there faults, or signs of fluid/gas flow in the area?

In the following some typical soil profiles from a few different settings will be presented in order to illustrate the relationship between setting and sediment properties.

2.2 *Soil Profiles*

Index parameters for a number of deep water sites are given in Table 7.6. There is usually nothing special about the relationships between the various index parameters and geotechnical properties for soils from different settings. However, the settings will determine soil composition and, for example, whether they are over-consolidated, normally consolidated or even "under-consolidated", as well as the variability of the soils within the area.

2.2.1 *Landslides*

Submarine landslides will have significantly different geotechnical properties inside and outside of the slide scar (Figure 2.1). Whereas the sediments on the outside have experienced normal sedimentation from before the slide event until the present, the sediments still inside the slide scar have experienced an unloading, at least those older than the slide itself. The slides outside the scar are therefore normally consolidated, whereas those inside are overconsolidated, perhaps with a drape of normally consolidated sediments that have deposited after the slide.

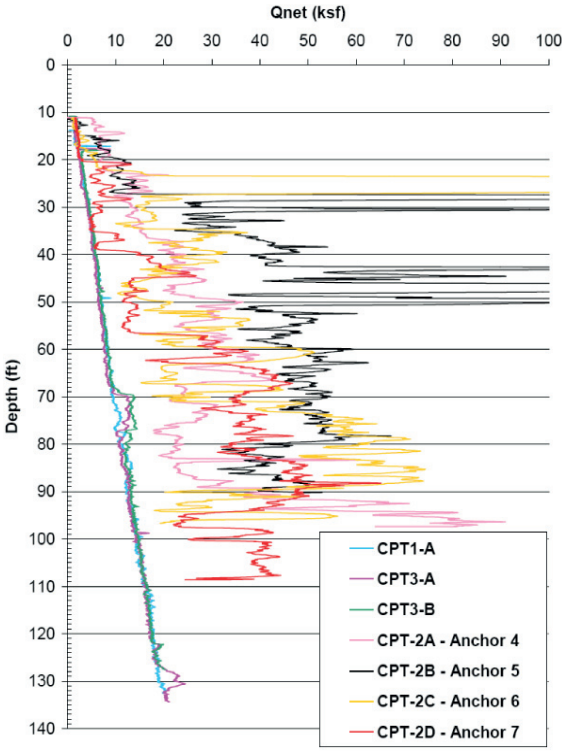

Figure 2.1. CPT results from the Mad Dog area in the Gulf of Mexico. CPT1-A, CPT3-A and CPT3-B are taken upslope from a slide scar. The rest are from inside the slide scar (from Liedtke *et al*., 2006). NB depth in ft.

2.2.2 *Cyclic sedimentation*

The Storegga slide off the Norwegian west coast is one of the largest submarine landslides discovered. It occurred in an environment characterized by repeated mega slide events, with the events occurring during interglacial periods such as the present. The preconditioning processes involved stacking of fine grained sediments deposited by ocean currents (contourites) and poorly sorted (well graded) glacial sediments (Figure 2.2). The contourites have a strain softening behaviour, whereas the glacial sediments do not. The triggering of the slide was helped by horizontal transfer to the base of the slope of excess pore water pressure caused by rapid glacial sedimentation on the neighbouring North Sea Fan. Once the slide had been triggered, strain softening focused the strain in the contourites causing these to form slip planes in a retrogressive slide. This example therefore demonstrates the possible influence of variable sediment composition, and especially the influence of strain softening and sensitivity.

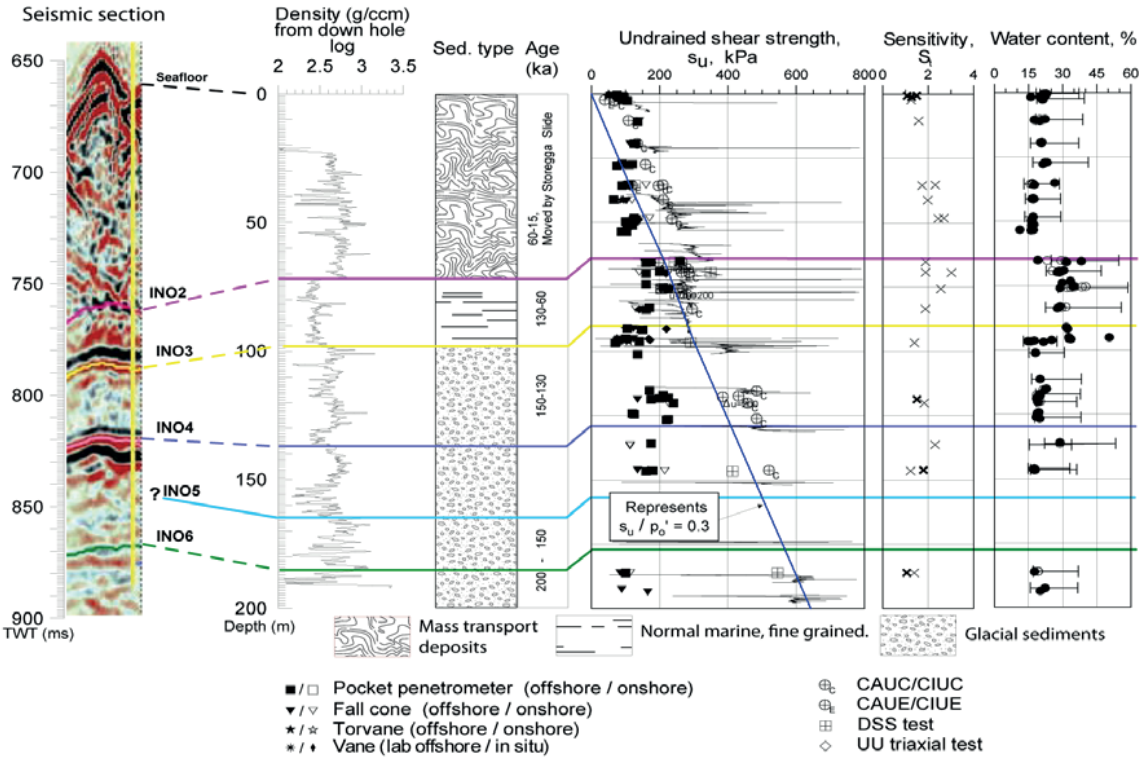

Figure 2.2. Fine grained sensitive layer below mass transport deposits has acted as a slip plane. Index tests below about 75m are not reliable due stress release during sampling. There is a mismatch of a few meters in depth between the down hole logs on the left and the borehole data on the right.

2.2.3 *High sedimentation rate*

Deltas are often sites of rapid sedimentation. The most rapid depositional rate is presently usual in relatively shallow water. The result is overpressuring, and growth faulting with thrusts perhaps developing in deep water (toe thrusts). The overpressured sediments are "under-consolidated" and thus relatively weak (Figure 2.3). Any slides occurring in shallow water will run down slope through canyons etc. and influence infrastructure situated in their path in deeper water.

The example in Figure 2.3 is from a site with a very high sedimentation rate, where the soil strength is low due to excess pore water pressure.

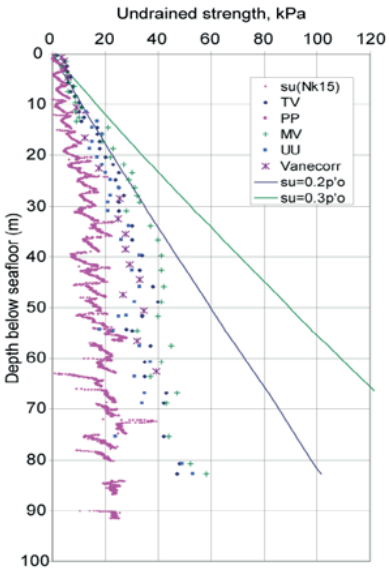

Figure 2.3. Underconsolidation as demonstrated by low shear strengths in a high sedimentation rate environment. The straight lines indicate usual limits for normally consolidated sediments.

2.2.4 *Cementation*

Cementation is part of the process of lithification that soils undergo during the rock forming process and is therefore not usually associated with deposits in the uppermost tens of metres below the seafloor. However certain settings can produce important cementation effects. The example in Figure 2.4 is from West Africa where degradation of organic matter has probably formed pyrite that cements the uppermost metre of the sediment, forming a stiffer crust that has consequences for pipeline design etc.

3 GEOHAZARDS IN DEEP WATER SITES

Deepwater sites are normally located on the continental slopes and gradually approaching the abyssal plains and in areas with thick deposits of sediments. In these areas the seafloor is often characterised by a low average slope inclination (typically less than 4°), but steep escarpments caused by previous submarine slide activity are found on many locations. Growth faulting and diapirism may alter the slope of the seabed on a local and regional basis like the salt driven Sigsbee Escarpment in the Gulf of Mexico.

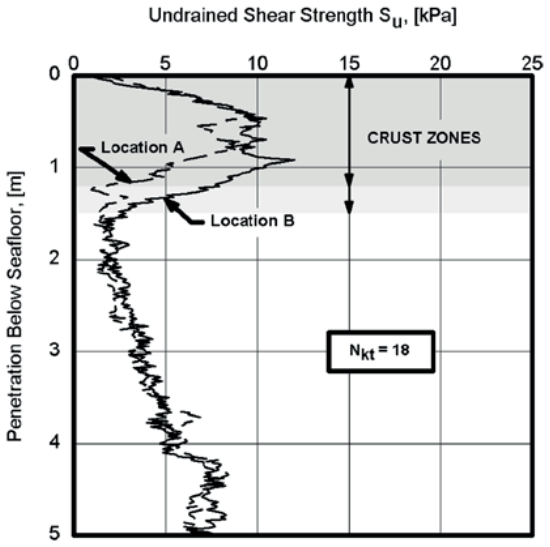

Figure 2.4. Crust-zone in sediments from deep water in the Gulf of Guinea (from Ehlers *et al*., 2005).

The density difference between salt and sediments and unevenly distributed overburden are the driving mechanisms. Salt is a viscous material with no or very low yield strength and will slowly deform and distort under shear loading, forming a rather peculiar landscape of salt domes and sediment basins (Figure 3.1). In delta areas, submarine channels or canyons starting at the shelf edge are typical, but deltas where channels cut deeply into the continental shelf area with sediment transport directly to the deeper slope and basin do also exist (Amazon, Zaire/Congo, Ganges-Bramaputra). The largest (cross sectional and incision area) submarine channel identified is the Zhemchug Canyon on the North-American margin of the Bering Sea with size well beyond Grand Canyon in the US. An overview of some of the largest submarine canyons is given by Normark and Carlson (2003). The side walls of submarine channels can be very steep, and

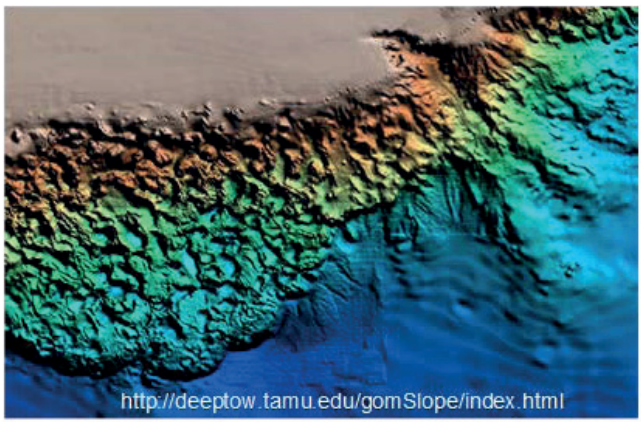

Figure 3.1. Bathymetry showing the Sigsbee escarpment with the salt deformation province behind (from Deep Tow Research Group, Texas A&M Univ.).

when reaching critical slope inclination, smaller slide

events will be initiated and run as debris flows and turbidity currents down the channel.

Geohazards can generally be sorted in two main groups:

– Hazards related to seabed instability (local and large scale)
– Hazards related to drilling and production

The former hazards are related to local and regional slope inclination and can be strongly influenced by excess pore water pressures (overpressure) in the upper sediments. The latter group is strongly related to presence of gas/gas hydrates and overpressured formations in deeper strata.

The triggering sources that may transform a potential hazard into a failure event can be divided in:

– Natural geological processes like sedimentation, erosion, diapirism and earthquake activity.
– Human induced changes in pressure and temperature conditions during drilling and production and load and stress changes introduced by field installations.

The consequences of geohazards type failure events may range from minimal damage due to limited displacements of wells, foundations and pipelines/flowlines, through severe damage to field installations and wells to multifield total damage and tsunami generation and 3rd party impact caused by severe submarine sliding.

3.1 *Submarine slope instability*

A large number of deepwater slides have been identified from seismic profiling (2D and 3D) and bathymetric mapping. The slide events range from local slumping in steeper areas to enormous slide events like the prehistoric (8200 yrs BP) Storegga slide off the west coast of Norway (Figure 3.2), the historic 1929 Grand Banks slide off New Foundland and major slide events offshore West Africa and in the Nile Delta (Figure 3.3) to mention a few. The Grand Banks slide was probably triggered by a major earthquake with epicentre in the slide area.

The factor of safety against slope failure can be defined as the ratio between soil resistance and mobilised shear stress along the most critical potential slip surface. Slope instability can thus be triggered by increased downslope loading or reduced soil strength. If the soil stress-strain behaviour is contractant and strain softening, post-failure strength may be reduced considerably giving a strong increase in mobility of the slide mass and opening up for retrogressive slide development and long run-out of the slide debris. This seems to be the dominant failure mode for the major submarine slides.

Rapid sedimentation may increase the downslope component of sediment weight faster than the increase in shear strength due to limited drainage possibility and increased pore water pressure.

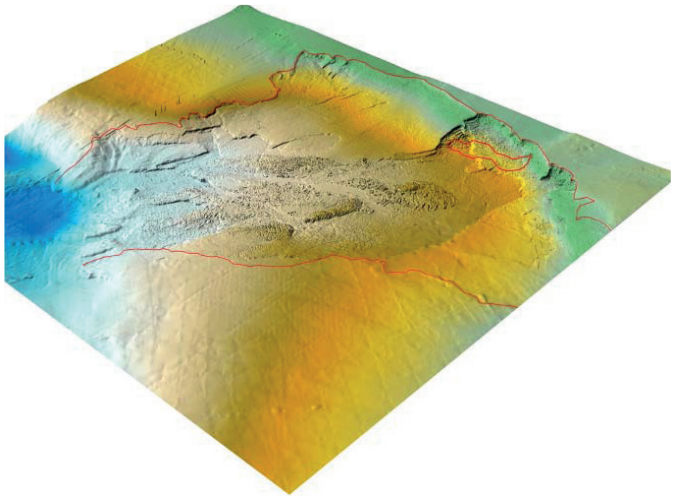

Figure 3.2. 3D perspective view of the Storegga slide scar with the Ormen Lange gas field. Note the terraced seabed showing slip surfaces at 5 to 7 different levels. (Courtesy Statoil-Hydro).

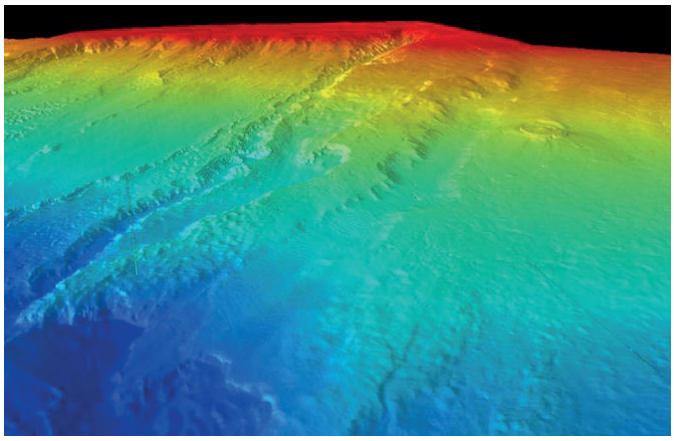

Figure 3.3. West Nile Delta bathymetry. 3D perspective view showing slide scars and submarine channels (Moore *et al*, 2007).

Earthquake loading causes cyclic variations in shear stress and shear strain. For contractant materials, like soft clays and loose sands, this will tend to compact the grain skeleton of the sediments and lead to increased pore water pressure. In sloping terrain the cyclic shear stress will be superimposed on the permanent, gravity induced, shear stress. The undrained strength of the clay may be exceeded repeatedly during the earthquake causing accumulation of shear strain and downslope displacement of the soil mass. In contractant materials the strain accumulation will lead to increased pore water pressure, and a gradual softening of the soil towards residual shear strength.

Erosion can be caused by sea water currents and by density currents (turbidity currents). Turbidity currents are gravity driven flows of turbid water with suspended particles and may form submarine channels extending from the shelf edge to the deepwater basins.

Variation in deepwater current velocity may give uneven deposition. High velocity deepwater currents, as observed in the Gulf of Mexico, may lead to severe

erosion. Erosion may reduce the soil resistance in the toe area of a slope.

Mud and salt diapirism as well as growth faulting are generally very slow processes, but in a geological time perspective a gradual increase in slope angle towards a critical value may develop. Numerous slumps and slides have been observed along the Sigsbee Escarpment in the Gulf of Mexico and locally in the salt diapir area behind (see Figure 3.1).

Submarine mud volcanoes are often seabed piercing mud diapirs where gas, water and mud from deeper sediments may travel up to the seabed, forming cone-shaped volcanoes. Mud diapirism is typically observed near subduction zones were the shallower sediments are scraped off the underlying subducting plate and compressed. (Mediterranean Ridge, Carribean Sea), in convergent tectonic settings, such as Azerbaijan-Caspian Sea, in front of deltas, such as the Mississippi and in the deeper part of delta fronts where the weight of the shelf sediments generates compression zones where mud diapirs are squeezed upwards (Niger Delta, Nile Delta). Mud volcano belts may also develop along deep faults. Extrusions of water and mud are traveling as mudflows down the hillside of the volcano (Figure 3.4). The mudflow may damage installations and bury equipment. Explosive eruptions of gas and rock material from deeper layers are typical for many onshore mud volcanoes (Guliyev and Feizullayev, 1997). Eruptions from deepwater submarine mud volcanoes are expected to be less violent due to the dampening effect of the water and the high water pressure.

Figure 3.4. Mudflow from erupting Azerbaijan mud volcano (from Guliyev and Feizullayev, 1997)

Large mud volcanoes located on the continental slopes represent areas with increased inclination on the down slope side of the volcano cone. Failure of the down slope part of the rim of mud volcanoes has been observed. This creates a pathway for later mudflows but can also be a release mechanism for larger slide events.

3.2 *Pockmarks*

Pockmarks are seen as depressions in the seabed, typically with nearly circular or elliptic shape created by fluid seeps (e.g. Figure 6.2). The diameter can range from a few meters to several hundred meters. Gas and water from overpressure strata may evacuate to seabed through nearly vertical channels/pipes and faults causing a slight erosion or reduction in sedimentation rate. Carbonate crust is often found in the pockmark area. In deep water, active seeps in pockmarks may generate gas hydrate accumulations. Along faults, series of pockmarks may line up.

In a geohazards context, uneven seabed may be a problem for routing of pipelines and flowlines. Intervention work might be required to even out the seabed, like trenching or installation of support structures. The local stability along the edge of the pockmark will have to be considered when installing pipeline supports or subsea structures near the rim of pockmarks. Carbonate hard ground in pockmark areas may be harmful to pipelines and subsea structures.

Avoidance is best remedial action, but if this is not possible, more extensive local investigations might be required to enable assessment of the local stability and the characteristics of hard ground material.

3.3 *Gas hydrate dissociation*

Gas hydrates are ice-like crystals formed by water molecule "cages" with enclosed guest molecules of natural gas. The most typical guest molecule is methane, CH_4. Methane gas hydrate has been detected in deepwater areas world wide and has for some years been considered a promising new energy source. Methane hydrate forms at pressure and temperature conditions shown in Figure 3.5.

The hazardous aspect of gas hydrates is the volume expansion that develops during dissociation (melting). At atmospheric pressure and 0°C temperature, $1m^3$ of methane gas hydrate will expand to $0.87m^3$ of water and about $164m^3$ of methane gas. Under deepwater pressure conditions, the expansion is considerably less dramatic, and at 1000m water depth the volume increase following dissociation is about 100%, i.e. 1 m^3 gas hydrate increases to about $1.1m^3$ of free gas and $0.87m^3$ of water.

Gas hydrates seem to form preferably in coarser sediments like sands and silts and to a lesser extent in clayey soils. The hydrate saturation (volume of gas hydrate/pore volume) will in general be low and in the range 0% to 8%, but close to fluid seeps structures where the supply of methane is high, more massive gas hydrates have been found at Blake ridge (Paull et al., 2000), at the Cascadia margin (Tréhu, A.M, et al., 2006), and on the Nigerian continental slope (Sultan et al, (2007).

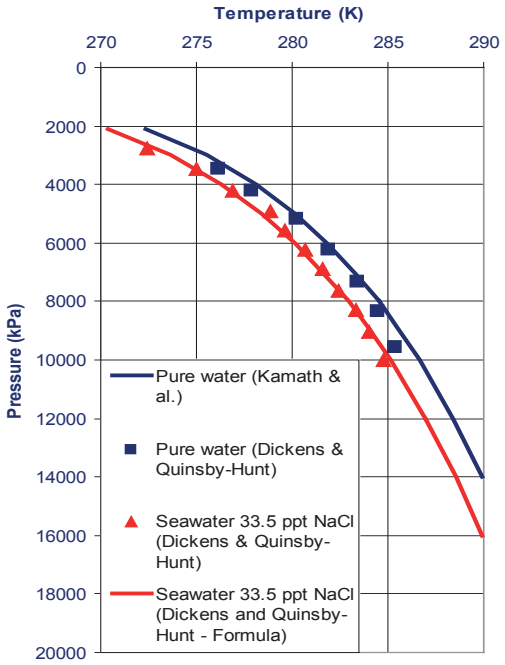

Figure 3.5. Gas hydrate stability diagram (Kamath *et al*, 1987, Dickens and Quinsby-Hunt, 1994)

The effect of gas hydrate melting on the soil behaviour is not well understood at present. Research is ongoing with focus directed towards production, and thus with focus on sandy sediments, but the geohazards aspect is also under investigation and research on clayey soils is also under way

A possible model can be described as follows: When gas hydrate dissociates in clayey soils, the increased volume of gas and water will increase the volume of the initial cavity, which was filled with gas hydrate. The gas/water pressure will increase and some of the methane will dissolve in the pore water. With increasing volume expansion, the fluid pressure will increase, hydraulic fracturing will be initiated, and the methane will force its way towards seabed or into sandy permeable formations. After fracturing the water/gas pressure will drop towards fracture closing pressure, which can be assumed to be about the minimum principal stress.

In the Gulf of Mexico, the seabed water temperature depends on the season and decreases with increasing water depth (Figure 3.6). This indicates that gas hydrates may be found in water depths greater than 600 to 700m in this area. The thickness of the gas hydrate stability zone (GHSZ) depends on the water depth. With a geothermal gradient of about 30°C/km in the north western part of the Gulf of Mexico, the theoretical thickness of the GHSZ at 800 m water depth will be about 200 m (Figure 3.6) and increases further with increasing water depth.

3.4 *Shallow gas*

Shallow gas is defined as natural gas deposit located near enough to the surface that a conductor or surface hole will penetrate that gas-bearing formation. If encountered while drilling, shallow gas is potentially dangerous because the well usually cannot be shut in to control it. Instead, the flow of gas must be diverted. Shallow gas is a geohazards which is not specific for deep water. Massive venting of shallow gas to the seabed may lead to cratering a local instability of the seabed. In sloping terrain this may spread upslope retrogressively and destabilize larger volumes.

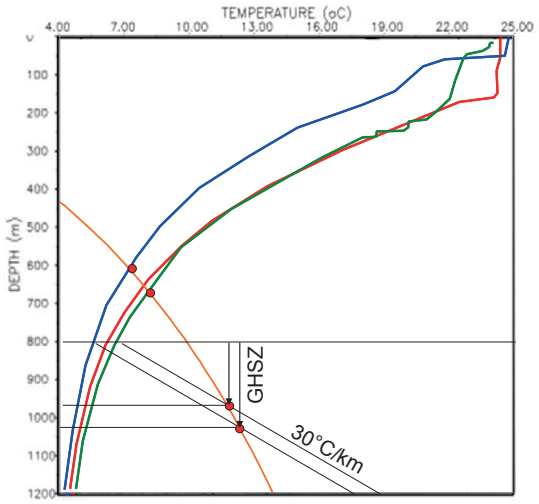

Figure 3.6. Temperature distributions from Mexican part of GOM (Vidal *et al*., 1994). Three curves showing seasonal variation. The theoretical methane hydrate stability zone is found below 600 to 700 m water depth. At 800 m water depth and with a geothermal gradient of 30°C/km, the thickness of the gas hydrate stability zone is about 200 m.

3.5 *Shallow water flow (SWF)*

SWF is defined as water or sand and water flowing within and around the outside of the structural well casing to the seafloor. Situations with SWF can occur when a well is drilled into an overpressured sandy formation under too low mud weight or the well casing is not cemented properly. If flow control is lost, severe underground erosion may develop in the sandy formation. This may lead to loss of lateral casing support and subsidence of the overlaying sediment column with casing damage, cratering around the wellhead and faulting to seabed. Shallow water flow is not restricted to deep water conditions, but is a general problem in areas with overpressured sediments (underconsolidated soils).

Gas hydrate melting around hot production wells may transform a normally (hydrostatic) consolidated sand formation to an overpressured formation if the gas hydrate content is high with full hydrate cementing of the sand and strongly reduced permeability.

3.6 *Overpressured clay formations*

Clays have a very low permeability compared with sand. This prevents shallow water flow, but instead hole closure may occur during drilling of exploration and production wells, as the underconsolidated clay can be considerably

softer than expected for normal pressure conditions. Hole closure may lead to severe problems for the drilling operations with high torque on the drill string, high resistance during pulling out of hole and increased need for reaming to reopen the hole.

3.7 *Underground blow-outs/cross-flow*

Wells may penetrate several sand formations with normal (hydrostatic) pressure or with overpressure. If cementing is not carried out with high quality, overpressured fluids may flow along the casing from a deeper permeable formation to a shallower permeable formation, so called cross-flow. This will increase the pore water pressure and reduce the shear strength in the shallower layer. In sloping terrain and in situations where wells are located upslope and close to erosional scarps, the potential slide risk associated with cross-flow to shallow permeable layers need to be considered (Figure 3.7).

Site investigations are required to identify the presence or lack of shallow sand layers with confidence. If sand layers are found at depths considered critical in case of cross-flow from certain wells, the cementing procedures may need to be sharpened and monitoring of pressure in the critical layer(s) may be required during drilling and production.

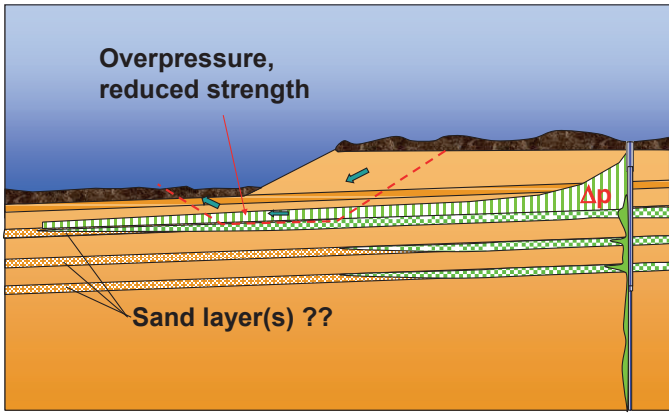

Figure 3.7. Underground blow-out generating cross-flow to shallower sand layers with overpressure and reduced strength in the toe area of a nearby slide scar.

4 DESIGN ISSUES AND REQUIRED SOIL PARAMETERS

This section identifies design issues, calculation procedures and required soil parameters for geotechnical design of anchoring units, seabed structures, pipelines and slope stability in deep water.

4.1 *Suction anchors*

4.1.1 *Concept*

A suction anchor is a large diameter cylinder; open-ended at the bottom and closed at the top (Figure 4.1). Mooring loads are applied by an anchor line usually attached to the side of the caisson. The length to diameter ratio of the caisson is typically six or less. The anchor may be equipped with stiffeners, like inside ring stiffeners and bulk head plates, and increased wall thickness over a height around the load attachment point. Once installed, the caisson acts much like a short rigid pile and is capable of resisting both lateral and axial loads. The maximum holding capacity is obtained if the chain is attached at a depth where the anchor failure mode is large translational displacements with minimal rotation ('optimum load attachment point').

The suction caisson is installed by applying underpressure ('suction') to its interior after it is allowed to penetrate under its own weight. The difference between the hydrostatic water pressure outside the cylinder and the reduced water pressure inside provides a differential pressure that acts as a penetration force in addition to the weight. After installation the caisson's interior is sealed off, and vertical loading creates an internal underpressure which in turn mobilizes the end bearing resistance of the soil at the caisson tip. Andersen *et al*. (2005) gives an overview of the more than 485 suction anchors installed at more than 50 locations in water depths to nearly 2000m by 2004, and summarizes and evaluates various calculation methods.

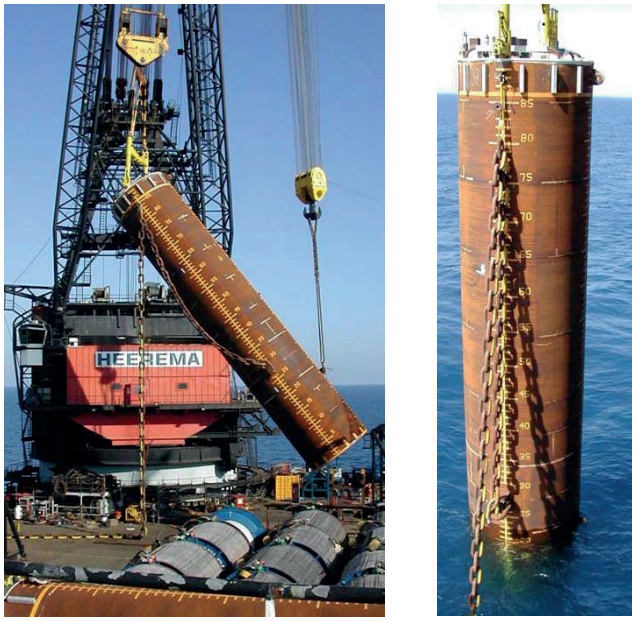

Figure 4.1. Suction caissons for the Horn Mountain field in the Gulf of Mexico. (Andersen *et al*, 2005; photo: E.C. Clukey, BP)

4.1.2 *Design issues and calculation procedures*

In the geotechnical design, one has to determine (1) the underpressure that is required to penetrate the anchor and (2) the holding capacity of the installed anchor.

4.1.2.1 Installation

The determination of the underpressure for penetrating the suction anchor involves calculation of skirt penetration

resistance, underpressure required to achieve target penetration depth, allowable underpressure (underpressure giving either large soil heave inside the caisson or cavitation in the water), and soil heave inside the caisson. The effect of inner stiffeners must be included in the penetration resistance, and the penetration resistance may be higher if there are sand layers or boulders in the clay.

The forces to penetrate a suction anchor without inner stiffeners and the calculation of the required underpressure are illustrated in Figure 4.2. The side shear resistance is normally calculated by using the remoulded shear strength. If the anchor is equipped with inside ring stiffeners, however, the upper part of the clay plug may not deform back to the anchor wall after passing the stiffener. This gives zero penetration resistance above the stiffener and increased heave inside the anchor. The depth to which the clay plug does not deform back to the wall can be calculated based on special triaxial extension-compression tests. If the depth to which the clay plug does not deform back to the wall exceeds the distance between two ring stiffeners, a mix of water and clay may be trapped between the stiffeners, giving zero penetration resistance over this part of the anchor. If the clay plug does deform back to the wall between two stiffeners, clay from the upper part of the profile is likely to be trapped between the stiffeners, and the penetration resistance between the stiffeners will be governed by the remolded strength of the top clay. Calculation of penetration resistance of anchors with inside ring stiffeners is described in Andersen and Jostad (2004).

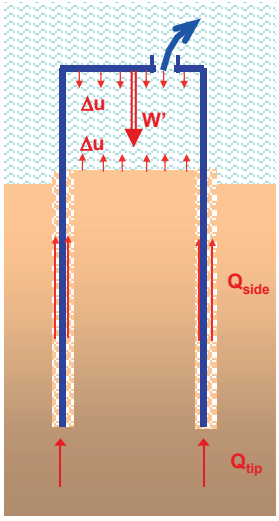

Penetration resistance

$Q_{total} = Q_{tip} + Q_{side}$

$Q_{tip} = (N_c \cdot s_u^{DSS} + \gamma' \cdot z) \cdot A_{tip}$

$Q_{side} = \alpha \cdot s_{u\,av}^{DSS} \cdot A_{wall\ (outside+inside)}$

$\alpha = 1/S_t$

Required underpressure

$\Delta u_{req} = (Q_{req} - W') / A_{in}$

Allowable underpressure

$\Delta u_a = N_c \cdot s_u^{DSS} + A_{inside\ wall} \cdot \alpha \cdot s_{u\,av}^{DSS} / A_{in}$

where:

A_{tip} = skirt tip area

A_{in} = horiz. inside area where underpr. is applied

N_c = bearing capacity factor

S_t = soil sensitivity

$s_{u\,av}^{DSS}$ = average s_u^{DSS} over penetration depth

Ref: Andersen and Jostad (1999)

Figure 4.2 Installation forces (case with no stiffeners)

The allowable underpressure is governed by the possibility of large soil heave inside the anchor due to bottom heave at skirt tip level and is calculated by considering the inverse bearing capacity at skirt tip level.

More details of calculation procedures for the various aspects can be found in Andersen and Jostad (1999 and 2004) and Andersen *et al*. (2005). Andersen *et al*. (2005) also presented comparison of calculated and measured behaviour of 6 prototype anchors with and without stiffeners.

4.1.2.2 Holding capacity

The holding capacity of a suction anchor is provided by self weight, shear strength along the skirt wall, inverse end bearing with vertical, horizontal and moment components at the anchor tip, passive and active pressures and side shear in the upper part, and flow around the anchor (Figure 4.3). The mobilization and the interaction between the various components depend on the depth/diameter ratio of the anchor, the load inclination, the shear strength profile, the shear strength anisotropy, and the set-up along the skirt wall.

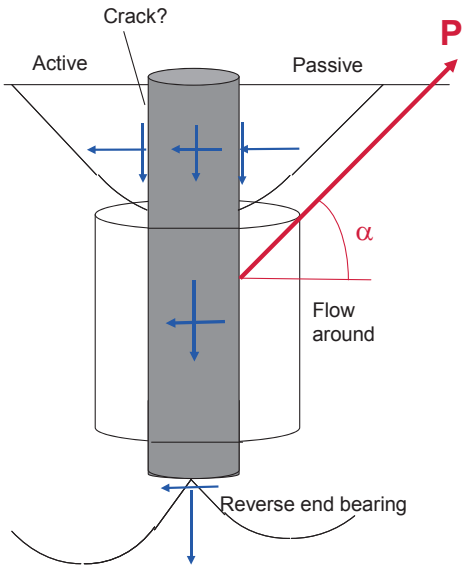

Figure 4.3 Limiting equilibrium model

The holding capacity analyses must model (1) the actual shear strength profile, including strength anisotropy and effects of rate and duration of loading and cyclic degradation, (2) a realistic failure mechanism, including coupling between vertical and horizontal resistances, 3D effects, and effects of tilt and misorientation from installation, (3) set-up effect in the remoulded clay along the skirt wall, and (4) a potential tension crack along the skirt wall on the active side.

In cases with inclined loading, the coupling between vertical and horizontal failure modes can reduce the resultant failure load, as illustrated in Figure 4.4.

The shear strength along the skirt wall will be reduced to the remolded shear strength during installation. After installation, the shear strength along the skirt wall will in most cases increase again due to increased total normal stresses during skirt penetration, redistribution and dissipation of the installation pore water pressures, and thixotropy. A method to determine the shear strength along the outside skirt wall with time after installation was presented by Andersen and Jostad (2002). They showed that the shear strength along the outside of the skirt may

be reduced due to the installation effects, even after full set-up has occurred. The shear strength along the inside skirt wall is of less importance for rapid loading, unless the anchor is not equipped with a permanent top lid. Determination of set-up along the inside skirt wall was presented in Andersen and Jostad (2004). In cases with inside stiffeners, the shear strength above and between the stiffeners may get significant reduction.

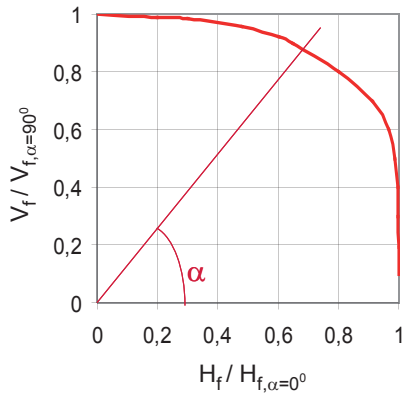

Figure 4.4 Vertical and horizontal failure load components, V_f and H_f, as function of load inclination, α.

The cyclic shear strength will depend on the ratio between cyclic and permanent load components, and the capacity can be calculated by the method proposed by Andersen and Lauritzsen (1988). This method is based on (1) the condition of equilibrium between the permanent loads and the average shear stresses in the soil and (2) the assumption of strain compatibility along the potential failure surface. A simplified approach is to determine the cyclic shear strength by assuming that the ratio between the cyclic shear stress and the change in average shear stress is equal to the ratio between cyclic and permanent environmental loads. With this ratio, one can determine the cyclic shear strength by plotting a line with this ratio in the cyclic shear strength diagrams. The cyclic shear strength can be determined based on the intersection of this line and the failure envelope for the number of load cycles in the specified design storm. Examples of cyclic shear strength diagrams are presented in Section 7.6.8.

The holding capacity can be calculated by limiting equilibrium models or by finite element analyses. In the limiting equilibrium model described in Andersen and Jostad (1999), the cross-sectional area is transformed to a rectangle with the same area as the real anchor and the width equal to its diameter. 3D effects are accounted for by side shear factors that were determined by calibration to 3D finite element analyses (e.g. Andersen *et al.*, 2005).

Finite element analyses can be performed as 2D or 3D analyses. In 2D analyses, the 3D effects must be accounted for by side shear factors, as in the 2D limiting equilibrium analyses. It is also important that the reduced shear strength along the skirt wall is modelled properly. An example of shear strains at failure in a 3D finite element analyses is shown in Figure 4.5.

The optimal load attachment point can be determined by running analyses with different attachment point locations. An example of an anchor with top loading and with optimized load attachment point is shown in Figure 4.6. The anchor with top loading has a rotational failure mode, whereas the anchor with optimal loading has a purely translational failure mode. In the example, the capacity of the optimized anchor is twice the capacity of the anchor with top loading. To avoid a potential tension crack at the active side of the anchor, the attachment point is often placed somewhat lower than optimal in order to get a ”backward” rotation that will prevent tensile stresses and crack formation.

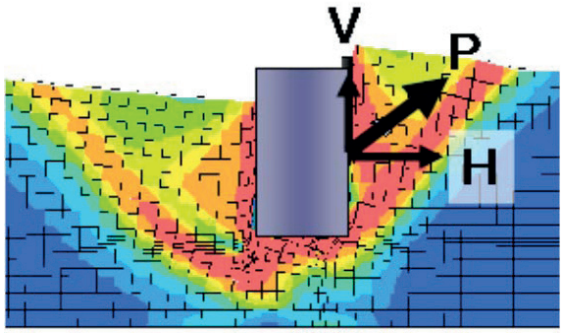

Figure 4.5 Shear strains at failure from 3D finite element analysis.

a) Anchor with load attachment point at top

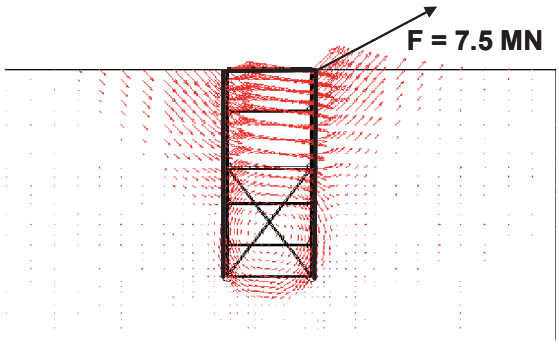

b) Anchor with optimal load attachment point

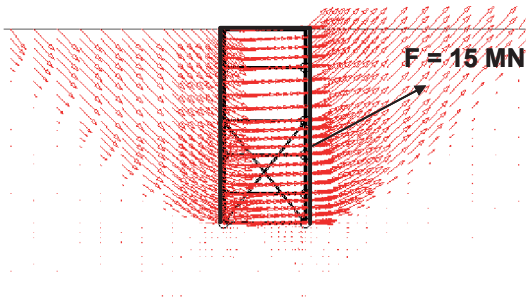

Figure 4.6 Displacements at failure from 3D finite element analysis.

The anchor loads are normally given at the seafloor elevation, and must be transformed to loads at the anchor attachment point by a chain-soil interaction analysis.

In cases when sustained loads act over a long time, the reduction in shear strength due to undrained creep, pore water flow and reduced effective stresses must be considered.

4.1.3 *Required soil parameters*

4.1.3.1 Installation

Calculation of the side shear during penetration requires the remoulded shear strength or the sensitivity.

Calculation of the tip resistance of skirts and stiffeners and the allowable underpressure require the anisotropic monotonic shear strength.

The soil parameters that are required for the installation analyses are summarized in Table 5.1.

4.1.3.2 Capacity

Soil elements along the potential failure surfaces will follow different stress paths, and the calculation of holding capacity requires anisotropic monotonic shear strengths and stress path dependent cyclic shear strengths.

The set-up in the clay along the skirt wall can be estimated based on recommendations in Andersen and Jostad (2002). If site specific set-up analyses are performed, however, one will need reloading compressibility and permeability of intact soil, virgin compressibility and permeability of remoulded soil, thixotropy factors, and reconsolidated remoulded shear strength.

In cases with sustained load, it is necessary to determine the effect of load duration on the shear strength. This may best be done by undrained static creep tests instead of constant rate of strain tests.

The soil parameters that are required for the holding capacity analyses are summarized in Table 5.1.

4.2 *Piles*

4.2.1 *Concept*

Piles can be used as anchors for floaters and as foundation elements for subsea structures.

Anchors and subsea structures can both be subjected to both vertical and horizontal loading.

For anchors, the loads will be cyclic and the vertical loads will be in tension. Anchors may also have high permanent load components. Displacements are normally not important for anchors.

For subsea structures, cyclic wave loading is normally not important, but there may be temperature induced cyclic loading with fewer cycles and time for drainage between the cycles. This is further discussed in Section 4.5 on subsea structures. Displacements can be important for subsea structures.

4.2.2 *Design issues and calculation procedures*

Vertical and horizontal pile capacities are often calculated by empirical formulas based on bearing capacity equations (e.g. API, 2000). Vertical and horizontal pile displacements can be calculated by means of t-z and p-y curves, respectively. The reference shear strength in the formulas can be from simple laboratory tests or from more advanced laboratory tests. API (2000) and Karlsrud *et al*., (2005) use strength from UU tests.

The empirical formulas assume that the vertical capacity under wave loading is not reduced by cyclic loading. The explanation why this may be reasonable is that the cyclic loading has a period of the order of 10s, whereas the static reference strength is related to a much longer duration. The positive rate effect for the fast cyclic load compared to the long duration reference strength may thus cancel the strength degradation due to cyclic loading. Data that supports this can be seen in the cyclic shear strength diagrams for Drammen Clay presented in Section 7.6.8.

For horizontal loading, separate p-y curves are applied for static and cyclic loading.

Capacity and displacements of piles can also be calculated by finite element analyses. Especially for lateral loading and in cases with cyclic loads, it is believed that finite element analyses can give more realistic displacements and capacities than the empirical formulas. It is important, however, that a relevant soil model is applied. It is also important that the reduced shear strength along the skirt wall is modelled. Karlsrud and Nadim (1990) developed a method to calculate capacity and displacements under vertical cyclic loading by modeling the pile-soil interface by non-linear "t-z"-springs with cyclic and permanent components. The cyclic and permanent spring components were determined through strain contour diagrams established from cyclic DSS tests.

The formulas and the analyses referred to above give the shear strength after full dissipation of the pore water pressure induced during installation. The installation pore water pressure can be significant and can take a long time to dissipate. The capacity is lower prior to full pore water pressure dissipation. The time required for pore water pressure dissipation can be calculated by analytical solutions.

4.2.3 *Required soil parameters*

The empirical formulas for capacity and displacements need the UU triaxial strength. The p-y curves also require some stiffness parameter. This is often given in the form of the strain at half the shear strength in the UU test (ε_{50}).

Calculation of time for pore water pressure dissipation needs information about the shear strength and modulus and the coefficient of horizontal consolidation for reloading conditions in the soil around the pile.

If more advanced analyses are performed, the soil model should use anisotropic shear strength and moduli in cases with static loading, and the effect of load duration

on the shear strength should be accounted for. In cases with cyclic loading, the model should use stress path dependent cyclic shear strengths and moduli.

4.3 *Plate anchors*

4.3.1 *Concept*

A plate anchor is installed by dragging the anchor through the soil or by pushing it in by gravity and/or underpressure. At the target penetration depth, the anchor is activated by orienting the anchor fluke such that it gets perpendicular to the load direction. The technique to activate the anchor varies between the anchor types.

There are many types of drag anchors. An example is shown in Figure 4.7. The deployment depth and the holding capacity of a drag anchor will depend on fluke area, fluke angel, fluke shape, anchor weight, stabilizer bars, soil strength, disturbance during installation, bearing capacity factor, etc. The capacity will also depend on whether the anchor line is a wire or a chain.

Drag anchors have mainly been used for temporary moorings, but they have also been used for permanent installations.

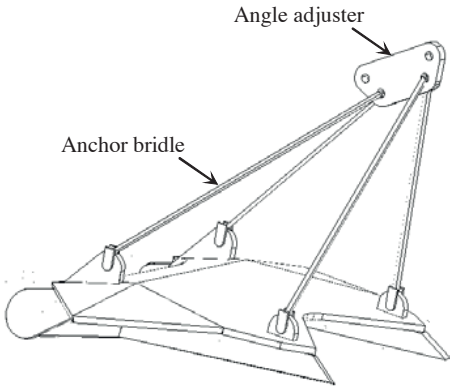

Figure 4.7. Schematic of Vryhof Stemanta (Murff *et al*., 2005).

4.3.2 *Design issues and calculation procedures*

Since the anchor capacity depends on many details, as described in the previous subsection, the prediction of the holding capacity of a drag anchor is complicated. The holding capacity is often based on empirical approaches, but analytical and numerical approaches are also available.

The empirical methods are based on simple design diagrams that have been established from prototype experience and model test results (e.g. NCEL, 1987, Vryhof Anchors, 1999). The empirical approaches generally assume that the holding capacity is not reduced due to cyclic loading. The explanation why this may be reasonable is the same as given for piles in Section 4.2.2.

The analytical and numerical tools are based on simple bearing capacity formulas, limiting equilibrium methods or finite element analyses. Since the holding capacity will depend on the deployment of the anchor, the analyses need to give information about anchor movement trajectory, anchor rotation and mooring line profile in the soil, in addition to the ultimate anchor capacity. An assessment of current design and analysis methods for vertically loaded plate anchors is presented in Murff *et al*. (2005).

The soil near the anchor will be remoulded, and the capacity of a drag anchor in normally consolidated clay will increase with time due to set-up effects similar to the set-up discussed for suction anchors.

Due to the uncertainty in the prediction of the capacity, test loading is normally required.

4.3.3 *Required soil parameters*

The empirical design diagrams are often not very specific with respect to details of soil data, and only require routine classification data and simple strength measurements.

Analytical and numerical methods will require information about the undrained intact shear strength and the remoulded shear strength. The type of intact shear strength data depends on the sophistication of the analysis. Today, design with analytical and numerical methods is often based on relatively simple shear strength measurements, like UU tests or isotropically consolidated triaxial tests. If more advanced analytical or numerical methods are used, however, one should consider using more advanced tests to determine the shear strength, like anisotropically consolidated triaxial tests and DSS tests, modelling both long term sustained loads and cyclic loads. An example of an advanced analytical model is the DIGIN-programme developed at DNV (Eklund and Strøm, 1998).

If attempts are made to calculate set-up effects, one will need reloading compressibility and permeability of intact soil, virgin compressibility and permeability of remoulded soil, thixotropy factors, and reconsolidated remoulded shear strength. The increased capacity due to set-up is generally disregarded in assessment of the anchor holding capacity, but should be considered in connection with increase in drag loads due to temporary stops during installation.

4.4 *Torpedo anchors*

4.4.1 *Concept*

Torpedo anchors (Figure 4.8) are free fall piles that have the advantage of being easier and faster to install than other anchor types. Torpedo anchors have been used offshore Brazil since the late 90´s (Brandao *et al*., 2006).

The piles in Figure 4.8 had a mass of 98 metric tons and were about 1m in diameter and 17m long. They had four 0.9m wide and 10m long wings. The maximum penetration depth was 20m, measured from the pile top. The holding capacity approached 10MN.

Figure 4.8. Photo of torpedo anchors used in the Albacora Leste Field, Brazil, in water depth up to 1384m (Brandao *et al*., 2006).

4.4.2 *Design issues and calculation procedures*

The holding capacity will depend on penetration depth. The penetration depth can be calculated by a drivability analysis.

The capacity analyses must evaluate the disturbance in the soil around the pile from installation and the amount of set-up with time. Whether full set-up can be assumed depends on the time from installation to hook-up.

For the Albacora Leste anchors the holding capacity was calculated by finite element analyses, assuming interface shear strength according to API (2000).

The holding capacity depends on the catenary of the anchor line, as the capacity will depend on the load inclination at the anchor and the forces taken by the anchor line. The catenary can be calculated as for other anchors.

Torpedo piles are not likely to be fully vertical at the end of penetration, and the effect of inclination at the end of penetration must be taken into account in the design analyses.

4.4.3 *Required soil parameters*

The soil will be disturbed when the pile penetrates into the soil, and both intact and remoulded shear strengths are needed. These strengths are also needed in the catenary analyses.

The penetration rate is high when the pile enters the soil and reduces as the pile penetrates. The rate will influence the shear strength, and the effect of rate on shear strength is needed. Rate effect or effect of load duration is also needed if the anchor shall carry sustained loads.

The capacity analyses should ideally use anisotropic static shear strengths and stress path dependent cyclic shear strengths.

To calculate set-up effects, one will need reloading compressibility and permeability of intact soil, virgin compressibility and permeability of remoulded soil, thixotropy factors, and reconsolidated remoulded shear strength.

4.5 *Subsea structures*

4.5.1 *Concept*

Subsea structures are used for various purposes, such as production, processing and transportation. Subsea structures include templates and foundations for (1) wells, (2) wellhead completions, (3) control and production systems for gas/liquid separation, gas dehydration (water removal), gas compression, water injection, etc, (4) manifolds, tie-in, and end termination of umbilicals, pipelines and flowlines, (5) risers support, and (6) protection systems to protect against falling objects and trawling.

The foundations for the subsea systems can be mudmats with short peripheral skirts, skirted foundations and piles. An example of a structure with skirted foundation is shown in Figure 4.9.

Mudmats and skirted foundations may be penetrated to base contact and even grouted to obtain good contact between the base and the soil. Another solution that is applied for skirted foundations is to penetrate the skirts to less than full contact. One may then have the possibility to correct for settlements and tilt later by increasing or decreasing the water pressure inside the different skirt compartments.

Foundations for pipelines must be able to accommodate temperature induced displacements of pipelines that can occur in connection with interruptions in production. These displacements can be accommodated by having connections that the pipelines can slide in. Some friction is still likely to occur and cause horizontal loads with corresponding overturning and rotational moments on the support structure. An alternative that has been used, is to have a fixed connection between the pipeline and the foundation structure, and to design the foundation such that it has a low horizontal capacity. The foundation will then act like a ”sledge” and slide on the seafloor when the horizontal force becomes larger than the sliding capacity of the foundation. The horizontal force on the pipeline will be limited to the sliding capacity of the foundation.

Cyclic loads from waves are likely to be negligible at large water depths. However, there may be cyclic loading from temperature induced movements of pipelines in connection with interruptions in production. Such movements would cause cyclic loading with a much longer load period than sea waves.

Figure 4.9. Template with skirted foundation at Ormen Lange (Neerland, 2006).

4.5.2 *Design issues and calculation procedures*

The foundation design must ensure that the structures are safe against a bearing capacity failure and that displacements are acceptable. The displacement requirement also includes differential displacements, as some of the functions of the subsea structures are sensitive to tilt. Foundations for pipelines must be designed for horizontal forces that may be cyclic, but with a longer period than waves.

The following subsections discuss design issues, calculation procedures and soil parameters for mudmats and skirted foundations. For piles, reference is made to Section 4.2.

4.5.2.1 Capacity

The capacity calculations of a foundation where the base is in contact with the seabed can be done with traditional limiting equilibrium analyses. An example of a potential failure surface in the soil beneath a foundation is illustrated in Figure 4.10. If there are horizontal loads, these must also be included as driving forces in addition to vertical loads from weight of the foundation and the facilities that it carries. If the vertical loads are eccentric, the analyses must account for the eccentricity by for instance working with an effective area. The loads may be static, but if cyclic loading occurs, the cyclic loads must be included in the driving forces. A procedure to calculate the bearing capacity of foundations under combined static and cyclic loading by limit equilibrium methods is described by Andersen and Lauritzsen (1988).

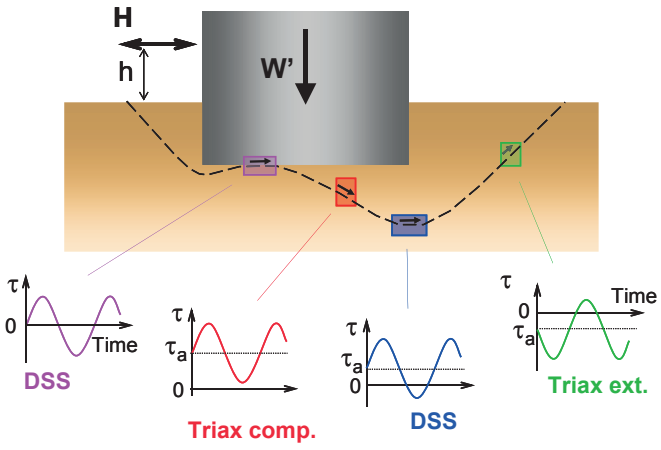

Figure 4.10. Potential failure surface beneath foundation under vertical, horizontal and moment static and cyclic loading.

The illustration in Figure 4.10 shows that elements along a failure surface will follow different stress paths. The shear strength will depend on the stress path, and it is important to use strengths that are representative for the different stress paths along the failure surface. The various stress paths can be simulated by triaxial compression, DSS and triaxial extension tests. If there are no cyclic loads, static shear strengths shall be used. However, since the shear strength is rate dependent, it is important that the tests are run with a rate of loading or a load duration that is representative for the loading that the foundation will experience. If cyclic loading occurs, this must also be accounted for in the shear strengths.

The bearing capacity can also be calculated by finite element analyses, but it is then important to apply a soil model that captures the factors discussed above.

For a structure resting on more than one foundation, like the template in Figure 4.9, the forces must be distributed on the different pods. Nature will find the most optimal way to distribute the forces, and the force distribution that gives the highest total capacity should be sought for.

In the foundation alternative where the skirts are not fully penetrated, the forces must be carried by the shear resistance along the skirt walls. The contribution from the resistance at the skirt tip is normally small in normally consolidated clays. Cyclic loads may be carried by the base area if the skirt compartments are not drained and the load period is short enough for undrained conditions to prevail. The shear strength along the skirt wall will be equal to the remoulded shear strength immediately after installation, but it will increase with time. This set-up is discussed in more detail in the section on holding capacity of suction anchors. One additional factor that needs to be considered if the skirts are not fully penetrated, is the effect that permanent shear stresses will have on the set-up. The vertical load has to be carried by permanent shear stresses along the skirt wall if the base is not in contact with the soil, and the permanent shear stresses can then be significant and influence the set-up.

In the ”sledge”-type foundation, the horizontal capacity will be governed by the remoulded shear strength. The pipelines may move several times, and the shear strength may increase between each time if the time between each occurrence is long enough for the excess pore water pressure in the remoulded zone to dissipate.

4.5.2.2 Displacements

The settlements under static loading can be calculated by traditional settlement calculation methods.

However, for skirted foundations, the load carrying mechanism may complicate the calculations. In soft clay, the compressibility of the clay is very high near the surface. When consolidation starts, the load taken by the clay plug inside the skirt will therefore be transferred to the skirt wall. The friction along the skirt wall will in this way transfer the loads deeper into the soil and reduce the settlements compared to what they would have been if the loads had to be transferred through the upper, more compressible, soft clay. Rough estimates can use a model where the shear stress distribution along the skirt wall is estimated. More accurate calculations require finite element analyses with consolidation formulation.

In cases with cyclic loading, there will also be cyclic displacements and increased settlements and other permanent displacements due to cyclic loading.

Calculation procedures for displacements due to cyclic loading were developed in connection with design of gravity structures in shallower water (e.g. Andersen, 1991 and Andersen and Høeg, 1991).

4.5.3 *Required soil parameters*

The distance between individual anchors, or group of anchors, can be kilometres, depending on the water depth. Seabed topography and soil conditions within the area should therefore be established by a shallow geophysical survey supplemented by soil sampling to interpret the geophysical data. The number of *in situ* tests and borings should be a function of the lateral soil variability. In case with lateral variability, one boring or *in situ* test at each anchor location should be considered.

4.5.3.1 Penetration

Penetration of skirts requires the same parameters as penetration of suction anchors, i.e. remoulded shear strength or sensitivity to calculate side shear, and anisotropic static shear strengths to calculate the tip resistance of skirts and stiffeners and allowable underpressure.

4.5.3.2 Capacity

Capacity analyses for structures with static loads require anisotropic monotonic shear strengths. In cases with large sustained static loads, it is necessary to determine the effect of load duration on the shear strength. This may best be done by undrained static creep tests instead of constant rate of strain tests.

The parameters to calculate set-up in the clay along the skirt wall are the same as for suction anchors. However, in cases where the anchors are not penetrated to contact at the base, one may need to evaluate the effect that the static shear stress acting during the set-up period will have on the reconsolidated remoulded shear strength.

Foundations with cyclic loads will need stress path dependent cyclic shear strengths. The strengths should be determined for a representative load period, which may differ from standard wave loading.

The capacity calculations for "sledge"-type foundations require reconsolidated remoulded shear strength after repeated series of remoulding.

4.5.3.3 Displacements

Calculation of settlements due to volumetric compression requires preconsolidation stress, compressibility and permeability (i.e. coefficient of consolidation).

Calculation of displacements under undrained static loading requires anisotropic stress-strain data from undrained tests. The tests must be representative for the load conditions, and undrained creep tests may be preferable.

Calculation of displacements due to cyclic loading requires information about development of cyclic and permanent shear strains, permanent pore water pressures, and recompression compressibility.

The soil parameters that are required for seabed structures are summarized in Table 5.1.

4.6 *Flowlines and pipelines*

4.6.1 *Concept*

Flowlines and pipelines are used to transport oil and gas between subsea structures and from oil and gas fields to land, as illustrated in Figures 1.1 and 1.2. The geotechnical problems are much the same for pipelines and flowlines. This paper will therefore not distinguish between flowlines and pipelines and use the term pipeline for both.

During pipe laying, the curvature of the pipeline, the penetration depth and stresses in the pipeline will depend on the strength and stiffness of the soil in the touchdown area.

During operation, pipelines will tend to expand due to temperature variations in connection with interruptions in production. This expansion is counteracted by friction between the pipeline and the soil. If the friction is exceeded, the pipeline will move, and if this expansion is not allowed to occur freely, it may cause lateral or vertical buckling of the pipeline. An example of lateral buckling is shown in Figure 4.11. The tendency for buckling can be reduced by trenching, burying and rock dumping. The tendency for buckling can also be reduced by designing supports and tie-in systems that allow the pipeline to move with low resistance, and to include bends (expansion spools) in the pipeline that can accommodate displacements. If the pipeline is allowed to displace, the stresses induced in the pipeline will also be smaller.

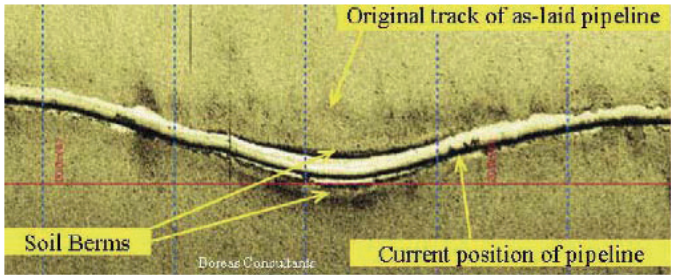

Figure 4.11. Example of lateral buckling of a pipeline (Bruton *et al.*, 2007).

The pipeline route has to be selected based on knowledge about the topography and to avoid areas with danger of submarine slides. Evaluation of potential for submarine slides is discussed in Section 4.7.

Stability of supports and tie-in systems is covered in Section 4.5 on seabed structures.

4.6.2 *Design issues and calculation procedures*

The axial and lateral load-displacement response from the soil is the most important parameter to evaluate pipeline penetration, pipeline stresses and pipeline displacement, and to design supports, tie-in systems and expansion

spools. The load-displacement responses depend on the penetration of the pipe into the soil during initial placement and during subsequent loading from the tendency for displacement.

Empirical axial and lateral load-displacement models based on physical model testing, as described in Section 8, are often used in design (e.g. Bruton *et al.*, 2006). Theoretical axial and lateral load-displacement models can be a valuable supplement to empirical models and may also provide insight into the mechanisms that govern the load-displacement relationships.

In theoretical models, the penetration can be calculated by bearing capacity theory that accounts for the reduction in vertical capacity due to horizontal loading. However, such calculations are complicated by changes in contact area between the pipe and the soil as the pipe penetrates into the soil (e.g. Murff *et al.*, 1989, Aubeny *et al.*, 2005). The change in contact area is due to the larger penetration depth and the soil heave due to displaced soil.

Lateral resistance will come from friction along the pipe and by passive resistance on the side. In principle, the lateral resistance can be calculated by formulas for horizontal sliding and passive resistance. In practice, however, such calculations are complicated due to the geometry of the pipe and the shape of the through and the soil berm that is generated with time.

Theoretical pre-failure load-displacement relationships require analytical or numerical analyses.

The axial force in the pipeline will be equal to the mobilized axial resistance in the soil along the pipeline integrated from a free end.

4.6.3 *Required soil parameters*

Seabed topography and soil conditions along the pipeline route should be established by a shallow geophysical survey supplemented by soil sampling to interpret the geophysical data. The soil sampling would typically be relatively shallow (less than about 5m) and relatively far apart (may be several km).

Empirical axial and lateral load-displacement models are generally based on index strength parameters and do not require sophisticated laboratory testing.

Advanced theoretical models require information about anisotropic undrained shear strengths and moduli, both under monotonic and cyclic loading. Since the pipe displacements during installation and later temperature variations may cause large shear strains in the soil both near the pipe/soil interface and further away from the pipe, both intact and remoulded shear strengths and moduli are needed. The cyclic loads are caused by the temperature variations during interruptions in production, and the load period will be significantly longer than for wave loading. The soil is likely to be undrained during the load changes, but may have the time to drain between each load cycle. This means that the soil may reconsolidate after each load cycle. The reconsolidation may increase the undrained shear strength and modulus of normally consolidated clay, but may cause a reduction in shear strength and moduli of overconsolidated clay. The remoulded clay may also gain strength from thixotropy effects. These effects should be accounted for by modelling in the laboratory tests or by utilizing existing experience.

The pipeline behaviour depends on the soil properties of the top soil. The best quality samples of the very soft top soil may be achieved by box cores that would provide samples of the upper 0.5m. While still inside the box, the soil should be tested by miniature T-bar and/or ball penetrometer tests and/or miniature field vane. Index tests for soil classification and additional strength tests can be performed on sub-samples from the box core sample.

The laboratory tests required to determine the strengths and moduli of intact and remoulded clay before and after reconsolidation should be run on samples from the top soil. Since the effective stresses and the shear strengths are very low in the top soil, such tests may not be feasible in existing laboratory equipment. As much testing as possible should therefore be performed *in situ* by T-bar and/or ball penetrometer tests, large diameter CPTU-tests or field vane. These tests should be run to provide both intact and remoulded shear strengths. The effect of reconsolidation after remoulding is difficult to achieve by the *in situ* tests, however. Qualitative effects of reconsolidation after remoulding may be found by extrapolation of results from tests at effective stresses that can be handled in advanced laboratory tests.

Equipment for special offshore pipe model tests has also been developed, as discussed in Section 7.3.4.

The strength at the interface between the pipe and the soil may also depends on the pipe surface, and ring shear, shear box or tilt table tests can be performed to evaluate whether the shear strength at the interface is smaller than in the soil itself.

The soil parameters that are required for pipeline/soil interaction are summarized in Table 5.1.

Riser/soil interaction

4.6.4 *Concept*

Risers are pipes used to transport oil and gas from the sea floor up to loading buoys or floaters, as illustrated in Figures 1.2 and 4.12.

Seabed stiffness can have important influence on the dynamic behaviour of the riser. Trenching and high lateral soil resistance can also lead to high stresses in the riser during lateral movements.

A riser will experience cyclic loading from wave-induced movements, and the cyclic period is shorter than for pipelines. The cyclic loading can thus be undrained during many cycles. However, since the cyclic loading occurs over the lifetime of the production, drainage and reconsolidation of both intact and remoulded clays can occur. The riser can also experience uplift and detach from the soil during a cycle.

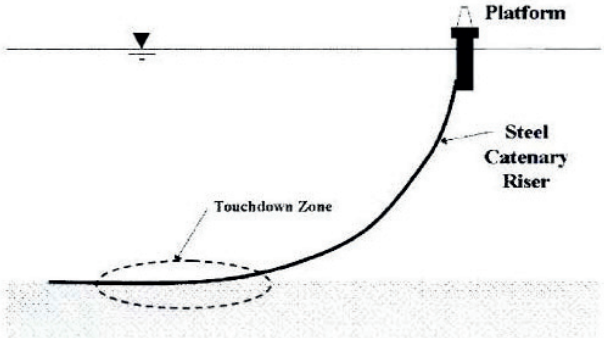

Figure 4.12 Sketch of steel catenary riser (Langford and Aubeny, 2008).

4.6.5 *Design issues and calculation procedures*

The riser-soil interaction is a complicated process where the soil reaction can be modelled with non-linear springs that vary along the riser as function of the distance from the touchdown point (e.g. Bridge *et al*., 2004). Part of the soil will be remoulded during initial penetration. The soil springs will vary with time due to increased riser penetration, cyclic soil degradation, drainage, reconsolidation of "intact" and remoulded soil and thixotropy.

The increased riser penetration is due to settlements due to plastic deformations in zones where the shear strength is exceeded and cyclic loading (permanent shear strain and dissipation of cyclically induced excess pore water pressure).

The stiffness is influenced by both the remoulded clay near the riser and the less disturbed clay further away from the riser.

The models that are generally used for non-linear stiffnesses and vertical and lateral resistances are analytical solutions and bearing capacity formulas. The formulas have to account for partial penetration and change in contact area, as discussed in the section on pipelines. Physical model tests (Section 8) are used to calibrate the theoretical formulas.

4.6.6 *Required soil parameters*

The calculation models for stiffness and capacity require information about undrained shear strength and moduli of "intact" and remoulded soil, both under monotonic and cyclic loading. Information about the initial shear modulus is important input. The soil is likely to be undrained during individual storms, but may have time to drain and reconsolidate between storms. The reconsolidation may increase the undrained shear strength and modulus of normally consolidated clay, but may cause a reduction in shear strength and moduli of overconsolidated clay. The remoulded clay may also gain strength from thixotropy effects. These effects should be accounted for by modelling in the laboratory tests or by utilizing existing experience.

As for pipelines, the riser behaviour depends on the properties of the top soil, and the discussion about box core sampling and laboratory testing in the section on pipelines is also valid for risers.

The strength at the interface between the riser and the soil may also depend on the riser surface, and ring shear, shear box or tilt table tests can be performed to evaluate whether the shear strength at the interface is smaller than in the soil itself.

The soil parameters that are required for riser/soil interaction are summarized in Table 5.1.

4.7 *Slope stability*

4.7.1 *Slide risk assessment*

Deepwater field development on continental slopes will often be located in areas with signs of previous slope instability. In addition to the average inclination, which typically is less than 4°, local escarpments from previous slide activity can be found upslope and down slope of the reservoir area. Often the petroleum reservoirs are related to anticlines and diapirism, which may give rise to local increase in seabed inclination. Assessment of the risk of slope instability is in these situations required as input to the total project risk analysis.

Risk can be defined as the product of probability of a failure event and the consequences of the failure. The risk is thus dependent on the probability of slide initiation, the extent and volume (depth affected, lateral extent, run-out and retrogression distance) of slide masses involved relative to the lay-out and type of the field installations and the damage potential of slide events. Extensive studies were performed for the Atlantis and Mad Dog fields located at the Sigsbee Escarpment in the Gulf of Mexico (Jeanjean, 2003 and a series of accompanying OTC papers) and for the Ormen Lange Field located in the Storegga slide scar (Nadim *et al*, 2005).

The slide risk assessment must be based on a thorough evaluation of site specific geological, geophysical and geotechnical information combined with modeling of the sedimentation process, pore water pressure history and present pore water pressure regime, sliding mechanisms and slide dynamics. This will allow analyses of today's stable situation under gravity loading (static slope stability analysis) and calculation of a deterministic factor of safety or a probability of failure based on uncertainty of analysis models and input parameters.

Then the influence of natural processes and human induced effects (see Section 3) on the stability during the lifetime of the project has to be evaluated. Finally, the potential influence zones of slide activity and the impact on field installations have to be evaluated.

Simulation of the sedimentation process and the pore water pressure history will also allow assessment of past soil strength and slope stability conditions, which can be applied in explanation of observed past slide activity.

4.7.2 *Pore water pressure and effective stress conditions*

Assessment of today's slope stability and explanation of

past slide events require evaluation of the past and present pore water pressure and effective stress conditions. In areas with high deposition rate (past and/or present), the potential for excess pore water pressure need to be evaluated. This must be based on detailed geological/geophysical assessment of seismic and chrono-stratigraphy combined with geotechnical data on permeability and compressibility.

The *required soil parameters* are:

– Depth converted seismic profiles with identified horizons
– Estimated or measured age of the horizons
– Compressibility (e-log p' curves from oedometer tests) representative for the different strata and for the stress range experienced during the sedimentation process, under slide events and during reloading under continued sedimentation following past slide events
– Permeability (hydraulic conductivity) from oedometer test or direct permeability measurements covering the range of stresses and void ratios.

Today's pore water pressure conditions may be measured in some points and at selected depths during site investigations with piezometers installed in boreholes or pore water pressure sensors inserted in the CPT equipment (see Section 7.3.3).

The calculation procedure is the following:

– Define stratigraphy (1D or 2D) with estimated material type and consolidation parameters for each stratum
– Define age profile
– Calculate/estimate sediment weight in each stratum based on measured unit weight and/or estimated effective stress based on compression test data
– Calculate sediment accumulation rates (kg/m^2/year) for each stratum based on sediment weight and time difference top-bottom of each stratum.
– Perform a stepwise simulation of the sedimentation and slide process (basin type analysis) from a selected depth to seabed to calculate distribution of excess pore water pressure and effective overburden stress during time
– Calculate undrained shear strength distributions with time

This allows assessment of a best estimate and variation range in excess pore water pressure, effective stress and undrained strength today and at the time of previous slide events. The uncertainty in the pore water pressure modeling is considerable, and it is recommended to try to verify the estimates against field measurement of undrained strength and pore water pressure, if and when such information is available.

4.7.3 *Slide initiation*

Slope stability analyses require definition of a seabed profile, soil layers and soil strength in the steepest part of a field development area or in the upslope and downslope area that can possibly affect the installations. Slide scars, faults and diapirs will typically be the critical areas with respect to slope inclination.

The selected profiles can then be analysed with different tools, like:

– infinite slope analysis
– limit equilibrium analysis
– upper bound plastic analysis
– finite element analysis

4.7.3.1 Infinite slope analysis

Infinite slope analysis is a 1D analysis of a slab sliding along a slip surface with inclination, α, vs. horizontal at depth, z, below seabed (Figure 4.13).

The effective normal stress σ'_n and the shear stress, τ, on the slip surface can be expressed as:

$$\sigma'_n = \gamma' z \cdot \cos^2 \alpha - \Delta u = \gamma' z(\cos^2 \alpha - r_u)$$

$$\tau = \gamma' z \cdot \sin \alpha \cdot \cos \alpha$$

where γ' = submerged unit weight and $r_u = \Delta u/\gamma' z$ is excess pore water pressure ratio.

The soil strength, τ_f, along the slip surface can then be expressed with drained or undrained soil parameters:

With drained parameters,

$\tau_f = \sigma'_n \cdot \tan\varphi + c$ or τ_f

where φ = friction angle, and c = cohesion.

or $\tau_f = \sigma'_n \cdot \tan\varphi(\sigma'_n)$,

using a nonlinear, stress dependent relationship between the friction angle and the consolidation stress (σ'_n).

With undrained parameters, $\tau_f = \sigma'_n \cdot (s_u/\sigma'_n) = k(\sigma'_n) \cdot \sigma'_n$, where s_u=undrained strength, $k(\sigma'_n)$=normalised undrained strength, which typically is stress dependent and decreasing with increasing consolidation stress.

The factor of safety, FoS, can be expressed as:

$$FoS_d = \frac{\tan\varphi \cdot (\cos^2 \alpha - r_u)}{\sin \alpha \cdot \cos \alpha}$$

for drained conditions, and as

$$FoS_u = \frac{k \cdot (\cos^2 \alpha - r_u)}{\sin \alpha \cdot \cos \alpha}$$

for undrained conditions (Figure 4.14).

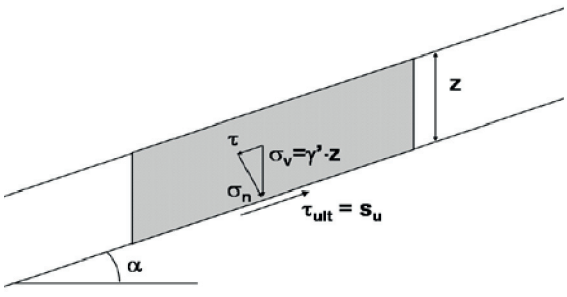

Figure 4.13. Infinite slope model

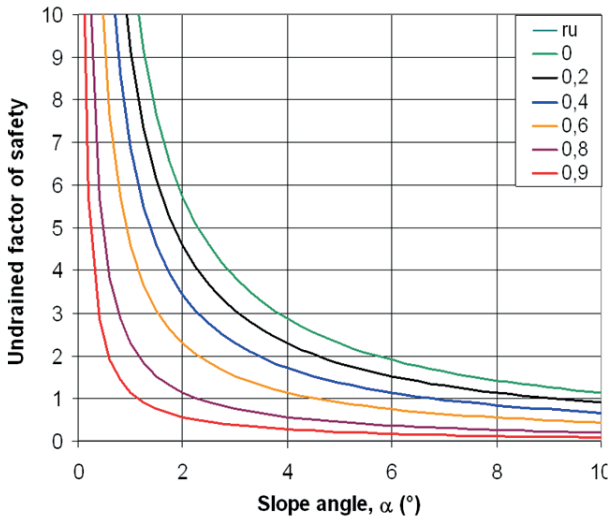

Figure 4.14. Infinite slope analysis. Factor of safety vs. slope angle and excess pore water pressure ratio, r_u, for undrained conditions. Normalised undrained strength, $k = s_u/\sigma'_n = 0.2$.

4.7.3.2 Limit equilibrium analysis

Limit equilibrium analysis (method of slices) has been the traditional tool for slope stability analysis. A number of different methods have been developed; Fellenius (1936), Bishop (1955), Morgenstern and Price (1965), Spencer (1967) and Janbu (1969), to mention some. This method allows 2D analyses of irregular seabed surface and also irregular stratigraphy to be modelled (Figure 4.15).

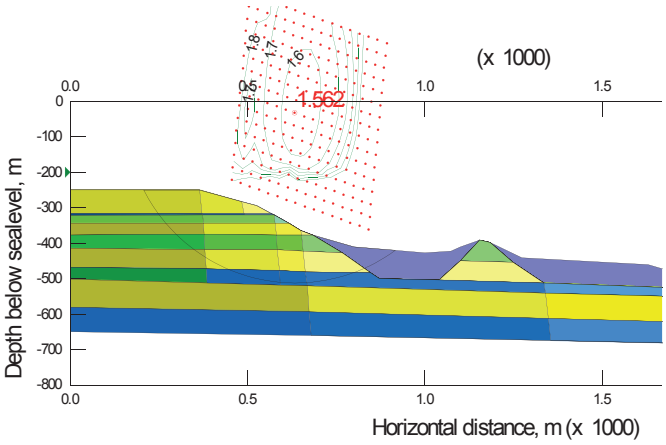

Figure 4.15. Slope stability analysis of a cross section of the upper headwall of the Storegga slide using SLOPE/W (Geoslope Inc.), The factor of safety was found to be 1.56.

The soil parameters are the same as for the infinite slope analysis, but some of the programs that have been developed allow anisotropic undrained strength to be modeled where the strength along the base of each slice is a function of the local inclination of the slip surface. Sophisticated algorithms for search of critical slip surfaces have been implemented in several of these programs.

4.7.3.3 Upper bound plasticity or energy equilibrium methods

An estimate of the plastic collapse load of a body is made by equating internal rate of dissipation of energy to the rate at which external forces do work in any postulated (kinematically admissible) mechanism of deformation of the body. By dividing the slope in a kinematically admissible set of rigid block and deformable shear blocks, close approximations to critical factor of safety can be calculated. The estimated factor of safety will be either on the high side or correct. The energy method can also be applied in modelling of slide dynamics, see Section 4.7.4.

4.7.3.4 Finite element analysis

Finite element analysis (FEA) is a very useful tool in assessment of slope stability. Several computer codes allow identification of the critical slip surface and calculation of the FoS against slope instability applying the shear strength reduction (SSR) method. The calculated FoS corresponds normally very well with the results from limit equilibrium analyses (see Figures 4.15 and 4.16). The elasto-plastic SSR FE approach offers advantages over traditional limit-equilibrium analysis as the need for a priori assumptions on failure mechanisms (the type, shape, and location of failure surfaces) is eliminated and the critical failure mechanism is automatically established. It eliminates artificial separation of slope problems into those involving slip surface failures, and those involving failure of deformed wedges.

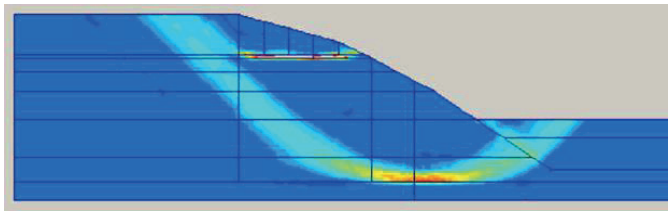

Figure 4.16. FE analysis of a cross section of the upper headwall of the Storegga slide using PLAXIS (Plaxis). The factor of safety was found to be 1.56 with the SSR method.

Non-linear elasto-plastic analyses in the time domain allow simulation of earthquake loading. Earthquake acceleration time histories are applied at the base of the analysed FE-grid and the responding stress-strain and displacement time histories are calculated. This allows estimates of cyclic and accumulated strains along the critical slip surface and assessment of earthquake induced strain softening to be made. 1D and 2D FE analysis tools for simulation of slope response under earthquake loading exist.

The required soil parameters may vary dependent on the stress-strain models implemented in the different computer codes, but in addition to undrained strength and submerged unit weight, parameters describing shear and volumetric stiffness vs. strain are required. For linear

elastic, ideal plastic models only the shear or Young's modulus (G or E) need to be defined.

4.7.4 *Slide run-out and slide retrogression*

After slide initiation, the slide mass will displace in the downslope direction. The shear strains along the slip surface and also internally in the slide mass will increase dramatically. Contractive and strain softening materials will generate increased pore water pressure in the shear zones, and the shear strength may drop towards residual or remoulded strength. This leads to a significant reduction in the FoS and the slide mass will accelerate downslope. If the mobility of the initial slide mass is sufficient, the slide head wall will be unloaded and the progressive spreading of shear concentration zones will be repeated in the soil mass behind the first developed headwall. Finite element analysis with strain softening material models allows simulation of this behaviour (Figure 4.17).

4.7.4.1 Multiblock energy approach

Modelling of run-out and retrogression has been developed with kinematically admissible block models at NGI (Kvalstad *et al*., 2005).

The method applied is based on an energy approach where the potential energy release of slide block systems with prescribed geometry and displacement pattern is calculated (Figure 4.18). The dissipated energy along the basal slip surface, between the individual blocks and in the distortion zones is calculated assuming that progressive development of shear zones has brought the shear strength down to residual or remoulded undrained strength. If the release of potential energy is higher than the dissipated energy, this difference has to be balanced by the kinematic energy in the slide block system, and the slide mass velocity can be calculated. The model has also been expanded to simulate retrogressive failure with a series of "triblocks" (Figure 4.19).

The results of the analyses are run-out and retrogression distances, frontal velocity and kinetic energy (Figure 4.20). These data are essential parameters in describing the influence zone of the slide mass and slide mass motion required as input to tsunami analyses.

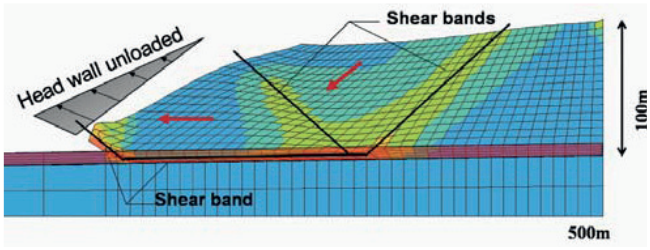

Figure 4.17. Displacement plot from FE modeling showing shear band development in slope with strain softening material in basal slip plane (Andresen, 2001).

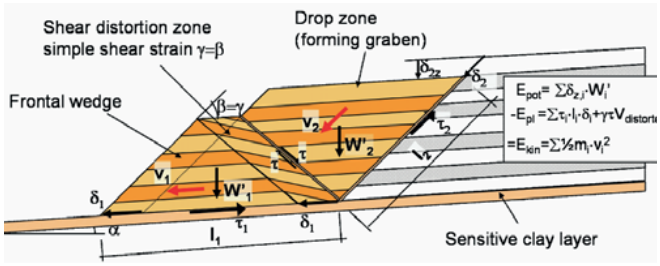

Figure 4.18 Kinematically admissible block slide model consisting of three blocks; frontal wedge, distortion zone and a drop zone forming a graben structure.

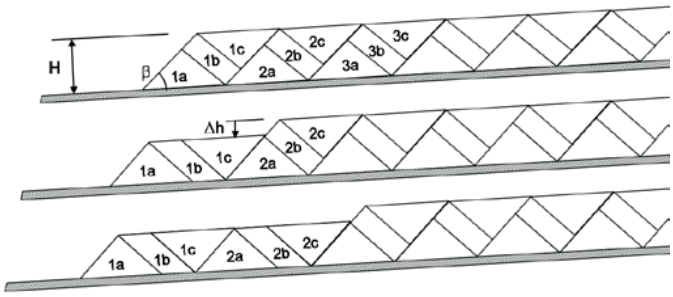

Figure 4.19. Series of "triblocks" with prescribed deformation pattern for estimate of slide run-out and retrogression.

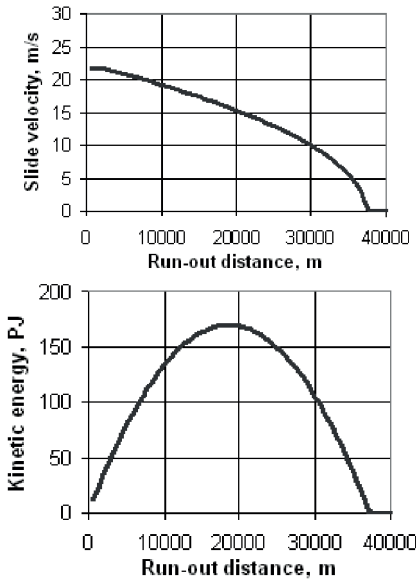

Figure 4.20. Example of simulation of the Storegga slide run-out with the triblock model with the block slide model.

The required soil parameters for the analyses are the intact and remoulded strength distribution vs. depth below seabed and the submerged unit weight.

4.7.4.2 Computational fluid dynamics analysis

More advanced simulation can be performed using computational flow dynamics (CFD) analyses (Gauer *et al*., 2005). The soil is modelled as a viscous fluid, and the viscosity in each element is adjusted individually in each time step to fit the selected viscoplastic material model. Figure 4.21 shows the results of a simulation of the last

phase of the Storegga slide towards the upper headwall. The material model applied was a Bingham model with initial yield strength increasing linearly with depth below seabed. A strain softening algorithm which reduces the yield strength as a function of experienced shear strain was implemented. The sensitivity of the slide mass was set to 3.0. The base slip plane was prescribed at 225 m depth. The simulations resulted in a slide block pattern very similar to what could be observed from seismic profiling near the headwall area (Figure 4.21).

The required soil parameters are basically the same as for the block model. The yield strength can be approximated with the remoulded strength, and a slight viscosity can be added to include strain rate effects.

Simulations can also been carried out with the debris flow model BING (Imran *et al*., 2001). This time-dependent model uses the depth-integrated momentum and continuity equations to calculate the movement of a simulated debris flow. The model allows only average parameters of the debris flow to be specified, while the typical behavior of clays is a rather linear increase in strength vs. depth below seabed.

5 SUMMARY OF REQUIRED SOIL PARAMETERS

The soil parameters that are needed for the various analyses described in Section 4 are summarized in Table 5.1. The table is based on typical designs. Special cases may require additional parameters. More details are given in Section 4.

Table 5.1 also indicates whether the parameters can be determined from *in situ* tests and/or from laboratory tests and the type of test. A detailed discussion of how the various parameters can be determined is discussed in detail in Section 7. For many of the parameters, empirical diagrams that can be used for a preliminary estimate of the parameters are also given. These diagrams are based on results from testing reported in the literature and in internal NGI files.

Classification, index testing, preconsolidation stress, *in situ* pore water pressure and overconsolidation ratio are general parameters that are needed in all cases to characterize a site.

The numerical values of the soil parameters will depend on the *in situ* effective stresses. It is therefore imperative to know the *in situ* pore water pressure. As discussed elsewhere in the paper, deep water soils can be underconsolidated. Strength and deformation properties will then be overestimated by assuming hydrostatic pore water pressure. In order to know the *in situ* pore water pressure, one will need to measure it *in situ*. Pore water pressure measurements are discussed in Section 7.3.3.

The temperature in the laboratory is normally different from the *in situ* temperature. The effect that this temperature difference may have on the soil parameters

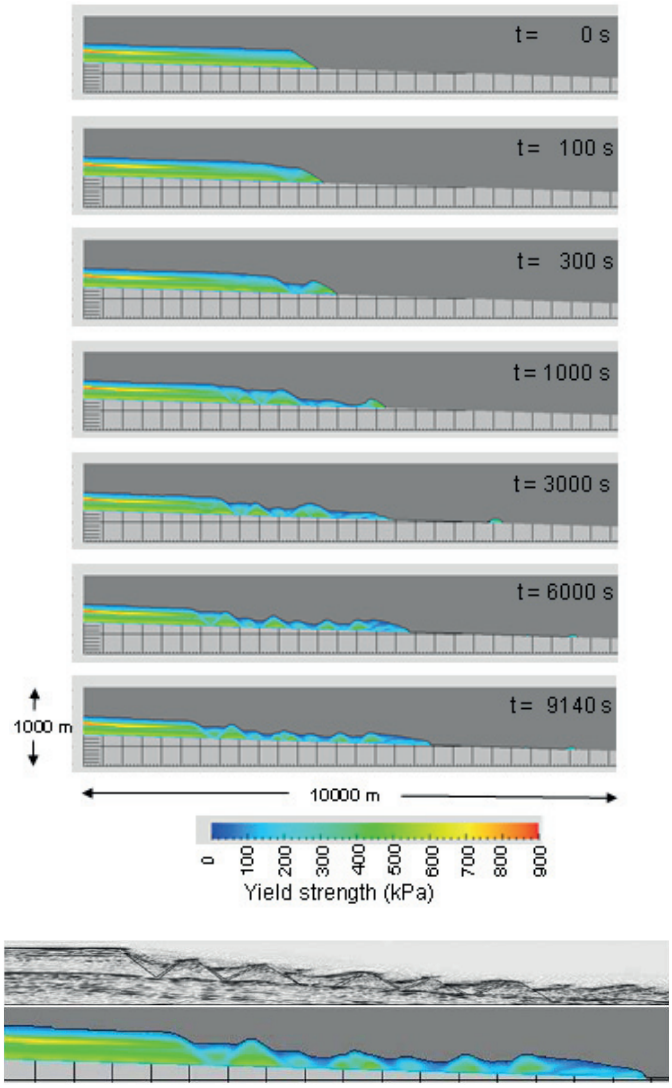

Figure 4.21. Comparison between seismic profile showing slide block pattern in upper part of the Storegga slide and CFD modeling of the same area. (Gauer *et al*., 2005)

has received relatively little attention in the past. Examples showing that this temperature difference may be important are presented in Section 7.6.18.

In some cases, like for pipelines and risers, the soil parameters need to be determined for the top soil, which is difficult to model in the laboratory due to low stresses and strength. It is also challenging to establish good calculation models. Physical model testing is therefore a supplement to establish and calibrate soil models for pipelines and risers. Model tests are discussed in Section 8

Earthquake analyses are only mentioned in connection with slope stability in Section 4. In earthquake areas, however, earthquake analyses may also be required for seabed structures, anchors and pipelines. Such analyses will require information about initial shear modulus, shear modulus as function of shear stress or shear strain, damping and cyclic shear strength.

Table 5.1 Summary of main parameters required for the various concepts.

Parameter	Suct. Anch. [3] Installation	Suct. Anch. [3] Capacity	Pile anchors	Drag anchors	Torpedo anchors	Seabed structures [11]	Piles [9]	Pipelines	Risers	Excess pore water pressure	Slope stability	Run-out/ retrogression	Determination method	
													In situ tests	Lab. tests
Classification and index testing [1]	x	x	x	x	x	x	x	x	x	x	x	x	CPT	Classification tests
In situ stresses	x	x	x	x	x	x	x	x	x	x	x	-		CK_0U triaxial
In situ pore water pressure	x	x	x	x	x	x	x	-	-	x	x	x	Piezometer Piezoprobe	
Precons. stress and OCR	x	x	x	x	x	x	x	x	x	x	x	-	CPT	Oedometer (CRS/IL) CK_0U triaxial
Compressibility; 1st loading and unload/reload	4)	x	x	8)	x	x	x	x	x	x	-	-		Oedometer
Permeability	4)	x	x	8)	x	x	x	x	x	x	-	-		Oedometer Const. head
Anisotropic monotonic strengths	x	x	7)	7)	x	x	7)	9)	10)	x	x	x	Field vane CPT Full flow pen. tests	CAUC, DSS, CAUE. Constant rate of strain or creep tests
Stress path dependent cyclic strengths	x	x	7)	7)	x	5)	-	9)	10)	-	x	-		CAUC, CAUE, DSS
Undrained anisotropic stress-strain relations	-	-	7)	-	-	x	7)	9)	10)	-	x	-		CAUC, DSS, CAUE. Constant rate of strain or creep tests
Initial shear modulus	-	-	7)	-	-	x	7)	-	10)	-	x	-	Seismic cone	Bender elements Resonant column
Permanent and cyclic shear strains under cyclic loading	-	-	7)	-	-	5)	-	-	10)	-	x	-		Cyclic CAU Cyclic DSS
Excess pore water pressure due to cyclic loading	-	-	-	-	-	5)	-	-	10)	-	-	-		Cyclic CAU Cyclic DSS
Strength, moduli and damping for earthq. loading	12)	12)	12)	12)	12)	12)	12)	12)	12)		12)	-		Cyclic/static CAU Cyclic/static DSS Cyclic/undr. creep
Effect of shear stress during consolidation	-	-	7)	8)	-	6)	7)	9)	-	-	x	-		CAUC, CAUE, DSS
Effect of rate of strain and load duration	x	x	x	7)	x	x	7)	9)	-	-	x	x		CAUC, DSS, CAUE. Constant rate of strain or creep tests
Remoulded strength	x	x	7)	x	x	x	7)	x	x	-	-	x	Field vane T-bar (or ball pen.)	Fall cone Lab vane
Sensitivity	x	x	7)	x	x	x	7)	x	x	-	-	x		
Thixotropy	4)	x	7)	8)	x	x	7)	7,10)	10)	-	-			Thixotropy tests
Compressibility and permeability of remoulded soil	4)	x	7)	8)	x	x	7)	7,10)	10)	-	-			Oedometer Const. head
Reconsolidated remoulded strength	4)	x	7)	8)	x	x	7)	7,10)	10)	-	-	-		CAUC, CAUE, DSS
Temperature effects	2)	2)	2)	2)	2)	2)	2)	2)	2)	2)	2)	2)	2)	2)

1) Includes water content, unit weight, grain size distribution, liquid and plastic limits, index strength (e.g. fall cone, lab. vane, UU, torvane, pocket penetrometer), carbonate content, mineralogy.
2) Temperature effects are important in all cases and for all laboratory tests (see Section 7.6.18)
3) As suction anchors are relatively shallow structures, deep soil borings are not needed, but requires more detailed soil data at shallow depths than piles.
4) May be relevant to determine set-up during stopping periods during installation.
5) In cases with cyclic loading
6) For skirted structures
7) In case of advanced analytical or numerical analyses
8) If set-up effects are taken into account
9) For seabed structures
10) Parameters may be difficult to determine in lab due to low effective stresses and strengths
11) For mudmats and skirted structures
12) In earthquake areas

6 GEOPHYSICAL AND GEOLOGICAL CHARACTERIZATION

6.1 *Geophysical characterization*

The most common tools used for geophysical characterization are various reflection seismic methods. The main difference between the tools is in their resolution and penetration ability.

The seismic reflection tools allow the determination of the thickness and shape of various soil units as well as the description of internal structures and internal acoustic appearance. These characteristics can be of help to determine soil type, but ultimately soil samples are needed. The geophysical data can however be of great help in determining where samples should be taken in order to obtain characteristic samples from all relevant layers and to extrapolate and interpolate information from sample/borehole locations.

6.1.1 *Geophysical methods*

6.1.1.1 Echo sounding/Multibeam echo sounding

Echo sounding is used for finding the bathymetry. The use of traditional echo sounders are increasingly being replaced by multibeam echo sounders / swath bathymetry that give a swath of measurements along the ship's track instead of only a single line. The multibeam data requires processing and calibration with sound velocities obtained from CTD (conductivity, temperature, depth) profiles through the water column. The grid of data points from swath bathymetry has a typical spacing of about 5m, but depends on the water depth at the site. Swath bathymetry recorded from ROVs can have a grid with a spatial resolution around 10 cm to 1 m. For deep water, ROV or AUV recordings are preferable to those from ships because the horizontal resolution decreases as the distance from the seafloor increases.

The DEMs (digital elevation models) obtained from multibeam data provide detailed pictures of seafloor features (e.g. slumps, pockmarks) and other artifacts.

6.1.1.2 Side scan sonar

Side scan sonar maps the acoustic reflectivity of the sea floor and thus shows changes in seafloor composition as exemplified by patches of sand and gravel on an otherwise muddy seafloor. The data do not contain depth information, however.

6.1.1.3 Sub bottom profiling

The frequency of sound waves used by these tools (~3.5 kHz) have given them the nickname "pinger" from the sound they make. The high frequency means that they have a high vertical resolution, but poor penetration. Pingers are therefore used to resolve the layering in the uppermost 10-50m of the sediment, and seldom penetrate more than this. For deep water ROV or AUV measurements provide better data than ship based measurements because of the smaller size of the Fresnel zone (Figure 6.1).

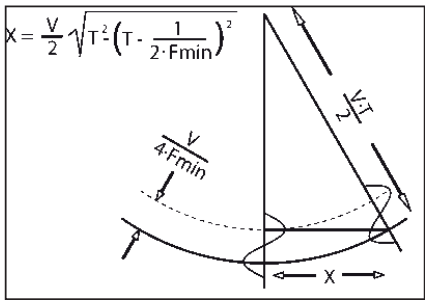

Figure 6.1. Horizontal resolution is defined by the Fresnel zone (X) and depends on water depth (two way travel time, T), frequency (F) and velocity (V).

6.1.1.4 Boomer/sparker

These use a frequency of a few hundred Hz and therefore have a better penetration, but a poorer resolution than sub bottom profilers (SBP). However, they are often used instead of SBPs where these signals are unable to penetrate sufficiently into the sea floor.

6.1.1.5 Multichannel reflection seismics

High resolution 2D data are often acquired prior to drilling wells as part of the evaluation of the shallow gas hazard and are therefore often available before geotechnical soil investigations in the same area take place. The frequency is about 500 Hz giving a penetration of about 1000m and a vertical resolution of about 0.8m (Table 6.1). The data can be very useful in extrapolating layering etc. from deep geotechnical boreholes.

Exploration 2D data usually have a resolution that is too poor to be very useful for soil investigations.

Although the vertical resolution may be poor, exploration 3D is very useful because of the very close spacing of data points. The seafloor reflector can give a very detailed picture of the topography of the area, especially in deep water. For buried layers, interpreted horizons can similarly be used to extract slip plane morphology etc. and in some cases the seismic attributes can be used to separate different soil types.

Table 6.1. Frequency, resolution and penetration of common seismic tools.

Tool	Approx. frequency and vertical resolution	Typical penetration depth
Echo sounders	> 20 kHz 0.02 m	0 m. Seafloor only
Pingers, sub bottom profilers (SBP)	~3.5 kHz 0.1 m	10-50 m
High resolution seismics	~500 Hz 0.8 m	100-1000 m
Exploration seismics	~50Hz 8 m	Several km

6.1.2 *Strategy of soil investigations*

The ideal strategy for a site investigation in a new area is to:

- Evaluate existing 2D high resolution and 3D data
- Perform additional multibeam and SBP surveys if deemed necessary.
- Design and carry out soil investigation.

During interpretation of the seismic data, several features of importance to the soil investigation and field development may be discovered. Examples of such features are given in the following.

6.1.3 *Submarine slides*

Submarine slide scars can be seen on the seafloor or as buried slides on seismic sections. They are often characterized by having a slip plane and one or more headwalls. The slide masses themselves (mass transport deposits) have a chaotic internal structure and an uneven surface. The slip plane is planar and can often be seen (on multibeam or 3D data) to contain striations parallel to the direction of mass movement. Submarine slides often occur as retrogressive slides on low angle slopes (down to ~1°). The size can vary from huge slides such as the Storegga Slide where the headwall is 300 km long to quite small features. The smallest features that can normally be observed on the seafloor reflector of topography from 3D seismic data are around 200 m wide and perhaps 5 m deep. Such a slide would be a threat to most seafloor installations. Turbidity currents generated by the slide may be a hazard to infrastructure some distance (depends on slope etc.) down slope from the slide itself.

6.1.4 *Shallow gas*

Shallow gas is a common drilling hazard. It can be recognized on seismic sections as enhanced reflectors (Figure 6.2) and zones where the acoustic signal is blanked out or noisy. Upward gas migration often creates columns of blanked reflectors or "chimneys".

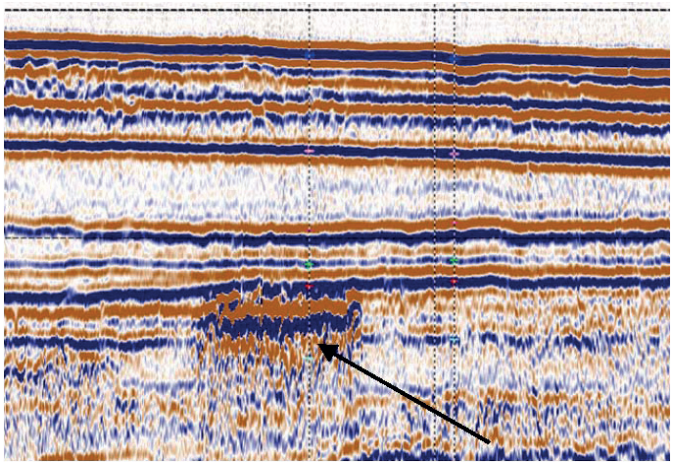

Figure 6.2. Example of a gas anomaly (arrow) on a high resolution 2D seismic section.

6.1.5 *Pockmarks*

Fluid or gas escaping through the seafloor often creates pockmarks (Figure 6.3) or crater-like depressions on the seafloor. Pockmarks can vary greatly in size from a diameter of about 1m to 500m with depths from only a few cm to tens of meters. The seafloor sediments have to be "pockmarkable" however, which means that they in general have to consist of fine grained sediments. The presence of pockmarks may not always indicate active gas or fluid venting, but can be an imprint left behind by activity in the past.

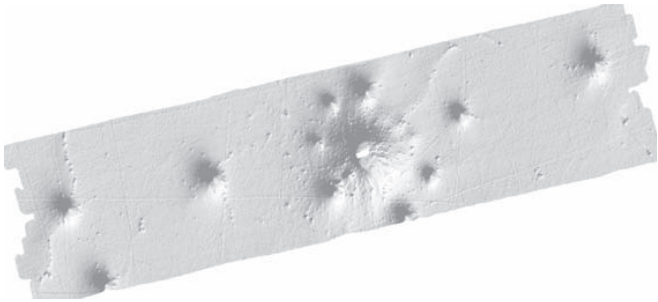

Figure 6.3. Multibeam bathymetry showing a complex pockmark with 7 satellites and 4 normal pockmarks (Forsberg et al., 2007).

6.1.6 *Gas hydrates*

The most common form of gas hydrate is methane hydrate that in general can form in water deeper than about 600m. The presence of hydrate is indicated by the presence of a bottom simulating reflector (BSR) on seismic sections (Figure 6.4). The BSR marks the base of the hydrate stability zone and is thought to be caused by the presence of some free gas in the sediments. Hydrates may form thick accumulations in areas with active venting and can be a hazard in these areas. The concentration in areas without active venting is probably quite low, but at present it is not known which concentration is a lower bound for the hydrates to be hazardous.

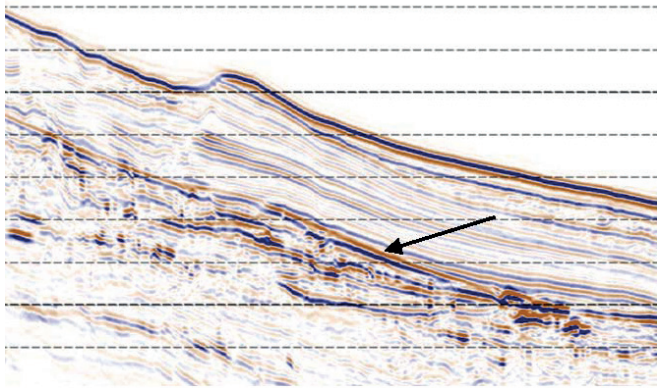

Figure 6.4. 2D high resolution seismic section showing the presence of a bottom simulating reflector (BSR, arrow), which is characteristic of the base of the gas hydrate stability zone.

6.1.7 *Mud volcanoes and salt domes*

Both mud volcanoes and salt are easily observed on seismic sections and will normally have been discovered during hydrocarbon exploration prior to soil investigations (Figure 6.5).

One common threat posed by these is that they may trigger sliding by over-steepening of the seafloor when they grow or, for the case of mud volcanoes, actually be a source of slide material that can inundate the surroundings. Salt domes are found in areas with thick salt deposits such as the Gulf of Mexico, whereas mud volcanoes are characteristic of tectonic thrust regimes (e.g. Trinidad) and areas with thick sediment accumulations. The mud volcanoes themselves are usually quite large (km-scale) features that vent both mud, fluids and gas and can therefore be associated with other types of hazard as well (e.g. excess pore water pressure and gas hydrates).

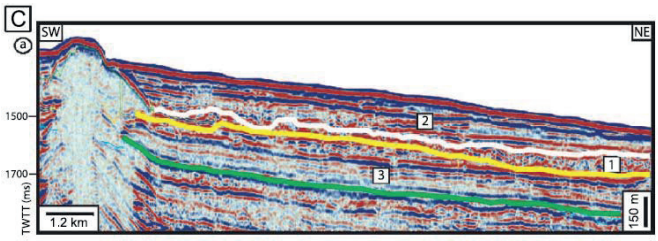

Figure 6.5. Seismic section from Trinidad showing a mud volcano (Moscardelli et al., 2006).

6.2 *Geological characterization*

Basic geological characterization is very similar to basic geotechnical characterization and includes a description where colour, soil structures, grain size, water contents and other index parameters are used. Somewhat more advanced characterization includes inspection of thin sections in optical microscopes or samples in a scanning electron microscope.

For stratigraphic analyses, age determinations and mineralogy can be useful. For hazard evaluations a concept of the time between or since events are needed and thus either direct dating of the sediments or correlations to layers of known age are needed.

6.2.1 *Geological testing*

6.2.1.1 Age Dating

The most common form of age determination is the radiocarbon method. It is based on the relative concentration of the radioactive isotope ^{14}C in the sample. ^{14}C is produced in the atmosphere and incorporated into plants, and thus the whole food chain, through photosynthesis. When an organism dies, the ^{14}C concentration is reduced through radioactive decay and is more or less completely depleted after about 50 000 years. This is therefore the maximum age on which radiocarbon dating can be used. Because the ^{14}C concentration in the atmosphere has varied through time, the radiocarbon age must be corrected to give calendar ages. ^{14}C dated tree rings etc. form the basis for the correction.

6.2.1.2 Mineralogy

Minerals, especially the clay minerals (e.g. smectite, illite, kaolinite and chlorite), determine many of the physical properties of the fine grained sediments. Thus a mineralogical analysis may prompt the need for special geotechnical tests. High smectite content may, for instance, warrant ring shear testing to find residual strength.

The most usual form for mineralogical analyses where clay minerals are included is X-ray diffraction. The method gives good qualitative results, but they are only semi-quantitative. This is because minerals vary in composition and have somewhat different diffraction peak intensities from place to place.

For sandy material microscopy and grain counts can be used for mineralogy.

6.2.1.3 Scanning Electron Microscopy (SEM)

SEM inspection is sometimes performed if the microstructure of the sample is suspected of influencing the physical properties of the soil. Small sub-samples (~0.5 cm^3) should be freeze-dried rather than dried in a normal manner to prevent deformation of the microstructure during desiccation. Once dried, the samples are mounted on sample holders and coated with a conducting material (e.g. gold, carbon) before inspection.

7 GEOTECHNICAL CHARACTERIZATION

7.1 *Introduction*

Basically, information about soil conditions can mainly be derived from two sources:

– results of laboratory tests on soil samples
– interpretation of results of *in situ* tests by means of theoretical solutions or empirical correlations

In general, one should not rely only on laboratory testing or only on *in situ* testing, but rather use a combination, as discussed in the following. Good overviews with guidelines for offshore soil investigations are given by SUT-OSIG's Guidance Notes (2000, 2004) and ISSMGE (2005). A new ISO standard on offshore soil investigation is under preparation. This will be a comprehensive document that can be used by all parties involved in offshore soil investigations. It is expected to be published in 2010.

7.2 *Deployment of sampling or in situ tools*

Sampling and *in situ* testing can basically be done in two modes of operation:

– seabed mode (SB) with penetration of sampler or *in situ* tool from sea bottom to refusal or to some predetermined depth. With presently available techniques,

penetration of *in situ* tools is normally limited to 30-45 m below sea bottom and sampling to about 20 m, although there are examples of larger penetrations being obtained. Usually, *in situ* testing is carried out with controlled pushing from the seabed, like the CPTU. Regarding sampling, traditionally seabed sampling in soft soils have been of the free fall gravity core type. A new deep water sampler that is penetrated with controlled pushing is given some emphasis in this paper (Section 7.4.2.3).

– down hole (DH) mode where sampling or *in situ* testing occurs in the bottom of the borehole. Large penetration below sea bottom can be achieved with this type of operation, which traditionally has been with the drill rig mounted on the ship.

A new alternative approach is to use an automated seabottom rig, the so-called PROD system (Figure 7.1). Problems related to heave of the vessel is avoided with this approach (e.g. Pennington and Kelleher, 2007).

It is important that, regardless of mode of operation, deployment of the *in situ* tool or sampler is done in such a way that the soil being tested or sampled is not disturbed.

Figure 7.1. PROD being launched.

7.3 *In situ testing*

7.3.1 *Introduction*

The main *in situ* testing tool has been and is the CPTU, but in some geographical areas the vane test has also been much used. Further the so-called full flow penetrometers have been increasingly used on several occasions during the last 10 years. The seismic cone and the piezoprobe are also used to some extent. The latter tool is also used for measurement of the *in situ* pore water pressure.

Since installation of piezometer, and possibly other instruments for long term measurements, can be done as part of an offshore soil investigation, this is also covered in the following. One additional type of *in situ* test is model testing which also is briefly covered.

7.3.2 *In situ tests to measure soil parameters*

7.3.2.1 Cone penetration test with pore water pressure measurements; CPTU.

The cone penetration test with pore water pressure measurement (CPTU) is now well standardized with respect to equipment and procedures in the NORSOK Standard (2004), which is the basis for the new ISO standard on marine soil investigations. One specific aspect that should be born in mind is that although the standard diameter of the cone penetrometer is 36 mm (equivalent to area= 10 cm^2), it is allowed to use diameters in the range 25 mm (area = 5 cm^2) and 50 mm (area = 200 cm^2) without using correction factors. However, for cone diameters outside the above range, such as mini cones with diameter < 25 mm, the results should be presented including a note that "non-standard" equipment has been used. When required, correction factors, based on parallel tests with 36 mm cone, should be applied before interpretation of the test results in terms of soil design parameters.

For very soft deep water soils it is important to monitor zero reference readings at the sea bottom since even relatively small zero shifts can have influence on the quality of the data. The new coming ISO standard recommends that the check on zero readings can be made by reporting of so-called deck to deck logging of the CPTU parameters. A similar scheme for deck to deck readings for down-hole mode CPTU will also be included in the new ISO standard.

A new cone design has been developed and patented by Gregg Drilling & Testing Inc. that provides greater accuracy in very soft sediments in deep water. The new cone design is based on a hydrostatically compensated cone using specially designed load cells. The load cell records the load that is independent of hydrostatic pressure. Traditional cone designs use Wheatstone bridge type stress gauges that produce an apparent load under high hydrostatic pressure, resulting in a loss of accuracy in very soft sediments in deep water. The new cone design uses specially designed load cells that are independent of applied hydrostatic pressure. The new cone records zero load at the seabed even in deep water. The load cells can therefore be designed to measure very small loads with improved accuracy in very soft sediments. Because the load cells are unaffected by the hydrostatic pressure they can be selected for greater accuracy and sensitivity in very soft sediments with resulting improved accuracy (Robertson, 2008).

7.3.2.2 Seismic cone; SCPT

With the seismic cone the shear wave velocity, V_s, is measured in addition to the standard CPTU parameters. Usually a seismic source mounted underneath the seabed frame is used as a shear wave source, and a geophone or seismometer in the cone penetrometer picks up the arrival of the shear wave. Knowing the time of travel and the

distance from the shear wave source to the geophone, the average shear wave velocity over the depth from seabed to geophone can be calculated. By repeating the seismic measurements at regular intervals, say every meter, the V_s value in each interval can be computed. One alternative that is more accurate is to have two geophones separated by 1 m in the cone penetrometer.

The important soil parameter, small strain shear modulus, G_0, can be computed from the formula:

$G_0 = \rho (V_s)^2$ where ρ is the soil mass density.

7.3.2.3 Full flow penetrometers

The so called full flow penetrometers were introduced to offshore soil investigation about 10 years ago (Randolph *et al*. 1998). Figure 7.2 shows the two full flow probes, the T-bar and the ball penetrometer, that are used in practice. The term full flow comes from the fact that the soil can flow round the device so that it is not necessary to subtract the full vertical total stress, as is done for the CPTU, before computing undrained shear strength. Only the vertical stress corresponding to the area of the rod needs to be subtracted. In most cases the ball or T-bar is just replacing the tip of a standard cone penetrometer, and the transducer used for measuring cone resistance can also be used to measure T-bar or ball resistance. The standard size of ball and T-bar (as will be given in the new ISO standard) are indicated in Figure 7.2, giving a cross sectional area of 100 cm^2, or 10 times the area of the cone penetrometer.

One advantage of the full flow penetrometers is that the area is much larger than for the CPT, so that the resolution of the measurement is higher.

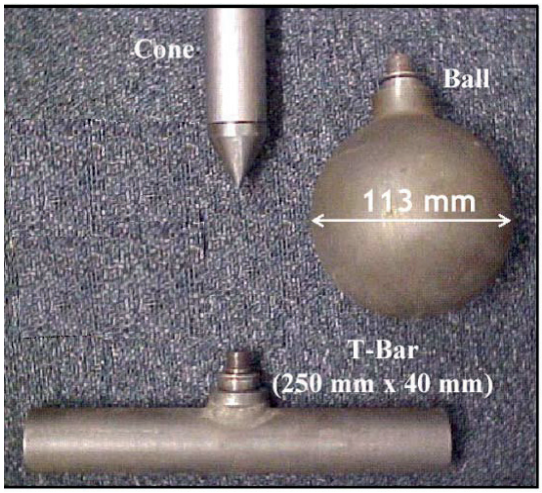

Figure 7.2 Full flow probes and cone penetrometer.

The measurement of T-bar and ball resistance still needs to be corrected for pore water pressure effects, as the cone penetrometer (e. g. Lunne *et al*., 1997), but the correction is much smaller relative to the cross sectional area of the penetrometer. The correction for vertical stress (acting over the area of the rod) and the water pressure acting at the slot behind the T-bar penetrometer reduces to:

$$q_{T\text{-}bar,corr} = q_{T\text{-}bar} - (\sigma_{v0} - u_2(1 - a))\,(A_s/A_p)$$

where σ_{v0} is the total vertical stress, u_2 is the water pressure acting in the slot behind the penetrometer and A_s and A_p are the areas of the rod and the penetrometer, respectively. Since u_2 is not normally measured, Randolph *et al*. (2007) recommends using the *in situ* pore water pressure, u_o, instead of u_2. The same correction should be applied to the measured ball resistance.

It is industry practice to also measure the T-bar (or ball) resistance during extraction of the penetrometer. This measurement is used for quality control of the data as recommended by Randolph *et al*. (2007).

By doing cyclic T-bar (or ball) tests at selected intervals during extraction of the probe, a remoulded T-bar resistance can be measured. This measurement can be interpreted in terms of remoulded shear strength, as discussed below. Figure 7.3 shows as an example the results of a complete T-bar test, including cycling, at NGI's soft clay test site at Onsøy.

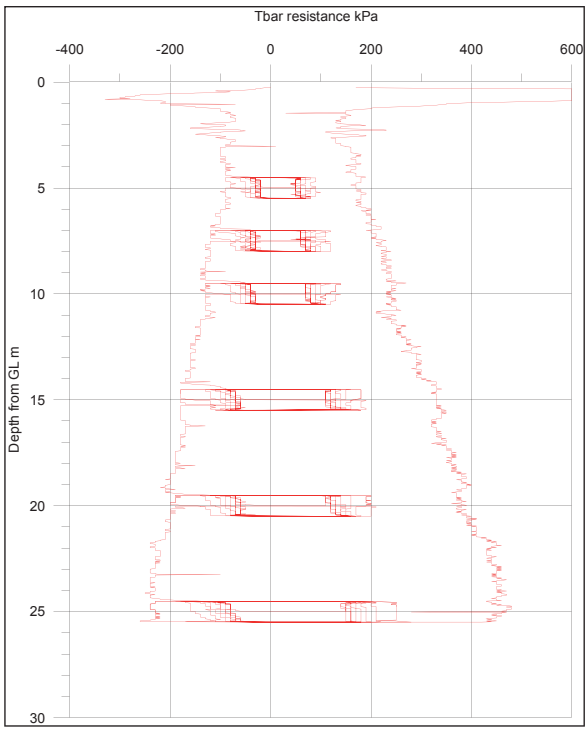

Figure 7.3 Result of T-bar test at Onsøy

7.3.2.4 *In situ* vane tests

The vane test has been used extensively for many years in the Gulf of Mexico. In the North Sea, it has been used only on relatively few projects. The offshore vane test can be used both in seabed and in down hole mode of operation. Peuchen and Mayne (2007) use the vane test for also measuring rate effects. Before use in foundation design or geohazards studies, correction of test results for rate and anisotropy effects need to be considered.

7.3.2.5 Interpretation of *in situ* penetration tests in terms of soil parameters

The main advantages of *in situ* penetration tests are that a continuous profile is obtained and that the issue of sample disturbance is eliminated.

However, the results of penetration tests are not direct measurements of the *in situ* shear strength, so an interpretation is needed in terms of some bearing capacity or N-factor. Recent theoretical and experimental research has confirmed that even if theoretical approaches exist for how to interpret the CPTU, T-bar and ball test results in terms of undrained shear strength parameters, there are many simplifications and assumptions that are required in the analyses (e.g. Andersen, 2002 and Randolph and Andersen, 2006). Thus empirical correlations are required for the various N-factors.

Numerous correlation studies have been carried out, especially for the CPTU, but also recently for the T-bar and the ball. The studies clearly indicate that it is not possible to define N-factors that are applicable for all types of soft clays, due to the fact that mineralogy, strength anisotropy, strain softening, sensitivity, degree of remoulding and rate effects vary from one soil to another. This is also in line with the theoretical work by Randolph and Andersen (2006). One advantage with the CPTU is that both the net corrected cone resistance, $q_t - p_o$, and the excess pore water pressure, Δu (= $u_2 - u_o$) can be used to evaluate the undrained shear strength, through the factors N_{kt} and $N_{\Delta u}$.

Based on the correlation studies and evaluations carried out by NGI and COFS, Table 7.1 summarises recommendations on which N-factors to use for practical projects (NGI/COFS, 2006).

The left column indicates the application; if there is limited experience in the area of the investigation, Application 1 should be used.

For Gulf of Guinea clays, Application 2 should be used, and for soft clays in the Norwegian Sea, Application 3 should be used as a guide.

The N-factors marked 1 (N_{kt1}, $N_{\Delta u1}$ and $N_{T\text{-}bar1}$) are based on correlations to undrained shear strength as measured in CAUC triaxial test on a good quality sample.

The N-factors marked 2 (N_{kt2}, $N_{\Delta u2}$ and $N_{T\text{-}bar2}$) are based on correlations to average undrained shear strength as measured in CAUC triaxial test, CAUE triaxial test and DSS tests on good quality samples. In some cases where CAUE tests have not been available, $s_{u,DSS}$ have been used. The mean values given in Table 7.1 can be used to calculate a mean shear strength. Regarding the range given, one should use the lower value to compute s_u when it is conservative to have a high shear strength and the higher value when it is conservative to have a low shear strength.

When using the CPTU, the undrained shear strength may be computed using both the N_{kt} values based on cone resistance and $N_{\Delta u}$ based on excess pore water pressure.

For the ball penetrometer test, the same N-factors as for the T-bar are recommended.

The recommendations given in Table 7.1 should be updated when local experience becomes available. However, extreme caution should be exercised if the correlations for a new site fall outside the ranges given, as this may indicate questionable data.

Table 7.1 Recommended N-factors

Application	Based on $s_{u,CAUC}$			Based on $s_{u,av}$ or $s_{u,DSS}$		
	N_{kt1}	$N_{\Delta u1}$	$N_{T\text{-}bar1}$	N_{kt2}	$N_{\Delta u2}$	$N_{T\text{-}bar2}$
1. Overall, if limited previous experience	11.5[1] (9.5 - 13.5)[2]	6 (4.5 - 7.5)	10 (8 to 12)	13 (11 - 15)	6.5 (5 - 8)	11 (9 - 13)
2. Gulf of Guineas	12.5 (10.5 - 14.5)	5.5 (4 - 7)	11 (9 – 13)	13.5 (11.5 – 15.5)	6 (4.5 – 7.5)	12 (10 – 14)
3. Norwegian Sea	11.5 (9.5 - 13.5)	5.5 (4 – 7)	11 (9 – 13)	14.5 (12.5 – 16.5)	7 (5.5 – 8.5)	14 (12 – 16)

Note: 1.Mean; 2. Range

Table 7.2 gives recommended $N_{T\text{-}bar}$ factors to calculate remoulded shear strength of clay from cyclic T-bar tests. It is presently proposed to use $N_{ball} = N_{T\text{-}bar.}$

Rate effect is a main reason why the N-factors as given in Table 7.2 depend on the type of test. This implies that one has to consider carefully the rate of shear strain in the case where one is going to apply the remoulded shear strength and to apply the N-factor appropriate for the strain rate in the design case.

Reasons why the N-factors are different for intact and remoulded shear strengths are discussed in Lunne and Andersen (2007).

Due to the uncertainties related to the CPTU sleeve friction measurements, as discussed by Lunne and Andersen (2007), it is recommended not to determine remoulded shear strength from CPTU sleeve friction measurements.

Table 7.2 Proposed N_T-bar factors to determine remoulded shear strength from cyclic T-bar penetrometer tests

Laboratory test type:	UU	Fall cone	Field vane
$N_{T\text{-}bar}$:	20	13.5	13.5

7.3.2.6 Guidance on when to use the different tests

Recommendations on which of the three *in situ* devices (cone, T-bar, ball or vane) should be used will depend on the project requirements, what soil conditions are likely to be encountered and the geotechnical problem(s) to be solved. Table 7.3 lists a number of geotechnical problems relevant for deep water field developments and how it is presently perceived that the various *in situ* tools can give reliable values of intact and remoulded shear strengths. Since an important part of a geotechnical evaluation is to consider layering and soil classification, an evaluation on how this information can be obtained from the four *in situ* tools is also included.

Table 7.3 is meant to be used as a guide for when to use the different *in situ* test types. The basis for the correlation for the ball test is much smaller than for the T-bar. However, since the tests at Onsøy, Burswood and Chinguetti indicate that the ball and T-bar resistances for these sites are very similar, the same N-factor is recommended for the ball and the T-bar.

Overall, the variability between the average N factors from the various sites has been found to be similar for the T-bar/ball and the cone penetrometer. Also the total range is about the same for the tools when comparing with laboratory tests.

Table 7.3 Applicability/reliability of interpreted soil parameters (adopted from NGI/COFS, 2006)

Geotechnical problem	Depth below seabed (m)	Soil parameters required[1,6]	Applicability / reliability			Comment
			CPTU	T-bar / ball	Vane	
Backfilled trenches: upheaval buckling	0-1	Soil profile	1-2	3	-	Extremely soft material may be encountered
		Classification	2	-	-	
		Soil density	2-3	-	-	
		Undrained shear strength	2-3	1-2	1-2	
Pipeline/riser soil interaction	0-3	Soil profile	1-2	3	-	Very soft material may be encountered
		Classification	2	-	-	
		Undrained shear strength	2	1-2	1-2	
		Remoulded shear strength	4	1-2[2]	1-2[5]	
Skirted foundations -penetration -bearing capacity	0-15/40	Soil profile	1-2	3	-	
		Classification	2	-	-	
		Undrained shear strength	2	1-2	1-2	
		Remoulded shear strength	4	1-2[2]	1-2[5]	
Seabed templates, pen.,stability, settlements	0-10	Soil profile	1-2	3	-	
		Classification	2	-	-	
		Undrained shear strength	2	1-2	1-2	
		Remoulded shear strength	5	1-2[2]	1-2	
		Settlements	(3-4)[4]	(-)[4]	(-)[4]	
Geohazards Slope stability	0-10/100[3]	Soil profile	1-2	3	-	Use of T-bar/ball and vane may be limited to 40 m depth
		Classification	2	-	-	
		Undrained shear strength	2	1-2	1-2	
		Remoulded shear strength	3-4	1-2[2]	1-2[5]	

Notes:
1. Scale of relative applicability/reliability: 1 High; 5 Very low. – No applicability. The values indicate to some extent NGI/COFS' view on the potential of a tool to derive a certain parameter.
2. Requires cyclic T-bar (or ball) tests
3. Table mainly covers interpretation of parameters to ~30 m.
4. Settlement parameters have not been covered
5. Requires at least 10 quick rotations.
6. Table does not include parameters to evaluate cyclic behaviour.
7. Seismic cone should be considered when small strain shear modulus is important

Note that the undrained shear strength from CPTU is rated lower in the case of backfilled material compared to original seabed soil due to the very low values of cone resistance and pore water pressure that are expected in this type of material.

At very shallow depths, where strengths are low, either the vane or the T-bar (or ball) may be capable of providing sufficient accuracy for estimating the shear strength. Both instruments show good agreement for both peak and residual (remoulded) strengths, with the advantage of the T-bar (or ball) that it gives a continuous profile of shear strength, and also is not subject to the same degree of scatter as is sometimes found with vane strengths. As such, it is recommended that the T-bar (or ball) is viewed as the primary tool, with the vane test as a supplementary test to increase reliability of the undrained shear strength.

In back-filled material, the material type is generally known and the shear strength is the main focus. In natural deposits, where the stratigraphy and type of material is uncertain, it is recommended that the CPTU is the primary investigation tool, since there is wide experience in interpreting the different parameters in order to deduce the material type. However, for direct estimation of shear strength, particularly in relatively soft material, in some cases the T-bar (or ball) may give a slightly tighter correlation (i.e. with smaller range of N value from site to site) than the cone, and therefore the T-bar (or ball) should be considered as a supplementary tool.

At this stage there is insufficient experience to assess the relative merits of the T-bar or ball. The T-bar, by its nature, is more susceptible to bending moments being induced in the load cell. These may result in spurious changes in the load cell measurements, since it is difficult to achieve complete independence of the load cell from the effects of bending. On the other hand, the T-bar may be viewed as a model pipeline element, and thus provides direct information for pipeline and riser design.

7.3.3 *Measurement of in situ pore water pressure*

7.3.3.1 Introduction

In situ pore water pressure is one of the fundamental parameters required for assessing the strength and stability of geo-materials. In particular, identification of pore water pressure regimes is necessary in geohazards studies. Offshore geological processes such as rapid sedimentation, minor slides, erosion, and fluid or gas seeps can result in non-hydrostatic pore water pressures in critical layers, leading to strength reductions and increased risk for instability.

7.3.3.2 Piezoprobe

In principle a CPTU dissipation test (e.g. Lunne *et al*., 1997a) can be used to define the *in situ* ambient pore water pressure. Excess pore water pressures are generated during penetration of the probe. After a stop in penetration, these excess pore water pressures will dissipate and come to rest at the *in situ* ambient pore water pressure. However, in clays the time to reach equilibrium is very long, up to several days with a standard size cone penetrometer (diameter = 36 mm). The time for full dissipation is proportional to the square of the probe diameter. Based on this, attempts have been made to reduce time for dissipation by having a tapered penetrometer with a reduced diameter at the filter, typically 5 – 8 mm. However, research at MIT showed that pore water pressure developed by the increased diameter behind the tapered cone eventually reaches the filter at the tip and influences the time for dissipation (Whittle *et al*., 2001). The extended small diameter tip should be as long as possible. The experience of the authors is that in some cases piezoprobes may give a reasonable estimate of the *in situ* pore water pressure; however, frequently there are uncertainties with the results, unless there are sand layers where quick dissipation occurs.

7.3.3.3 Piezometers

NGI concluded some years ago (Strout and Tjelta, 2004) that by far the most reliable measurements of *in situ* pore water pressure is to install piezometers and take readings after some time when one is absolutely confident that all excess pore water pressures have dissipated. As reported by Strout and Tjelta (2007), it is now possible to install piezometers as part of a soil investigation, using soil investigation techniques. Strout and Tjelta outline the possible ways of installing single or multilevel piezometers:

– In a drilled bore hole (which can be a standard soil boring with sampling and/or *in situ* testing), which is grouted after the piezometer string is in place, as shown in Figure 7.4.

– Using a seabed CPT frame to push in a piezometer as shown in Figure 7.5.

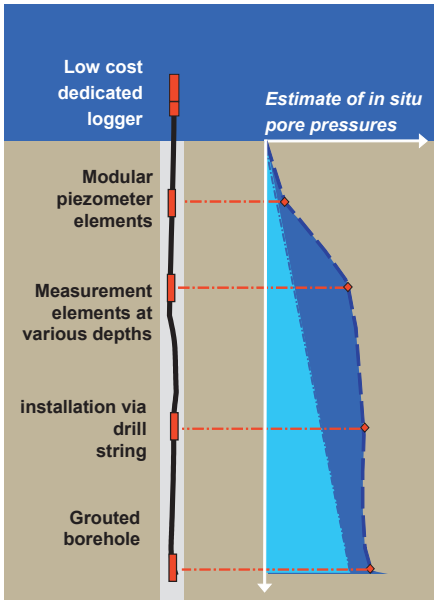

Figure 7.4. Example of multi-piezometer string (Strout and Tjelta, 2007).

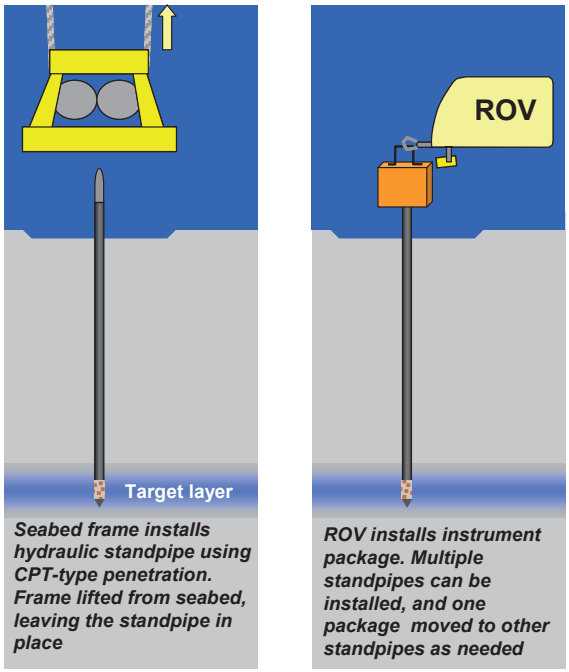

Figure 7.5. Example of piezoemeter installed with CPT equipment (Strout and Tjelta, 2007).

Three basic approaches may be used for measuring the pore water pressure (Figure 7.6):

– Direct measurement of total pressure *in situ* and at seabed; excess pore water pressure is the difference of these values minus the calculated hydrostatic pressure head at the sensor.

– Utilize a differential pressure sensor *in situ*, and establish a hydraulic connection to the seabed. Note that this requires that the fluid in the reference line has a density representative for the average density of the pore fluid in the soil column.

– Utilize a differential pressure sensor at seabed, and establish the measurement port *in situ*. The same requirements for the density of the hydraulic fluid apply for this case. Note that the differential sensor can also be two total pressure sensors, where one measures the seabed reference. Pore water pressure is the difference between these sensor readings.

Strout and Tjelta (2007) discuss the advantages and disadvantages of the three approaches described above.

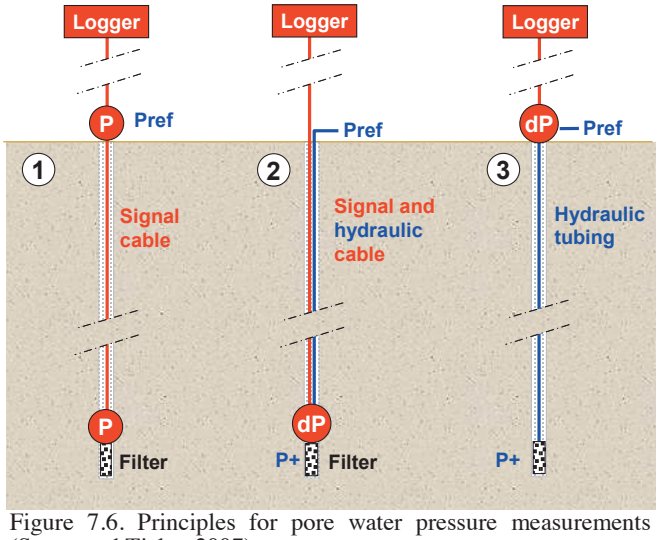

Figure 7.6. Principles for pore water pressure measurements (Strout and Tjelta, 2007).

7.3.4 *In situ model tests*

In some cases it is necessary to test larger volumes of soil and also to load the soil in a manner that simulates the full scale structure that is going to be installed. The results from such model tests can then be used to check both the soil design parameters evaluated from the soil investigation and the foundation analyses procedure.

As mentioned in Section 8, model testing can be both in the laboratory, as 1g or in the centrifuge, or in the field. The most realistic, but also the most complicated and costly, is to carry out field model tests at the actual offshore site. In this section only model tests that can be done from soil investigation vessels will be mentioned. Other field model tests are discussed in Section 8.

One recent example is *in situ* measurement of pipe-soil interaction, as presented by Hill and Jacob (2008). Figure 7.7 shows the pipe model that can be used to measure seabed soil-pipe interaction forces in vertical, axial and lateral directions.

7.4 *Soil sampling*

7.4.1 *Evaluation of sample disturbance*

The issue of sample disturbance needs to be accounted for when establishing design parameters, especially for soft

Figure 7.7. Pipe model tester (from Hill and Jacob, 2008).

clays. Lunne and Andersen (2007) presented a thorough review of most aspects related to sample disturbance.

Sample disturbance is caused by several factors:

– preparation and drilling of borehole (relevant for down hole mode sampling only);
– pressure of the tube into the soil;
– stress relief;
– gas coming out of solution in the sample;
– handling, transportation and storage of the sample;
– preparation equipment and testing techniques in the laboratory.

In most cases, the first three causes above are the most significant. The two last causes are usually of less importance if careful procedures are followed (SUT-OSIG, 2000 and 2004, ISSMGE, 2005, NORSOK, 2004).

Neglecting the effects of sample disturbance usually results in strength and deformation parameters that are on the low side; however, in some cases, the derived strength may be too high. The behaviour of samples taken with 54 and 75mm samplers are compared to behaviour high quality block samples in Figure 7.8. One should always attempt to take samples as undisturbed as possible.

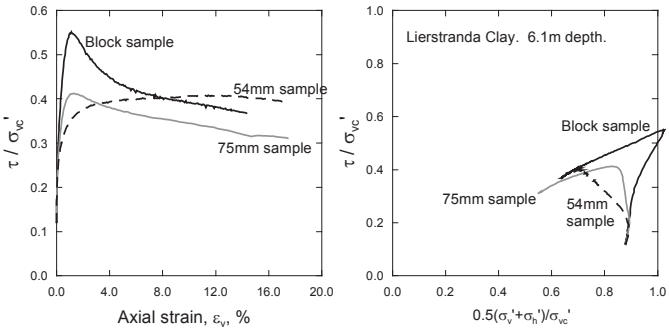

Figure 7.8. Stress-strain and stress paths for CAUC tests on soft clay specimens from various sampler types.

To ensure a reliable and cost-effective design, it is important to assess, as clearly as possible, the effects of sample disturbance. For many years, sample quality has been assessed based on results of oedometer tests, and to some extent, the anisotropic consolidation phase of triaxial

tests. A recent trend is to use non-destructive techniques, which have the advantage that the best samples can be identified before carrying out the laboratory tests.

Based on a systematic study of the results of triaxial and oedometer (constant rate of strain) tests on Lierstranda and Bothkennar clays, Lunne *et al*. (1997b) concluded that the change in pore volume relative to the initial pore volume, $\Delta e/e_o$, after reconsolidation to the *in situ* effective stress p'_o, was a more useful indicator than the in volumetric strain in the oedometer, $\Delta\varepsilon/\varepsilon_o$. (The *in situ stresses* must include any excess pore water pressures). They established the NGI sample disturbance criterion (Table 7.4) for evaluating the importance of sample disturbance on mechanical properties. Figure 7.9 illustrates the criterion and the results for three Norwegian clays.

The sample disturbance criterion proposed in Table 7.4 is based on the results on marine clays with a plasticity index between 6 and 43%, water content between 20 and 67%, and depth below ground between 0 and 25 m.

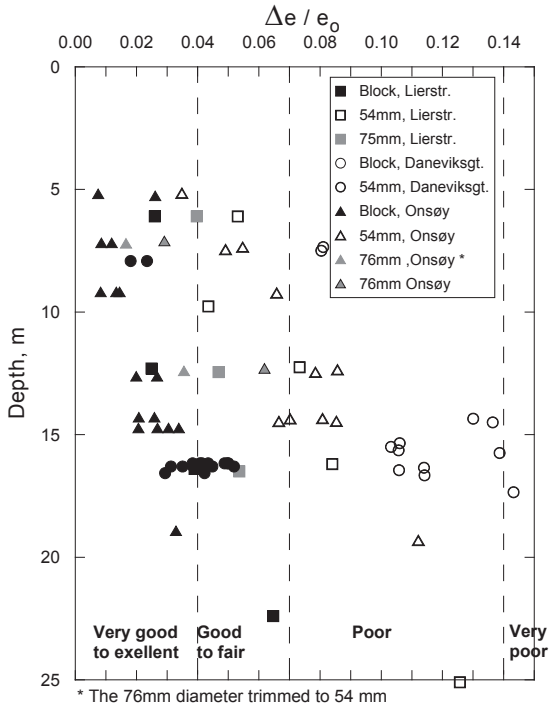

Figure 7.9 Δe/eo vs depth for three Norwegian clays (anisotropically consolidated triaxial tests) (Lunne and Andersen 2007).

Table 7.4. Proposed criterion for evaluation of sample disturbance (Lunne *et al*. 1997b).

OCR	Δe/eo at *in situ* stresses for sample quality 1, 2, 3 and 4			
	1. Very good to excellent	2. Good to fair	3. Poor	4. Very poor
1-2	<0.04	0.04-0.07	0.07-0.14	>0.14
2-4	<0.03	0.03-0.05	0.05-0.10	>0.10

OCR = overconsolidation ratio

A potential alternative technique to assess degree of disturbance is the measurement of shear wave velocity, V_s, using bender elements (Landon *et al*. 2007; Donohue and Long, 2007).

Landon *et al*. (2007) and DeGroot *et al*. (2007) proposed a methodology where V_s measurements on an extruded, unconfined sample is compared to V_s measured *in situ* using the seismic cone (V_{vh}/V_{SCPT}). The V_s measurements on the samples, in the vertical direction (denoted V_{vh}), were carried out after extrusion in the field. Figure 7.10 illustrates the good correlation between V_{vh}/V_{SCPT} and $\Delta e/e_o$ for the soft clays in Onsøy (Norway), Boston Blue clay (USA) and Burswood clay (Australia). Donohue and Long (2007) reported similar results for Onsøy clay and two soft Irish clays, thus confirming the potential of the approach. Provided shear wave velocity measurements *in situ* are available, the correlation in Figure 7.10 may be used to quantify sample disturbance.

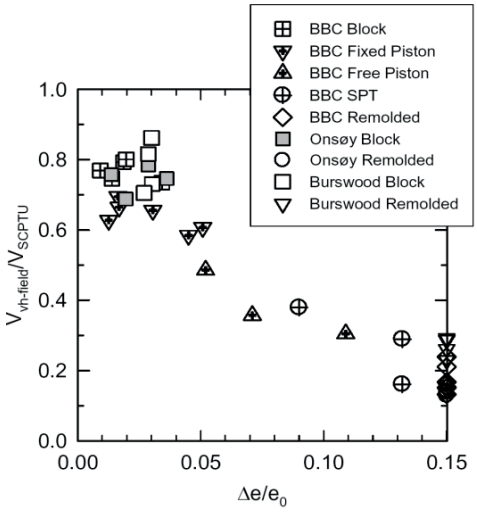

Figure 7.10. Shear wave velocity vs. $\Delta e/e_o$ for Onsøy, Boston Blue (BBC) and Burswood clays ($\Delta e/e_o$ from constant rate of strain oedometer tests) (Landon *et al*. 2007).

The above non-destructive techniques are believed to have good potential for assessing degree of disturbance. It is however, important to evaluate the quality of the samples tested in triaxial and oedometer tests based on the $\Delta e/e_o$ criterion. When selecting design parameters, more emphasis can then be given to the results from samples with the highest quality.

7.4.2 *Seabed samplers*

7.4.2.1 Box core sampling

Box cores were mainly developed for taking samples of the upper 0.3 to 0.5 m of the seabed for purpose of biological and geochemical studies. However, experience has shown that this type of sampler can also be very useful for geotechnical characterisation of the seabed soil. Basically, a cubic sample is normally taken with $0.5 \cdot 0.5 \cdot 0.5 m^3$ being the largest dimensions. Usually, the seabed soil is very soft in deep water. Therefore, it is important to test out the soil while the soil is intact inside the box corer.

7.4.2.2 Gravity core samplers with piston

Kullenberg type samplers, with a piston attached to a wire that runs all the way to the ship, can give very long samples (>50 m in extreme cases). However, one serious problem is that the sample recovery (=measured sample length/estimated penetration of the sampler) can be low, e.g. 0.7–0.8 is quite common (e.g. Lunne and Long, 2006). This means that for a sampler that penetrates 20m, the recovered sample may only be 14 to 16m.

One gravity core sampler that has improved features is the STACOR which was developed in France in the 1960ies. This has a piston that is truly stationary relative to seabed. Lunne and Long (2006) showed some examples illustrating that STACOR samples can be of good quality, but sampler penetration cannot be measured reliably.

7.4.2.3 New deep water sampler

One recently developed sampler not included in ISSMGE (2005) is the Deep Water Sampler (DWS). The sampler was designed to minimize sample disturbance by carefully considering the factors influencing sample quality.

The criteria for development of the new sampler for softer clays was the following: 15 to 20m penetration below seabed in 2000m of water, minimum 95% recovery, and sample quality comparable to that of a thin wall piston sampler in the drilling mode. Lunne *et al*. (2008) presented the main aspects influencing sample quality and made recommendations for an "ideal" design. Lunne and Long (2006) also reviewed the factors that influence sample quality.

Figure 7.11 presents the most important characteristics, in particular:

– stationary piston;
– sharp cutting shoe: with an angle of 5° for soils susceptible to sample disturbance;
– area ratio smaller than 17%, combined with a length sufficient to satisfy this criterion for enlarged diameters;
– inside friction as small as possible;
– steady speed penetration of sampler;
– accurate measurement of penetration to ensure a reliable calculation of the recovery ratio can be made.

The new sampler was tested both onshore and offshore, and penetration was modelled with finite element analyses. The deepwater sampler (DWS) was shown to provide high quality samples. Figure 7.12 presents the results of constant rate of strain oedometer tests illustrating the quality of the samples recovered (from onshore testing out of sampler) compared with the results for high quality block samples and a 54-mm piston samples. The shape of the stress-strain curves show that the quality of the DWS samples is very good.

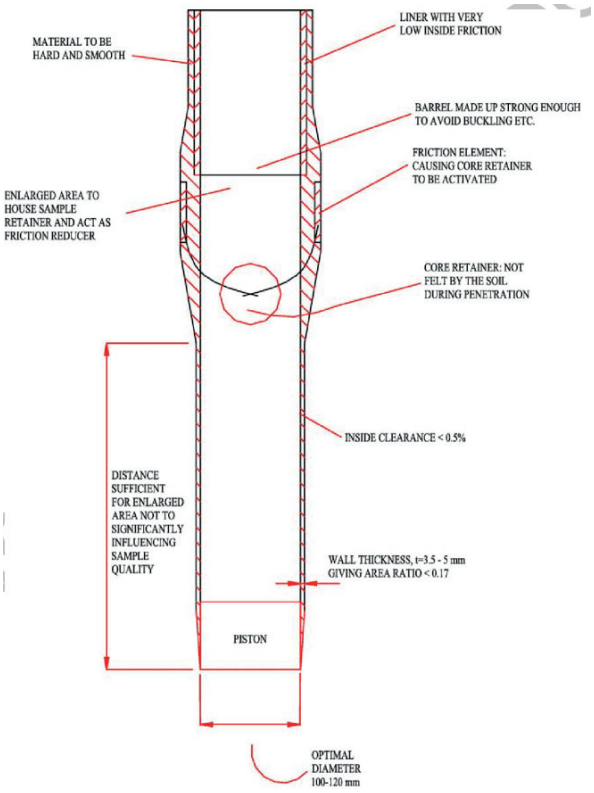

Figure 7.11. Design of lower end of ideal sampler (Lunne and Long, 2006).

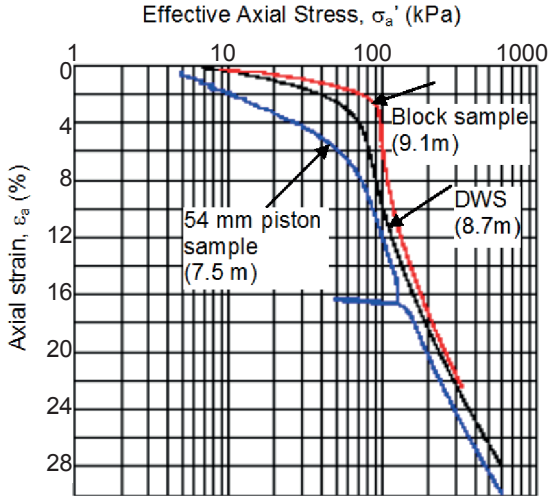

Figure 7.12. Oedometer test results with deepwater sampler (DWS) at Onsøy (Lunne *et al*., 2008).

Figure 7.13 shows a plot of the parameter $\Delta e/e_o$ as measured in CRSC and CAU tests on the DWS samples. Figure 7.13 includes results of laboratory tests on thin walled piston tube samples taken in a borehole during soil investigations at Troll in 1983 and 1989. The figure also includes results of CRSC and CAU tests on some gravity core samples taken at the Fram field, where the soil conditions are relatively similar to the Troll field. Figure 7.13 shows that all the lab tests carried out on DWS samples indicate the samples to be in Very Good to

Excellent and Good to Fair categories. This is similar or better compared to the samples taken with thin walled piston tube samples in a borehole (1983 and 1989 investigations). Furthermore, the DWS sample quality is more consistent with depth (i.e. there is less variation in the parameter $\Delta e/e_o$) compared to the thin walled piston tube samples. As expected, the laboratory tests on the Fram gravity core samples had much lower quality.

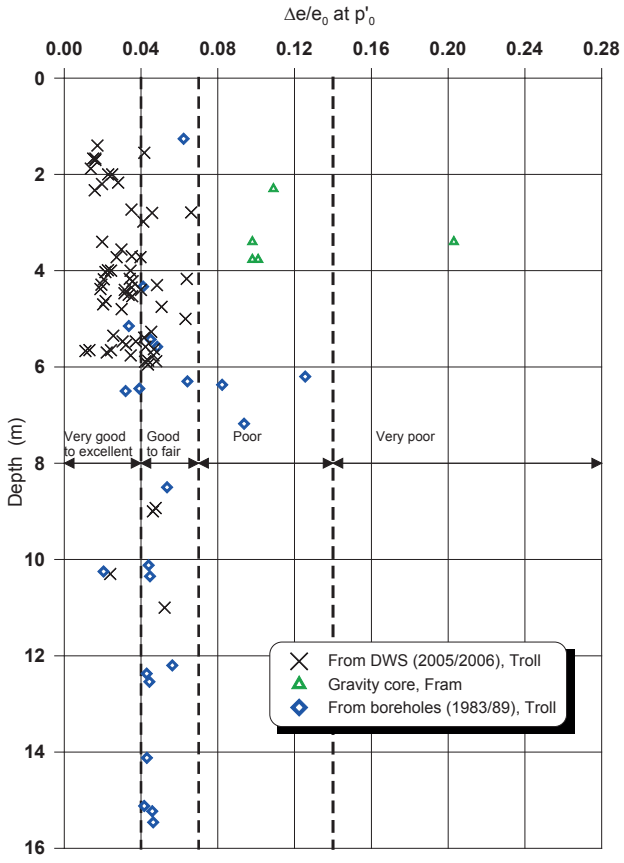

Figure 7.13 Assessment of sample quality with NGI criterion (Lunne *et al*., 2008).

7.4.3 *Down hole samplers*

Due to the limited inside diameter of drill pipes normally used, the practical limited sample diameter for down hole samplers is about 75 mm. Best quality samples are obtained with samplers pushed in by a hydraulic cylinder, or in very deep water, using pressurised drilling fluid inside the drill string. In soft to stiff soils a piston sampler should be used.

It is also very important that the drill string is controlled, like with the hard tie system where the heave compensator is "tied" to the seabed frame placed on the sea bottom (Zuidberg *et al*.1986).

7.5 *Laboratory testing*

7.5.1 *Field vs. offshore laboratory testing*

Due to logistic reasons, the laboratory testing that can be done in the offshore laboratory is usually limited to classification and index strength testing. The offshore laboratory tests can be used to get first knowledge about soil conditions and to evaluate if more samples are required.

In some cases it can be very advantageous to carry out CRSC oedometer tests offshore in order to get an early knowledge of stress history of the various soil layers. This knowledge is very important for detailed specification of advanced testing to be done in the onshore laboratory, as discussed below. In addition, results of oedometer tests can be used to evaluate sample disturbance, as discussed above.

A very important part of the offshore laboratory work is also to preserve samples for transport to onshore laboratory for advanced testing. For very soft to soft clays, it is in NGI's opinion very important to keep the samples in the sample tubes and not extrude them offshore.

7.5.2 *7.4.2 Classification and index tests*

It is very important that samples are described by technicians or engineers with a geological and geotechnical perspective. The following classification tests should be carried out on samples from all important layers:

- water content
- soil unit weight
- liquid and plastic limits (clay samples only)
- maximum and minimum density (sand samples)
- unit weight of solid particles
- grain size distribution
- organic content
- carbonate content

Photography of samples can also be very useful.

Intact and remoulded shear strength, and hence determination of sensitivity can be done with a range of index tests, including:

- fall cone
- motorvane
- pocket penetrometer
- torvane
- unconsolidated undrained triaxial tests (UU)

For identifying layering and for evaluation of sample quality and detecting any cracks, shells or stones in the samples, X-raying is a very useful method. NGI has for several years now used X-ray with tomography. As a routine, as shown in the example in Figure 7.14, images are presented as two longitudinal sections perpendicular to each other, plus one cross section per 100mm along the tube axis. The results are presented as positive images, so that the voids are white and solid material dark grey or black.

As an example of the usefulness of doing X-ray tomography, Figure 7.14 shows the presence of a 30 mm diameter calcareous tube worm in a sample tube, and Figure 7.15 shows the calcareous tube worm after extrusion and cleaning. Obviously no advanced tests

should be done over this part of the sample. Based on the X-ray results, this was included in the detailed planning.

7.5.3 *Tests to measure strength, deformation and flow parameters*

7.5.3.1 Overview of test types

Section 5 discussed the type of laboratory tests that are needed in order to obtain input parameters in the various geotechnical analyses. Table 7.5 lists all these test types. All tests should be run according to the requirements given in appropriate ASTM, BS and Norwegian standards, with further detailed requirements to be given in the new ISO standard for Marine Soil Investigations. It is essential that the consolidation stresses and other test specifications are accurate and representative for *in situ* conditions and for the loading the soil elements will be subjected to. Prior to starting any advanced testing programme, it is necessary to make a best estimate of the *in situ* stresses and stress history.

7.5.3.2 Correction for sample disturbance

Lunne *et al*. (2006) and Berre *et al*. (2007) observed that for soft Norwegian marine clays the mobilised shear stress at small shear strains (up to ≈3%) is lower the more disturbed the sample is. At large shear strains (>15%); however, the mobilised shear stress/strength becomes higher the more disturbed the sample is (Figure 7.8). Berre *et al*. (2007) used this experience to develop procedures to correct for the effect of sample disturbance.

The correction procedure involves a correction at small strain resulting in an increase in the mobilised shear stress at small strains and a correction at large strain resulting in a reduction in the mobilised shear stress at large strains The corrections provide only estimates that can be used to assess (1) the potential increase in strength if high quality samples were taken and (2) the cost/benefit of additional sampling and testing. The corrected shear stresses should not be used for design without further testing.

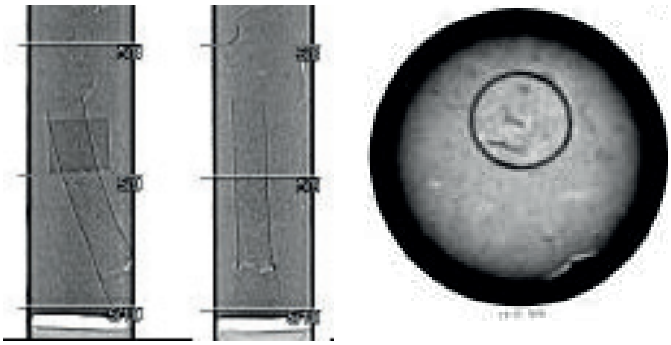

Figure 7.14 Example of X-ray tomography of sample (Schjetne, 2008)

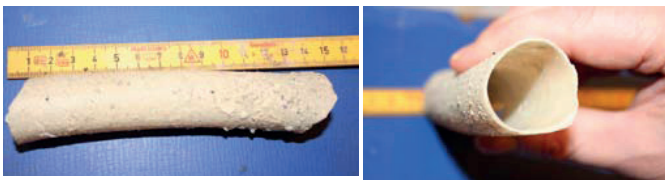

Figure 7.15 Calcareous tube worm" shown on X-ray in Figure 7.14 (Schjetne, 2008)..

Table 7.5. Overview of required test specifications and main parameters measured in advanced tests.

Test type	Required test specifications	Main parameters measured	Notes	Key reference(s)
IL oedometer	p_c'estimate, unload-reload loop	p_c', M, m, c_v, k_v	Need to consider low increment ratio for good definition of p_c'	Sandbækken *et al*. (1986)
CRS oedometer	p_c'estimate, unload-reload loop	p_c', M, m, c_v, k_v	Rate of strain so that pore water pressure < 15 % of σ_v	Sandbækken *et al*. (1986)
CAUC static	σ_{vc}', σ_{hc}', rate of shearing	s_u^C, φ_u, shear modulus	Sufficient consolidation time to reach stable conditions	Berre (1981)
CAUE static	σ_{vc}', σ_{hc}', rate of shearing	s_u^E, φ_u, shear modulus	Sufficient consolidation time to reach stable conditions	Berre (1981)
DSS static	σ_{vcmax}', $\sigma_{vcfinal}$', rate of shearing	s_u^{DSS}, shear modulus	Normally σ_{vcmax}' is conservative estimate of p_c' and $\sigma_{vcfinal}$'= p_o'	Bjerrum and Landva (1966)
CK_oUC	σ_{vcmax}', $\sigma_{vcfinal}$', rate of shearing	s_u^C, φ_u, shear modulus	Used for SHANSEP type consolidation. Can give p_c'	Berre (1981)
CK_oUE	σ_{vcmax}', σ_{vcfin}', rate of shearing	s_u^E, φ_u, shear modulus	Used for SHANSEP type consolidation. Can give p_c'	Berre (1981)
CAU cyclic	σ_{vc}', σ_{hc}', cyclic stress level, frequency	Cyclic strength and deformation parameters	Sufficient consolidation time to reach stable conditions	Berre (1981) Andersen (2004)
DSS cyclic	σ_{vcmax}', σ_{vcfin}', cyclic stress level, frequency	Cyclic strength and deformation parameters	Normally σ_{vcmax}' is conservative estimate of p_c' and σ_{vcfin}' = p_o'	Andersen (2004)
Resonant column	σ_{vc}', σ_{hc}'	V_s (G_{max}), damping	Preferably anisotropic consol.	ASTM (2007)
Bender element	σ_{vc}', σ_{hc}'	V_s (G_{max})	Usually part of CRSC, CAU or DSS test	Dyvik & Madshus (1985)
Ring shear	σ_{vc}', rate of rotation	Residual strength	Frequently several rates	Bishop *et al*. (1971)

Note: For good quality samples, NGI generally recommends reconsolidation to the best estimate *in situ* stresses. If samples are not of so good quality, SHANSEP type consolidation (Ladd and Foott, 1974 and Ladd and DeGroot, 2003) should be considered. See Lunne *et al*. (2006) for more detailed discussion. Results of oedometer tests and consolidation phase of triaxial and DSS tests may be used to evaluate sample quality (see Section 7.4.1).

Figure 7.16 illustrates the correction at small strain for triaxial compression tests (Berre *et al*., 2007). The stress path for the partly disturbed sample is represented by curve ABC. The correction is done by drawing a vertical line from the *in situ* stresses (point O) to the intersection with the line between the origin and passing through the peak shear stress of the disturbed stress path (point B). Point D represents the shear stress close to the undrained shear strength for a comparable high quality block samples. Berre *et al*. (2007) showed that the stress path for e.g. block samples tends to follow an "elastic" stress path with no shear induced pore water pressure (i.e. no tendency for dilation or contraction) almost entirely up to the peak shear stress. In the stress path diagram in Figure 7.16, the soil would then follow a path with inclination of 3:1.

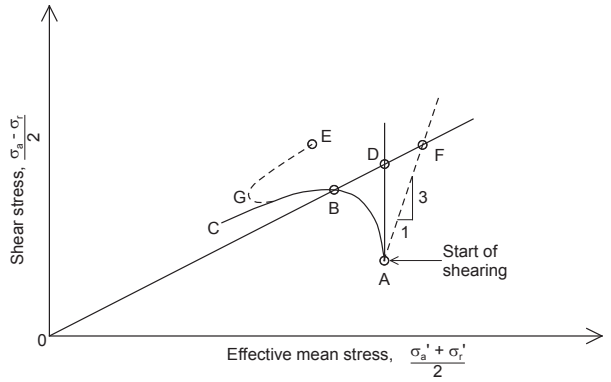

Figure 7.16. Correction at small strain for sample disturbance, triaxial compression tests (Berre *et al*., 2007).

For clays with overconsolidation ratio (OCR) no greater than 2, the stress path before failure shows some contractive behaviour even for block samples and "bends over" slightly towards the left before peak shear stress is reached. It is thus proposed to use the AD-line for correction. Clays with OCR between 2 and 4 show less contractive or even dilative behaviour, and one may consider the line with inclinations of 3:1 as more representative. For silty clays, the stress path may start to dilate after first exhibiting contractive behaviour, as illustrated by curve ABGE in Figure 7.16. The correction should in this case be done by drawing the line from the origin through the peak shear stress of the stress path before the dilation starts (Point B). Lacasse *et al*. (2001) and Berre *et al*. (2007) provide examples for several clays. Berre *et al*. (2007) also presented procedures for correcting triaxial extension and direct simple shear tests.

Figure 7.17 illustrates the correction at large strain. The correction can be found from the results of oedometer tests. The correction is based on the reduction in water content during reconsolidation to the *in situ* stress. The virgin part of the oedometer stress-strain curve is used. The correction can be applied to triaxial compression and extension and direct simple shear tests. Berre *et al*. (2007) provide examples. A comparative study of several clays in NGI's database of 54-mm tube samples suggests correction factors from 0.4 to 0.85, with an average of 0.60. The large-strain correction is less empirical than the small-strain correction, and always results in a shear stress reduction for soft clays. This correction should therefore always be made.

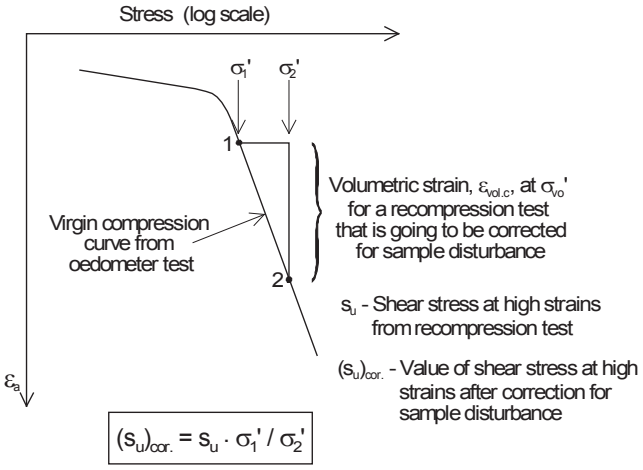

Figure 7.17. Correction at large strain for sample disturbance (Berre *et al*., 2007).

7.6 *Soil parameters*

7.6.1 *Index parameters*

Table 7.6 gives some typical values of index parameters for locations in deep water areas. Range of values for the upper 10 – 15 m of soil is given for a number of deep water sites around the world.

Table 7.6 Index parameters for a number of deep water sites

Area	Water depth, m	w, %	γ' kN/m^3	w_l%	I_p%	% clay particles	Organic cont., %	Carbonate cont., %
Norwegian Sea	800	80 - 140	13.5 – 14.0	85 - 107	51 - 54	43 - 50	NA	NA
Gulf of Guineas	953	106 - 137	12.8 –13.8	120 - 135	87 - 104	65 - 75	2	NA
Gulf of Mexico	1225	70-150	13.0–14.5	70 -150	55 - 105		NA	NA
Mediterranean	400-700	100 - 160	13.0 – 15.0	75 - 120	40 - 75	50 - 75	1 – 1.5	5 - 60
Offsh. Australia	410	66 - 77	15.4 – 16.0	60 - 70	20 - 38	20 - 26		70
Bay of Bengal	1100	75-150	130-160	80-160	45-70	50-80	0.9-2.1	4-50

7.6.2 *Preconsolidation stress, p'$_c$, and stress history*

7.6.2.1 Interpretation of oedometer tests

The methods to determine the preconsolidation stress, p'$_c$, whether apparent due to aging (Bjerrum, 1967), or due to unloading, include the Casagrande (1936) and Janbu (1969) approaches. Casagrande used the semi-logarithmic stress strain (one-dimensional compression) curve (Figure 7.18a) while Janbu used the linear stress-strain and linear tangent constrained modulus-effective axial stress curves (Figure 7.18b). Janbu did not specify how to exactly select p'$_c$. NGI uses the graphic method shown in Figure 7.19.

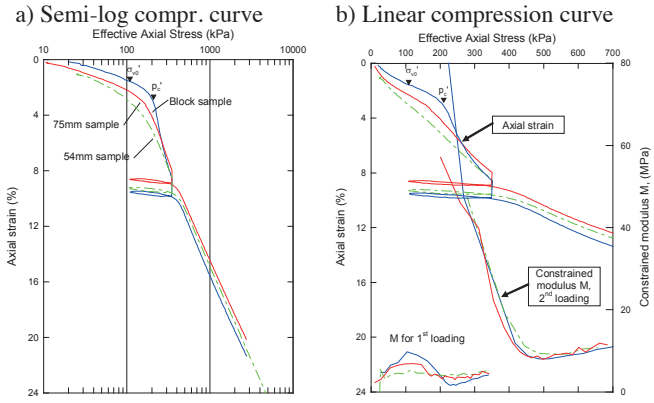

Figure 7.18. Oedometer tests on block and tube samples from Lierstranda at depth 12.3 m.

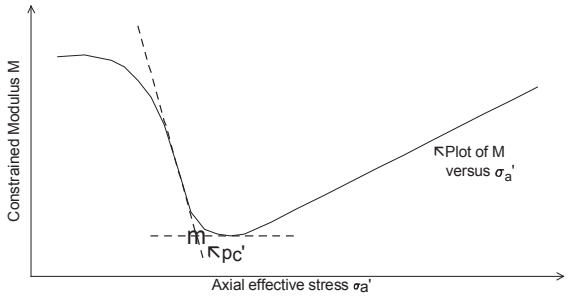

Figure 7.19. NGI-determination of p'$_c$ from constrained modulus curve in Janbu's method (Lunne *et al*., 2008).

Berre (2005) and Lunne *et al*. (2008) suggested an empirical method where p'$_c$ is taken as the axial stress at the shear strain at p'$_o$ plus 2% strain. If the vertical strain at p'$_o$ is 3%, p'$_c$ is taken at a vertical strain of 5%. The "Berre approach" seems to work reasonably well for a large number of soft marine non-quick Norwegian clays. The approach needs further checking with other clays. One important advantage is that the method allows a person-independent determination of the preconsolidation stress.

The results of the study made by Lunne *et al*. (2008) indicated the following:

– There is no significant difference among p'$_c$ derived by the Casagrande, Janbu and Berre approaches.

– p'$_c$ was typically 20 to 30% lower for 54-mm tube than for block samples.

In addition to above mentioned methods NGI uses the method presented by Becker *et al*. (1986).

Finally it should be mentioned that in some cases, it has been found that the consolidation phase of a SHANSEP CK$_o$U test can be used to determine p$_c$'.

7.6.2.2 Interpretation of *in situ* tests and empirical correlations

Preliminary estimates of p$_c$' and OCR are frequently needed before results of oedometer tests are available. Also in many cases it is difficult to get reliable determination of p$_c$' from oedometer tests. In these cases it can be very beneficial to interpret CPTU results using empirical correlations as given by for instance Lunne *et al*. (1997).

Correlations among s$_u$/p$_o$', I$_p$ and OCR are also available, e.g. Andresen *et al*. (1979).

7.6.3 *Compressibility*

Compressibility can be expressed in terms of the constrained modulus, M, as determined in an oedometer test. Fig. 7.18 and 7.19 show results of CRSC oedometer tests illustrating how M is a function of the effective vertical stress. For first loading, Fig. 7.19 shows that in the overconsolidated range, i.e. below p$_c$', M is high, and obviously sensitive to sample disturbance. The value of M becomes higher and more realistic with increasing quality of the sample. Above p$_c$', M is usually proportional to the vertical effective stress, σ_{vo}', according to M = m (σ_{vo}' – p$_r$') where m and p$_r$' are constants.

As discussed in Chapter 4, it is also important to determine the moduli for unloading and reloading situations. As can be seen from Fig. 7.18, the unloading and reloading moduli are much higher than the first loading. In some cases the unloading and reloading moduli are so high that false deformations and equipment compressibility can significantly influence the modulus. These false deformations and compliance need to be determined and corrected for by running special tests with a steel dummy. It is important that the steel dummy test follows the same loading/unloading/reloading sequence as the test on the actual sample.

7.6.4 *Permeability and coefficient of consolidation*

The coefficient of permeability, k$_v$, (or hydraulic conductivity) is usually calculated from the time settlement readings in an incremental oedometer test and from the measured excess pore water pressure in a CRSC oedometer test as described by Sandbækken *et al*. (1986). The computed permeability is plotted as function of strain, as the so-called k-line, as shown in Figure 7.20. In some cases, a check on the computed permeability can be made by doing a constant head permeability test at some stage in the oedometer test.

To correct for sample disturbance the procedure at NGI is to assume the permeability at zero strain to be representative for the permeability at the in situ effective vertical stress. With reference to the case shown in Figure 7.20, the coefficient of permeability at the *in situ* stresses will be about $1.5 \cdot 10^{-9}$m/s.

Once the constrained modulus, M, and the coefficient of permeability, k, have been established, the coefficient of consolidation, c_v, can be computed according to $c_v = k \cdot M/\gamma_w$, where γ_w is the unit weight of water.

Normally samples are oriented vertically so that k and c are valid for vertical flow or consolidation. It is however, possible to orient samples horizontally and to measure k and c in the horizontal direction. In this case coefficients should be denoted k_h and c_h respectively.

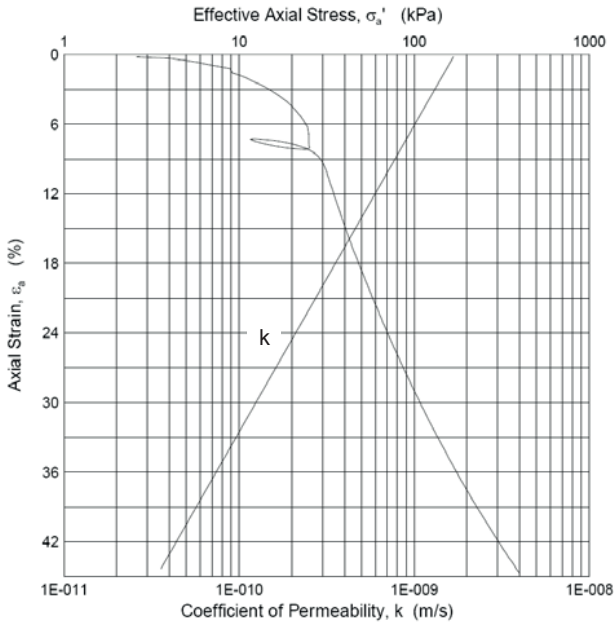

Figure 7.20. Example of CRSC test result in soft clay including k-line

7.6.5 *Monotonic strength anisotropy*

NGI has used an anisotropy model as discussed in Section 4 for several decades (see Figure 4.10). For a reliable design, it is essential to obtain stress-strain parameters characteristic of the stress system the soil *in situ* will be subjected to. In practice, this means that it in many cases is necessary to define undrained shear strength profiles for triaxial compression, direct simple shear and triaxial extension (s_u^C, s_u^{DSS} and s_u^E). The undrained shear strengths should be derived from both laboratory tests and *in situ* tests (see section 7.3).

The laboratory test specimens are normally re-consolidated to the *in situ* stresses (anisotropic, if so *in situ*) and then sheared to failure. Ideally, a sufficiently large number of triaxial compression and extension and direct simple shear tests should be run in each layer on high quality samples. In practice, the number of samples available for testing and the quality of the samples impose limitations on the testing programme. For large testing programs, NGI follows the following approach (Lunne and Andersen, 2007):

– Choose one representative soil boring and carry out a sufficient number of anisotropically consolidated triaxial compression tests to define a reliable s_u^{CAUC} profile. Select the most undisturbed part of the samples (e.g. based on X-ray imaging, measured shear wave velocity or measured suction). Ensure that weaker layers are included, as they may be governing for design.

– In the same borehole, do a few direct simple shear and triaxial compression tests to establish the anisotropy ratios s_u^{DSS}/s_u^{CAUC} and s_u^{CAUE}/s_u^{CAUC}.

– Correlate values of s_u^{CAUC} with the results of *in situ* tests (CPTU and other tests) to develop local correlation between the continuous *in situ* data and the site specific laboratory results (see Section 7.3). Use the NGI sample quality criterion parameter $\Delta e/e_o$ described earlier to evaluate the quality of the laboratory test data and ascertain whether any data is of insufficient quality.

– If possible, do a few triaxial compression and direct simple shear tests in the other borings.

NGI has found it very useful to compare the results of laboratory tests with correlations developed from a database of earlier laboratory test results on soft clays. If the preconsolidation stress, p_c', can be determined with adequate reliability, it correlates well with undrained shear strength for the three stress systems. Figures 7.21 to 7.23 illustrate the undrained shear strength correlations developed so far. Tables 7.7 and 7.8 present the statistics for the normalised undrained shear strength anisotropy ratios for the three figures.

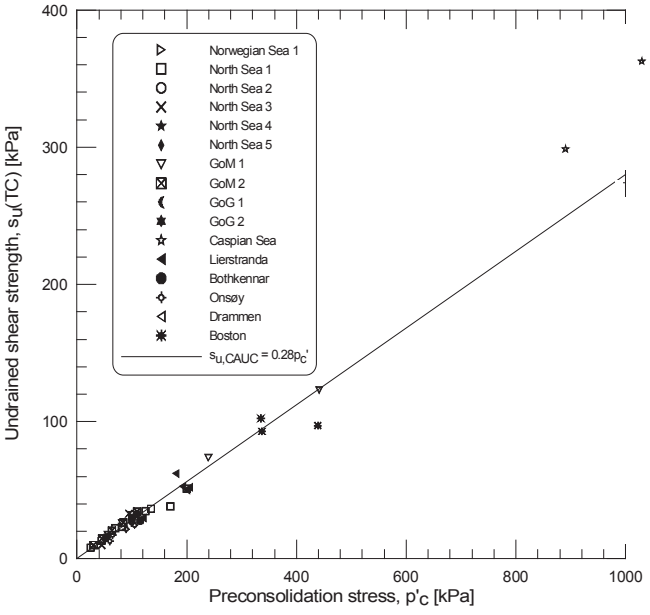

Figure 7.21. Correlation between s_u^{CAUC} and p_c' (Lunne and Andersen, 2007).

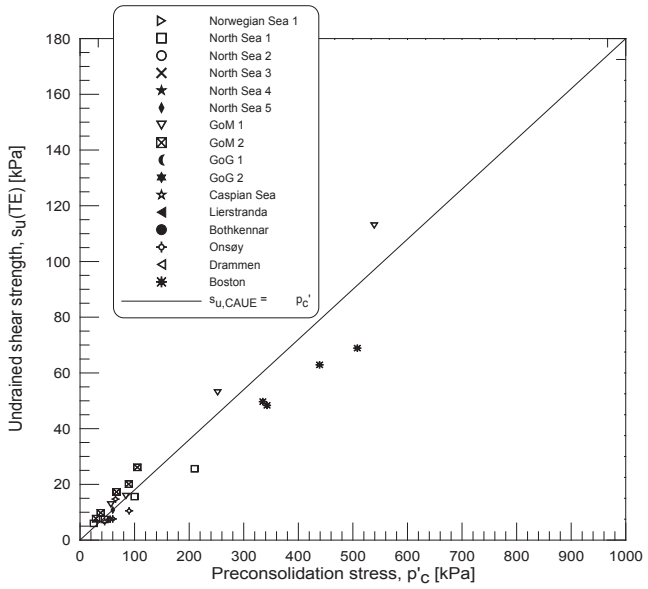

Figure 7.22. Correlation between $s_{u,}^{CAUE}$ and p_c' (Lunne and Andersen, 2007).

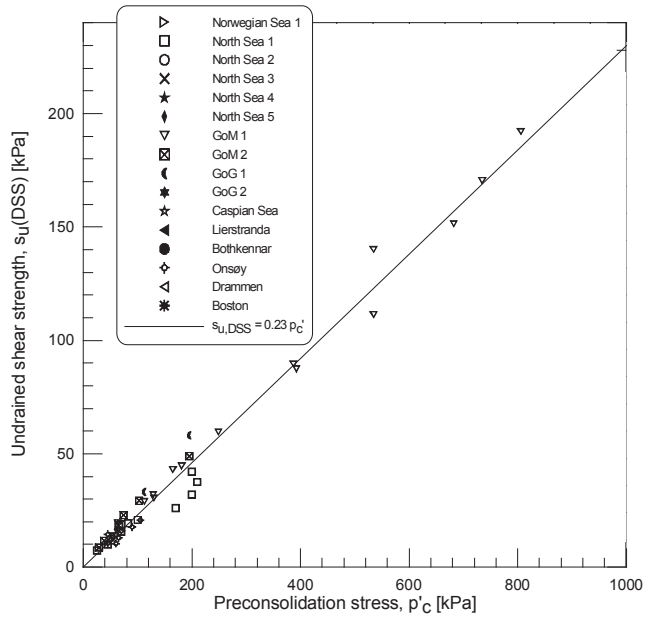

Figure 7.23. Correlation between $s_{u,}^{DSS}$ and p_c' (Lunne and Andersen 2007).

The data shown in Figures 7.21 to 7.23 and Tables 7.7 and 7.8 are for soft, slightly overconsolidated clays that fall around the 'sedimentary compression line' as defined by Burland (1990). Table 7.9 summarises the strength anisotropy ratios obtained for the Norwegian onshore soft clays used in the sample disturbance study at NGI (Lunne *et al.*, 2006).

Table 7.7. Statistics for normalised undrained shear strength in Figures 7.21 to 7.23 (NGI, 2002).

Test	n	μ	r^2
s_u^{CAUC}/p'_c	41	0.28	0.99
s_u^{DSS}/p'_c	36	0.23	0.96
s_u^{CAUE}/p'_c	18	0.18	0.94

n = number of data points μ = mean value r^2 = regression coefficient

Table 7.8. Undrained shear strength anisotropy ratios from Figures 7.21 -7.23 (NGI, 2002).

Anisotropy ratio	n	μ	SD	COV
s_u^{CAUE}/s_u^{CAUC}	54	0.62	0.13	0.21
s_u^{DSS}/s_u^{CAUC}	45	0.80	0.07	0.09

n=number of data points μ= mean value
SD=standard deviation COV=coefficient of variation

Table 7.9 Results of regression analyses of strength anisotropy ratios for onshore clays (Lunne and Andersen, 2007).

Anisotropy ratio	Block samples			54- or 95-mm samples		
	μ	n	r^2	μ	n	r^2
s_u^{DSS}/s_u^{CAUC}	0.69	20	0.99	0.74	16	0.99
$ss_u^{CAUE}/s_{Su}^{CAUC}$	0.42	19	0.98	0.50	12	0.97

n=number of data points μ=mean value r^2=regression coefficient

7.6.6 *Stress-strain relationship for monotonic loading*

An example of stress-strain relationship for undrained monotonic loading in triaxial compression is presented in the left diagram in Figure 7.8. The example shows that the stress-strain relationship can be strongly influenced by sample disturbance and that it is important to use samples of high quality.

The example in Figure 7.8 also shows that the stress-strain relationship is very non-linear. The modulus at low shear strain can be very high and difficult to measure accurately in conventional triaxial and DSS equipment. One way to determine the shear modulus at low shear stresses, is to calculate the shear modulus from the stress-strain curve and plot it as function of shear stress as far as the data is reliable. This curve can be extended to higher values by drawing it to the initial shear modulus at the initial shear stress, τ_0. An example is shown in Figure 7.24. The initial shear modulus (Section 7.6.12) can be determined from shear wave velocity measurements by means of bender elements on the same specimen, or from a parallel resonant column test.

The shear modulus will be different for triaxial compression, triaxial extension and DSS. As for shear strength, it is therefore important to use anisotropic, stress path dependent modulus in cases where displacements are important. A model that works with anisotropic stress-strain behaviour is described by Andresen and Jostad (2002). This model also incorporates strain softening.

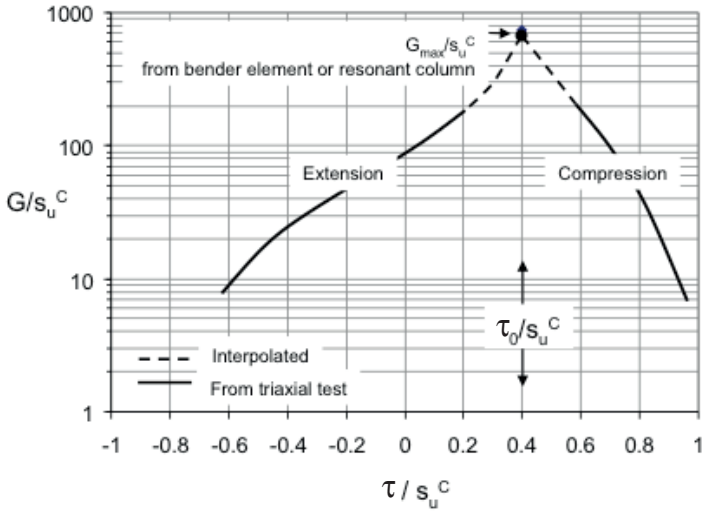

Figure 7.24. Determination of shear modulus at low shear stresses and strains.

7.6.7 *Effect of rate of strain and load duration*

The undrained shear strength depends on the rate of loading, and it is essential to account for differences in rate and duration of loading between the prototype and laboratory and *in situ* tests. Undrained monotonic laboratory tests are typically run with a rate of shear strain of about 2-5 %/hr or about 30-140 minutes to failure. Cyclic laboratory tests are typically run with 1-10 s load period. In the prototype, the soil can, as discussed in Section 4, be subjected to loads of different rate and duration, like sustained loading from weight, current and wind, impact load from icebergs and trawler equipment, and cyclic loads from waves earthquakes and temperature variations. These loads can have a rate or a duration that are significantly different from the laboratory tests. The strain rate in the shear zone in the soil around *in situ* tests can also be different from the strain rate in the laboratory and in the prototype. In the T-bar, for instance, Randolph and Andersen (2006) showed that the rate of shear strain in the shear zone can be 6-7 orders of magnitudes higher than in typical laboratory tests.

The undrained shear strength of clay in strain-controlled undrained triaxial compression, triaxial extension, DSS and UU tests is plotted as function of time to failure in Figure 7.25 and as function of rate of shear strain in Figure 7.26. The data include clays with plasticity index and overconsolidation ratio in the range I_p=5-88% and OCR=1-4.5. The shear strength is normalized by the shear strength in tests with 140 minutes to failure in Figure 7.25 and by the shear strength in tests with a rate of shear strain of 4.5 %/hr in Figure 7.26.

The data in Figures 7.25 and 7.26 show that the change in strength per log-cycle increases with increasing rate of strain and decreasing time to failure. There is no systematic effect of plasticity or overconsolidation ratio in the range of OCR=1-4.5. Lunne and Andersen (2007) also presented additional diagrams that seem to indicate that the effect of rate or duration is not significantly influenced by sample disturbance and that the rate effect is the same for remoulded and intact clays. Lunne and Andersen (2007) also show data that seem to indicate that the time to failure in tests with constant shear stress, i.e. undrained creep tests, agree with the data in Figure 7.25.

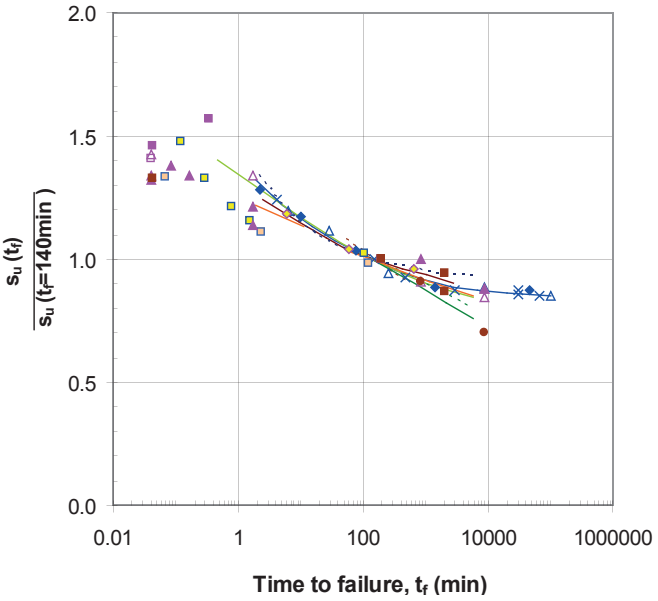

Figure 7.25. Static shear strength of several clays as function of time to failure (based on Lunne and Andersen, 2007).

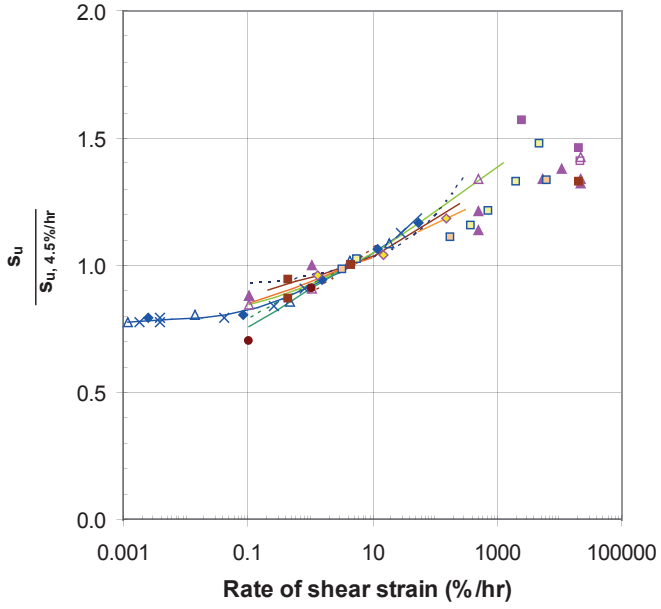

Figure 7.26. Static shear strength of several clays as function of rate of shear strain (based on Lunne and Andersen, 2007).

7.6.8 *Cyclic shear strength*

Cyclic loading may reduce the shear strength of a soil, and the cyclic shear strength may be lower than the static shear strength. The reason is that cyclic loading tends to break down the soil structure and cause a tendency for volumetric reduction in the soil. If the conditions are undrained, volumetric changes will be prevented by the low volumetric compressibility of the water. The normal

stresses that were carried by the soil will then be transferred to the pore water, and the effective stresses in the soil will decrease accordingly. This is illustrated by the effective stress paths for monotonic and cyclic loading in Figure 7.27.

The development of pore water pressure and shear strain with time for a soil element subjected to undrained cyclic loading with a constant cyclic shear stress is illustrated in Figure 7.28. The load cycles with a single amplitude shear stress, τ_{cy}, around a constant shear stress, τ_a. The cyclic loading generates a pore water pressure characterized by a permanent pore water pressure component, u_p, and a cyclic pore water pressure component, u_{cy}. The increased pore water pressure reduces the effective stresses in the soil, resulting in increased permanent and cyclic shear strains, γ_p and γ_{cy}, with time.

The stress-strain behaviour of a soil element under the cyclic loading in Figure 7.28 is illustrated in Figure 7.29.

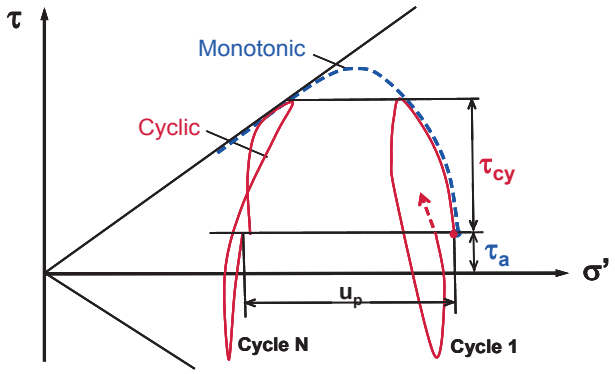

Figure 7.27. Effective stress paths for undrained tests with monotonic and cyclic loading.

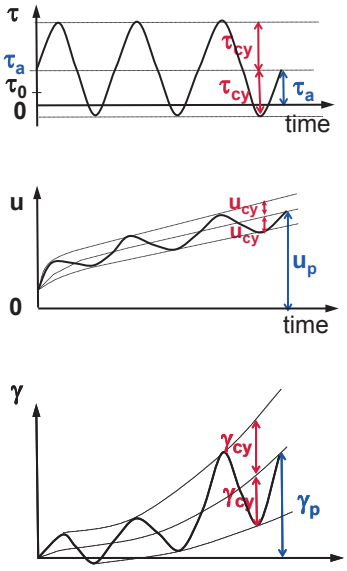

Figure 7.28. Pore water pressure and shear strain as function of time under undrained cyclic loading.

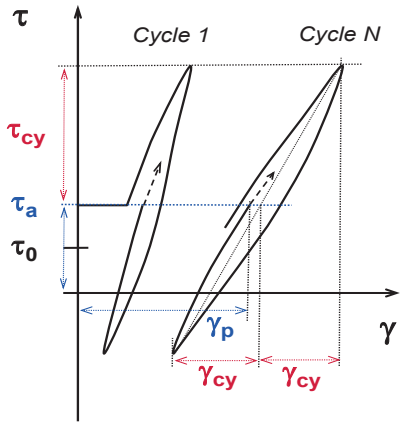

Figure 7.29. Stress-strain behaviour under cyclic loading.

The cyclic shear strength depends strongly upon the average shear stress (e.g. Andersen *et al.*, 1988 and Andersen, 2004). It has therefore been suggested to plot the number of cycles to failure, N_f, as function of the average and cyclic shear stress components. Examples of such diagrams are given in Figures 7.30 and 7.31 for DSS and triaxial tests, respectively. The shear stresses are normalized by the static shear strength for DSS and triaxial compression tests, respectively. The diagrams are valid for normally consolidated Drammen Clay, assuming stress-controlled undrained cyclic loading and a load period of 10s.

The contour diagrams define the number of cycles to failure as function of average and cyclic shear stresses. The diagram also defines the failure mode; i.e. the combination of permanent and cyclic shear strains at failure, γ_p and γ_{cy}. The diagram in Figure 7.30 shows that in DSS tests, the failure will occur as large cyclic shear strains when the average shear stress is small, and as large permanent shear strains when the average shear stress approaches the static shear strength. For average shear stresses between zero and the static shear strength, the failure mode will be a combination of permanent and cyclic shear strains.

The diagram in Figure 7.31 shows that in triaxial tests, the failure will occur as large cyclic shear strains for a range of average shear stresses about halfway between the compression and extension static shear strengths. For average shear stresses approaching the compression shear strength, the failure mode will be dominated by large permanent compression shear strains, whereas for average shear stresses approaching the extension strength, the failure mode will be dominated by large permanent extension shear strains. Strains in compression are defined as positive and strains in extension are defined as negative in Figure 7.31 and later figures.

The intersection of the contours with the τ_a-axis and the location of the contours for values of τ_a approaching the static undrained shear strength depend upon the duration of τ_a. The reason is the undrained creep that occurs under high average shear stress. In the diagrams in this paper, the contours have been drawn to intersect the horizontal

axis at the undrained shear strength in standard laboratory tests. If the duration of τ_a deviates from the approximately 2 h time to failure in standard monotonic laboratory test, this can be corrected for when applying the diagrams by using a shear strength corrected for load duration when denormalizing τ_a/s_u. The shear strength correction can be based on the data in Figure 7.25, which shows the shear strength of several clays as function of time to failure.

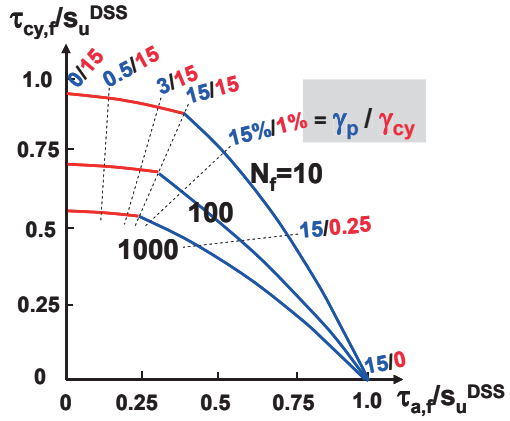

Figure 7.30. Number of cycles to failure and failure mode as function of average and cyclic shear stresses for cyclic DSS tests on normally consolidated Drammen Clay. Based on diagrams in Andersen *et al*., 1988.

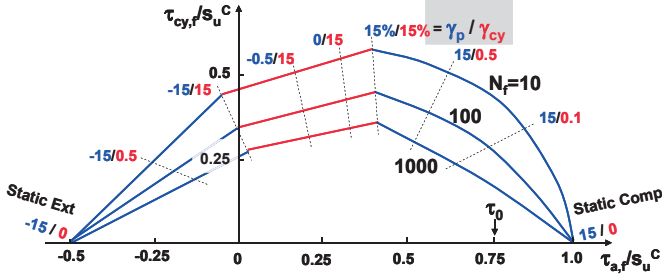

Figure 7.31. Number of cycles to failure and failure mode as function of average and cyclic shear stresses for cyclic triaxial tests on normally consolidated Drammen Clay. Based on diagrams in Andersen *et al*., 1988.

The diagrams in Figures 7.30 and 7.31 show the combinations of average and cyclic shear stresses that will cause failure in a given number of cycles. In a stability analysis, one needs to know the maximum shear stress that can be mobilized. As illustrated in Figure 7.32, the maximum shear stress that can be mobilized is the sum of average and cyclic shear stresses at failure, i.e.

$\tau_{f,cy} = \tau_{a,f} + \tau_{cy,f}$, where

$\tau_{f,cy}$ is the cyclic shear strength

$\tau_{a,f}$ is the average shear stress at failure. $\tau_{a,f}$ is composed of the initial consolidation shear stress, τ_0, plus the change in average shear stress, $\Delta\tau_a$, due to an additional average load or redistribution of average stresses, i.e. $\tau_{a,f} = \tau_0 + \Delta\tau_a$. The diagrams in this paper assumes that $\Delta\tau_a$ acts under undrained conditions. The effect of drained $\Delta\tau_a$ is presented in Andersen (1991).

$\tau_{cy,f}$ is the cyclic shear stress at failure

The equation above means that the cyclic shear strength for a given number of cycles to failure can be established by simply adding average and cyclic shear stresses for various given values of average shear stress, and plot this sum as a function of the average shear stress. This is done for DSS tests in Figure 7.33 and for triaxial tests in Figure 7.34. The reason for the discontinuity in the curves for triaxial tests in Figure 7.34 is that the average stress has opposite sign for compression and extension. Compression is defined as a failure mode where the permanent shear strain is positive, and extension is defined as the failure mode where the permanent shear strain is negative.

The cyclic shear strength diagrams show that the cyclic shear strength can be higher than the static shear strength, since $\tau_{f,cy}/s_u > 1$ for low number of cycles in some cases. The reason for this is that the clay strength is rate dependent (e.g. Figures 7.25 and 7.26). Since the cyclic tests are run with a load period of 10 s and the monotonic tests are brought to failure in about 2 hours, the cyclic strength may thus be higher than the static shear strength.

The diagrams in Figures 7.33 and 7.34 provide the data required to define the cyclic shear strength for the various stress conditions shown in Figure 4.10.

Figures 7.30, 7.31, 7.33 and 7.34 present diagrams for normally consolidated Drammen Clay. The cyclic shear strength for 10 cycles for a number of other normally consolidated clays are compared to Drammen Clay in Figures 7.35 and 7.36. There is a tendency for the normalized cyclic shear strength to increase with increasing plasticity index.

Diagrams for overconsolidated Drammen Clay with overconsolidation ratio of 4 and 40 can be found in Andersen (2004).

The diagrams in Figures 7.30 to 7.36 give the cyclic shear strength for cases with a constant cyclic shear stress during the cyclic load history. In a storm, however, the cyclic shear stress is likely to vary from one cycle to the next. The equivalent number of cycles of the maximum cyclic shear stress, N_{eqv}, that would give the same effect as the real cyclic load history must therefore be determined in order to be able to use the diagrams.

Procedures to determine N_{eqv} are presented by Andersen (1976) and Andersen *et al*. (1992). The procedures use shear strain or pore water pressure contour diagrams of the type presented in Figures 7.37 and 7.38. The diagrams are established from the same tests as used to establish the diagrams in Figures 7.30 and 7.31. The diagrams in Figures 7.37 and 7.37 are for DSS tests with an average shear stress of τ_a=0. Similar diagrams can be established for other average shear stresses and for triaxial

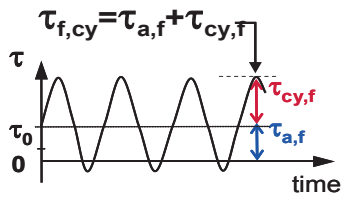

Figure 7.32. Definition of cyclic shear strength, $\tau_{f,cy}$.

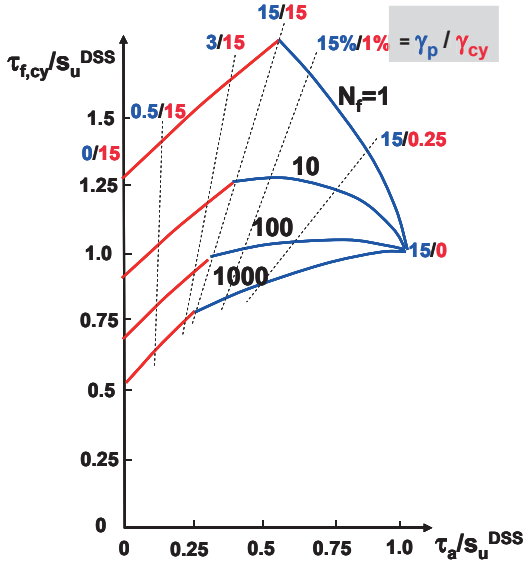

Figure 7.33. Cyclic DSS shear strength. Normally consolidated Drammen Clay.

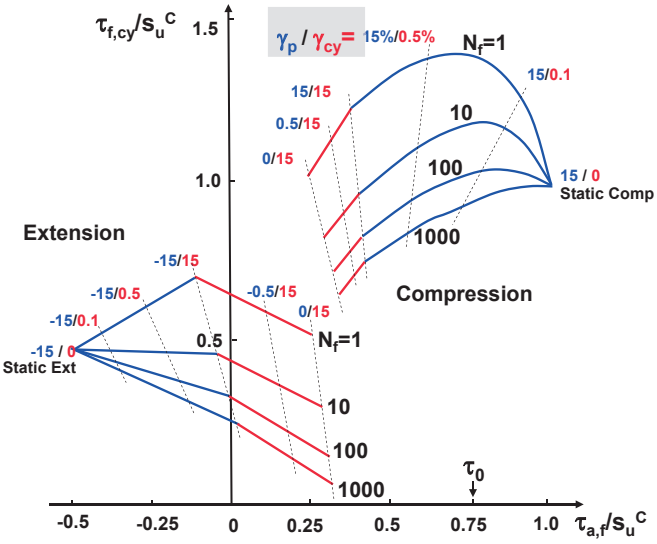

Figure 7.34. Cyclic triaxial compression and extension shear strengths. Normally consolidated Drammen Clay.

tests. Various such diagrams are given in Andersen (2004).

For clays, N_{eqv} may be determined by the "strain accumulation" procedure where the cyclic shear strain is used as memory of the cyclic effect by keeping track of the cyclic shear strain during the cyclic load history.

For sands or situations where drainage can occur during the storm, it is necessary to account for the effect of the drainage. The equivalent number of cycles, Neqv, can then be determined by keeping track of the permanent pore water pressure accumulated during the cyclic load history, accounting for the simultaneous generation and dissipation of the excess pore water pressure.

In principle, the pore water pressure accumulation procedure could also be used for clays. In practice, however, accurate laboratory measurement of pore water pressure is more difficult to perform in clays than in sand. Since drainage is not likely to occur during the cyclic load history in clays, it is preferable to use the cyclic strain accumulation procedure for clays.

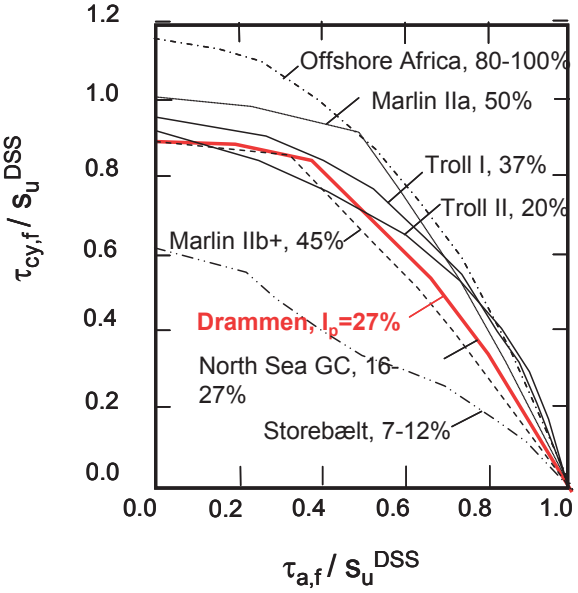

Figure 7.35. Normalized average and cyclic shear stresses for N_f=10 in DSS tests, for different normally consolidated clays (based on Andersen, 2004).

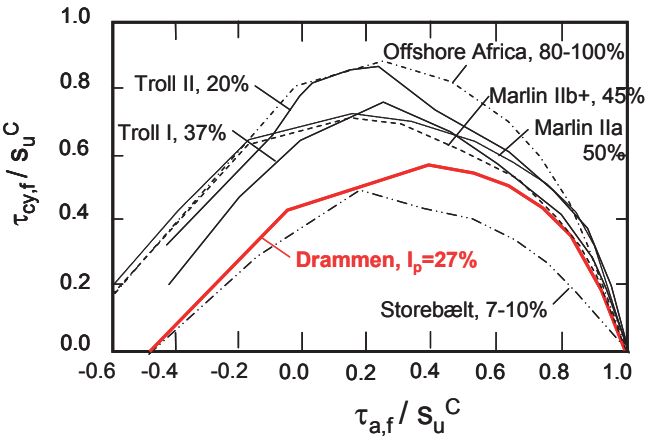

Figure 7.36. Normalized average and cyclic shear stresses for N_f=10 in triaxial tests, for different normally consolidated clays (based on Andersen, 2004).

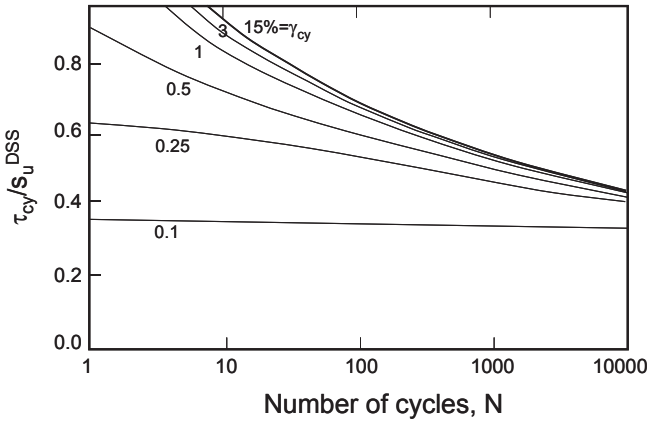

Figure 7.37. Cyclic shear strain as function of number of cycles (DSS tests with τa=0 on Drammen Clay with OCR=1).

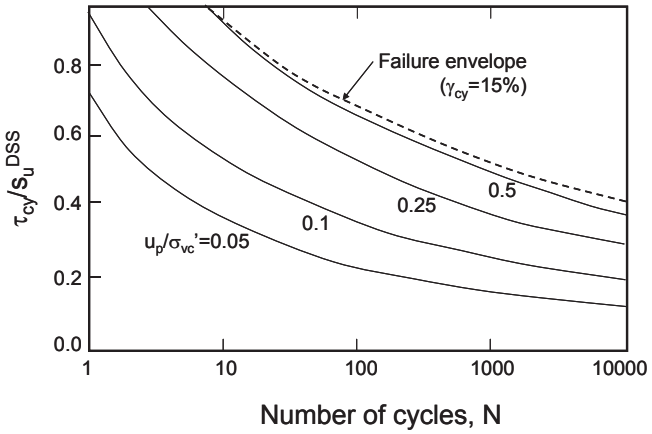

Figure 7.38. Permanent pore water pressure as function of number of cycles (DSS tests with τ_a=0 on Drammen Clay with OCR=1).

7.6.9 *Shear strains and pore water pressure due to cyclic loading*

As described in Section 7.6.8, cyclic loading will generate an excess pore water pressure, and the reduced effective stresses will lead to permanent and cyclic shear strains that increase with number of cycles.

Permanent pore water pressure and permanent and cyclic shear strains can be presented in the same type of diagrams as in Figures 7.30 and 7.31. Diagrams of this type are given in Andersen (2004).

7.6.10 *Effect of shear stress during consolidation*

A permanent slope will consolidate under a shear stress from its own weight, τ_c, as illustrated in Figure 7.39. The existence of a shear stress under consolidation will influence the undrained shear strength, as illustrated in Figure 7.40 for DSS tests on high quality samples of a Norwegian normally consolidated soft quick clay. The data in Figure 7.40 should only be regarded as an example, as available data do not show a consistent trend. The effect of the shear stress during consolidation may depend on the overconsolidation ratio and be less pronounced for overconsolidated than for normally consolidated clays.

However, the data in Figure 7.40 illustrate that it can be important to consolidate the clay under the appropriate stresses. If this strength increase due to shear stress under consolidation is neglected, the stability of a slope under additional undrained loading may be significantly underestimated. On the other hand, a laboratory test is normally run to failure in less than 2 hours, and the slope will remain undrained for a much longer period than this after additional loading. The undrained shear strength may then be reduced by about 20%, according to Figure 7.25.

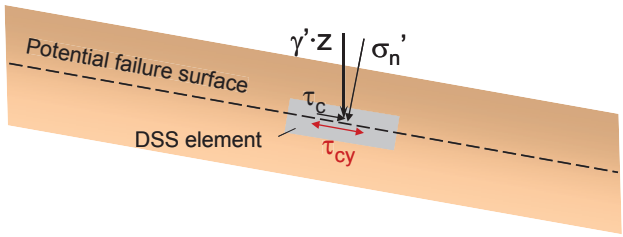

Figure 7.39. Simplified stress conditions in infinite slope.

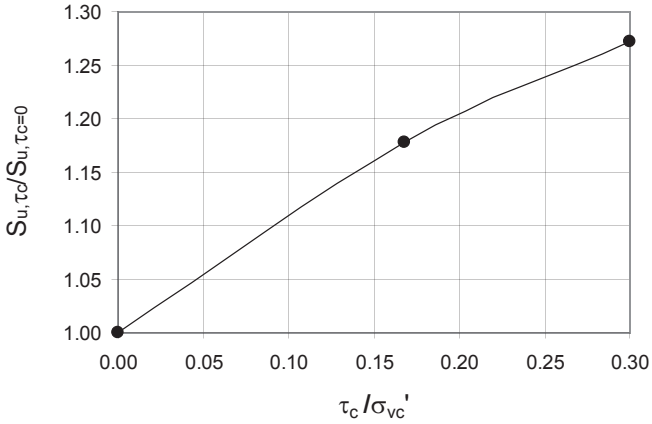

Figure 7.40. Undrained static DSS shear strength of a Norwegian normally consolidated soft quick clay as function of normalized consolidation shear stress, τ_c/σ_{vc}'.

7.6.11 *Shear strength of slopes under earthquake loading*

For slopes subjected to earthquake loading, the stress conditions and the failure mechanism require special considerations. A permanent slope will consolidate under a shear stress from its own weight, τ_c, as illustrated in Figure 7.39. For relatively steep slopes, this average shear stress may be of about the same magnitude as the cyclic shear stress due to the earthquake. The earthquake has a cyclic load period of about one tenth of offshore wave loading.

A slope that is subjected to earthquake loading may fail in three different ways; (1) large permanent and/or cyclic displacements during the earthquake, (2) large undrained creep displacements, and (3) due to reduced static shear strength. The creep displacements and the reduced static shear strength are both caused by reduced effective stresses due to cyclically induced pore water pressures during the earthquake.

Due to the large soil mass that has to be accelerated during the short time of an earthquake load cycle, cyclic displacements are not likely to be the critical mechanism. The critical mechanism is likely to be development of large permanent shear strains and displacements during or after the earthquake. The critical period may be some time after the earthquake before the excess pore water pressure generated by the cyclic loading has dissipated. During this period the clay will creep under undrained conditions and a delayed failure may occur. The reduced static shear strength will reduce the safety against external load changes after the earthquake, like erosion at the toe of the slope, sedimentation in the upper part of the slope, or other external loads.

Preliminary laboratory testing has been performed on a Norwegian normally consolidated quick clay under stress conditions that are representative for the stresses under earthquake loading of a slope (Andersen, 2009). These tests are used to propose a procedure to determine the shear strength of a slope under earthquake loading. The procedure is described in the following.

The effect that the shear stress during consolidation will have on the static shear strength was discussed in the previous subsection. The effect that the shear stress during consolidation will have on cyclic behaviour, initiation of undrained creep and post cyclic static shear strength is discussed in the following.

The effect of earthquake loading on undrained creep is illustrated by the test results in Figure 7.41. The tests in Figure 7.41 have been consolidated with an average shear stress of 62% of the undrained static shear strength, corresponding to a slope of about 13^0. One specimen was cycled to a permanent shear strain of 5% and left with the average shear stress under undrained conditions. It can be seen that the specimen develops shear strains that accelerate and fails after 136 minutes. A reference creep test that was not subjected to cyclic loading also is included in Figure 7.41. The reference test was run by just closing the drainage after the same consolidation period as in the cyclic test. The reference test did not develop noticeable shear strains. This demonstrates that the earthquake loading can initiate undrained creep and that undrained creep is a likely failure mode for slopes subjected to earthquakes.

The effect of earthquake loading on the static shear strength is illustrated by the test results in Figure 7.42. Figure 7.42 shows examples of cyclic tests consolidated with τ_c/σ_{vc}'=0.16, corresponding to a slope of about 10^0. The figure shows one reference monotonic test and 2 cyclic tests that were run with monotonic loading to failure after cycling. The cyclic tests were run stress-controlled with a load period of 1s. The monotonic tests were run strain-controlled with a rate of shear strain of ~4.5%/hr.

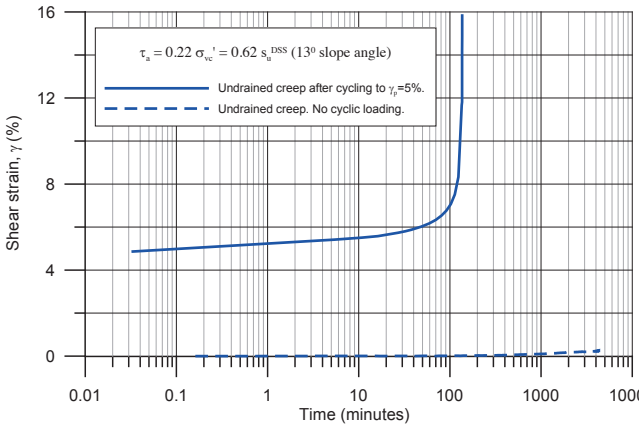

Figure 7.41. Development of shear strain in undrained DSS tests with constant shear stress.

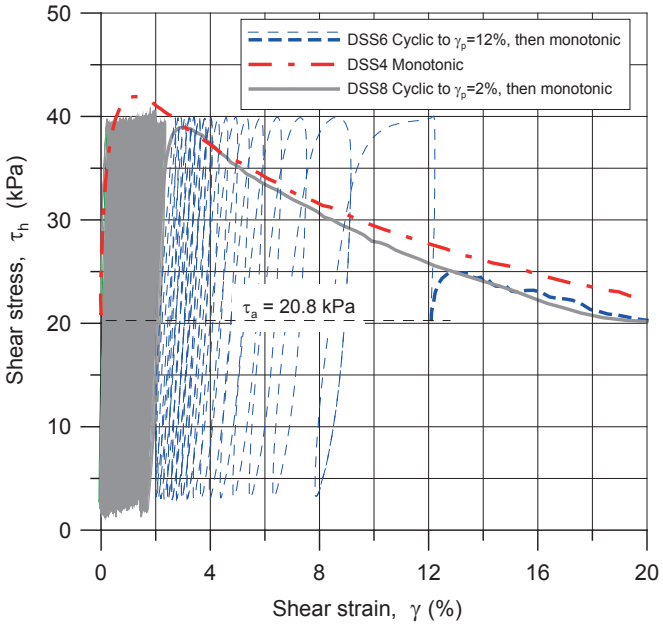

Figure 7.42. Stress-strain behaviour in monotonic, cyclic and post-cyclic monotonic DSS tests with $\tau_a=\tau_c$=20.8 kPa=0.16·σ_{vc}'.

It can be seen from the plot that the cyclic stress-strain curves go beyond the monotonic stress-strain curve. The reason for this is that the cyclic tests are run stress-controlled and that the rate of strain is significantly higher in the cyclic tests when they develop large strains than the rate of strain in the strain-controlled monotonic tests.

The cyclic loading was stopped when a permanent shear strain of γ_p=2% was reached in the first cyclic test (DSS8) and when γ_p=12% was reached in the other cyclic test (DSS6). The results in Figure 7.42 show that the post-cyclic monotonic stress-strain curve rapidly joins the virgin monotonic stress-strain curve and that the monotonic peak shear strength is reduced by the cyclic loading. Differences in the monotonic curves are believed to be due to soil variability. It thus appears that the post cyclic static shear strength is governed by the virgin

monotonic stress-strain curve and the permanent shear strain that is developed during cyclic loading. Similar results have been found on Drammen Clay (Andersen, 1988), but the behaviour is even more evident for the quick clay due to the more pronounced strain-softening. In the tests in Figure 7.42, the post-cyclic monotonic tests were run immediately after the cyclic tests without drainage or time for undrained creep.

Tests with symmetrical loading ($\tau_a=\tau_c=0$) show a somewhat different picture, where the post cyclic monotonic stress-strain curve does not reach the virgin monotonic stress-strain curve (Andersen, 1988).

Based on the results presented above, the safety of a slope subjected to earthquake loading may be analysed by first running a dynamic analysis to determine the permanent shear strain due to the earthquake. The post cyclic shear strength may then be determined as the shear stress on the monotonic stress-strain curve at a shear strain equal to the calculated permanent shear strain. This shear strength should be reduced by 15-25% to account for the following two effects:

– Undrained creep occurring before significant dissipation of the earthquake-induced excess pore water pressure. The time before significant pore water pressure dissipation is significantly longer than the time to failure in the monotonic laboratory test, and the effect of the undrained creep during this period has been corrected for based on the effect of time to failure on the shear strength in Figure 7.25.

– The post-cyclic stress-strain curve reaches the virgin curve at a somewhat larger strain than the permanent strain developed during the earthquake.

When applying the shear strengths discussed above, one must take into consideration that there can be progressive failure mechanisms in slopes (e.g. Andresen and Jostad, 2004).

7.6.12 *Initial shear modulus*

The initial shear modulus from shear wave velocity measurements on a number of clays in laboratory tests is plotted as function of plasticity index in Figures 7.43 and 7.44. The initial shear modulus is normalised with respect to the undrained static DSS strength in Figure 7.43 and with respect to the vertical effective consolidation stress in Figure 7.44. The plots distinguish between data for close to normally consolidated clays (OCR=1–1.5) and overconsolidated clays (OCR>1.5). For overconsolidated clays, the OCR-value is identified in the plot.

There is a clear tendency for the normalised shear modulus to decrease with increasing plasticity index, I_p. There is also a reduction in G_{max}/s_u^{DSS} and an increase in G_{max}/σ_{vc}' with increasing OCR.

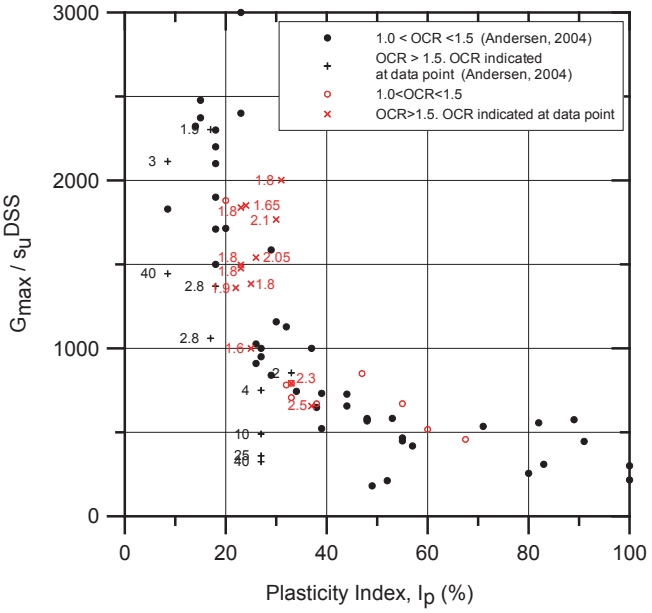

Figure 7.43 Initial shear modulus normalized by s_u^{DSS} as function of plasticity index, I_p.

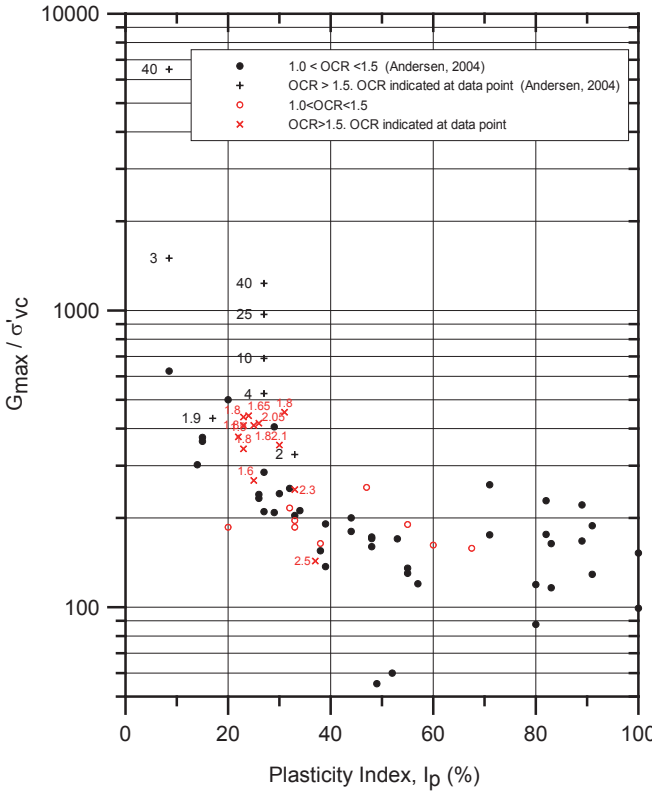

Figure 7.44 Initial shear modulus normalized by σ_{vc}' as function of plasticity index, I_p.

7.6.13 *Damping*

The damping coefficient, D, is plotted as function of cyclic shear strain in Figure 7.45. The curves are mainly based on results from stress-controlled two-way cyclic DSS tests with 10s load period and resonant column tests on Great Belt Clay with OCR=3 (Kleven and Andersen, 1991). The Great Belt Clay is a low plasticity clay till with

I_p=13%. However, tests on normally consolidated offshore clay with I_p=25-30% have given very similar results.

The curves in Figure 7.45 show that the damping coefficient depends on the number of cycles. The Seed and Idriss (1970) curve would be close to a curve for about 25 cycles. The curves are not checked for various different clays, and should therefore be used with caution. The curves may also be different for non-symmetrical cyclic loading and in triaxial tests. The tests on Great Belt clay indicated that the damping ratio may decrease with decreasing load period.

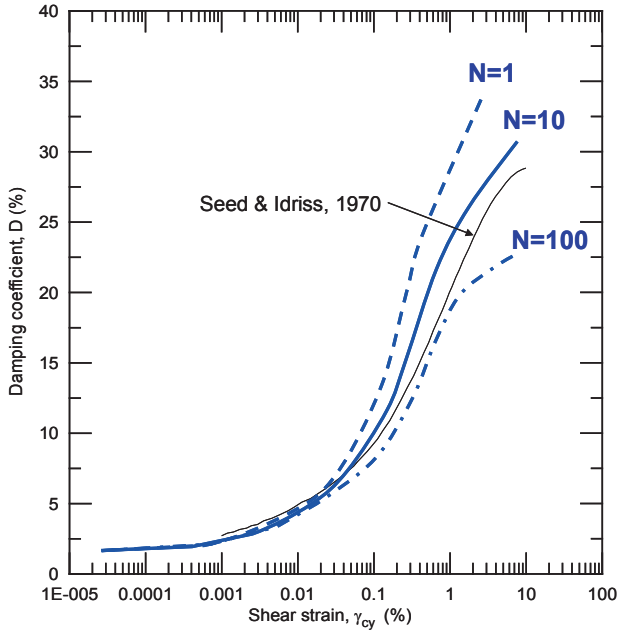

Figure 7.45. Damping coefficient as determined in stress-controlled two-way cyclic DSS tests.

7.6.14 *Remoulded shear strength*

The remoulded shear strength can be measured by different tests, like UU, fall cone, miniature vane tests in the laboratory, and field vane and T-bar and ball penetrometer tests in the field. These measurements often give different values of the remoulded shear strength. Lunne and Andersen (2007) presented examples showing that UU tests give smaller shear strengths than field vane and fall cone. A main reason for this difference is believed to be rate effect. UU tests are typically run to failure in 5 to 10 minutes, whereas the rate of shear strain in the shear zone in the clay around the field vane may be three orders of magnitudes faster. The fall cone is often calibrated against the field vane, and thus represents fast loading. According to the rate effect presented in Figure 7.26, this may give about 50% higher remoulded strength measured by field vane and fall cone than by UU tests.

The remoulded shear strength may also be measured by T-bar and ball penetrometer tests where the penetrometer is moved about 0.5 m up and down several times until the resistance becomes more or less constant. The measured resistance is converted to remoulded shear strength by dividing by an N-factor. Recommended N-factors to determine remoulded strength are given in Table 7.2.

7.6.15 *Sensitivity*

The sensitivity is the ratio between the shear strengths of intact and remoulded clay. Data presented by Lunne and Andersen (2007) seem to indicate that the rate effect is the same in remoulded and intact clay. This means that the sensitivity should be less dependent on the type of test than the strengths, provided the same type of test is used to determine intact and remoulded shear strengths. The sensitivity may be underestimated due to sample disturbance; however, as the intact shear strength may be reduced by sample disturbance.

When using the T-bar or the ball penetrometers one should keep in mind that the true sensitivity of the clay will be higher than the ratio of initial to cyclic resistance. The reason is that (a) the initial penetration resistance will be reduced by the disturbed zone behind the penetrometer and (b) the cyclic resistance may be increased by varying degree of disturbance radially away from the penetrometer.

Since the remoulded shear strength depends on the rate of strain, it is important to take rate effect into account and use a remoulded strength representative for the rate and duration of the design load, just as for intact strength. If the remoulded shear strength is determined based on intact strength and sensitivity through $s_{u,rem}=s_u/S_t$, the rate effect should be included in the intact shear strength and the rate independent sensitivity can be used.

7.6.16 *Reconsolidated remoulded shear strength*

The shear strength of remoulded clay that has been reconsolidated to the effective stresses it had before remoulding is presented in Figure 7.46. The figure shows the DSS strength normalised to the shear strength of the clay before remoulding as function of overconsolidation ratio. The strength for normally consolidated clay is roughly 0 – 10 % higher than the strength for intact clay. The reason for the strength increase is believed to be the reduction in water content when remoulded normally consolidated clay is reconsolidated. With increasing overconsolidation ratio, the ratio between reconsolidated and intact strengths deceases, meaning that overconsolidated clay does not regain its original strength after remoulding. The diagram in Figure 7.46 contains data for clays with plasticity and sensitivity in the range of I_p=10-90% and S_t=2-5.

The reconsolidation stresses will not in all cases come back to the original *in situ* effective stresses, however. This can for example be the case in the disturbed zone along the outside wall of a suction anchor, where arching may cause reduced effective normal stresses compared to the original *in situ* stresses. It will also take time before excess pore water pressures after installation have dissipated, and the governing condition may occur at effective stresses lower than those at equilibrium. It is

therefore of interest to know the reconsolidated remoulded strength as function of the reconsolidation stress. Figure 7.47 therefore presents the shear strength from DSS tests of remoulded clay, $s_{u,rr}^{DSS}/\sigma_{vc}'$, after being reconsolidated to different percentages of the original consolidation stress of $\sigma_{vc}'=p_0'$, $0.68 \cdot p_0'$ or $0.5 \cdot p_0'$, where p_0' is the original *in situ* vertical effective stress prior to remoulding. The p_0'-value varies from clay to clay. Some clays have been consolidated to p_0' only, whereas others have been reconsolidated to more than one stress level. The different reconsolidation levels are marked by different symbols, and, when available, strengths for different reconsolidation stress levels for one particular clay are connected by lines.

The data in Figure 7.47 show that $s_{u,rr}^{DSS}/\sigma_{vc}'$ increases with decreasing consolidation stress for a given OCR and increases with increasing OCR. This is the same trend as observed for shear strength of intact normally consolidated clay (Lunne and Andersen, 2007). It is interesting to observe that the increase in $s_{u,rr}^{DSS}/\sigma_{vc}'$ for tests reconsolidated to $0.68 \cdot p_0'$ or $0.5 \cdot p_0'$ compared to tests reconsolidated to p_0' for individual clays seems to follow the general trend for tests reconsolidated to p_0'. The increase in $s_{u,rr}^{DSS}/\sigma_{vc}'$ for tests reconsolidated to $0.5 \cdot p_0'$ compared to tests reconsolidated to p_0' was on average 15% for the 7 clays where both reconsolidation levels were available. The increase will, however, depend on the magnitude of p_0', as one can see on Figure 7.47.

The data in Figure 7.47 does not shown a clear tendency for $s_{u,rr}^{DSS}/\sigma_{vc}'$ to vary with I_p or S_t, but the data base is too small to draw definite conclusions about such tendencies.

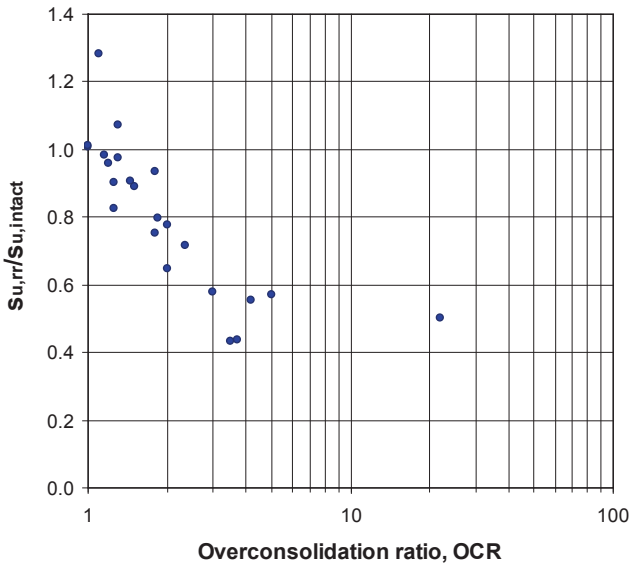

Figure 7.46. DSS shear strength of remoulded clay after reconsolidation to original *in situ* vertical effective stress, normalised to intact shear strength.

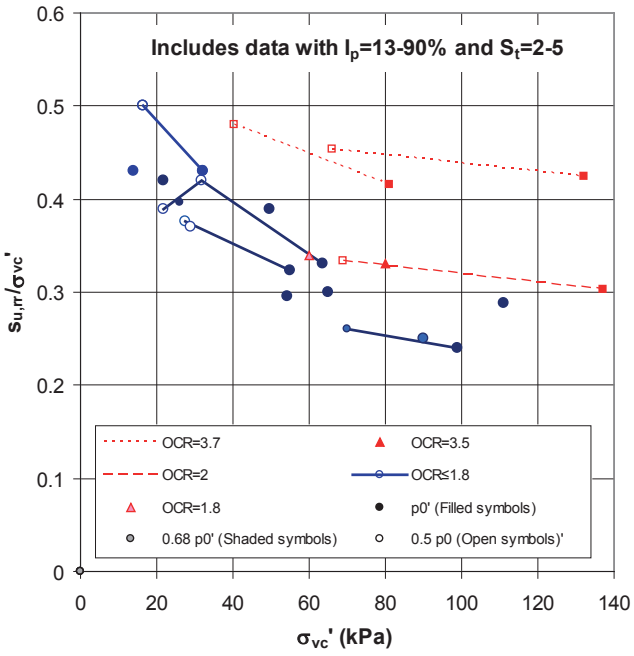

Figure 7.47. DSS shear strength of remoulded clay after reconsolidation to original vertical effective stress (modified from Lunne and Andersen, 2007).

7.6.17 *Thixotropy*

Thixotropy can be defined as a process of softening caused by remoulding, followed by a time dependent return to the original harder state at a constant water content and constant porosity (Mitchell, 1960). In a purely thixotropic material, this process is fully reversible. The ratio between the shear strength after a time with thixotropic strength gain and the shear strength just after remoulding is referred to as the thixotropy strength ratio. Sensitivity of clays can partly be explained by thixotropy, but other factors also contribute to the sensitivity of clays, like cementation, leaching or other factors not related to thixotropy.

Thixotropy can result in strength increase of more than 100% after remoulding, and thus be significant from an engineering standpoint when dealing with clays in their remoulded state. For instance, the thixotropy effect means that it is possible to rely on a shear strength along the wall of piles and suction anchors soon after installation which is higher than the remoulded shear strength, even before pore water pressure dissipation occurs. Procedures to calculate the increase in the shear strength along the outside and inside wall of suction anchors due to thixotropy and pore water pressure dissipation are proposed in Andersen and Jostad (2002 and 2004).

An example of thixotropy measured on a clay from the Gulf of Mexico is plotted in Figure 7.48. It can be seen that the thixotropy effect gives a very rapid increase in strength in the first few days or even hours and that strength continues to increase even after 2 months.

Andersen and Jostad (2002) plotted the thixotropy strength ratio after 1, 10 and 60 – 90 days for a number of

natural clays as function of the plasticity index. They found that the thixotropy strength ratio tended to increase with increasing plasticity index, but there was considerable scatter in this relationship. Skempton and Northey (1952) found that natural clays exhibited a significant strength increase, kaolin exhibited almost no thixotropy, illite showed a moderate strength increase, and bentonite showed a large strength gain. The thixotropy of natural clays is therefore likely to depend strongly on their mineral composition. Lunne and Andersen (2007) therefore plotted the thixotropy strength ratio against the inverse of the activity of the soil. The activity is defined as I_p / %clay, and reflects the clay mineralogy. The plot from Lunne and Andersen (2007) is reproduced in Figure 7.49, supplemented with some more recent data. The plot shows that there is some relationship between the thixotropy strength ratio and the activity, but there is still considerable scatter. There is an effect of the sensitivity, and the scatter is reduced when sorting the data according to the sensitivity. Most of the data are based on fall cone measurements. The data for kaolin, illite and bentonite form a lower bound to the data for the natural clays.

There is not enough data on overconsolidated clays to determine if there is an effect of overconsolidation on the thixotropy.

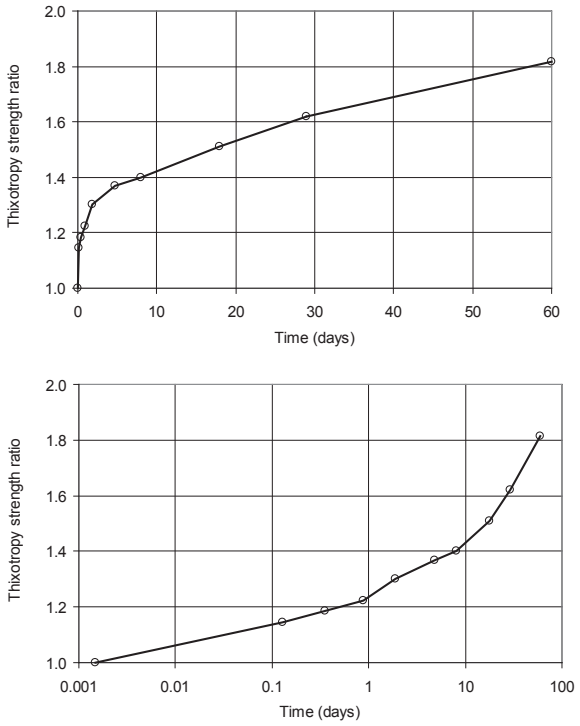

Figure 7.48. Thixotropy ratio with time for a Gulf of Mexico clay with I_p=40%, w=, S_t=3.5 and 50% clay content.

If the data in Figure 7.49 is used in design, a low value within the thixotropy strength ratio scatter for the given activity should be used when a low strength is conservative, like in capacity analyses. If a high strength is conservative, like in retrieval of suction anchors, a high value should be selected. If the thixotropy strength factor turns out to be important for the design, thixotropy tests on site specific soil should be considered.

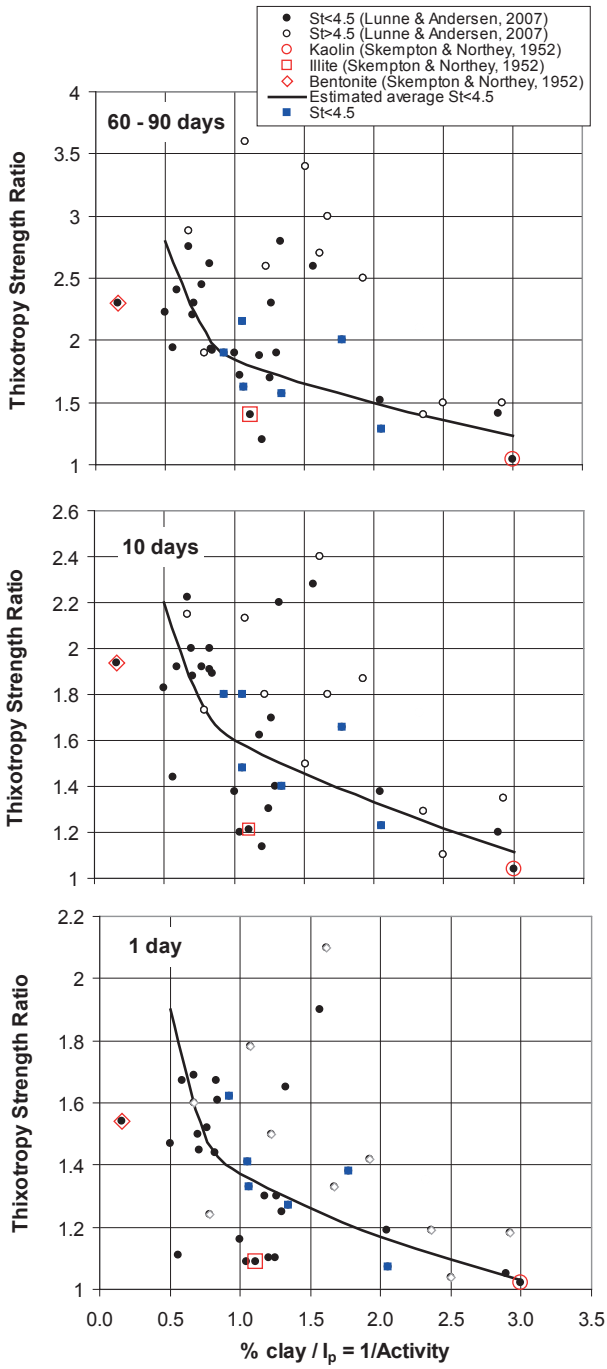

Figure 7.49. Thixotropy strength ratio as function of Activity^{-1}=% clay/I_p after 1, 10 and 60-100 days.

7.6.18 *Temperature effects*

In the Norwegian Sea, and in many other deep water areas, the temperature at the seabed can be continuously around 0°C or even below with the salt content of the pore fluid allowing the soil to remain unfrozen. For example, Bugge (1983) has shown that for a location on the

Norwegian continental margin at latitude of 64°N, the sea water reaches a temperature of 0°C at a depth of 850m and reaches an equilibrium temperature of -0.9°C at a depth of 1300m. In the Mexican part of the Gulf of Mexico temperatures lower than 5°C have been measured in 1200m water depth (Vidal et al., 1994). In the Barents Sea seabed temperatures can be lower than -2°C in some areas.

It is presently normal practice to test deep water soils at room temperature in the laboratory. A review has recently been carried out at NGI (Perkins and Sjursen, 2008), which confirms that testing at room temperature (about 20°C) may lead to strength and deformation properties that can be different to what had been obtained if the samples had been stored, transported and tested at the in situ temperature. The study showed that the preconsolidation stress, p_c', and undrained triaxial shear strength, s_u, can be 10–20% too low when tested at room temperature compared to when tested at 0°C. This experience was in the line with previous work reported by Mitchell (1993) and Leroueil and Marques (1996). Figure 7.50 shows considerable scatter, but indicates that the preconsolidation stress measured near 0°C can be about 20% higher than measured near 20°C. Undrained shear strength has often been found to be proportional to p_c', so a similar effect is expected to be valid for undrained shear strength.

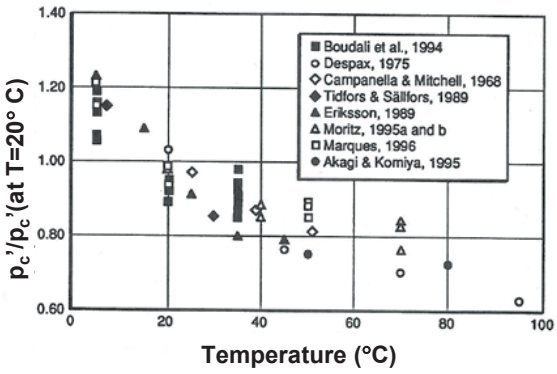

Figure 7.50 Variation of normalized preconsolidation pressure or vertical effective stress with temperature (from Leroueil and Marques, 1996).

However, one limitation with the tests carried out so far is that the samples were stored in one period at room temperature and also in a period at about 7°C before the sample was cooled to 0°C before testing. Leroueil and Marques (1996) argued that warming a sample from in situ to room temperature will results in some consolidation, and cooling the sample back to in situ temperature will cause some swelling, but not all the way back to it's original void ratio. The effect of this consolidation and swelling cycle could be that the measured undrained shear strength could be higher than if the sample had not experienced the warming and cooling cycle. NGI is presently carrying out a join industry project where the effects of temperature will be comprehensively investigated.

8 PROTOTYPE OBSERVATIONS AND FIELD AND MODEL TESTING

8.1 *General*

It has been tradition in geotechnical engineering to check foundation design and calculation models by prototype observations and field and model testing. This has also been the case offshore. Such information has given confidence in the foundation design procedures for new concepts that have been introduced and allowed these new concepts to be applied. Some examples of prototype observations and field and model tests related to soft clays where NGI has been involved are given in the following.

8.2 *Brent B GBS prototype observations*

The Brent B Condeep gravity platform was one of the first large gravity structures (GBS) installed offshore. The oil and gas industry therefore established a joint industry sponsored project where the Brent B platform was heavily instrumented to verify that the platform behaved as expected and to gain knowledge for future projects.

The platform was instrumented as shown in Figure 8.1 to measure wave height, soil stiffness, displacements (from accelerometers), settlements, pore water pressure, base contact stresses, resonance periods and stresses in the structure. The observations gave valuable feedback about the behaviour of skirted gravity base structures under severe storm loading and rendered confidence in the design procedures that had been applied (Andersen and Aas, 1980). As an example of results, the acceleration spectra as calculated from measured accelerations are shown in Figure 8.2. The two first modes of 0.56 and 0.58Hz represent bending in the two horizontal directions, and the third mode of 0.84Hz is torsion about the vertical axis.

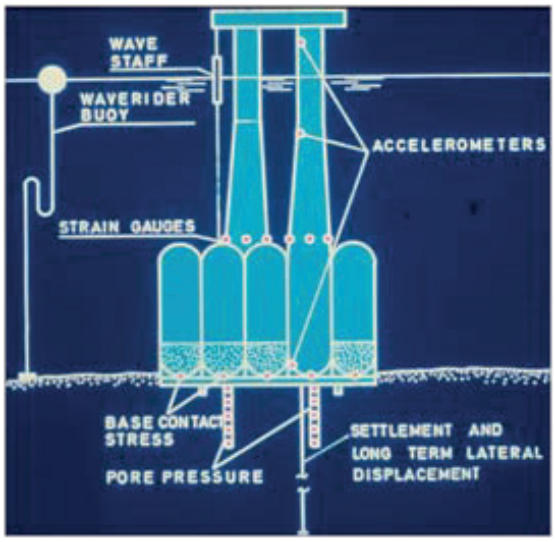

Figure 8.1. Instrumentation of the Brent B Condeep platform.

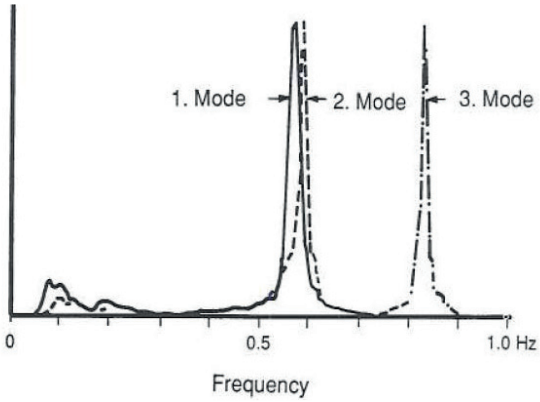

Figure 8.2. Measured acceleration spectra for the Brent B Condeep platform (Hansteen, 1980).

8.3 *Troll GBS prototype observations*

The Troll A Condeep platform is a huge GBS located in the Norwegian trench in 303m water depth (Figure 8.3). The submerged platform weight is 2820MN, and the foundation area is 16597m^2. As the soil is normally consolidated clay, the 19 concrete foundation cells are extended by cylindrical concrete skirts penetrating 36m into the seabed to obtain the required bearing capacity.

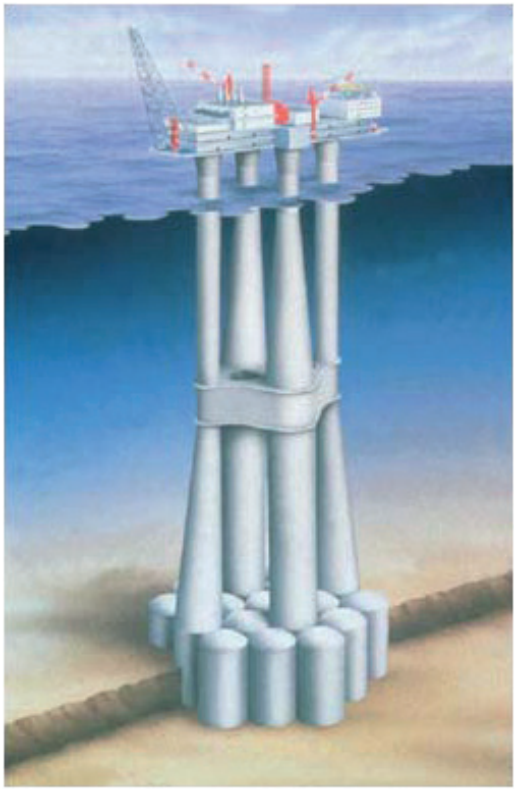

Figure 8.3. Troll A GBS Condeep platform.

The Troll A platform is equipped with a structural and environmental monitoring system that has been in operation and given information about the condition of the platform and its foundation since the platform was installed in 1995 (Tjelta *et al.*, 2007). The monitored parameters include settlement, earth pressures, pore water pressures in the soil, water pressure in the skirt compartments, and accelerometers and strain gauges at several elevations on the structure. The system also monitors environmental parameters such as waves and wind.

The monitoring system proved its value when it was suspected that gas might migrate along the well path and into one of the skirt cells beneath the structure. The information from the monitoring system made it possible to exclude that gas migrated from the reservoir into the foundation cells. Based on the information from the monitoring system, it is also possible to adjust the water pressure in the foundation cells to prevent high local contact stresses against the base.

8.4 *Gullfaks C skirt penetration test*

The Gullfaks C Condeep Gravity Base structure was installed in 1989. The water depth is 220 m, and at the time the platform was the largest gravity base structure installed. The soil conditions at Gullfaks C comprise normally consolidated clays, relatively loose clayey, silty sands and medium dense sands in the upper 45 m. The platform was designed with 1200 m running meters of 22 m high concrete skirts. In the design phase Statoil became concerned that penetration of the skirts could become difficult, and it was decided to carry out a model test at the actual platform site. The test structure (Figure 8.4) was made up of two steel cylinders, height 23 m and diameter 6.5 m, attached to each other through a concrete panel 2.4 m·0.4 m. Penetration of the concrete panel was achieved by the submerged weight and suction inside the two steel cylinders. The structure was heavily instrumented to measure a number of parameters including the penetration

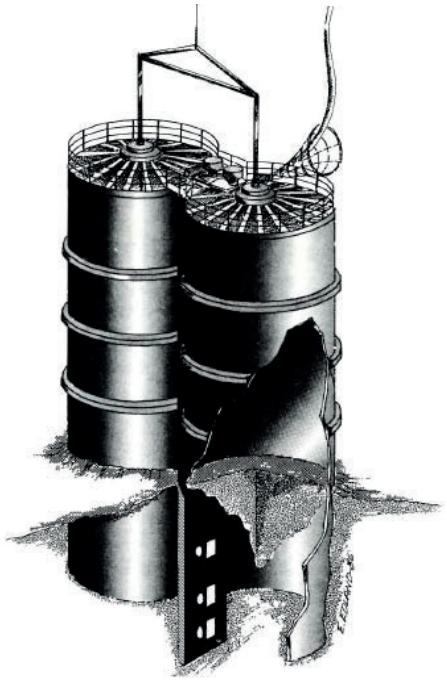

Figure 8.4. Artist view of Gullfaks C penetration model.

force and underpressure in the steel cylinders as function of penetration. Two tests were carried out and included variation in penetration rate, check for set-up effects, cyclic tests and water injection at tip of the penetration panel. As reported by Tjelta *et al*. (1986), the tests were successful and proved the feasibility of achieving full penetration of the concrete skirts.

8.5 *GBS laboratory model tests*

Five 1g laboratory model tests with a diameter of 0.4m were run to verify the foundation design procedures for offshore gravity base structures in soft clay. The calculated and measured capacities, displacements and failure mode (large permanent displacements, large cyclic displacements, or a combination) agreed very well. A comparison between calculated and measured failure surfaces is presented in Figure 8.5. More details can be found in Andersen *et al*. 1989.

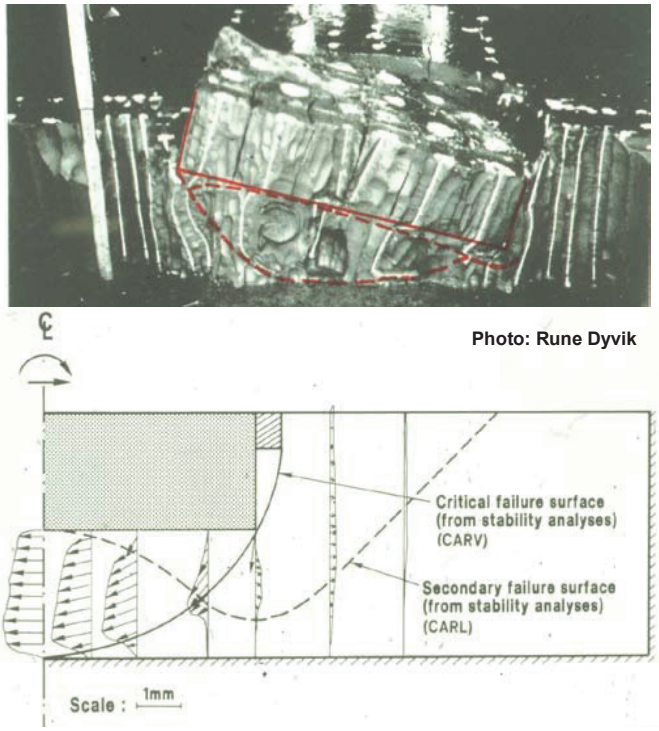

Figure 8.5. Observed and calculated failure surfaces in GBS laboratory model tests.

8.6 *Suction anchor field tests*

Two series of large scale field tests were run to verify the calculation procedures for offshore suction anchors in soft clay (Figures 8.6 and 8.7). One series was run with a load inclination of 10° with the vertical to simulate anchors for a tension leg platform (Andersen *et al*. 1993). The other series was run with a load inclination of 10° with the horizontal to simulate anchors with more horizontal loading (Keaveny *et al*. 1994). The calculated holding capacity, type of failure surface, failure surface location, and failure mode (large permanent displacements, large cyclic displacements, or a combination) were in excellent agreement with the measurements for all the model tests. This gave confidence in the suction anchor concept and the design procedures that were applied. Details can be found in the references given above.

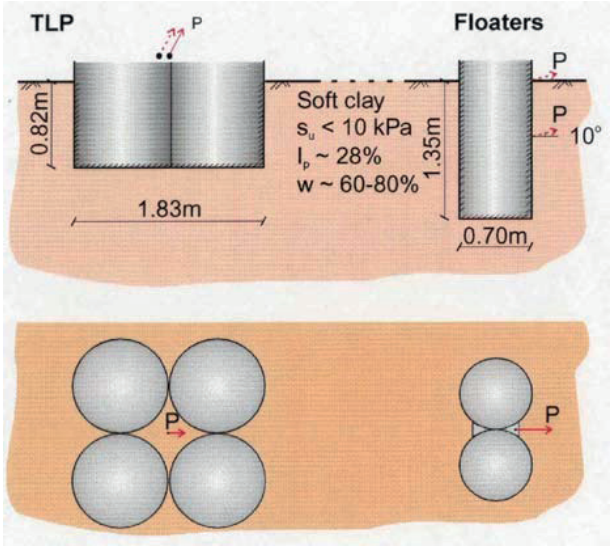

Figure 8.6. Geometry and key soil data for the large scale field model tests of offshore suction anchors.

Figure 8.7. TLP model after failure (photo by Rune Dyvik, NGI).

8.7 *Pipelines and risers*

The axial and lateral load displacement response from the soil is the most important input to evaluate pipeline displacement and riser-soil interaction. As discussed in Section 4, this response depends on various aspects of the soil behaviour and is complicated to calculate theoretically. A number of model tests on pipe elements in various clays under load conditions representative for pipelines and risers have therefore been performed in the NGI test bin shown in Figure 8.8.

These model tests have been used to study mechanisms under typical load conditions, establish soil models directly from the model tests, and check and calibrate theoretical models (e.g. Clukey *et al*., 2005, Langford and Aubeny, 2008).

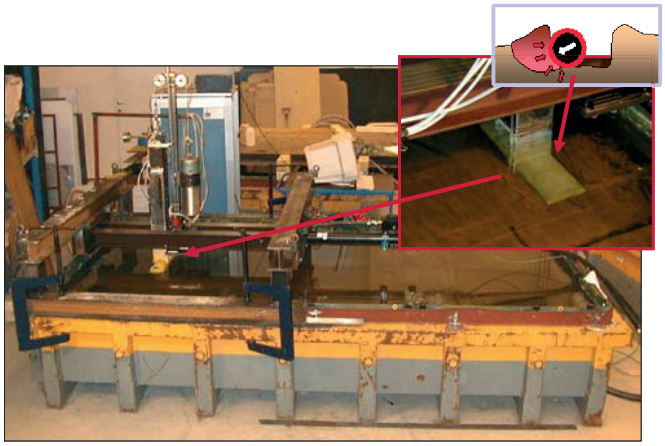

Figure 8.8. NGI test bin for pipelines and risers (L=3.6m, B=1.7m).

9 SUMMARY AND CONCLUSIONS

Oil and gas from deep water fields can be produced by transportation through pipelines to shore or loaded onto tankers. In both cases it is necessary with different subsea structures on the seabed. In cases with tankers, anchoring systems are necessary, and in cases with pipelines, a safe pipeline route must be found. All these structures require foundation design and geotechnical considerations.

The soil in deep water areas is generally soft and normally consolidated, or even underconsolidated. In slide areas, the clay can also be overconsolidated.

Both for the production site and for the pipeline route, it is necessary to consider possible geohazards. Of major concern are changes in seabed conditions caused by local or large scale instability as well as unexpected pressure changes and uncontrolled fluid flow during drilling and maintenance of wells... Possible geohazards include rapid sedimentation, erosion, mud and salt diapirism, mud volcanoes, growth faulting, gas hydrates, shallow gas, excess pore water pressures, shallow water flow, pockmarks and earthquakes. Several of these phenomena can trigger submarine slides and have a severe impact on well bore stability.

Geohazards, bathymetry and thickness and variation of soil units can be mapped by geophysical methods. Reflection seismic methods are the most common. The main difference between the methods is their resolution and penetration ability. Ground truthing by geological/ geotechnical boreholes and pore water pressure measurements is required to calibrate the seismic information and to extrapolate/interpolate data over larger areas. For assessment of geohazards risk, full integration of the geological, geophysical and geotechnical disciplines is recommended.

The foundation design of subsea structures, pipelines and anchors and the evaluation of slope stability require knowledge about the soil. The necessary soil parameters will depend on the structure, but one will always need classification and index parameters, like water content, unit weight, grain size distribution, liquid and plastic limits, index shear strength data, mineralogy and carbonate content. It is also necessary to know in situ stresses, pore water pressure and preconsolidation stress. Parameters that depend on the structures are compressibility, permeability, undrained shear strength, strength anisotropy, stress-strain relationships, initial shear modulus, stress path dependant cyclic shear strength, permanent and cyclic shear strains and permanent pore water pressure under cyclic loading, shear strength, stiffness and damping under earthquake loading, effect of shear stress during consolidation, effect of rate of strain and load duration, remoulded shear strength, sensitivity, compressibility of remoulded clay, strength of reconsolidated remoulded clay, and thixotropy.

Of special concern for characterization of deep water soils are the very low strength in the upper part of the soil profile, sample disturbance and the effect of the difference in temperature between in situ and laboratory. It is also important to determine the in situ pore water pressure, as deep water deposits can be underconsolidated.

The soil parameters can be determined by *in situ* and laboratory testing.

In situ testing includes cone penetrometer tests (CPT), full flow penetrometers (T-bar and ball), field vane, seismic cone and piezoprobe. The interpretation of the CPT and the full flow penetrometer tests requires N-factors, which can depend on the clay and are different for intact and remoulded shear strengths. Recommended N-factors are given in the paper. Pore water pressure measurement by piezoprobe involves uncertainties, and single or multilevel piezometers installed as part of the soil investigation will be more reliable.

Sample disturbance can have a significant influence on the deep water soil parameters measured in the laboratory, and one should always attempt to take samples that are as undisturbed as possible. Sample quality can be evaluated by the change in void ratio when consolidating a sample back to the in situ stresses, and by comparing laboratory and in situ shear wave velocities. NGI has recently contributed to the development of a deep water sampler designed to retrieve good quality, 15-20m long samples in 2000m water by carefully considering the factors influencing sample quality. The quality should be comparable to that of a thin walled piston sampler in drilling mode. For the upper very soft part of the soil profile, box core sampling should be considered.

Laboratory testing includes, in addition to the index testing, oedometer tests, monotonic and cyclic triaxial compression, triaxial extension and DSS tests, permeability tests, bender element tests, resonant column tests and thixotropy tests. The laboratory tests are normally run at a room temperature of about 20^0C, whereas the temperature at seabed may be closer to 0^0C in deep water. This temperature difference may lead to in

situ preconsolidation stress and shear strength being underestimated by 10-20%. The effect of temperature is a topic that should be studied further.

In a feasibility study and in an early stage of a project, it is necessary to have an idea about the soil parameters. Diagrams with typical parameters are then very useful for preliminary estimates of the parameters. Diagrams for a number of parameters are given in the paper. The diagrams are also very helpful when planning in situ and laboratory testing programs and for evaluating the parameters from site specific tests.

A tradition in geotechnical engineering has been to check foundation design and calculation models by prototype observations and field and model testing. Such information has given confidence in the foundation design procedures for new concepts that have been introduced and allowed these new concepts to be applied. Model testing and prototype observations should therefore also be considered for deep water concepts. Some examples of previous prototype observation and field and model testing related to soft clays are given in the paper.

10 ACKNOWLEDGEMENT

The authors would like to thank the Mexican Society of Soil Mechanics and the Mexican Petroleum Institute (IMP) for the invitation to present this paper at the Mexican Soil Mechanics National Meeting. The paper is based on results from R&D and advisory projects at NGI, financed by the Research Council of Norway and the oil and gas industry, and takes advantage of the work of numerous colleagues at NGI.

11 REFERENCES

Andersen, K.H. (1976): Behaviour of clay subjected to undrained cyclic loading. *Proc., Int. Conf., Behaviour of Offshore Structures, BOSS'76, Trondheim,* (1) 392-403.

Andersen, K.H. and Aas, P.M. (1980): Foundation performance. *Seminar; Shell Brent "B" Instrumentation Project. SUT.* Proc., 57-77. London 1979. Also NGI Publ. 137.

Andersen, K.H. and Lauritzsen, R. (1988): Bearing capacity for foundation with cyclic loads. *ASCE, J. Geotech. Eng., 114 (5)*, 540-555.

Andersen, K.H. (1988): Properties of soft clay under static and cyclic loading. *Int. Conf. on Engrg. Problems of Regional Soils,* Proc., p. 7-26, Beijing, China, 1988. Ed. by Chinese Inst. of Soil Mech. and Found. Engrg. Also in NGI Pub. 176.

Andersen, K.H., Dyvik, D., Lauritzsen, R., Heien, D., Hårvik, L. and Amundsen, T. (1989): Model tests of offshore platforms. II. Interpretation. *ASCE, J. of Geotech. Engrg.*, 115 (11) 1550-1568.

Andersen, K.H. (1991): Displacement of structures subjected to combined static and cyclic loads. *Int. Conf. on Geotech. Engrg. for Coastal Development, GEOCOAST'91,* Yokohama, Japan, Proc., (1) 537-542.

Andersen, K.H. and Høeg, K. (1991): Deformations of soils and displacements of structures subjected to combined static and cyclic loads. *X ECSMFE,* Firenze, May 1991, Proc., (4) 1147-1158.

Andersen K.H., Dyvik, R., Kikuchi, Y. and Skomedal, E. (1992): Clay behaviour under irregular cyclic loading. *Proc. Int. Conf., Behaviour of Offshore Structures,* London, (2), 937-950.

Andersen, K. H., Dyvik, R., Schrøder, K., Hansteen, O. E. and Bysveen, S. (1993): Field tests of anchors in clay. II: Predictions and interpretation. *ASCE, J. Geotech. Engrg*, 119 (10), 1532-1549.

Andersen, K.H. and Jostad, H.P. (1999): Foundation design of skirted foundations and anchors in clay. *Proc., OTC, Houston,* Paper 10824.

Andersen, K. H. and Jostad, H. P. (2002): Shear strength along outside wall of suction anchors in clay after installation. *Proc., XII ISOPE, Kyushu,* Japan, 26–31.

Andersen, K.H. (2002): Characterization of soft seabed soils in deep water by *in situ* tests. Theoretical analyses of the T-bar. *NGI Rep.* 20011026-2, 25 Sept.2002.

Andersen, K.H. (2004): Cyclic clay data for foundation design of structures subjected to wave loading. *Proc., Int. Conf. on Cyclic Behaviour of Soils and Liquefaction Phenomena, CBS04, Bochum, Germany*, 371-387, A.A. Balkema Publishers, Ed Th. Triantafyllidis.

Andersen, K.H. and Jostad, H.P. (2004): Shear strength along inside of suction anchor skirt wall in clay. *Proc., OTC, Houston,* Paper 16844.

Andersen, K.H., Murff, J.D., Randolph, M.F., Clukey, E., Erbrich, C., Jostad, H.P., Hansen, B., Aubeny, C., Sharma, P. and Supachawarote, C. (2005): Suction anchors for deepwater applications. *Proc., ISFOG, Int. Symp. on Frontiers in Offshore Geotech.*, 13-30. Perth, Australia.

Andersen, K.H. (2009): Bearing capacity under cyclic loading – offshore, along the coast and on land. *21st Bjerrum Lecture,* pres. in Oslo, Norway, 23 Nov. 2007. Subm. for possible publ. in CGJ.

Andresen, A., Berre, T., Kleven, A. and Lunne, T. (1979): Procedures used to obtain soil parameters for foundation engineering in the North Sea. *Marine Geotechnology,* 3(3), 201-266.

Andresen, L. (2001): Effect of strain softening on stability analyses. Analysis of retrogressive sliding due to strain softening – Ormen Lange case study. *NGI report* No. 521001-10, 29.03.2001.

Andresen, L. and Jostad, H.P. (2002): A constitutive model for anisotropic and strain softening clay. *NUMOG VIII*, Proc., p-79-84.

API (2000): Recommended practice for planning, designing and constructiong fixed offshore platforms – Working stress design., *RP2A-WSD, American petroleum Institute.*

ASTM (2007): Standard Test Methods for Modulus and Damping of Soils by Resonant Column Method. *ASTM D4015-07.*

Aubeny, C.P., Shi, H. and Murff, J.D. (2005): Collapse load for a cylinder embedded in trench in cohesive soil. Int. J. of Geomechanics, ASCE, 5(4), 320-325.

Baerheim,M. and Tjelta, T.I. (1992): Skirt-plate foundations for offshore jackets. *Int. Symp. Offshore and Polar Engrg., ISOPE*, San Fransisco, June 1992.

Becker, D. E., Crooks, J.H.A., Been, K. and Jefferies, M.G. (1987): Work as a criterion for determining in situ yield stresses in clays. *Can, Geot. J.*, 24, 549-564.

Berre, T. (2005): An alternative method for determination of preconsolidation stress. *Personal communication. NGI*, June 2005.

Berre, T., Lunne, T., Andersen, K.H., Strandvik, S. and Sjursen, M.A. (2007): Potential improvements of design parameters by taking block samples of soft marine Norwegian clays. *Canadian Geotechnical Journal*. V 44, pp. 698-716.

Bishop, A.W. (1955): The use of the slip circle in the stability analysis of slopes. *Geotechnique,* 5 (1), 7-17.

Bishop, A.W., Green, G.E., Garga, V.K., Andresen, A. and Brown, J.D. (1971): A new ring shear apparatus and its application to the measurement of residual strength. *Geotechnique,* 21 (4) 273-328.

Bjerrum, L. and Landva, A. (1966): Direct simple shear tests on a Norwegian quick clay. *Geotechnique,* 16 (1), 1-20. Also publ. in: NGI Publ. 70.

Bjerrum, L. (1967): Engineering geology of Norwegian normally consolidated marine clays as related to settlements of buildings. 7. Rankine Lecture, *Géotechnique*, V 17 (2), pp. 81-118.

Brandao, F.E.N., Henriques, C.C.D., de Araujo, J.B., Ferreira, O.C.G. and Dos santos Amaral, C. (2006): Albacora Leste field development-FPSO P-50 mooring system concept. *Proc., OTC,* Paper OTC18243.

Bridge, C., Lave, K., Clukey, E. and Evans, T. (2004): Steel catenary riser touch-down point vertical interaction model. *Proc., OTC,* Paper OTC16628.

Bruton, D.A.S., White, D.J., Cheuk, C.Y., Bolton, M.D. and Carr, M.C. (2006): Pipe-spoil interaction behaviour during lateral buckling, including large amplitude cyclic displacement tests by the SAFEBUCK JIP. *Proc., OTC, Houston*, Paper OTC17944.

Bruton, D.A.S., Carr, M. and White, D.J. (2007): The influence of pipe-spoil interaction on lateral buckling and walking of pipelines – The SAFEBUCK JIP. *Proc., 6th Intern.Offshore Site Investigation and Geotechnics Conf., London*, 133-148, Sept. 2007.

Bugge, T. (1983): Submarine Slides on the Norwegian Continental Margin, with Special Emphasis on the Storegga Area. *IKU,* Publication 110, 152 p.

Burland, J.B. (1990): On the compressibility and shear strength of natural clays. *Geotechnique*, 40 (3), 329-378.

Casagrande, A. (1936): The determination of the preconsolidation load and its practical significance. Proc. *First Intern. Conf. on Soil Mech. and Found. Eng.*, Cambridge, Mass USA V. 3, pp. 60-64.

Clukey, E. Haustermans, L. and Dyvik, R. (2005): Model tests to simulate riser-soil interaction effects in touch-down point region. *Proc., ISFOG, Int. Symp. on Frontiers in Offsh. Geotech.*, 651-658. Perth, Australia.

DeGroot, D.J., DeJong, J.T., Yafrate, N.J., Landon, M.M. and Sheahan, T.C. (2007): Application of Recent Developments in Terrestrial Soft Sediment Characterization Methods to Offshore Environments. *38th OTC*, Houston, USA.

Dickens, R. and Quinsby-Hunt, M.S. (1994): Methane hydrate stability in seawater. *Geophysical Research Letters* 21, 2115-2118.

Donohue, S. and Long, M. (2007): Rapid determination of sample quality using shear wave velocity and suction measurements. *Proc. Conf. on Soil Invest. and Found. Behaviour, SUT*, London, Sept. 2007, 63-72.

Dyvik, R. and Madshus, C. (1985): Lab measurements of G_{max} using bender elements. *Conf. on Advances in the art of testing soil under cyclic conditions,* Detroit, MI, Oct., Proc., p. 186 – 196.

Ehlers, C. J., Chen, J. Roberts, H. H., and Lee, Y. C. (2005): The origin of near-seafloor "crust zones" in deepwater. *Proc., ISFOG, Int. Symp. on Frontiers in Offshore Geotech.*, 927-933. Perth, Australia.

Eklund, T. and Strøm, P. (1998): DIGIN. User's manual Ver. 5.3. *DNV Report 96-3637*, Rev. 03, 20 Apr. 1998.

Fausa (2006): Generell orientering om subsea produksjonssystemer. *Seminar om Subsea Produksjonsanlegg, Norwegian Structural Steel Association,* Oslo, 9 March, 2006.

Fellenius, W. (1936): Calculation of the stability of earth dams. *Proc., 2. ICOLD*, Washington, D.C., Vol. 4, 445.

Forsberg, C.F., Planke, S., Tjelta, T., Svanø, G., Strout, J. and Svensen, H. (2007): Formation of Pockmarks in the Norwegian Channel. *Proc., 6th OSIG, SUT,* London. 221-230.

Gauer, P., Kvalstad, T.J., Forsberg, C.F., Bryn, P. and Berg, K. (2005): The Last Phase of the Storegga Slide: Simulation of Retrogressive Slide Dynamics and Comparison with Slide-Scar Morphology. *Marine and Petroleum Geology*, 22 (1-2), Jan./Feb. 2005.

Geo-Slope Inc., http:\\www.geo-slope.com.

Imran, J., Harff, P., and Parker, G., (2001): A numerical model of submarine debris flow with graphical user interface. *Computers and Geosciences*, 27, 717-729.

Guliyev, I. and Feizullayev, A. (1997): All about mud volcanoes. *Baku Publishing House, Nafta Press*, 1997.

Hansteen, O.E. (1980): Dynamic performance. *Seminar; Shell Brent "B" Instrumentation Project. SUT.* Proc., 89-107. London 1979. Also NGI Publ. 137.

Hill, A.J. and Jacob, H. (2008): In-situ measurement of pipe-soil interaction in deep water. *Proc. OTC,* Paper OTC 19528.

Imran, J., Harff, P., and Parker, G. (2001): A numerical model of submarine debris flow with graphical user interface. *Computers and Geosciences*, 27, p. 717-729.

ISSMGE (2005): Geotechnical and geophysical investigations for offshore and nearshore developments. *Int. Society for Soil Mechanics and Geotechnical Engineering*, Handbook, Sept. 2005.

Janbu, N. (1969): The resistance concept applied to the deformation of soils. Proc. 7^{th} *Int. Conf. on Soil Mech. and Found. Eng.*, Mexico City. Vol 1, 191-196.

Janbu, N. (1973): Slope stability computation. *Embankment dam engineering. Ed.by R.C. Hirschfeld & S.J. Poulos. John Wiley & Sons*, New York, 47–86.

Jeanjean, P., Hill, A, and Taylor, S. (2003): The challenge of siting facilitites along the Sigsbee Escarpment in the Southern Green Canyon area of the Gulf of Mexico. *Proc. OTC*, Houston, Paper 15156.

Kamath, A., Godbole, S.P., Ostermann, R.D. and Collett, T.S. (1987): Evaluation of the stability of gas hydrates in northern Alaska. *Cold Regions Science and Technology* 14, 107-119.

Karlsrud, K. and Nadim, F. (1990): Axial capacity of offshore piles in clay. *Proc., 22 OTC*, Houston, 404-416, Paper OTC6245.

Karlsrud, K., Clausen, C.J.F. and Aas, P.M. (2005): Bearing capacity of driven piles in clay. *Proc., ISFOG, Int. Symp. on Frontiers in Offshore Geotechniques*, 775-782. Perth, Australia.

Keaveny, J.M., Hansen, S.B., Madshus, C. and Dyvik, R. (1994): Horizontal capacity of large scale model anchors. *XIII ICSMFE.* New Delhi, 1994. Proc. (2) 677-680.

Kleven, A. and Andersen, K.H. (1991): Cyclic laboratory tests on Storebælt clay till. *Seminar, Design of Exposed Bridge Piers. Danish Soc. of Hydr. Engrg. Copenh., Denmark,* Jan. 1991. Also publ. in NGI Publ. 199.

Kvalstad, T.J., Andresen, L., Forsberg, C.F., Berg, K. and Bryn, P., (2005): The Storegga Slide: Evaluation of triggering sources and slide mechanisms. *Marine and Petroleum Geology*, 22 (1-2), Jan./Feb. 2005.

Kvalstad, T.J., Nadim, F., Kaynia, A.M., Mokkelbost, K.H. and Bryn, P. (2005): Soil conditions and slope stability in the Ormen Lange area. *Marine and Petroleum Geology*, 22 (1-2), Jan/Feb 2005.

Lacasse, S., Hermann, S. and Jensen, T.G. (2001): Improved engineering solutions because of improved site characterisation. *Chuck Ladd Symp., Soil Behavior and Soft Ground Construction*, ASCE Geotechnical Spec. Pub. 119, MIT, Cambridge, USA, 239-254.

Ladd, C.C. and Foott, R. (1974): New design procedure for stability of soft clays. *JGED, ASCE,* 100 (7) 763-786.

Ladd, C.C. and DeGroot, D.J. (2003): Recommended practice for soft ground site characterization: *A. Casagrande Lecture. Proc. 12th Panamerican Conf. on Soil Mech. and Geotech. Engrg.*, Boston, MA, 3.

Landon, M.M., DeGroot, D.J., and Sheahan, T.C. (2007): Non-Destructive Sample Quality Assessment of a Soft Clay using Shear Wave Velocity. *J. of Geotechnical and Geoenvironmental Enrg.*, 133 (4), 424-432.

Langford, T. and Aubeny, C. (2008): Model tests for steel catenary riser in marine clay. *Proc., OTC,* Houston, Paper 19495.

Leroueil, S. and Marques, E.S. (1996) : Importance of strain rate and temperature effects in geotechnical engineering". Measurement and Modeling Time Dependent Soil Behaviour. *ASCE Geotech. Spec. Pub.* 61, 1-60.

Liedtke, E., Jeanjean, P., and Humphrey, G. (2006.): Geotechnical site investigation for the Mad Dog Spar anchors", *Proc., OTC*, Houston, Paper 17862.

Lunne, T., Robertson, P.K. and Powell, J.J.M. (1997a): *Cone Penetration Testing in Geotechnical Practice*, SponPress, London, 312 p.

Lunne, T., Berre, T. and Strandvik, S. (1997b): Sample disturbance effects in soft low plastic Norwegian clay. Proc. *Recent Developments in Soil and Pavement Mechanics*. Rio de Janeiro, Brazil, 81-102.

Lunne, T. and Long, M. (2006): Review of long seabed samplers and criteria for new sampler design. *Marine Geology*, 226, 145-165.

Lunne, T., Berre, T., Andersen, K.H., Strandvik, S. and Sjursen, M. (2006): Effects of sample disturbance and consolidation procedures on measured shear strength of soft marine Norwegian clays. *Can. Geot. J.*, 43, 726-750.

Lunne, T. and Andersen, K.H. (2007): Soft clay shear strength parameters for deepwater geotechnical design. *Proc., 6th OSIG*, London, UK, 151-176.

Lunne, T., Tjelta, T.I., Walta, A. and Barwise, A. (2008): Design and testing out of deepwater seabed sampler. *Proc. OTC*, Houston, USA, Paper 19290.

Lunne, T., Berre, T., Andersen, K.H., Sjursen, M. and Mortensen, N. (2008): Effects of sample disturbance on consolidation behaviour of soft marine Norwegian clays. *ISC-2,* Taiwan (on CD only).

Marques, M.E.S., Leroueil, S. and Almeida, M. de S.S. (2004): Viscous behaviour of St-Roch-de-l'Achigan clay. *Can. Geot. J.*, 41 (1) 25-38.

Mitchell, J.K. (1960): Fundamental Aspects of Thixotropy in Soils, *J. of Soil Mech. & Found. Div., ASCE*, 86, (3), 19-53.

Mitchell, J.K. (1993): Fundamentals of Soil Behavior, 2nd Edition, *John Wiley and Sons, Inc.*

Moore, R., Usher, N. and Evans, T. (2007): Integrated multidisciplinary assessment and mitigation of West Nile Delta geohazards. *Proc., 6th OSIG*. p. 11-13.

Morgenstern, N.R. and Price, V.E. (1965): The analysis of the stability of general slip surfaces. *Géotechnique*, 15: 79–93.

Moscardelli L., Wood L., and Mann P. (2006): Mass-transport complexes and associated processes in the offshore area of Trinidad and Venezuela. *AAPG Bulletin* 90 (7): 1059-1088.

Murff, J.D., Wagner, D.A. and Randolph, M.F. (1989): Pipe penetration in cohesive soil. *Geotechnique*, 39 (2), 213-229.

Murff, J.D., Randolph, M.F., Elkhatib, S., Kolk, H.J., Ruinen, R.M., Strom, P.J. and Thorne, C.P. (2005): Vertically loaded plate anchors for deepwater applications. *Proc., ISFOG,* 31-48. Perth, Australia.

Nadim, F., Kvalstad, T.J., and Guttormsen, T. (2005): Quantification of risk associated with seabed instability at Ormen Lange. *Marine and Petr. Geology*, 22 (1-2).

NCEL (1987): Drag embedment anchors for navy moorings. *Techdata sheet 83-08R*, Naval Civil Engineering Laboratory, Port Hueneme, California.

Neerland (2006): Ormen Lange – en gigant på dypt vann. *Seminar om Subsea Produksjonsanlegg, Norwegian Structural Steel Association*, Oslo, 9 March, 2006.

NGI (2002): Early soil investigations for fast track projects: Assessment of soil design parameters from index measurements in clays. Summary Rep./Manual, *NGI Report 521553-3*, 15 Jan. 2002.

NGI/COFS (2006): Shear Strength Parameters Determined by In situ Tests for Deep Water Soft Soils. Summary Report/Manual. *NGI Report* 20041618-6, 20 July 2006.

Normark, W.R. and Carlson, P.R. (2003): Giant submarine canyons: Is size any clue to their importance in the rock record?. *Ed. by Chan, M.A. & Archer, A.W., Extreme depositional environments: Mega end members in geologic time: Boulder, Colorado. Geological Society of America*, Paper SPE370-10.

NORSOK Standard (2004): Marine soil investigations, G-001, Rev. 2, Oct. 2004.

Paull, C.K., Matsumoto, R., Wallace, P.J., and Dillon, W.P. (Eds.) (2000): *Proc. ODP*, Sci. Results, 164: College Station, TX (Ocean Drilling Program). doi:10.2973/odp.proc.sr.164.2000.

Pennington, D. and Kelleher, P. (2007): PROD delivers accurate site investigation at Maari. *Proc., Conf. on Soil Invest. and Found. Behaviour, SUT*, London, Sept., 2007, 81-90.

Perkins, S. and Sjursen, M. (2007): Effect of cold temperature of unfrozen Troll clay. *Submitted for possible publ in Can. Geot. J.*

Peuchen, J. and Mayne, P. (2007): Rate effects in vane shear testing. *Proc., Conf. on Soil Invest. and Found. Behaviour, SUT*, London, Sept. 2007,. 187-194.

PLAXIS (2001): http:\\www.plaxis.nl.

Posamentier, H.W. and Kolla, V. (2003): Seismic geomorphology and stratigraphy of depositional elements in deep-water settings. *J. of Sedimentary Research* 73 (3): 367-388.

Randolph, M.F., Hefer, P.A., Geise, J. and Watson, P.G. (1998): Improved seabed strength profiling using T-bar

penetrometer. *Proc. Int. Conf. Offsh. Site Inv. and Found. Beh.-"New Frontiers", SUT*, London, 221-235.
Randolph, M.F. and Andersen, K.H. (2006): Numerical analyses of T-bar penetration in soft clay. *ASCE Int. J. of Geomechanics* 6(6), 411-420.
Randolph, M.F., Low, H.E. and Zhou, H. (2007): In situ testing for design of pipeline and anchoring systems. *Proc., Conf. on Soil Invest. and Found. Behaviour, SUT*, London, Sept., 2007, 251-262.
Robertson, P.K. (2008): Personal communication.
Sandbækken, G., Berre, T. and Lacasse, S. (1986): Oedometer testing at the Norwegian Geotechnical Institute. "Consolidation of soils: Testing and Evaluation". *ASTM, STP 892 1986*, 329-353.
Schjetne, K. (2008): Personal communication.
Seed, H.B. and Idriss, I.M. (1970): Soil moduli and damping factors for dynamic response analysis. *Earthq. Engrg. Res, Center*. Report EERC70-10.
Skempton, A.W. and Northey, R.D. (1952): The sensitivity of clays. *Geotechnique,* 3, (1), 30-53.
Spencer, E. (1967); A method of analysis of the stability of embankments assuming parallel interslice forces. *Geotechnique*, 17(1), pp. 11-26.
Strout, J.M. and Tjelta, T.I. (2004): *In situ* pore pressures: What is their significance and how can they be reliably measured? *Marine and Petroleum Geology*, 22 (1-2) Jan/Feb 2005.
Strout, J.M. and Tjelta, T.I. (2007): Excess pore pressure measurements and monitoring for offshore instability problems.*Proc. OTC*, Paper18706.
Sultan, N., Voisset, M., Marsset, T., Vernant, A.M., Cauquil, E., Colliat, J.L. and Curinier, V., (2007): Detection of free gas and gas hydrate based on 3D seismic data and cone penetration testing: An example from the Nigerian Continental Slope**.** *Marine Geology* Vol. 240, Issues 1-4, 5 June 2007, Pages 235-25.
SUT-OSIG (2000): Guidance Notes on Geotechnical Investigations for Subsea Structures. *OSIG-Rev. 2, Aug. 2000. Prep. by Subsea Working Group of Offsh. Soil Invest. Forum*. Updated 2000 by SUT.
SUT-OSIG (2004): Guidance Notes on Geotechnical Investigations for Marine Pipelines. *OSIG-Rev. 3, Sept. 2004. Prep. by Pipeline Working Group of Offsh. Soil Invest. Forum*. Updated 2004 by SUT.
Tjelta, T.I., Guttormsen, T. and Hermstad, J. (1986): Large scale penetration test at a deep water site. *Proc. OTC*, Houston, Paper 5103.
Tjelta, T.I, Svanø, G., Strout, J.M., Forsberg, C.F., Johansen, H. and Planke, S. (2007): Shallow gas and its multiple impact on a North Sea production platform. *Proc., 6th OSIG*, London, UK, 205-220.
Tréhu, A.M., Bohrmann, G., Torres, M.E., and Colwell, F.S. (Eds.) (2006): *Proc. ODP, Sci. Results,* 204: College Station, TX (Ocean Drilling Program), 1–40. doi:10.2973/odp.proc.sr.204.101.2006.
Vidal, V.M.V., Vidal, F.V., Hernandez, A.F., Meza, E. and Zambrano, L. (1994): Winter Water Mass Distributions in the Western Gulf of Mexico Affected by a Colliding Anticyclonic Ring, *J. of Oceanography*, 50, 559-588.
Vist (2006): Snøhvit, Loboco-Tomboco and Seven Heads. *Seminar om Subsea Produksjonsanlegg, Norwegian Structural Steel Association*, Oslo, 9 March, 2006.
Vryhof Anchors (1999): *Anchor Manual 2000*, Krimpen and Yjssel, The Netherlands.
Whittle, A.J., Sutabutr, T., Germaine, J.T. and Varney, A. (2001): Prediction and measurements of pore pressure dissipation for a tapered piezoprobe. *Proc. OTC,* Paper 13155.
Zuidberg, H.M., Richards, A.F. and Geise, J.M. (1986): Soil exploration offshore. Field Instrumentation and *in situ* Measurements. *Proc. 4. Int. Geot. Seminar,* 3-11.

Program (1/2)

33rd IGC in Lillestrøm Norway
GEOHAZARDS - A TRIBUTE TO KAARE HØEG
Friday, August 8, 2008

A Life in GeoSciences

The Symposium is a tribute to Kaare Høeg's career and achievements. Lecturers from around the world who have contributed to and benefited from Kaare Høeg's outreach in the geosciences will present keynote lectures on geology and geohazards, including landslides, shallow gas, floods, erosion, early warning systems, safety of dams subjected to erosion, and hazard analysis. Professor R.V Whitman, of MIT, will introduce the session with a retrospective of Kaare Høeg's work in the USA and how his ideas and work influence the profession today.

08:30-08:45	Introduction Dr. Suzanne Lacasse International Centre for Geohazards (ICG), NGI, Norway
08:45-09:30	Kaare Høeg in the United States Professor Robert V. Whitman MIT, Cambridge, MA, USA
09:30-10:00	Bayesian method: a natural tool for processing geotechnical information Professor Wilson Tang Hong Kong University of Science and Technology, Hong Kong
10:00-10:30	*Coffee break*
10:30-11:00	An Early Warning System for Risk Mitigation at Lake Sarez in Tajikistan Dr. Elmo DiBiagio International Centre for Geohazards (ICG), NGI, Norway
11:00- 11:30	Managing Landslides in the Panama Canal Professor J. Michael Duncan Virginia Polytechnic Institute, Blacksburg, VA, USA
11:30-12:00	Effects of long term groundwater change on basement design Dr. Hugh St John Geotechnical Consulting Group, UK

Lunch Break

14:00-14:30	Safeguarding Venice from High Tides Professor Dr. Michel Jamiolkowski Studio Geotecnico Italiano, Politecnico di Torino, Italy

Program (2/2)

33rd IGC in Lillestrøm Norway
GEOHAZARDS - A TRIBUTE TO KAARE HØEG
Friday, August 8, 2008

14:30-15:00	Perceived Problems of Shallow Gas beneath a North Sea Production Platform Tor Inge Tjelta Statoilhydro AS, Norway
15:00-15:30	Internal erosion, the ageing of water retaining structures: failures, incidents and preventive maintenance Profesor Dr. Jean-Jacques Fry Electricité de France et Ecole Centrale de Lyon, France
15:30-16:00	*Coffee break*
16:00-16:30	How the glaciers formed a challenging playground for prominent geotechnical engineers Professor Anders Elverhøi University of Oslo (UiO), Norway
16:30-17:15	The Changing Pattern of Landslide Risk in Europe Professor Dr. Farrokh Nadim International Centre for Geohazards (ICG), NGI, Norway
17:15-17:30	Retrospective Professor Kaare Høeg UiO/ICG/NGI, Norway
17:30	Closure Dr. Suzanne Lacasse ICG, NGI, Norway

Program (1/2)

33rd IGC in Lillestrøm Norway
Theme of the Day GEOHAZARDS
Saturday, August 9 2008

Geohazards: can society cope?

Landslides, sea level rise, subsidence in deltas, violent storms, earthquakes, floods and tsunamis hit our communities, causing loss of life and huge damage. Can we protect these communities, should we build in areas threatened by natural hazards? Can we develop effective warning and emergency preparedness systems?

GEOSCIENCE PROGRAM

08:30-08:33 Introduction
Dr. Suzanne Lacasse
International Centre for Geohazards, NGI (Norway)

08:33-09:00 Rock Slide Hazards: Detection, Assessment and Warning
Professor D. Jean Hutchinson
Queen's University (Canada)

09:00-09:30 Earthquake Vulnerability: An Engineer's Perspective with a Difference
Dr. Tiziana Rossetto
University College London (UK)

09:30-10:00 Tsunamis
Professor Costas Synolakis
University of Southern California Los Angeles (USA)

10:00-10:30 Coffee break

10:30-11:00 Volcanoes and their Impact on Human Society
Professor Stephen Sparks
University of Bristol (UK)

11:00- 11:30 Geological Considerations in Quantitative Offshore Geohazards Risk Assessment
Dr. Philippe Jeanjean
BP Corporation (USA)

11:30-12:00 Early Warning Systems for Landslides
Professor Farrokh Nadim
University of Oslo and International Centre for Geohazards, NGI (Norway)

PLENARY LECTURE

13:00-13:45 Reducing the Risks Associated with Natural Threats
Professor Herbert H. Einstein
Massachusetts Institute of Technology (MIT) (USA)

Program (2/2)

33rd IGC in Lillestrøm Norway
Theme of the Day GEOHAZARDS

SOCIETAL PROGRAM

14:00-14:30	Global Approach to Slope Safety in Hong Kong Mr. Raymond Chan GEO Civil Engineering and Development Department (Hong Kong)
14:30-14:45	Global Patterns of Disaster Risk Dr. Bob Chen The Earth Institute, Columbia University (USA)
14:45-15:00	Hazard and Risk Mapping for Landslides Mr. Kjell Karlsrud International Centre for Geohazards and NGI (Norway)
15:00-15:15	The Ms 8.0 Wenchuan Earthquake of May 12th, 2008, Sichuan, China Dr. Shuwen Dong Chinese Academy of Geological Sciences (China)
15:15-15:30	Social Vulnerability and Resilience to Geohazards Dr. Carsten Felgentreff University Osnabrück (Germany)
15:30-16:00	*Coffee break*
16:00-16:30	Geophysical Risks and Society Dr. Tom Beer CSIRO (Australia)
16:30-17:00	Geo-Risks: Global Trends, Losses and Risk Management Dr. Anselm Smolka Geo Risks Research, Munich Reinsurance Company (Germany)
17:00-17:15	Geohazards in Iceland Ms. Thorunn Sveinbjarnardottir Ministry for the Environment (Iceland)
17:15-17:30	*Coffee break*
17:30-18:30	Panel debate: Policy-Making for Mitigation of Risks Associated with Geohazards *Moderator:* Marianne Moen, Norwegian Space Centre *Panellists:* Minister Thorunn Sveinbjarnardóttir, Ministry for the Environment (Iceland) Professor Herbert .H. Enstein, MIT (USA) Dr. Tom Beer, CSIRO (Australia) Dr. Carsten Felgentreff, University Osnabrück (Germany) Mr. Kjell Jogerud, Åknes-Tafjord Project (Norway) Dr. Hallvard Berg, Norwegian Water Resources and Energy Directorate (Norway)
18:30	Press conference